Fall 2014

Probabilistic engineering analysis and design under time-dependent uncertainty

Zhen Hu

Department: Mechanical and Aerospace Engineering

PROBABILISTIC ENGINEERING ANALYSIS AND DESIGN UNDER TIME-DEPENDENT UNCERTAINTY

by

ZHEN HU

A DISSERTATION

Presented to the Faculty of the Graduate School of the

MISSOURI UNIVERSITY OF SCIENCE AND TECHNOLOGY

In Partial Fulfillment of the Requirements for the Degree

DOCTOR OF PHILOSOPHY

in

MECHANICAL ENGINEERING

2014

Approved

Associate Prof., Xiaoping Du, Advisor

Professor, K. Chandrashekhara

Associate Prof., Serhat Hosder

Associate Prof., Joshua Rovey

Associate Prof., Xuerong Wen

PUBLICATION DISSERTATION OPTION

This dissertation consists of the following five articles that have been published or submitted for publication as follows:

Pages 7-39 have been published in Structural and Multidisciplinary Optimization.

Pages 40-74 have been accepted for publication in the proceedings of the 2014 ASME International Design and Engineering Technical Conferences & Computers and Information in Engineering Conference (IDETC/CIE 2014), August 17-20, 2014, Buffalo, NY, and submitted for publication to ASME Journal of Mechanical Design.

Pages 75-113 have been published in Structural and Multidisciplinary Optimization.

Pages 114-146 have been submitted to ASCE-ASME Risk and Uncertainty in Engineering Systems, Part B. Mechanical Engineering.

Pages 147-179 have been submitted to ASCE-ASME Risk and Uncertainty in Engineering Systems, Part B. Mechanical Engineering.

All of them have been prepared in the format for publication in the corresponding journals.

ABSTRACT

Time-dependent uncertainties, such as time-variant stochastic loadings and random deterioration of material properties, are inherent in engineering applications. Not considering these uncertainties in the design process may result in catastrophic failures after the designed products are put into operation. Although significant progress has been made in probabilistic engineering design, quantifying and mitigating the effects of time-dependent uncertainty is still challenging. This dissertation aims to help build high reliability into products under time-dependent uncertainty by addressing two research issues. The first one is to efficiently and accurately predict the time-dependent reliability while the second one is to effectively design the time-dependent reliability into the product. For the first research issue, new time-dependent reliability analysis methodologies are developed, including the joint upcrossing rate method, the surrogate model method, the global efficient optimization, and the random field approach. For the second research issue, a time-dependent sequential optimization and reliability analysis method is proposed. The developed approaches are applied to the reliability analysis of designing a hydrokinetic turbine blade subjected to stochastic river flow loading. Extension of the proposed methods to the reliability analysis with mixture of random and interval variables is also a contribution of this dissertation. The engineering examples tested in in this work demonstrate that the proposed time-dependent reliability methods can improve the efficiency and accuracy more than 100% and that high reliability can be successfully built into products with the proposed method. The research results can benefit a wide range of areas, such as life cycle cost optimization and decision making.

ACKNOWLEDGMENTS

First and foremost, I would like to express my sincere gratitude to my advisor, Dr. Xiaoping Du, for his encouragement, insightful guidance, and support during my graduate study at Missouri University of Science and Technology. He patiently guided me through every stage of my research while granted me a great deal of independence. His encouragement endowed me with tremendous confidence in exploring unknown scientific territory and challenging myself to be my best. His diligence and rigorous altitude to research and work will have a significant influence on my future life. It has been a privilege and a great honor to have worked with him.

I would also like to extend my appreciation to all my dissertation committee members, Dr. K. Chandrashekhara, Dr. Serhat Hosder, Dr. Joshua Rovey, and Dr. Xuerong Wen. Without their guidance and valuable comments, it is impossible for me to complete my dissertation.

The dissertation was supported by the National Science Foundation through Grant No. CMMI 1234855, the Office of Naval Research through contract ONR N000141010923, and the Intelligent System Center, which are gratefully acknowledged. I would like to express my deep thanks to my labmates and friends, Dr. Yi Zhang, Mr. Zhifu Zhu, Ms. Yao Cheng, Mr. Liang Xie, Mr. Yao Wang, Mr. Haifeng Li, Mr. Zhen Huo, Ms. Xueyang Chen, Mr. Wenyong Lu, Mr. Thomas West, Mr. Harsheel Shah, Mr. Andrew Brune, and Mr. Joe-Ray Gramanzini for their support during my study in Rolla. I also would like to express my sincere gratitude to Dr. Daniel Conrad and Mr. Michael Walmsley at Hussmann Corporation for their help and support during my summer internship.

Last but not the least, I wish to extend my special and sincere thanks to my wife, Dan Ao, my parents, sister, and my parents in law, for their love and unwavering support.

TABLE OF CONTENTS

LIST OF ILLUSTRATIONS

Page

PAPER IV

PAPER V

LIST OF TABLES

Page

PAPER I

PAPER II

PAPER III

PAPER IV

PAPER V

1. INTRODUCTION

1.1. BACKGROUND

Natural variations or uncertainties are inevitable in engineering systems. The uncertainties are in-eliminable but usually reducible. Some examples include manufacturing variations in dimensions, variations in material properties, and noises in loadings. Accounting for such uncertainties in the design is vital for the safety of many complex engineering systems such as aircraft [1], automobiles [2], and offshore structures [3]. As an effective way of mitigating the effects of design bias stemmed from the inherent uncertainties in the design environment, probabilistic engineering design methodologies have been increasingly used in recent years [4-7]. In the probabilistic engineering design, uncertainties in the design environment are addressed through three ways. The first one is uncertainty propagation, which propagates uncertainties through the design models to investigate the effects of uncertainties on designs. The second one is uncertainty quantification, which quantifies the uncertainty in simulation or analysis results. The third one is calibration under uncertainty, which is an inverse uncertainty propagation process. The focus of this work is the uncertainty propagation.

There are many kinds of uncertainties. According to the time variant characteristics, the uncertainties can be grouped into two categories: time-independent uncertainties and time-dependent uncertainties. The time-independent uncertainties are usually described as random variables while time-dependent uncertainties are modeled as stochastic processes. For example, the manufacturing tolerance is a typical time-independent uncertainty; the stochastic wind loading, river flow loading, and aerodynamic loading, on the other hand, are time-dependent uncertainties. The reliability of systems subjected to time-dependent uncertainties is also time dependent [8, 9]. Even for some systems with only time-independent uncertainties, their reliability may also be time dependent due to the responses are time dependent [8]. Time-dependent reliability methodologies should be employed for systems under time-dependent uncertainties or with time-dependent responses.

The time-dependent reliability gives the reliability of the system over a specific time interval instead of the reliability at a certain time instant. For instance, the time-dependent reliability of a vehicle over ten years indicates the probability that there is no failure over the ten years' operation. It is different from the conventional time-instantaneous reliability, which only tells the reliability at a time instant. Time-dependent reliability is directly related to the lifecycle cost (LCC) of a product [10, 11]. Based on the relationship between reliability and time, failure rates of the system can be easily obtained. Moreover, in order to guarantee the reliability of a system over a certain time interval and maintain a low operation cost, engineers can schedule maintenance activities with reference to the time-dependent reliability. It is of great interest to not only designers with concerns about reliability, but also decision makers focusing on product lifecycle costs. The prediction of time-dependent reliability is therefore vital.

In the past decades, many efforts have been devoted to evaluating the time-dependent reliability. For example, the time-dependent reliability model developed in the area of reliability engineering based on post-design failure rates [12]. The time-dependent reliability analysis method proposed by researchers using the Rice's formula in the area of probabilistic engineering design [8]. Even if the failure rate based time-dependent reliability model can effectively predict the time-dependent reliability, it is not applicable in the early design stage as no failure data are available. The Rice's formula based method is applicable to some problems. But its accuracy and efficiency are not satisfactory for many problems with low failure thresholds [8, 13, 14]. How to effectively quantify and mitigate the effects of time-dependent uncertainties is still an ongoing research issue. There are many challenges need to be solved.

To accurately and efficiently approximate the time-dependent reliability and effectively build the time-dependent reliability into the design, the underlying statistical characteristics of time-dependent uncertainties need to be understood. Technical developments in new reliability analysis methodologies are required. This dissertation contributes to solving these problems. The technical developments of probabilistic engineering analysis and design under time-dependent uncertainties in this work will bridge the gap between engineering design and reliability engineering. It makes the

design with an optimal lifecycle cost possible. The outcomes will benefit many areas, such as aerospace engineering, automobile engineering, and marine engineering.

1.2. RESEARCH OBJECTIVES

The main objective of this research is to explore new analysis and design methodologies for the quantification and mitigation of the effect of time-dependent uncertainties. Four research tasks are carefully studied to achieve this overall objective. The first research task concentrates on the time-dependent reliability analysis. Based on the outcomes of the first research task, the second research task focuses on reliability-based design optimization (RBDO) with time-dependent reliability constraints. Since fatigue reliability is a very important issue for structures under stochastic loadings, the third research task studies the fatigue reliability analysis method under stochastic loadings. Research results from the first three research tasks are then evaluated through engineering design examples in the fourth research task.

More specifically, research task 1 (RT1) answers the following question: Given the information of time-independent and time-dependent uncertainties in the input variables, what is the uncertainty in the output of a system. The main challenge for answering this question is how to account for the time-varying statistical properties of the response with the minimal computational cost. The widely used Rice's formula based method is efficient, but it overestimates the time-dependent probability of failure [8]. Directly solving the time-dependent reliability is computationally expensive. To address these challenges, the joint-upcrossing rate method is employed to release the independent assumption used in the Rice's formula based method [15]. The correlations between upcrossing events are considered to obtain an accurate first-time failure rate. With the first-time failure rate, the time-dependent reliability is approximated. In addition to that, an efficient global optimization reliability analysis method is proposed for time-variant problems with random variables and time [16]. A mixed efficient global optimization method is developed to identify the global extremes. Surrogate model of the extreme value response is then established. Time-dependent reliability is estimated by performing Monte Carlo sampling on the surrogate model. The applications of series expansion

method and sampling approach to the time-variant problems are investigated as well [17, 18].

Research task 2 (RT2) addresses the question of how to design specific time-dependent reliabilities into a product. The way of designing high reliability into a product is achieved by optimally changing the design variables to satisfy reliability constraints. Design optimization algorithms are usually used to adjust the design variables and check the constraints. Since time-dependent reliability analysis is computationally expensive, design optimization with time-dependent reliability constraints is far more computationally costly. A time-dependent sequential optimization and reliability assessment (t-SORA) approach is proposed by decoupling the design optimization model into a deterministic design optimization model and a time-dependent reliability analysis model. The design optimization and reliability analysis are performed sequentially and thus improves the efficiency of time-dependent reliability based design optimization. The most critical part of the method is the identification of an equivalent Most Probable Point (MPP). The equivalent MPP is obtained using the inverse saddlepoint approximation method and series expansion method.

RT1 and RT2 concern about the global extreme values of the time-variant response. For structures subjected to stochastic loadings, the local extreme values are also very important as they are related to the fatigue life of the structure. Research Task 3 (RT3) studies the fatigue reliability analysis method. The challenge is how to efficiently obtain the stress cycle distribution of the structure and incorporate uncertainties of material properties and experimental data into the analysis. A design oriented fatigue reliability analysis method is developed based on the peak counting method [19]. An efficient numerical algorithm is proposed to approximate the fatigue reliability. Considering the stress-dependent uncertainties in the S-N curve of material fatigue properties, an efficient reliability analysis method is developed for structures with known loading trend [20].

Research Task 4 (RT4) applies the developed methodologies to the reliability analysis of hydrokinetic turbine blades under stochastic river flow loadings. It is a typical time-variant problem. The uncertainties in the composite material of the turbine blades and river velocity are considered. The reliability of the turbine blades is evaluated using

the joint-upcrossing rate method proposed in RT1. Two failure modes of the turbine blades are investigated. The extension of the proposed method to other similar problems is also studied. A random field approach is developed for the reliability analysis under mixture of random and interval variables by extending the series expansion method from time-dependent problems to interval problems.

The outcomes of above research tasks are expected to advance the knowledge of probabilistic engineering design under time-dependent uncertainties. The technical developments may benefit not only the area of engineering design, but also other areas such as engineering management, statistics, and reliability engineering.

1.3. ORGANIZATION OF DISSERTATION

Many technical developments have been made in this study on above research objectives. In this dissertation, only the five major developments are presented due to the page limit. The five articles are organized in the way shown in Fig. 1.1. Paper I and II focus on the time-dependent reliability analysis. Paper III is an application of the proposed method to a composite hydrokinetic turbine blade. Paper IV is an extension of the proposed method to the reliability analysis under mixture of random and interval variables. Paper V studies the time-dependent reliability-based design optimization method.

All of the five articles share a same research topic: the time-dependent reliability analysis, while each of them has a different focus. Paper I presents a joint-upcrossing rate method which is applicable for general problems with random variables, stochastic processes, and time. The Poisson assumption is released in the join-upcrossing rate method by considering the correlation of upcrossing events at different time instants. For problems with only random variables and time, a surrogate model method is given in Paper II. Even if the method presented Paper I can also be applied to the problems with only random variables and time, its accuracy and efficiency are worse than the method given in Paper II. The joint upcrossing rate method is applied to the reliability analysis of a composite hydrokinetic turbine blade in Paper III. The uncertainties in the design environment of the hydrokinetic turbine blades are investigated and summarized. The

reliability of the turbine blades is analyzed according to two kinds of failure modes. Since the time-dependent reliability problem is very similar as the reliability analysis problem under random and interval variables, in Paper IV, the series expansion method developed for the time-dependent reliability analysis is extended to the reliability analysis with random and interval variables. In order to incorporate the time-dependent reliability analysis method into design optimization, Paper V develops a time-dependent sequential optimization and reliability assessment approach for structures under stationary stochastic loadings. The approach is developed based on the new time-dependent reliability analysis method.

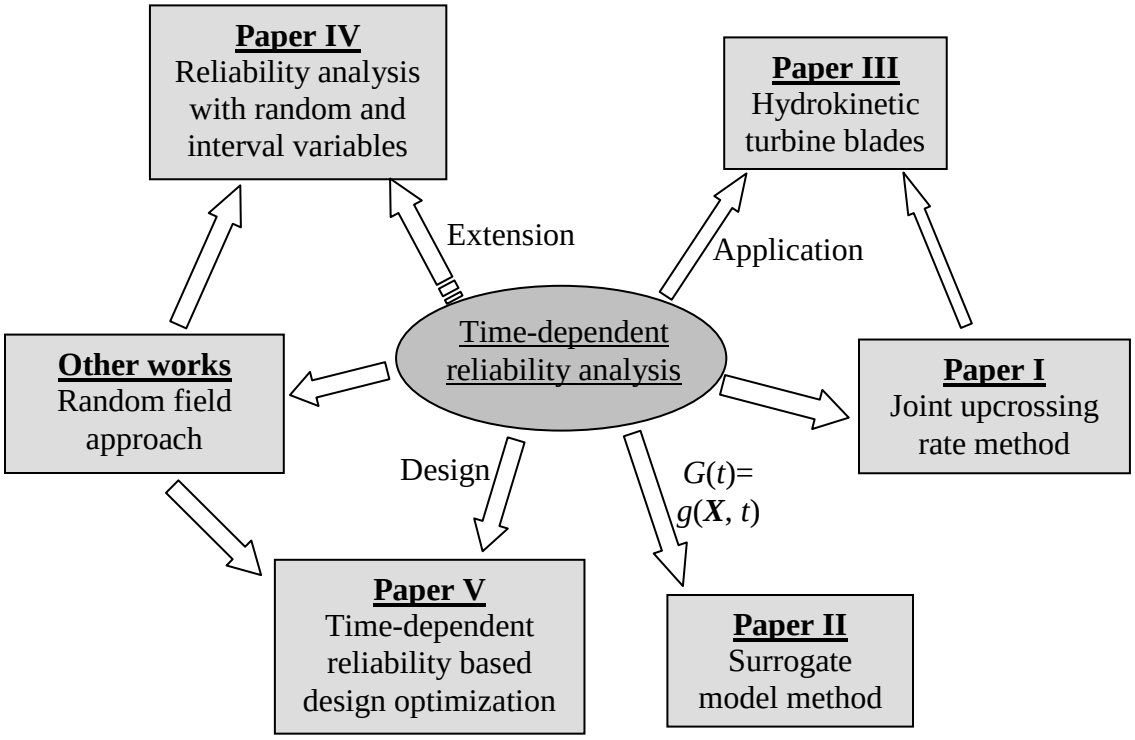

Figure. 1.1 Framework of this dissertation

PAPER

I. TIME-DEPENDENT RELIABILITY ANALYSIS WITH JOINT UPCROSSING RATES

Zhen Hu and Xiaoping Du

Department of Mechanical and Aerospace Engineering
Missouri University of Science and Technology, Rolla, Missouri 65409, U.S.A.

Abstract

In time-dependent reliability analysis, an upcrossing is defined as the event when a limit-state function reaches its failure region from its safe region. Upcrossings are commonly assumed to be independent. The assumption may not be valid for some applications and may result in more than 50% errors. In this work, a new method that relaxes the assumption by using joint upcrossing rates is developed. The method extends the existing joint upcrossing rate method to general limit-state functions with both random variables and stochastic processes. The First Order Reliability Method (FORM) is employed to derive the single upcrossing rate and joint upcrossing rate. With both rates, the probability density of the first time to failure can be solved numerically. Then the probability density leads to an easy evaluation of the time-dependent probability of failure. The proposed method is applied to the reliability analysis of a beam and a mechanism, and the results demonstrate improvements in accuracy.

Keywords: Time-dependent reliability, stochastic processes, first passage, autocorrelation

1. Introduction

Reliability is the probability that a product performs its intended function over a specified period of time and under specified service conditions [1]. Depending on whether the performance of the product is time-dependent or not, reliability can be

classified into two types: time-variant (time-dependent) reliability and time-invariant reliability.

For a time-invariant performance, its reliability and probability of failure remain constant over time. The time-invariant probability of failure is defined by

$$p_f = \Pr\{D = g(\mathbf{X}) > e\} \tag{1}$$

where $\mathbf{X} = (X_1, X_2, \cdots X_n)$ is a random vector, $g(\cdot)$ is a time-invariant performance function or limit-state function, D is a performance variable, e is a limit state, and Pr{·} stands for a probability. Many reliability methods are available for calculating the time-invariant reliability, including the First Order Second Moment Method (FOSM), FORM, and Second Order Reliability Method (SORM) [2-8].

On the other hand, limit-state functions may vary over time. For instance, over the service life of the Thermal Barrier Coating (TBC) of aircraft engines, the stresses and strains of the TBC are time dependent [9]. Many mechanisms also experience time varying random motion errors due to random dimensions (tolerances), clearances, and deformations of structural components [10-14]. In the systems of wind turbines, hydrokinetic turbines, and aircraft turbine engines, the turbine blade loading always varies over time. Likewise, the wave loading acting on offshore structures fluctuates randomly with time [15-17]. Almost all dynamic systems involve time-dependent parameters [18-20]. For all the above problems, reliability is a function of time and typically deteriorates with time.

Therefore, a general limit-state function is a function of time t. In addition to random variables $\mathbf{X} = (X_1, X_2, \cdots X_n)$, stochastic processes $\mathbf{Y}(t) = (Y_1(t), Y_2(t), \cdots Y_m(t))$ may also appear in the limit-state function. A stochastic process can be considered as a random variable that varies over time. Hence a general time-dependent limit-state function is given by

$$D(t) = g(\mathbf{X}, \mathbf{Y}(t), t) \tag{2}$$

If the likelihood of failure at a particular instant of time t is expected to be evaluated, the time-invariant probability of failure can still be used because t is fixed at the instant. Using Eq. (1), the instantaneous probability of failure is obtained by

$$p_f(t) = \Pr\{g(\mathbf{X}, \mathbf{Y}(t), t) > e(t)\} \tag{3}$$

The aforementioned methods, such as FOSM, FORM, or SORM, are ready to calculate $p_f(t)$.

For time-dependent problems, the time-dependent probability of failure is of great interest because it provides engineers with the likelihood of a product performing its intended function over its service time, or a system fulfilling its task during its mission time. The time-dependent probability of failure over a time interval $[t_0, t_s]$ is defined by

$$p_f(t_0, t_s) = \Pr\{g(\mathbf{X}, \mathbf{Y}(\tau), \tau) > e(\tau),\ \exists\, \tau \in [t_0, t_s]\} \tag{4}$$

where t_0 is the initial time when the product is put into operation, and t_s is the endpoint of the time interval, such as the service time of the product.

Let the first time to failure (FTTF) be T_1, which is the time that $g(\cdot)$ reaches its limit state for the first time. T_1 is also the working time before failure and is obviously a random variable. $p_f(t_0, t_s)$ can also be given by

$$p_f(t_0, t_s) = F_{T_1}(t_s) = \Pr\{T_1 < t_s\} \tag{5}$$

where $F_{T_1}(\cdot)$ is the cumulative distribution function (CDF) of the FTTF.

Time-dependent reliability methodologies are classified into two categories. The first includes the extreme-value methods, which use the time-invariant reliability analysis methods (FOSM, FORM, SORM, etc.) if one can obtain the distribution of the extreme value of $g(\mathbf{X}, \mathbf{Y}(\tau)) - e(\tau)$over $[t_0, t_s]$ [21-24]. The reason is that the failure event $\{g(\mathbf{X}, \mathbf{Y}(\tau), \tau) > e(\tau),\ \exists\, \tau \in [t_0, t_s]\}$is equivalent to the event $\left\{\max_{\tau}\left[g(\mathbf{X}, \mathbf{Y}(\tau)) - e(\tau)\right] > 0,\ \exists\, \tau \in [t_0, t_s]\right\}$. However, it is difficult to obtain the distribution of the extreme value. The extreme distribution may be available for limit-state functions in the form of $D(t) = g(\mathbf{X}, t)$ [24] or $D(t) = g(\mathbf{X}, Y(t))$ [25]. The associated methods, however, are not applicable for the general problems as indicated in Eq. (2). Therefore, in most cases, the methods in the second category are used.

The second category includes the first-passage methods because they directly use the first-passage time or the first time to failure (FTTF) T_1 in Eq. (5). The failure event

$\{g(\mathbf{X}, \mathbf{Y}(\tau), \tau) > e(\tau),\ \exists\, \tau \in [t_0, t_s]\}$ is equivalent to the event that at least a failure occurs over $[t_0, t_s]$ or equivalent to the event of $t_0 \le T_1 \le t_s$. The most commonly used method is the Rice's formula [26], which is based on the concept of upcrossing.

Define $N(t_0, t_s)$ as the number of upcrossings that $g(\cdot)$ reaches the limit state e from the safe region $g(\cdot) < 0$ over the time period $[t_0, t_s]$. The basic probability theory shows that $N(t_0, t_s)$ follows a binomial distribution. When the probability of upcrossing is very small, it is equal to the mean number of upcrossings per unit time (the upcrossing rate). Because the binomial distribution converges to the Poisson distribution when the time period is sufficiently long or the dependence between crossings is negligible, the upcrossings are assumed to be statistically independent [27]. With this assumption, the upcrossing rate becomes the first-time crossing rate or the failure rate. Then the probability of failure can be estimated from the upcrossing rate.

Since the development of the Rice's formula, many improvements have been made [28-40]. For example, an analytical outcrossing rate [31] has been derived for Gaussian stationary processes. An analytical outcrossing rate has also been given for general Gaussian stochastic processes [32, 33] and has been applied to mechanism analysis [34]. An important sampling method has been proposed to approximate the outcrossing rate [41], and a lifecycle cost optimization method was developed using the outcrossing rate as the failure rate [42]. If upcrossing events are rare over the considered time period [34], the Poisson assumption-based approaches [28-40] have shown good accuracy.

When upcrossings are strongly dependent, however, the above approaches may leads to large errors. In this case, the memory of failure should be considered to guarantee that the obtained first passage failure is indeed the first. Even though the Markov process methods have a property of memory, such memory is weak and is only valid for Markov or similar processes [43, 44]. Vanmarcke [45] and Preumont [46] have made some empirical modifications to the Poisson assumption-based formulas. These modifications are good for Gaussian processes.

A promising way to improve accuracy is to relax the independent assumption for upcrossing events. In other words, considering the dependence between two or more

instants of time [47, 48], instead of considering a single upcrossing at one instant. The accuracy improvement has been shown in [48] for a Gaussian process in vibration problems.

Inspired by the work in [48], a time-dependent reliability analysis method with joint upcrossing rates is developed, which extends the method in [48] to more general limit-state functions that involve time, random variables, and stochastic processes. Because the method combines the joint upcrossing rates (JUR) and First Oder Reliability Method (FORM), it is called JUR/FORM.

In section 2, the commonly used time-dependent reliability analysis methods is reviewed, upon which JUR/FORM is built. The JUR/FORM is then discussed in Section 3 followed by two case studies in Section 4. Conclusions are made in Section 5.

2. Review of time-dependent reliability analysis methods

In this section, the integration of the Poisson assumption based method with the First Order Reliability Method (FORM) is reviewed. By this method, $p_f(t_0, t_s)$ is calculated by [34, 48, 49]

$$p_f(t_0, t_s) = 1 - [1 - p_f(t_0)] \exp\left\{-\int_{t_0}^{t_s} v^+(t)dt\right\} \tag{6}$$

where $p_f(t_0)$ is the instantaneous probability of failure at the initial time point t_0, and $v^+(t)$ is the upcrossing rate at t.

$p_f(t_0)$ can be calculated by any time-invariant reliability methods, such as FOSM, FORM, and SORM. If $v^+(t)$ is known, then $p_f(t_0, t_s)$ can be calculated by integrating $v^+(t)$ over $[t_0, t_s]$ as indicated in Eq. (6).

For a general limit-state function $D(t) = g(\mathbf{X}, \mathbf{Y}(t), t)$, at a given instant t, the stochastic proceses $\mathbf{Y}(t)$ become random variables. If FORM is used, random variables $(\mathbf{X}, \mathbf{Y}(t))$ are first transformed into standard normal variables $\mathbf{U}(t) = (\mathbf{U_X}, \mathbf{U_Y}(t))$[2-6, 34]. Then the Most Probable Point (MPP) $\tilde{\mathbf{U}}(t) = (\tilde{\mathbf{U}}_\mathbf{X}, \tilde{\mathbf{U}}_\mathbf{Y}(t))$ is searched. The MPP is a point at the limit sate, and at this point the limit-state function has its highest probability

density. After the limit-state function is linearized at the MPP, the failure event $g(\mathbf{X},\mathbf{Y}(t),t) > e(t)$ is equivalent to the event given by [1].

$$W(\mathbf{U}(t),t) = \boldsymbol{\alpha}(t)\mathbf{U}(t)^T > \beta(t) \tag{7}$$

where

$$\begin{aligned}\boldsymbol{\alpha}(t) &= \left.\frac{\partial \mathbf{g}(T[\mathbf{U}(t)],t)}{\partial \mathbf{U}(t)}\right|_{\tilde{\mathbf{U}}(t)} \Bigg/ \left\| \left.\frac{\partial \mathbf{g}(T[\mathbf{U}(t)],t)}{\partial \mathbf{U}(t)}\right|_{\tilde{\mathbf{U}}(t)} \right\| \\ &= \nabla \mathbf{g}(T[\tilde{\mathbf{U}}(t)],t) \Big/ \left\| \nabla \mathbf{g}(T[\tilde{\mathbf{U}}(t)],t) \right\|\end{aligned} \tag{8}$$

$\beta(t)$ is the reliability index, which is the length of $\tilde{\mathbf{U}}(t)$. $T(\cdot)$ is the operator of transforming non-Gaussian random variables $(\mathbf{X},\mathbf{Y}(t))$ into Gaussian random variables $\mathbf{U}(t)$. $\|\cdot\|$ stands for the magnitude of a vector.

Then the upcrossing rate $v^+(t)$ is [50]

$$v^+(t) = \|\dot{\boldsymbol{\alpha}}(t)\| \phi(\beta(t)) \Psi\left(\dot{\beta}(t) / \|\dot{\boldsymbol{\alpha}}(t)\|\right) \tag{9}$$

where $\dot{\boldsymbol{\alpha}}(t)$ and $\dot{\beta}(t)$ are the derivatives of $\boldsymbol{\alpha}(t)$ and $\beta(t)$, respectively, with respect to time t, and $\Psi(\cdot)$ is a function defined by

$$\Psi(x) = \phi(x) - x\Phi(-x) \tag{10}$$

in which $\phi(x)$ and $\Phi(-x)$ stand for the probability density function (PDF) and cumulative density function (CDF) of the standard normal random variable, respectively.

As mentioned previously, the above method may produce large errors if upcrossings are strongly dependent. Next the joint upcrossing rate is used to improve the accuracy of time-dependent reliability analysis.

3. Time-dependent reliability analysis with joint upcrossing rates and FORM

In this section, the equations given in [48] is provided first for a Gaussian stochastic process. Based on these equations and FORM, complete equations are then derived in the subsequent subsections.

3.1. Time-dependent reliability analysis with joint upcrossing rates

Now the methodology in [48] is summarized, where the joint upcrossing rates are used. Based on the methodologies, necessary equations are developed in Secs. 3.2 and 3.3.

For a general stochastic process $Q(t)$, suppose its failure event is defined by $\{Q(t) > e(t)\}$. $p_f(t_0, t) = \Pr\{Q(\tau) > e(\tau),\ \exists\, \tau \in [t_0, t_s]\}$ is then given by

$$p_f(t_0, t_s) = \Pr\{Q(t_0) > e(t_0)\} + \Pr\{Q(t_0) < e(t_0)\} \Pr\{Q(\tau) > e(\tau),\ \exists\, \tau \in [t_0, t_s]\} \quad (11)$$

or

$$p_f(t_0, t_s) = \Pr\{Q(t_0) > e(t_0)\} + \Pr\{Q(t_0) < e(t_0)\} \int_{t_0}^{t_s} f_{T_1}(t)\, dt \quad (12)$$

where $f_{T_1}(t)$ is the probability density function (PDF) of the first time to failure (FTTF). The first term in the above equation is the probability of failure at the initial time, and the second term is the probability of failure over $[t_0, t_s]$ and no failure occurs at t_0.

The upcrossing rate $\nu^+(t)$ is the probability that an upcrossing occurs at time t per unit of time. It is equal to the summation of two probabilities. The first probability is the PDF $f_{T_1}(t)$, which is the upcrossing rate occurring for the first time at t. The second probability is the probability rate that the upcrossing occurred at time t given that the first-time upcrossing occurs at time τ prior to t. Thus [48]

$$\nu^+(t) = f_{T_1}(t) + \int_{t_0}^{t} \nu^+(t|\tau) f_{T_1}(\tau) d\tau \quad (13)$$

According to the characteristics of conditional probability for two events A and B, the probability is given by $P(\mathrm{A}|\mathrm{B}) = P(\mathrm{A}, \mathrm{B}) / P(\mathrm{B})$. Thus, the conditional probability $\nu^+(t|\tau)$ is equal to $\nu^{++}(t, \tau) / \nu^+(\tau)$, and Eq. (13) is rewritten as

$$\nu^+(t) = f_{T_1}(t) + \int_{t_0}^{t} \nu^{++}(t, \tau)\, f_{T_1}(\tau) / \nu^+(\tau) d\tau \quad (14)$$

where $\nu^{++}(t, \tau)$ is the second order upcrossing rate or the joint outcrossing rate at t and τ. It indicates the joint probability that there are outcrossings at both t and τ.

Eq. (14) is a Volterra integral equation, for which a closed-form solution may not exist. Numerical methods are therefore necessary [51-55]. In this work, the compounded

trapezoidal rule method [53] is used. Other integration methods can also be used. How to solve the Volterra integral equation is briefly presented below.

The time interval is first discretized into p time intervals or $p+1$ time instants with $t_i = t_0 + (i-1)h$, where $h = \dfrac{t_s - t_0}{p}$ and $i = 1, 2, \cdots, p+1$. With the compounded trapezoidal rule [53], $\int_{t_0}^{t_s} v^{++}(t_s, \tau) f_{T_1}(\tau) / v^{+}(\tau) d\tau$ is approximated as follows:

$$\begin{aligned} &\int_{t_0}^{t_s} v^{++}(t_s, \tau) f_{T_1}(\tau) / v^{+}(\tau) d\tau \\ &\approx \frac{1}{2} h \frac{v^{++}(t_s, t_0)}{v^{+}(t_0)} f_{T_1}(t_0) + h \sum_{i=2}^{p} \frac{v^{++}(t_s, t_i)}{v^{+}(t_i)} f_{T_1}(t_i) + \frac{1}{2} h \frac{v^{++}(t_s, t_s)}{v^{+}(t_s)} f_{T_1}(t_s) \end{aligned} \tag{15}$$

Combining Eq. (15) with (14) yields

$$v^{+}(t_s) \approx (1 + \frac{h}{2}) f_{T_1}(t_s) + \frac{1}{2} h \frac{v^{++}(t_s, t_0)}{v^{+}(t_0)} f_{T_1}(t_0) + h \sum_{i=2}^{p} \frac{v^{++}(t_s, t_i)}{v^{+}(t_i)} f_{T_1}(t_i) \tag{16}$$

Applying Eq. (16) to every time instant t_i, $i = 1, 2, \cdots, p+1$, it is given by

$$\begin{cases} v^{+}(t_1) = f_{T_1}(t_1) \\ v^{+}(t_2) \approx (1 + \frac{h}{2}) f_{T_1}(t_2) + \frac{1}{2} h \frac{v^{++}(t_2, t_1)}{v^{+}(t_1)} f_{T_1}(t_1) \\ v^{+}(t_3) \approx (1 + \frac{h}{2}) f_{T_1}(t_3) + h \frac{v^{++}(t_3, t_2)}{v^{+}(t_2)} f_{T_1}(t_2) + \frac{1}{2} h \frac{v^{++}(t_3, t_1)}{v^{+}(t_1)} f_{T_1}(t_1) \\ v^{+}(t_4) \approx (1 + \frac{h}{2}) f_{T_1}(t_4) + h \frac{v^{++}(t_4, t_3)}{v^{+}(t_3)} f_{T_1}(t_3) + h \frac{v^{++}(t_4, t_2)}{v^{+}(t_2)} f_{T_1}(t_2) + \frac{1}{2} h \frac{v^{++}(t_4, t_1)}{v^{+}(t_1)} f_{T_1}(t_1) \\ \quad \vdots \qquad\qquad\qquad\qquad \vdots \\ v^{+}(t_{p+1}) \approx (1 + \frac{h}{2}) f_{T_1}(t_{p+1}) + h \sum_{i=2}^{p} \frac{v^{++}(t_{p+1}, t_i)}{v^{+}(t_i)} f_{T_1}(t_i) + \frac{1}{2} h \frac{v^{++}(t_{p+1}, t_1)}{v^{+}(t_1)} f_{T_1}(t_1) \end{cases} \tag{17}$$

Eq. (17) forms a matrix given by

$$\begin{bmatrix} v^{+}(t_1) \\ v^{+}(t_2) \\ \vdots \\ v^{+}(t_{p+1}) \end{bmatrix} = \begin{bmatrix} 1 & 0 & 0 & 0 \\ \dfrac{h v^{++}(t_2, t_1)}{2 v^{+}(t_1)} & 1 + \dfrac{h}{2} & 0 & 0 \\ \vdots & \vdots & \ddots & 0 \\ \dfrac{h v^{++}(t_{p+1}, t_1)}{2 v^{+}(t_1)} & \dfrac{h v^{++}(t_{p+1}, t_2)}{v^{+}(t_2)} & \cdots & 1 + \dfrac{h}{2} \end{bmatrix} \begin{bmatrix} f_{T_1}(t_1) \\ f_{T_1}(t_2) \\ \vdots \\ f_{T_1}(t_{p+1}) \end{bmatrix} \tag{18}$$

The discretized $f_{T_1}(t)$ is then be solved by the following equation:

$$\begin{bmatrix} f_{T_1}(t_1) \\ f_{T_1}(t_2) \\ \vdots \\ f_{T_1}(t_{p+1}) \end{bmatrix} = \begin{bmatrix} 1 & 0 & 0 & 0 \\ \dfrac{hv^{++}(t_2,t_1)}{2v^{+}(t_1)} & 1+\dfrac{h}{2} & 0 & 0 \\ \vdots & \vdots & \ddots & 0 \\ \dfrac{hv^{++}(t_{p+1},t_1)}{2v^{+}(t_1)} & \dfrac{hv^{++}(t_{p+1},t_2)}{v^{+}(t_2)} & \cdots & 1+\dfrac{h}{2} \end{bmatrix}^{-1} \begin{bmatrix} v^{+}(t_1) \\ v^{+}(t_2) \\ \vdots \\ v^{+}(t_{p+1}) \end{bmatrix} \tag{19}$$

After $f_{T_1}(t)$ is solved numerically, $p_f(t_0, t_s)$ can be obtained with Eq. (12).

The above methodology is applicable for a single stochastic process. It is extended to a general limit-state function $D(t) = g(\mathbf{X}, \mathbf{Y}(t), t)$. As $D(t)$ can be converted into a Gaussian process at the MPP, the extension is possible. From Eq. (19), it can be found that the single upcrossing rate $v^{+}(t)$ and joint upcrossing rate $v^{++}(t, \tau)$ are the bases for solving $f_{T_1}(\tau)$, equations are first derived for these two rates by using FORM and Rice's formula. After that, it discusses how to obtain the time-dependent probability of failure based on these rates.

3.2. Single upcrossing rate $v^{+}(t)$

Recall that after the MPP is found, the general limit-state function $g(\mathbf{X}, \mathbf{Y}(t), t)$ becomes $W(\mathbf{U}(t), t)$, and the failure event is $W(\mathbf{U}(t), t) = \boldsymbol{\alpha}(t)\mathbf{U}(t)^T > \beta(t)$. According to the Rice's formula [26, 56], the single upcrossing rate $v^{+}(t)$ is given by

$$v^{+}(t) = \omega(t)\,\phi(\beta(t))\,\Psi\left(\dot{\beta}(t) / \omega(t)\right) \tag{20}$$

where $\omega(t)$ is the standard deviation of $\dot{W}(t)$, which is the time derivative process of $W(t)$. $\omega^2(t)$ is given in terms of the correlation function $\rho(t_1, t_2)$ of $W(t)$ as follows:

$$\omega^2(t) = \partial^2 \rho(t_1, t_2) / (\partial t_1 \partial t_2)\Big|_{t_1 = t_2 = t} \tag{21}$$

The finite difference method is used to estimate $\dot{\beta}(t)$. This means that the MPP search needs to be performed twice. Ref. [50] also uses the finite difference method but introduces additional random variables for the second MPP search. As will been seen, the method presented here does not introduce any extra random variables.

As mentioned above, $W(t) = \boldsymbol{\alpha}(t)\mathbf{U}(t)^T$, and from Eq. (8), it gives $\|\boldsymbol{\alpha}(t)\| = 1$. $W(t)$ is therefore a standard normal stochastic process, and its coefficient of correlation is given by

$$\rho(t_1, t_2) = \boldsymbol{\alpha}(t_1)\mathbf{C}(t_1, t_2)\boldsymbol{\alpha}(t_2)^T \tag{22}$$

where $\mathbf{C}(t_1, t_2)$ is the covariance matrix of $\mathbf{U}(t_1)$ and $\mathbf{U}(t_2)$.

Since $\mathbf{U}(t) = (\mathbf{U_X}, \mathbf{U_Y}(t))$ is a vector of standard normal random variables and stochastic processes, $\mathbf{C}(t_1, t_2)$ is given by:

$$\mathbf{C}(t_1, t_2) = \begin{bmatrix} \mathbf{I}_{n\times n} & 0 \\ 0 & \mathbf{C}^Y(t_1, t_2) \end{bmatrix} \tag{23}$$

where $\mathbf{I}_{n\times n}$ is an $n \times n$ identity matrix, which is the covariance matrix of the normalized random variables $\mathbf{U_X}$ from $\mathbf{X}$. The covariance matrix of the normalized stochastic processes $\mathbf{U_Y}(t)$ from $\mathbf{Y}(t)$ is given in terms of its correlation coefficients as

$$\mathbf{C}^Y(t_1, t_2) = \begin{bmatrix} C^{Y_1}(t_1,t_2) & 0 & \cdots & 0 \\ 0 & \ddots & \cdots & 0 \\ \vdots & \vdots & \ddots & \vdots \\ 0 & 0 & \cdots & C^{Y_m}(t_1,t_2) \end{bmatrix} = \begin{bmatrix} \rho^{Y_1} & 0 & \cdots & 0 \\ 0 & \ddots & \cdots & 0 \\ \vdots & \vdots & \ddots & \vdots \\ 0 & 0 & \cdots & \rho^{Y_m} \end{bmatrix} \tag{24}$$

where $C(\cdot, \cdot)$ standard for the covariance, $C^{Y_i}(t_1,t_2)$ is the covariance of the normalized stochastic process $U_{Y_i}(t)$ at time instants t_1 and t_2. $\rho^{Y_i}$is the corresponding correlation function of the normalized stochastic process $U_{Y_i}(t)$ at these two time instants and is given by

$$\rho^{Y_i} = \rho^{Y_i}(t_1,t_2) \tag{25}$$

Substituting Eq. (22) into Eq. (21) yields

$$\begin{aligned} \omega^2(t) &= \partial^2\rho(t_1, t_2) / (\partial t_1 \partial t_2)\big|_{t_1=t_2=t} \\ &= \dot{\boldsymbol{\alpha}}(t)\dot{\mathbf{C}}_2(t, t)\boldsymbol{\alpha}(t)^T + \dot{\boldsymbol{\alpha}}(t)\mathbf{C}(t, t)\dot{\boldsymbol{\alpha}}(t)^T \\ &\quad + \boldsymbol{\alpha}(t)\ddot{\mathbf{C}}_{12}(t, t)\boldsymbol{\alpha}(t)^T + \boldsymbol{\alpha}(t)\dot{\mathbf{C}}_1(t, t)\dot{\boldsymbol{\alpha}}(t)^T \end{aligned} \tag{26}$$

Since the MPP search is performed at two instants and Eq. (26) also needs two instants (t, t), equations are now derived for two general instants t_1 and t_2. For time derivatives, such as $\dot{\beta}(t)$, let $t_1 = t_1$, $t_2 = t_1 + \Delta t$, where Δt is a small step size.

Differentiating Eq. (23), it yields

$$\dot{\mathbf{C}}_1(t_1, t_2) = \partial \mathbf{C}(t_1, t_2) / \partial t_1 = \begin{bmatrix} \mathbf{0} & 0 \\ 0 & \dot{\mathbf{C}}_1^Y(t_1, t_2) \end{bmatrix} \tag{27}$$

$$\dot{\mathbf{C}}_2(t_1, t_2) = \partial \mathbf{C}(t_1, t_2) / \partial t_2 = \begin{bmatrix} \mathbf{0} & 0 \\ 0 & \dot{\mathbf{C}}_2^Y(t_1, t_2) \end{bmatrix} \tag{28}$$

and

$$\ddot{\mathbf{C}}_{12}(t_1, t_2) = \begin{pmatrix} \mathbf{0} & 0 \\ 0 & \ddot{\mathbf{C}}_{12}^Y(t_1, t_2) \end{pmatrix} \tag{29}$$

$\dot{\mathbf{C}}_1^Y(t_1, t_2)$, $\dot{\mathbf{C}}_2^Y(t_1, t_2)$, and $\ddot{\mathbf{C}}_{12}^Y(t_1, t_2)$ are given by

$$\dot{C}_1^{Y_i}(t_1, t_2) = \partial \rho^{Y_i}(t_1, t_2) / \partial t_1, \ \ i = 1, 2, \cdots, m \tag{30}$$

$$\dot{C}_2^{Y_i}(t_1, t_2) = \partial \rho^{Y_i}(t_1, t_2) / \partial t_2, \ \ i = 1, 2, \cdots, m \tag{31}$$

and

$$\ddot{C}_{12}^{Y_i}(t_1, t_2) = \partial^2 \rho^{Y_i}(t_1, t_2) / (\partial t_1 \partial t_2), \ \ i = 1, 2, \cdots, m \tag{32}$$

Specially, for a pair of the same time instant (t, t),

$$\rho^{Y_i}(t, t) = 1 \tag{33}$$

$$\mathbf{C}(t, t) = \mathbf{I}_{n \times m} \tag{34}$$

$$\partial \rho^{Y_i}(t, t) / \partial t_1 = C\left(\dot{W}(t), W(t)\right) = 0 \tag{35}$$

$$\dot{\mathbf{C}}_1(t, t) = \mathbf{O}_{n \times m} \tag{36}$$

$$\partial \rho^{Y_i}(t, t) / \partial t_2 = C\left(W(t), \dot{W}(t)\right) = 0 \tag{37}$$

and

$$\dot{\mathbf{C}}_2(t, t) = \mathbf{O}_{n \times m} \tag{38}$$

Therefore, Eq. (26) is rewritten as

$$\omega(t)^2 = \dot{\boldsymbol{\alpha}}(t)\dot{\boldsymbol{\alpha}}(t)^T + \boldsymbol{\alpha}(t)\ddot{\mathbf{C}}_{12}(t, t)\boldsymbol{\alpha}(t)^T \tag{39}$$

where $\ddot{\mathbf{C}}_{12}(t, t)$ is computed by substituting $(t_1, t_2)$with (t, t)in Eq. (29), $\dot{\boldsymbol{\alpha}}(t)$ and $\dot{\beta}(t)$are calculated by

$$\dot{\boldsymbol{\alpha}}(t) = (\boldsymbol{\alpha}(t+\Delta t) - \boldsymbol{\alpha}(t))/\Delta t \tag{40}$$

and

$$\dot{\beta}(t) = (\beta(t+\Delta t) - \beta(t))/\Delta t \tag{41}$$

All the equations are obtained for the single upcrossing rate $\nu^{+}(t)$ in Eq. (20).

3.3. Joint upcrossing rate $\nu^{++}(t_1, t_2)$

Now the joint upcrossing rate $\nu^{++}(t_1, t_2)$ is derived between two arbitrary time instants t_1 and t_2. The joint upcrossing rate $\nu^{++}(t_1, t_2)$, which indicates the joint probability that outcrossing events occur at both t_1 and t_2, is defined by the Rice's formula as follows [26, 56] :

$$\nu^{++}(t_1, t_2) = \int_{\dot{\beta}_1}^{\infty}\int_{\dot{\beta}_2}^{\infty} f_{\dot{\mathbf{W}}\mathbf{W}}(\mathbf{Z}, \boldsymbol{\beta})(z_1 - \dot{\beta}_1)(z_2 - \dot{\beta}_2)dz_1 dz_2 \tag{42}$$

where $f_{\dot{\mathbf{W}}\mathbf{W}}(\dot{\mathbf{W}}, \mathbf{W})$ is the joint normal density function of $\dot{\mathbf{W}} = (\dot{W}(t_1), \dot{W}(t_2))$, and $\mathbf{W} = (W(t_1), W(t_2))$, $\boldsymbol{\beta} = (\beta_1, \beta_2)$, $\beta_1 = \beta(t_1)$, and $\beta_2 = \beta(t_2)$. The covariance matrix of $\dot{\mathbf{W}}$ and $\mathbf{W}$ is given by [48]

$$\mathbf{c} = \begin{bmatrix} \mathbf{c}_{\dot{\mathbf{W}}\dot{\mathbf{W}}} & \mathbf{c}_{\dot{\mathbf{W}}\mathbf{W}} \\ \mathbf{c}_{\mathbf{W}\dot{\mathbf{W}}} & \mathbf{c}_{\mathbf{W}\mathbf{W}} \end{bmatrix} = \begin{bmatrix} \omega^2(t_1) & \rho_{12} & 0 & \rho_1 \\ \rho_{21} & \omega^2(t_2) & \rho_2 & 0 \\ 0 & \rho_2 & 1 & \rho \\ \rho_1 & 0 & \rho & 1 \end{bmatrix} \tag{43}$$

in which

$$\rho = \rho(t_1, t_2) \tag{44}$$

$$\rho_1 = \partial\rho(t_1, t_2)/\partial t_1 \tag{45}$$

$$\rho_2 = \partial\rho(t_1, t_2)/\partial t_2 \tag{46}$$

$$\rho_{12} = \partial^2\rho(t_1, t_2)/(\partial t_1 \partial t_2) \tag{47}$$

and

$$\rho_{21} = \partial^2\rho(t_1, t_2)/(\partial t_2 \partial t_1) \tag{48}$$

Substituting Eq. (22) into Eqs. (45)-(48) yields

$$\rho_1 = \dot{\boldsymbol{\alpha}}(t_1)\mathbf{C}(t_1, t_2)\boldsymbol{\alpha}(t_2)^T + \boldsymbol{\alpha}(t_1)\dot{\mathbf{C}}_1(t_1, t_2)\boldsymbol{\alpha}(t_2)^T \tag{49}$$

$$\rho_2 = \boldsymbol{\alpha}(t_1)\mathbf{C}(t_1,t_2)\dot{\boldsymbol{\alpha}}(t_2)^T + \boldsymbol{\alpha}(t_1)\dot{\mathbf{C}}_2(t_1,t_2)\boldsymbol{\alpha}(t_2)^T \tag{50}$$

$$\begin{aligned}\rho_{12} &= \dot{\boldsymbol{\alpha}}(t_1)\dot{\mathbf{C}}_2(t_1,t_2)\boldsymbol{\alpha}(t_2)^T + \dot{\boldsymbol{\alpha}}(t_1)\mathbf{C}(t_1,t_2)\dot{\boldsymbol{\alpha}}(t_2)^T \\ &+\boldsymbol{\alpha}(t_1)\ddot{\mathbf{C}}_{12}(t_1,t_2)\boldsymbol{\alpha}(t_2)^T + \boldsymbol{\alpha}(t_1)\dot{\mathbf{C}}_1(t_1,t_2)\dot{\boldsymbol{\alpha}}(t_2)^T\end{aligned} \tag{51}$$

and

$$\begin{aligned}\rho_{21} &= \dot{\boldsymbol{\alpha}}(t_1)\mathbf{C}(t_1,t_2)\dot{\boldsymbol{\alpha}}(t_2)^T + \boldsymbol{\alpha}(t_1)\dot{\mathbf{C}}_1(t_1,t_2)\dot{\boldsymbol{\alpha}}(t_2)^T \\ &+\boldsymbol{\alpha}(t_1)\ddot{\mathbf{C}}_{21}(t_1,t_2)\boldsymbol{\alpha}(t_2)^T + \dot{\boldsymbol{\alpha}}(t_1)\dot{\mathbf{C}}_2(t_1,t_2)\boldsymbol{\alpha}(t_2)^T\end{aligned} \tag{52}$$

in which

$$\ddot{\mathbf{C}}_{21}(t_1,t_2) = \begin{pmatrix} \mathbf{0} & 0 \\ 0 & \ddot{C}_{21}^{Y}(t_1,t_2) \end{pmatrix} \tag{53}$$

and

$$\ddot{C}_{21}^{Y_i}(t_1,t_2) = \partial^2 \rho^{Y_i}(t_1,t_2)/(\partial t_1 \partial t_2),\ i = 1, 2, \cdots, m \tag{54}$$

$\mathbf{C}(t_1,t_2)$, $\dot{\mathbf{C}}_1(t_1,t_2)$, $\dot{\mathbf{C}}_2(t_1,t_2)$, and $\ddot{\mathbf{C}}_{12}(t_1,t_2)$ in Eqs. (49)-(52) are computed using Eqs. (23), and (27) through (29).

With the above equations derived, the equations in [48] can now be used directly to calculate $v^{++}(t_1,t_2)$. The equations are summarized blow.

$$\begin{aligned}v^{++}(t_1,t_2) &= \lambda_1\lambda_2 f_{\mathbf{W}}(\boldsymbol{\beta})\Psi\left((\dot{\beta}_1-\mu_1)/\lambda_1\right)\Psi\left((\dot{\beta}_2-\mu_2)/\lambda_2\right) \\ &+\lambda_1\lambda_2 f_{\mathbf{W}}(\boldsymbol{\beta})\kappa\Phi\left((\mu_1-\dot{\beta}_1)/\lambda_1\right)\Phi\left((\mu_2-\dot{\beta}_2)/\lambda_2\right) \\ &+\lambda_1^2\lambda_2^2 f_{\mathbf{W}}(\boldsymbol{\beta})\int_0^{\kappa}(\kappa-K)\, f_{\dot{\mathbf{W}}|\mathbf{W}}\left(\dot{\boldsymbol{\beta}}\,|\,\boldsymbol{\beta};K\right)dK\end{aligned} \tag{55}$$

in which

$$f_{\mathbf{W}}(\boldsymbol{\beta}) = (\exp((\beta_1^2 - 2\rho\beta_1\beta_2 + \beta_2^2)/(2-2\rho^2)))/(2\pi\sqrt{1-\rho^2}) \tag{56}$$

μ_1 and μ_2, λ_1 and λ_2, κ are the mean values, standard deviations, and correlation coefficient of $\dot{W}(t_1)\big|\boldsymbol{\beta}$ and $\dot{W}(t_2)\big|\boldsymbol{\beta}$, respectively. They are calculated by substituting the covariance matrix in Eq. (43) into the following equations

$$\boldsymbol{\mu} = \begin{bmatrix}\mu_1 \\ \mu_2\end{bmatrix} = \mathbf{c}_{\dot{\mathbf{W}}\mathbf{W}}\mathbf{c}_{\mathbf{W}\mathbf{W}}^{-1}\boldsymbol{\beta} = \begin{bmatrix}(\beta_2-\rho\beta_1)\rho_1 \\ (\beta_1-\rho\beta_2)\rho_2\end{bmatrix}/(1-\rho^2) \tag{57}$$

$$\sum = \mathbf{c}_{\dot{\mathbf{W}}|\mathbf{W}} = \mathbf{c}_{\dot{\mathbf{W}}\dot{\mathbf{W}}} - \mathbf{c}_{\dot{\mathbf{W}}\mathbf{W}}\mathbf{c}_{\mathbf{W}\mathbf{W}}^{-1}\mathbf{c}_{\mathbf{W}\dot{\mathbf{W}}} = \begin{bmatrix}\lambda_1^2 & \kappa\lambda_1\lambda_2 \\ \kappa\lambda_1\lambda_2 & \lambda_2^2\end{bmatrix} \tag{58}$$

After the derivation of $v^{+}(t)$ and $v^{++}(t_1,t_2)$, $p_f(t_0, t_s)$ is computed with Eqs. (12), (19), (20), and (55).

3.4. Numerical implementation

There are many equations involved in JUR/FORM. In this section, its numerical implementation is summarized. From Eq. (11) and (12), it is known that to obtain $p_f(t_0, t_s)$, the PDF $f_{T_1}(t)$ needs to be integrated over $[t_0,t_s]$ numerically. At each of the integration point between t_0 and t_s, the integral equation in Eq. (14) should be solved. To maintain good efficiency, the following numerical procedure is proposed.

It starts to evaluate the PDF at the last instant t_s. To do so, the time interval $[t_0,t_s]$ is discretized into $p+1$ instants t_i $(i=0,1,2,\cdots,p)$, at each of which the integral equation in Eq. (14) for $f_{T_1}(t_s)$ will be solved. The PDFs at all these instants are then obtained. Thus the total number of the MPP will be $2(p+1)$. This procedure is summarized below, and the associated flowchart is given in Fig. 1.

- Step 1: Initialize the random variables and stochastic processes, including transforming non-Gaussian variables into Gaussian ones, discretizing the time interval $[t_0, t_s]$ into $p+1$ time instants $t_0, t_1, \cdots, t_i, \cdots, t_{p+1}=t_s$, and setting a time step Δt for the MPP search at $t_i+\Delta t$ $(i=1,2,\cdots,p+1)$.
- Step 2: Perform the MPP search at every discretized point t_i, as well as at $t_i+\Delta t$; calculate $\boldsymbol{\alpha}(t_i)$, $\boldsymbol{\beta}(t_i)$, $\dot{\boldsymbol{\alpha}}(t_i)$, $\dot{\boldsymbol{\beta}}(t_i)$, covariance matrix $\mathbf{C}(t_i,t_j)$ $(i,\ j=1,2,\cdots,p+1)$, and $\mathbf{c}$ by using Eqs. (23), (40), (41) and (43)-(54).
- Step 3: Solve for the single upcrossing rate $v^{+}(t_i)$ using Eq. (20), joint upcrossing rate $v^{++}(t_i,t_j)$ $(i,\ j=1,2,\cdots,p+1)$ using Eq. (55), and compute the PDF $f_{T_1}(t_i)$ at each time instant using Eq. (19).
- Step 4: Calculate $p_f(t_0, t_s)$.

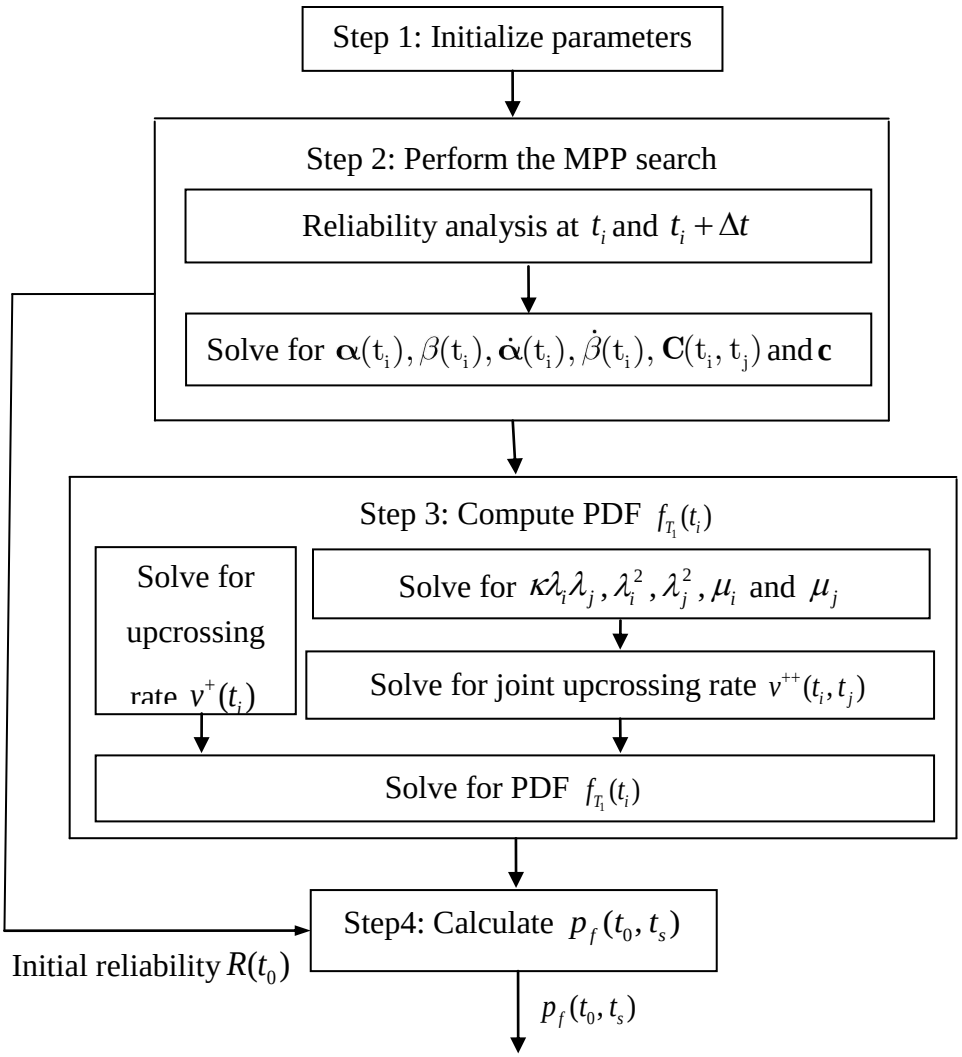

Fig. 1 Flowchart of the JUR/FORM

4. Numerical Examples

In this section, two examples are used to demonstrate the developed methodology. The first one is the reliability analysis of a corroded beam under time-variant random loading, and the second one is the reliability analysis of a two-slider crank mechanism. The two examples are selected because they represent two kinds of important applications. Specifically, the first example involves both of a stochastic process and random variables in the input of the limit-state function. The stochastic process is the time-variant random load acting on the beam. In the second example, there are no

stochastic processes in the input of the limit-state function. But the limit-state function is still time-dependent because it is an explicit function of time.

To show the accuracy improvement of JUR/FORM, its results are compared with those of the traditional Poisson assumption based single upcrossing rate method, which has been reviewed in Sec II. Because the exact solutions are not available, the Monte Carlo Simulation (MCS) is used as a benchmark.

In order to investigate the effects of parameter settings on the accuracy of JUR/FORM, numerical studies were also performed for Example 1. The effects studied include the effects of number of discretization points for the time interval $[t_0, t_s]$, the time step size Δt, the level of probability of failure, and the dependency of the limit-state function between two successive time instants.

Next the MCS is briefly reviewed.

4.1. Monte Carlo Simulation

When there are stochastic processes involved in the limit-state function, to generate the samples of the stochastic process Y_i, the stochastic process is treated as correlated random variables $\mathbf{Y}_i = (Y_i(t_1), Y_i(t_2), \cdots, Y_i(t_N))^T$ after discretizing the time interval $[t_0, t_s]$ into N instants. For a Gaussian stochastic process, the correlated random variables $\mathbf{Y}_i$ are generated after transforming the correlated random variables into uncorrelated ones as follows [57]

$$\mathbf{Y}_i = \boldsymbol{\mu}_{y_i} + \mathbf{L}\boldsymbol{\xi} \tag{59}$$

where $\boldsymbol{\xi} = (\xi_1, \xi_2, \cdots, \xi_N)^T$ is the vector of N independent standard normal random variables; $\boldsymbol{\mu}_{Y_i} = (\mu_{Y_i}(t_1), \mu_{Y_i}(t_2), \cdots, \mu_{Y_i}(t_N))^T$ are the vector of mean values of $\mathbf{Y}_i = (Y_i(t_1), Y_i(t_2), \cdots, Y_i(t_N))^T$; and $\mathbf{L}$ is a lower triangular matrix obtained from the covariance matrix of $\mathbf{Y}_i$.

Let matrix $\mathbf{A}_{N\times N}$ be the covariance matrix of $\mathbf{Y}_i$. $\mathbf{L}$ can be obtained by

$$\mathbf{A}_{N\times N} = \mathbf{P}\mathbf{D}\mathbf{P}^{-1} = \mathbf{L}\mathbf{L}^T \tag{60}$$

in which $\mathbf{D}$ is a diagonal eigenvalue matrix of the covariance matrix $\mathbf{A}$, and $\mathbf{P}$ is the $N \times N$ square matrix whose i-th column is the i-th eigenvector of $\mathbf{A}$.

4.2. Example 1: Corroded beam under time-variant random loading

4.2.1. Problem statement

The beam problem in [50] is modified as the first example. As shown in Fig. 2, the cross section A-A of the beam is rectangular with its initial width a_0 and height b_0. Due to corrosion, the width and height of the beam decrease at a rate of r. A random load F acts at the midpoint of the beam. The beam is also subjected to a constant load due to the weight of the steel beam.

A failure occurs as the stress of the beam exceeds the ultimate stress of the material, and the limit-state function is given by

$$g(\mathbf{X}, \mathbf{Y}, t) = \left(F(t)L/4 + \rho_{st} a_0 b_0 L^2/8\right) - \left(a_0 - 2rt\right)\left(b_0 - 2rt\right)\sigma_u/4 \qquad (61)$$

where σ_u is the ultimate strength, ρ_{st} is the density, and L is the length of the beam.

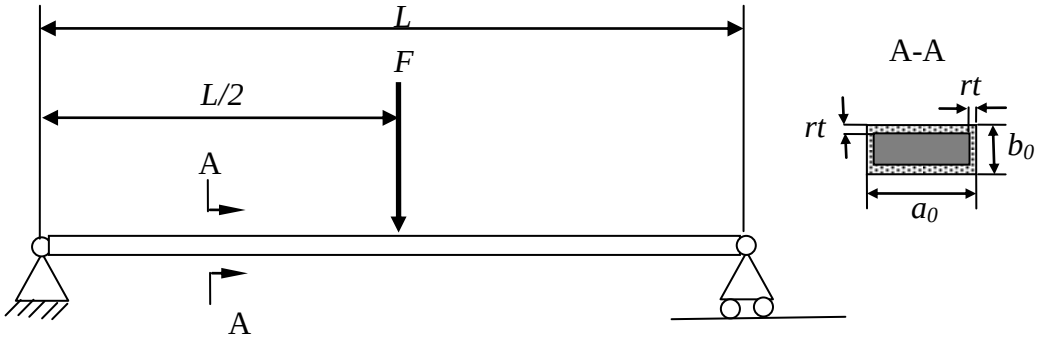

Fig. 2 Corroded beam under time-variant random loading

The variables and parameters in Eq. (61) are provided in Table 1.

Table 1 Variables and parameters of Example 1

Variable	Mean	Standard deviation	Distribution	Autocorrelation
a_0	0.2 m	0.01 m	Lognormal	N/A
b_0	0.04 m	4×10^{-3} m	Lognormal	N/A
σ_u	2.4×10^{8} Pa	2.4×10^{7} Pa	Lognormal	N/A
$F(t)$	3500 N	700 N	Gaussian	In Eq. (63)
L	5 m	0	Deterministic	N/A
ρ_{st}	78.5 kN/m^3	0	Deterministic	N/A
r	5×10^{-5} m/year	0	Deterministic	N/A

The covariance function of $F(t)$ is given by

$$C^F(t_1, t_2) = \rho^F(t_1, t_2)\sigma^F(t_1)\sigma^F(t_2) \tag{62}$$

where

$$\rho^F(t_1, t_2) = \exp(-((t_2 - t_1)/\zeta)^2) \tag{63}$$

where $\zeta = 1$ year is the correlation length. The auto-correlation becomes weaker with a longer time interval $t_2 - t_1$, $\sigma^F(t_1) = \sigma^F(t_2) = 700\ N$ is the standard deviation of $F(t)$ at time instants t_1 and t_2.

Since $F(t)$ is a Gaussian stationary stochastic process, it has

$$\rho_{U_F}(t_1, t_2) = \rho^F(t_1, t_2) \tag{64}$$

in which $\rho_{U_F}(t_1, t_2)$ is the auto-correlation function of the underlying Gaussian standard stochastic process $U_F(t)$.

4.2.2. Results

Following the numerical procedure of JUR/FORM in Fig.1, the time-dependent probabilities of failure over different time intervals up to [0, 30] years were computed. The time intervals were discretized into 80 small intervals, and the time size for the second MPP search was taken as 0.001 years. To eliminate the accuracy difference caused by different numerical integration methods, for the traditional method, the same integration method was used as the proposed method to eliminate the accuracy difference caused by different numerical integration methods; namely, the time interval was discretized into 80 small intervals and then used the rectangle integration method to calculate the integral in Eq. (6). For MCS, the evaluated time intervals were discretized into 600 time instants with a sample size of 2×10^6 at each time instant to generate the stochastic loading $F(t)$. The results of the three methods are plotted in Fig. 3 and are given in Table 2. The relative errors, ε, with respect to the MCS solutions, and the confidence intervals (CI) of the MCS solutions, are also given in Table 2.

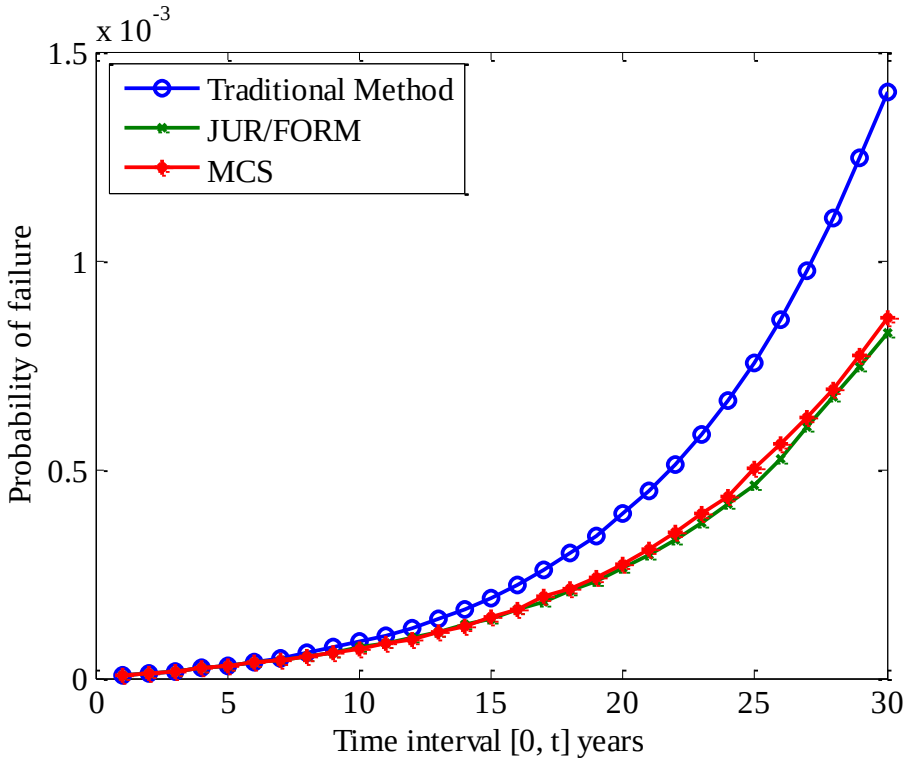

Fig. 3 Probability of failure of the beam over different time intervals

Table 2 Time-dependent probabilities of failure

TI	Traditional		JUR/FORM		MCS	
	p_f	ε (%)	p_f	ε (%)	p_f	95% CI
[0, 5]	0.309×10^{-4}	6.55	0.292×10^{-4}	0.69	0.29×10^{-4}	$[0.215\times10^{-4}, 0.365\times10^{-4}]$
[0, 10]	0.864×10^{-4}	25.22	0.727×10^{-4}	5.36	0.69×10^{-4}	$[0.575\times10^{-4}, 0.805\times10^{-4}]$
[0, 15]	1.930×10^{-4}	31.29	1.450×10^{-4}	1.36	1.47×10^{-4}	$[1.302\times10^{-4}, 1.638\times10^{-4}]$
[0, 20]	3.924×10^{-4}	44.80	2.669×10^{-4}	1.51	2.71×10^{-4}	$[2.482\times10^{-4}, 2.938\times10^{-4}]$
[0, 25]	7.553×10^{-4}	50.76	4.706×10^{-4}	6.07	5.01×10^{-4}	$[4.700\times10^{-4}, 5.320\times10^{-4}]$
[0, 30]	14.027×10^{-4}	62.73	8.393×10^{-4}	2.63	8.62×10^{-4}	$[8.213\times10^{-4}, 9.027\times10^{-4}]$

- "TI" stands for time interval

The results indicate that the proposed JUR/FORM method is much more accurate than the traditional method. The traditional method leads to unacceptable errors while JUR/FORM shows excellent agreement with the MCS solution

Table 3 gives the numbers of function calls, N_{func}, as measures of efficiency. The number of function calls is defined as the times that the limit-state function is evaluated

with the inputs of $\mathbf{x}, \mathbf{y}(t_i)$ and t_i. The actual computational cost (times) is also given. The computational times were based on a Dell computer with Intel (R) Core (TM) i5-2400 CPU and 8GB system memory.

Table 3 Number of function calls and computational times

Time interval	Traditional Method		JUR/FORM		MCS	
	Time (s)	N_{func}	Time (s)	N_{func}	Time (s)	N_{func}
[0, 5]	4.85	5495	6.19	5560	127.66	2×10^8
[0, 10]	4.59	5220	6.16	5280	1.29×10^3	4×10^8
[0, 15]	4.55	5115	6.27	5175	2.08×10^3	6×10^8
[0, 20]	4.55	5135	6.26	5195	2.70×10^3	8×10^8
[0, 25]	4.43	5070	6.23	5125	4.19×10^3	10×10^8
[0, 30]	4.36	4955	6.17	5005	4.51×10^3	12×10^8

With the same integration method, the results show that the accuracy improvement from JUR/FORM indeed comes from the consideration of the dependencies between upcrossing events. Table 3 also indicates that the numbers of function calls by both methods are almost the same. This is because of the use of the same integration method.

The traditional method, however, may need less number of function calls because other integration methods could be used. The cursive adaptive Lobatto quadrature method was also applied to the traditional method. The probabilities of failure obtained are identical to those given in Table 2, but with fewer numbers of function calls and less computational time as shown in Table 4. This means that the traditional method is more efficient than the proposed method for this example.

The results given in Tables 1 to 4 demonstrated that JUR/FORM produced much higher accuracy with a cost of increased computational effort, but the increased computational cost is moderate.

4.2.3. Numerical studies

(a) Effect of discretization and time step size

As shown in the numerical procedure, the time interval $[t_0, t_s]$ is discretized into $p+1$ time instants t_i $(i = 0,1,2,\cdots, p)$ or p small intervals. The number of discretization points may affect the accuracy of the analysis result. If the number is too small, the error will be large. On the contrary, if the number is too large, the error will be small but the efficiency will be low. To study the effect of the number of discretization points, the time interval [0, 30] years was discretized into 20, 30, 40, 50, 60, 70 and 80 small intervals.

Table 4 Number of function calls and computational times of traditional method using direct integration method

Time interval	[0, 5]	[0, 10]	[0, 15]	[0, 20]	[0, 25]	[0, 30]
Time (s)	1.07	1.04	1.02	1.03	0.99	2.61
N_{func}	1250	1170	1155	1165	1135	2965

Table 5 shows the results from JUR/FORM with different numbers of discretization points. When the time interval is divided into 20 small intervals, as expected, the error is the largest; however, the result is still more accurate than the traditional method. With the higher number of discretization points, the accuracy of JUR/FORM is higher.

Table 5 Time-dependent probability of failure with different discretization points

	MCS	Traditional Method	JUR/FORM with p small intervals						
			20	30	40	50	60	70	80
p_f (10^{-4})	8.6	14.027	7.83	7.98	8.09	8.13	8.21	8.24	8.25
ε (%)	N/A	62.73	9.16	7.42	6.15	5.68	4.76	4.41	4.33

In addition to the number of discretization, there is another parameter that may affect the performance of JUR/FORM. This parameter is the time-step size Δt, which is used for numerically evaluating the derivatives $\dot{\alpha}(t_i)$ and $\dot{\beta}(t_i)$ in Eqs. (40) and (41), respectively. $\Delta t = 0.0005, 0.001, 0.005$ and 0.01 were used to study its effect. Table 6 provides the results, which show that the time-step size does affect the accuracy, but the

effect is not significant. The general discussions regarding the effect of a step size for numerical derivatives can be also found in [48-50].

Table 6 Time-dependent probability of failure with different Δt

Method	MCS	Traditional Method	JUR/FORM with different Δt			
			5×10^{-4}	0.001	0.005	0.01
$p_f(10^{-4})$	8.62	14.03	8.41	8.25	8.0	7.98
ε (%)	N/A	62.73	2.47	4.33	7.16	7.40

(b) Effect of larger probability of failure

To investigate the accuracy of JUR/FORM when the probability of failure becomes larger, the results of MCS, JUR/FORM and traditional method were compared for six cases at different probability levels. Table 7 show that the larger is the probability of failure, the worse is the traditional method, while JUR/FORM is always much more accurate than the traditional method.

Table 7 Time-dependent probability of failure JUR/FORM at different probability levels

Traditional Method		JUR/FORM		MCS	
p_f	ε (%)	p_f	ε (%)	p_f	95% CI
14×10^{-4}	71.15	8.25×10^{-4}	0.86	8.18×10^{-4}	$[7.62\times10^{-4}, 8.74\times10^{-4}]$
19×10^{-4}	72.73	10×10^{-4}	9.09	11×10^{-4}	$[10.4\times10^{-4}, 11.6\times10^{-4}]$
95×10^{-4}	93.88	46×10^{-4}	6.12	49×10^{-4}	$[47.6\times10^{-4}, 50.4\times10^{-4}]$
176×10^{-4}	97.75	83×10^{-4}	6.74	89×10^{-4}	$[87.2\times10^{-4}, 90.8\times10^{-4}]$
1083×10^{-4}	127.52	444×10^{-4}	6.72	476×10^{-4}	$[472\times10^{-4}, 480\times10^{-4}]$
3101×10^{-4}	137.81	1246×10^{-4}	4.44	1304×10^{-4}	$[1297\times10^{-4}, 1311\times10^{-4}]$

(c) Effect of the auto-covariance of the limit-state function

JUR/FORM is developed to better account for dependent failures over a time period. To demonstrate this, the accuracy of JUR/FORM was analyzed for five cases with

different levels of dependency. In the five cases, the coefficients of auto-correlation ρ, ranging from 0.108 to 0.961, between two successive time instants $[t_i, t_{i+1}]$, $i = 1, 2, \cdots, 99$ over [0, 30] years. Note that the coefficient of auto-correlation of the limit-state function is almost constant given the auto-correlation function of the stochastic process for the external force in Eq. (62).

Table 8 shows that the error of the traditional method decreases when the dependency becomes weaker while the accuracy of JUR/FORM method is always better than the traditional effort.

Table 8 Time-dependent probability of failure with different dependencies

ρ	Traditional Method		JUR/FORM		MCS	
	p_f (10^{-4})	ε (%)	p_f (10^{-4})	ε (%)	p_f(10^{-4})	95% CI (10^{-4})
0.961	4.756	24.5	5.83	7.46	6.30	[5.81, 6.79]
0.914	6.952	23.18	8.52	5.86	9.05	[8.46, 9.64]
0.698	13.54	20.07	16.60	2.01	16.94	[16.13, 17.75]
0.368	22.32	17.27	27.36	1.41	26.98	[25.96, 28.00]
0.108	33.29	12.12	38.65	2.03	37.88	[36.68, 39.08]

4.3. Example 2: Two-slider crank mechanism

A two-slider crank mechanism is shown in Fig. 4. This type of mechanism is widely used in engines. The crank is rotating at an angular velocity of ω. The motion error is defined as the difference between the desired displacement difference and the actual displacement difference between sliders *A* and *B*. The error should not exceed 0.94 mm over one motion cycle.

The limit-state function is given by

$$g(\mathbf{X}, \mathbf{Y}, t) = \Delta s_{desired} - \Delta s_{actual} \tag{65}$$

in which

$$\Delta s_{actual} = R_1\cos(\theta-\theta_0)+\sqrt{R_2^2-R_1^2\sin^2(\theta-\theta_0)} - R_3\cos(\theta_1+\theta_0-\theta-\delta_0)-\sqrt{R_4^2-R_3^2\sin^2(\theta_1+\theta_0-\theta-\delta_0)} \tag{66}$$

$$\Delta s_{desired} = 108\cos(\theta-\theta_0)+\sqrt{211^2-108^2\sin^2(\theta-\theta_0)} -100\cos(\theta_1+\theta_0-\theta-\delta_0)-\sqrt{213^2-100^2\sin^2(\theta_1+\theta_0-\theta-\delta_0)} \tag{67}$$

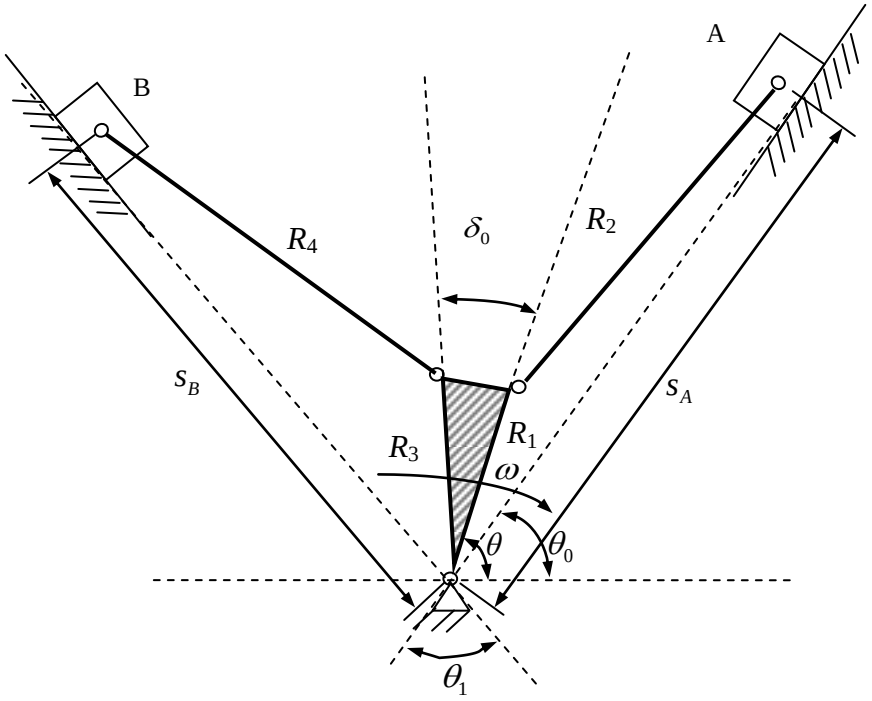

Fig. 4. Two-slider crank mechanism

The variables and parameters in the limit-state function are given in Table 9.

This mechanism problem is different from the beam problem in the follow two aspects. First, this problem does not involve any input stochastic processes, but the limit-state function is still a stochastic process because it is a function of time. Second, the dependence of the limit-state function at any two time instants is strong. The auto-dependence does not decay with a longer time period. On the contrary, in the first problem, the auto-dependency between the performance values at t_1 and t_2 will be weaker and weaker when $t_2 - t_1$ becomes larger and larger as indicated in Eq. (62).

The angular velocity of the crank is $\omega = \pi$ rad/s, and the time period of one motion cycle is then [0, 2] seconds**.** Following the numerical procedure of JUR/FORM,

the probabilities of failure were computed over different time intervals. Each of the evaluated time intervals were discretized into 60 smaller intervals. The step size for the second MPP search was 8×10^{-5} seconds. The traditional method and MCS with a sample size of 10^6 were also applied. The same integration method was used for both the traditional method and the proposed method to eliminate the accuracy difference caused by different numerical integration methods. The time interval was discretized into 60 small intervals and then used the rectangle integration method to calculate the integral in Eq. (6). The results from the three methods are plotted in Fig. 5 and are given in Table 10.

Table 9 Variables and parameters in Example 2

Variable	Mean	Standard deviation	Distribution
R_1	108 mm	0.05 mm	Normal
R_2	211 mm	0.2 mm	Normal
R_3	100 mm	0.05 mm	Normal
R_4	213 mm	0.2 mm	Normal
θ_0	45°	0	Deterministic
θ_1	60°	0	Deterministic
δ_0	10°	0	Deterministic
ω	π rad/s	0	Deterministic

Table 10 Time-dependent probabilities of failure

Time interval	Traditional		JUR/FORM		MCS	
	p_f (10^{-3})	ε (%)	p_f (10^{-3})	ε (%)	p_f (10^{-3})	95% CI (10^{-3})
[0, 0.4]	1.76	22.03	1.51	4.27	1.45	[1.37, 1.52]
[0, 0.8]	3.06	53.84	1.97	1.01	1.99	[1.90, 2.08]
[0, 1.2]	3.92	81.48	2.16	0.17	2.16	[2.07[3], 2.25]
[0, 1.6]	4.67	112.27	2.31	4.92	2.20	[2.10, 2.29]
[0, 2.0]	6.01	161.30	2.33	1.14	2.30	[2.20, 2.39]

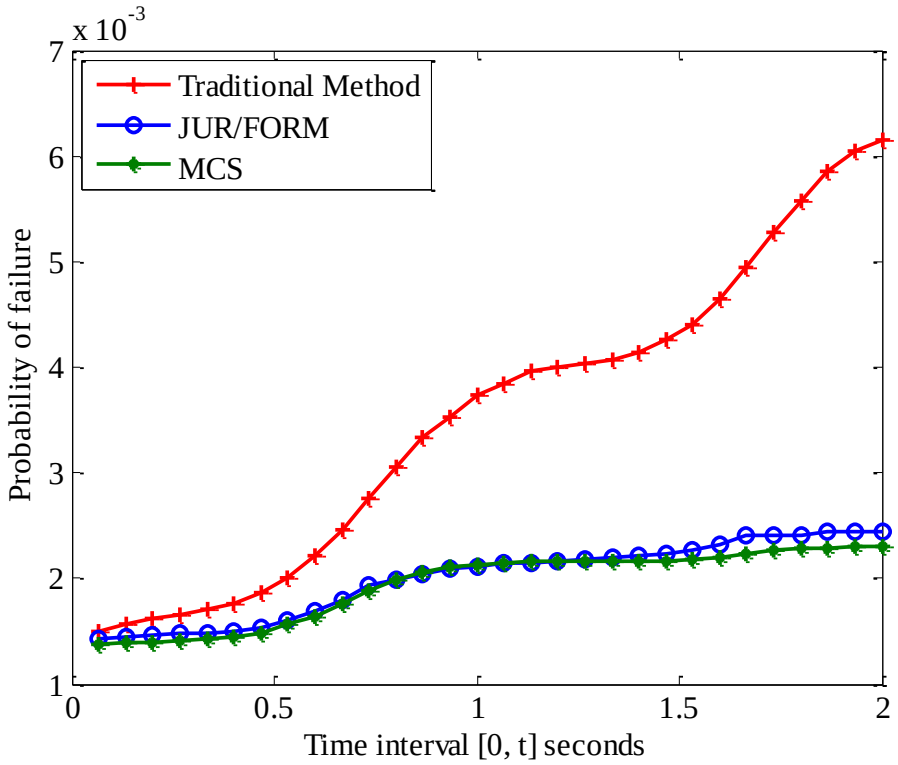

Fig. 5. Time-dependent probabilities of failure

The results indicate that JUR/FORM is significantly more accurate than the traditional method. With the same integration method, Table 10 indicates that the accuracy improvement is indeed due to the consideration dependent upcrossings by JUR/FORM.

The number of function calls and the computational time are given in Table 11, which shows that the proposed method is almost as efficient as the traditional method.

As what has been done in Example 1, Eq. (6) was also solved using the direct cursive adaptive Lobatto quadrature method. The probabilities of failure obtained are almost identical to those in Table 10. Contrary to Example 1, The efficiency of the traditional method, however, varies for different time periods as shown in Table 12.

The results show that the increased computational cost by JUR/FORM is reasonable given its significantly improved accuracy.

5. Conclusion

Time-dependent reliability analysis is needed in many engineering applications. When multiple dependent upcrossings occur over a time interval, the single upcrossing rate method with Poisson assumption may produce large errors in estimating the time-dependent probability of failure.

This work demonstrates that the joint upcrossing rates proposed in [48] can be extended to a general time-dependent limit-state function with much higher accuracy. This work integrates the FORM with the joint upcrossing rates so that high computational efficiency can be maintained. Analytical expressions of the single and joint upcrossing rates are also derived based on FORM.

Table 11 Number of function calls and MPP searches

Time interval	Traditional		JUR/FORM		MCS	
	MPP searches	Function Calls	MPP searches	Function Calls	MPP searches	Function Calls
[0, 0.4]	122	2394	122	2452	N/A	6×10^{7}
[0, 0.8]	122	2398	122	2455	N/A	1.2×10^{8}
[0, 1.2]	122	2394	122	2437	N/A	1.8×10^{8}
[0, 1.6]	122	2400	122	2451	N/A	2.4×10^{8}
[0, 2.0]	122	2391	122	2437	N/A	3.0×10^{8}

Table 12 Number of function calls of traditional method using direct integration method

Time interval	[0, 0.4]	[0, 0.8]	[0, 1.2]	[0, 1.6]	[0, 2.0]
N_{func}	1927	720	4320	3140	16531

The proposed method has shown good accuracy when the probability of failure is small and the dependency between failures is strong. When the probability of failure becomes larger or the dependency becomes weaker, the proposed method remains more accurate than the traditional upcrossing rate method. Since the proposed method requires

a numerical method in solving the integral equation and derivatives, its accuracy may be affected by the number of discretization points and the time size between two consecutive MPP searches. The proposed method can be used for general stochastic processes, including non-Gaussian non-stationary processes. To do this, a general stochastic process at first needs to be transformed into a standard Gaussian process. The transformation should make not only the CDF functions but also the auto-covaraince functions be equal to each other before and after the transformation.

Possible future work includes improving the efficiency and robustness of the method and applying it to time-dependent reliability-based design optimization.

Acknowledgement

The authors gratefully acknowledge the support from the Office of Naval Research through contract ONR N000141010923 (Program Manager – Dr. Michele Anderson), the National Science Foundation through grant CMMI 1234855, and the Intelligent Systems Center at the Missouri University of Science and Technology.

Reference

[1] Choi, S. K., Grandhi, R. V., and Canfield, R. A., 2007, Reliability-based structural design, Springer.

[2] Du, X., Sudjianto, A., and Huang, B., 2005, "Reliability-based design with the mixture of random and interval variables," Journal of Mechanical Design, Transactions of the ASME, 127(6), pp. 1068-1076.

[3] Huang, B., and Du, X., 2008, "Probabilistic uncertainty analysis by mean-value first order Saddlepoint Approximation," Reliability Engineering and System Safety, 93(2), pp. 325-336.

[4] Zhang, J., and Du, X., 2010, "A second-order reliability method with first-order efficiency," Journal of Mechanical Design, Transactions of the ASME, 132(10).

[5] Madsen, H. O., Krenk, S., Lind, N.C., 1986, Methods of Structural Safety, Englewood Cliffs, New Jersey.

[6] Banerjee, B., and Smith, B. G., 2011, "Reliability analysis for inserts in sandwich composites," pp. 234-238.

[7] Kim, D. W., Jung, S. S., Sung, Y. H., and Kim, D. H., 2011, "Optimization of SMES windings utilizing the first-order reliability method," Transactions of the Korean Institute of Electrical Engineers, 60(7), pp. 1354-1359.

[8] Millwater, H., and Feng, Y., 2011, "Probabilistic sensitivity analysis with respect to bounds of truncated distributions," Journal of Mechanical Design, Transactions of the ASME, 133(6).

[9] Miller, R. A., 1997, "Thermal barrier coatings for aircraft engines: History and directions," Journal of Thermal Spray Technology, 6(1), pp. 35-42.

[10] Dubowsky, S., Norris, M., Aloni, E., and Tamir, A., 1984, "Analytical and experimental study of the prediction of impacts in planar mechnical systems with clearances," Journal of mechanisms, transmissions, and automation in design, 106(4), pp. 444-451.

[11] Dupac, M., and Beale, D. G., 2010, "Dynamic analysis of a flexible linkage mechanism with cracks and clearance," Mechanism and Machine Theory, 45(12), pp. 1909-1923.

[12] Tsai, M. J., and Lai, T. H., 2008, "Accuracy analysis of a multi-loop linkage with joint clearances," Mechanism and Machine Theory, 43(9), pp. 1141-1157.

[13] Meng, J., and Li, Z., "A general approach for accuracy analysis of parallel manipulators with joint clearance," pp. 790-795.

[14] Szkodny, T., 2001, "The sensitivities of industrial robot manipulators to errors of motion models' parameters," Mechanism and Machine Theory, 36(6), pp. 673-682.

[15] Nielsen, U. D., 2010, "Calculation of mean outcrossing rates of non-Gaussian processes with stochastic input parameters - Reliability of containers stowed on ships in severe sea," Probabilistic Engineering Mechanics, 25(2), pp. 206-217.

[16] Kuschel, N., and Rackwitz, R., 2000, "Optimal design under time-variant reliability constraints," Structural Safety, 22(2), pp. 113-127.

[17] Ditlevsen, O., 2002, "Stochastic model for joint wave and wind loads on offshore structures," Structural Safety, 24(2-4), pp. 139-163.

[18] Rice, J. R., Beer, F.P.,, 1965, "First-Occurrence Time of Hih-Level Crossings in a Continuous Random Process," The Journal of Acoustical Society of America, 39(2), pp. 323-335.

[19] Richard, V. F., Mircea, D.G., 2006, " Reliability of Dynamic Systems Under Limited Information."

[20] Song, J., and Der Kiureghian, A., 2006, "Joint first-passage probability and reliability of systems under stochastic excitation," Journal of Engineering Mechanics, 132(1), pp. 65-77.

[21] Chen, J. B., and Li, J., 2008, "The inherent correlation of the structural response and reliability evaluation," Jisuan Lixue Xuebao/Chinese Journal of Computational Mechanics, 25(4), pp. 521-528.

[22] Li, J., Chen, J. b., and Fan, W. l., 2007, "The equivalent extreme-value event and evaluation of the structural system reliability," Structural Safety, 29(2), pp. 112-131.

[23] Chen, J. B., and Li, J., 2007, "The extreme value distribution and dynamic reliability analysis of nonlinear structures with uncertain parameters," Structural Safety, 29(2), pp. 77-93.

[24] Wang, Z., and Wang, P., 2012, "A nested extreme response surface approach for time-dependent reliability-based design optimization," Journal of Mechanical Design, Transactions of the ASME, 134(12), pp. 12100701-12100714.

[25] Hu, Z., and Du, X., 2013, "A Sampling Approach to Extreme Value Distribution for Time-Dependent Reliability Analysis," Journal of Mechanical Design, Transactions of the ASME, DOI: 10.1115/1.4023925.

[26] Rice, S. O., 1944, "Mathematical Analysis of Random Noise," Bell System Technical Journal, , 23, pp. 282–332.

[27] Rui, V. d. M. P., 1985, "The Theory of Statistics of Extremes and EL NINO Phenomena-A Stochastic Approach," Massachusetts Institute of Technology, Boston.

[28] Schall, G., Faber, M. H., and Rackwitz, R., 1991, "Ergodicity assumption for sea states in the reliability estimation of offshore structures," Journal of Offshore Mechanics and Arctic Engineering, 113(3), pp. 241-246.

[29] Engelund, S., Rackwitz, R., and Lange, C., 1995, "Approximations of first-passage times for differentiable processes based on higher-order threshold crossings," Probabilistic Engineering Mechanics, 10(1), pp. 53-60.

[30] Rackwitz, R., 1998, "Computational techniques in stationary and non-stationary load combination - A review and some extensions," Journal of Structural Engineering (Madras), 25(1), pp. 1-20.

[31] Lutes, L. D., and Sarkani, S., , 2004, Random Vibrations: Analysis of Structural and Mechanical Systems, Elsevier, New York.

[32] Lutes, L. D., and Sarkani, S., , 2009, "Reliability Analysis of Systems Subject to First-Passage Failure."

[33] Sudret, B., 2008, "Analytical derivation of the outcrossing rate in time-variant reliability problems," Structure and Infrastructure Engineering, 4(5), pp. 353-362.

[34] Zhang, J., and Du, X., 2011, "Time-dependent reliability analysis for function generator mechanisms," Journal of Mechanical Design, Transactions of the ASME, 133(3).

[35] Lin, Y. K., 1967, Probabilistic Theory of Structural Dynamics., McGraw-HilI, New York.

[36] Cramer, H., 1966, "On the intersections between the trajectories of a normal stationary stochastic process and a high level," Arkiv för Matematik 6, pp. 337-349.

[37] Hagen, O., 1992, "Conditional and joint failure surface crossing of stochastic processes," Journal of Engineering Mechanics, 118(9), pp. 1814-1839.

[38] Li, C. W., and Melchers, R. E., 1994, "Structural systems reliability under stochastic loads," Proceedings of the Institution of Civil Engineers: Structures and Buildings, 104(3), pp. 251-256.

[39] Parkinson, D. B., 1999, "Second order stochastic simulation with specified correlation," Advances in engineering software, 30(7), pp. 489-494.

[40] Streicher, H., and Rackwitz, R., 2004, "Time-variant reliability-oriented structural optimization and a renewal model for life-cycle costing," Probabilistic Engineering Mechanics, 19(1), pp. 171-183.

[41] Singh, A., Mourelatos, Z., and Nikolaidis, E., 2011, "Time-Dependent Reliability of Random Dynamic Systems Using Time-Series Modeling and Importance Sampling," SAE International Journal of Materials and Manufacturing, 4(1), pp. 929-946.

[42] Singh, A., Mourelatos, Z. P., and Li, J., 2010, "Design for lifecycle cost using time-dependent reliability," Journal of Mechanical Design, Transactions of the ASME, 132(9), pp. 0910081-09100811.

[43] Yang, J. N., and Shinozuka, M., 1971, "On the first excursion probability in stationary narrow- band random vibration," Journal of Applied Mechanics, Transactions ASME, 38 Ser E(4), pp. 1017-1022.

[44] Yang, J. N., and Shinozuka, M., 1972, "ON THE FIRST-EXCURSION PROBABILITY IN STATIONARY NARROW-BAND RANDOM VIBRATION - 2," Journal of Applied Mechanics, Transactions ASME, 39 Ser E(3), pp. 733-738.

[45] Vanmarcke, E. H., 1975, "On the distribution of the first-passage time for normal stationary random processes," Journal of Applied Mechanics, Transactions ASME, 42 Ser E(1), pp. 215-220.

[46] Preumont, A., 1985, "On the peak factor of stationary Gaussian processes," Journal of Sound and Vibration, 100(1), pp. 15-34.

[47] Bernard, M. C., and Shipley, J. W., 1972, "The first passage problem for stationary random structural vibration," Journal of Sound and Vibration, 24(1), pp. 121-132.

[48] Madsen, P. H., and Krenk, S., 1984, "Integral equation method for the first-passage problem in random vibration," Journal of Applied Mechanics, Transactions ASME, 51(3), pp. 674-679.

[49] Hu, Z., and Du, X., 2012, "Reliability analysis for hydrokinetic turbine blades," Renewable Energy, 48, pp. 251-262.

[50] Andrieu-Renaud, C., Sudret, B., and Lemaire, M., 2004, "The PHI2 method: A way to compute time-variant reliability," Reliability Engineering and System Safety, 84(1), pp. 75-86.

[51] Burchitz, I. A., and Meinders, T., 2008, "Adaptive through-thickness integration for accurate springback prediction," International Journal for Numerical Methods in Engineering, 75(5), pp. 533-554.

[52] Dickmeis, W., Nessel, R. J., and van Wickeren, E., 1984, "A general approach to counterexamples in numerical analysis," Numerische Mathematik, 43(2), pp. 249-263.

[53] Diethelm, K., 1994, "Modified compound quadrature rules for strongly singular integrals," Computing, 52(4), pp. 337-354.

[54] Navascués, M. A., and Sebastián, M. V., 2012, "Numerical integration of affine fractal functions," Journal of Computational and Applied Mathematics.

[55] Ujević, N., 2008, "An application of the montgomery identity to quadrature rules," Rendiconti del Seminario Matematico, 66(2), pp. 137-143.

[56] Rice, S. O., 1945, "Mathematical analysis of random noise," Bell Syst.Tech. J.,, 24, pp. 146-156.

[57] Gupta, A. K., Móri, T. F., and Székely, G. J., 2000, "How to transform correlated random variables into uncorrelated ones," Applied Mathematics Letters, 13(6), pp. 31-33.

PAPER
II. EFFICIENT GLOBAL OPTIMIZATION RELIABILITY ANALYSIS (EGORA) FOR TIME-DEPENDENT LIMIT-STATE FUNCTIONS

Zhen Hu and Xiaoping Du[1]
Department of Mechanical and Aerospace Engineering
Missouri University of Science and Technology

Abstract

If a limit-state function involves time, the associated reliability is defined within a period of time. The extreme value of the limit-state function is needed to calculate the time-dependent reliability, but the extreme value is usually highly nonlinear with respect to random input variables and may follow a multimodal distribution. For this reason, a surrogate model of the extreme response along with Monte Carlo simulation is usually employed. The objective of this work is to develop a new method, called the Efficient Global Optimization Reliability Analysis (EGORA), to efficiently build the surrogate model. EGORA is based on the Efficient Global Optimization (EGO) method. Different from the current method that draws samples of random variables and time independently, EGORA draws samples of the two types of input variables simultaneously and therefore accounts for their interaction effects. The other improvement is that EGORA only focuses on high accuracy at or near the limit state. With the two improvements, the new method can reduce the number of samples to almost half of that of the traditional method. Once the surrogate model of the extreme response is available, Monte Carlo simulation is applied to calculate the time-dependent reliability. The accuracy and efficiency of EGORA are demonstrated by three examples.

---

[1]400 West 13th Street, Toomey Hall 290D,Rolla, MO 65409, U.S.A., Tel: 1-573-341-7249, e-mail: dux@mst.edu

1. Introduction

If a response variable is a function (limit-state function) of time, the associated reliability is defined within a period of time and usually decreases over time. For this case, time-independent reliability analysis methodologies [1,2] are not applicable. Even though other methods [3-5] exist, the first passage methods and extreme value methods are usually used to calculate time-dependent reliability. The former methods are easier to use and are more popular, but may not be as accurate as the latter methods. The two types of methods are briefly reviewed below.

The first-passage methods calculate the probability that the response exceeds its failure threshold (limit state) for the first time in the predefined period of time. The event that the response reaches its limit state is called an upcrossing, and the upcrossing rate is the rate of change of the upcrossing probability with respect to time. If the first-time upcrossing rate is available, the time-dependent probability of failure can be easily found. But it is difficult to obtain the first-time upcrossing rate. For this reason, approximation methods are widely applied. The most commonly used method is the Rice's formula [6], which uses upcrossing rates throughout the entire period of time and assumes that all the upcrossings are independent.

Many latter methods have been developed based on the Rice's formula. For instance, an asymptotic outcrossing rate for stationary Gaussian processes was derived by Lindgren [7] and Breitung [8, 9]. The bounds of the upcrossing rate of a non-stationary Gaussian process were given by Ditlevsen [10]. To solve general time-dependent reliability problems, Hagen and Tvedt [11, 12] proposed a parallel system approach. A PHI2 method was then developed by Sudret [13]. Hu and Du also developed a time-dependent reliability analysis method based on the Rice's formula [14]. Even if some modifications have been made [15-18], the upcrossing methods may produce large errors when upcrossings are strongly dependent.

The extreme value methods approach the time-dependent reliability from another aspect – using the extreme value of the response with respect to time. If the extreme value and its distribution can be found, the accuracy will be higher than the upcrossing methods since the independent upcrossing assumption is eliminated. The distribution of

the extreme response, however, may not be obtained accurately and efficiently without using expensive global optimization repeatedly.

In general, the extreme value of the response is much more nonlinear than the response itself with respect to the input random variables. For many problems, the distribution of the extreme response is multimodal with different modes (peaks of probability density) even though the response itself follows a unimodal distribution [19]. For this reason, using Design of Experiments (DOE) to obtain a surrogate model of the extreme response becomes promising and practical. For example, Wang and Wang [20] proposed an extreme response method using the Efficient Global Optimization (EGO) approach [22], which is a DOE method. Chen and Li [21] also studied how to evaluate the distribution of the extreme response using the probability density evolution method [21].

The efficiency of the existing extreme value methods with DOE, such as the approach in [20], can be improved. Suppose the response Y is computed though a limit-state function $g(\mathbf{X}, t)$, where $\mathbf{X}$ is a vector of random variables and t is time. The current methods draw samples of $\mathbf{X}$ first. Then at each sample point of $\mathbf{X}$, samples of t are drawn through EGO [22], which produces the extreme response with respect to time. Then the values of the extreme response are available at all the sample points of $\mathbf{X}$, and a surrogate model of the extreme response is built. Sampling on $\mathbf{X}$ and t is performed at two nested and independent levels, and the method is therefore called the *independent EGO method*. The interaction effects of $\mathbf{X}$ and t are not considered at the two separate sampling levels. The efficiency could be improved if $\mathbf{X}$ and t are simultaneously sampled. This motivated us to develop a new method with higher efficiency.

This work develops a new time-dependent reliability method based on EGO, and the strategy proposed in [19] is also employed. The new method is named the *Efficient Global Optimization Reliability Analysis* (EGORA). The contributions of this work consist of the following elements:

- A new efficient sampling strategy for generating samples of random input variables $\mathbf{X}$ and time t simultaneously so that the interaction effects of both types of variables can be considered. The strategy significantly increases the efficiency of the existing independent EGO method.

- The extension of the sampling update approach proposed in [19] for time-independent problems to time-dependent problems. This makes the surrogate model of the extreme response accurate near or at the limit state and therefore makes the reliability obtained later by Monte Carlo simulation accurate.
- A complete numerical algorithm that implements the new sampling strategy robustly.
- The integration of the above algorithm and Monte Carlo simulation.

Time-dependent limit state functions may be given in different forms [23, 24]. This work is concerned with limit-state functions in the form of $Y = g(\mathbf{X}, t)$, where $\mathbf{X} = [X_1, X_2, \cdots, X_n]$ is a vector of random variables.

The remainder of this paper starts from Section 2 where the EGO is reviewed and time-dependent reliability. The new method is discussed in Section 3 followed by its numerical algorithm in Section 4. Three examples are presented in Section 5, and conclusions are given in Section 6.

2. Background

The Efficient Global Optimization (EGO) is used for time-dependent reliability analysis in this work. The EGO is first reviewed and then discuss the definition of the time-dependent reliability. The current method or the independent EGO method is also discussed in Section 1.

2.1. Efficient Global Optimization (EGO)

Since being proposed by Jones in 1998 [22], EGO has been widely used in various areas [25-28]. It is based on the DACE model [29] or the Kriging model. Both of the EGO and DACE methods update their models by adding training points gradually. The two methods use different criteria for model updating. The EGO model is updated with a new training point that maximizes the expected improvement function (EIF) while the DACE model is updated with a new training point that minimizes the mean square error. A maximum EIF helps find a point with the highest probability to produce a better

extreme value of the response than the current ones. Many studies have demonstrated that EGO can significantly reduce the number of function evaluations for global optimization.

EGO at first constructs a Kriging model using initial training points. The expected improvements (EI) is calculated using the mean and covariance of the Kriging model. The model is then updated by adding a new point with the maximum EI. The procedure continues until convergence.

The Kriging model $\hat{g}(\mathbf{x})$ is given by

$$\hat{y} = \hat{g}(\mathbf{x}) = \mathbf{h}(\mathbf{x})^T \boldsymbol{\beta} + Z(\mathbf{x}) \tag{1}$$

in which $\mathbf{h}(\cdot)$ is called the trend of the model, $\boldsymbol{\beta}$ is the vector of the trend coefficients, and $Z(\cdot)$ is a stationary Gaussian process with a mean of zero and the covariance given by

$$Cov[Z(\mathbf{a}), Z(\mathbf{b})] = \sigma_Z^2 R(\mathbf{a}, \mathbf{b}) \tag{2}$$

where σ_Z^2 is the variance of the process, and $R(\mathbf{a}, \mathbf{b})$ is the correlation function. The commonly used correlation functions include the squared-exponential and Gaussian [29].

At a general point $\mathbf{x}$, $\hat{y}$ is a Gaussian random variable denoted by

$$\hat{y} = \hat{g}(\mathbf{x}) \sim N(\mu(\mathbf{x}), \sigma^2(\mathbf{x})) \tag{3}$$

in which $N(\cdot, \cdot)$ stands for a normal distribution; $\mu(\cdot)$ and $\sigma(\cdot)$ are the mean and standard deviation of $\hat{y}$, respectively. At a training point $\mathbf{x}$, $\mu(\mathbf{x}) = g(\mathbf{x})$ and $\sigma(\mathbf{x}) = 0$. This means that $\hat{g}(\mathbf{x})$ passes all the sampled points $\{\mathbf{x}, g(\mathbf{x})\}$.

When EGO is used to find the global maximum of $g(\mathbf{x})$, the improvement at $\mathbf{x}$ is defined by $I = \max(y - y^*, 0)$, where y^* is the current best solution (the maximum response) obtained from the existing training points. The expected improvement EI is given by [22]

$$\mathrm{EI}(\mathbf{x}) = (\mu(\mathbf{x}) - y^*)\Phi\left(\frac{\mu(\mathbf{x}) - y^*}{\sigma(\mathbf{x})}\right) + \sigma(\mathbf{x})\phi\left(\frac{\mu(\mathbf{x}) - y^*}{\sigma(\mathbf{x})}\right) \tag{4}$$

where $\Phi(\cdot)$ and $\phi(\cdot)$ are the Cumulative Distribution Function (CDF) and Probability Density Function (PDF) of a standard Gaussian variable, respectively, and y^* is computed by

$$y^* = \max_{i=1,2,\cdots,k} \{g(\mathbf{x}^{(i)})\} \tag{5}$$

in which k is the number of current training points.

By maximizing EI, a new training points is then identified as follows

$$\mathbf{x}^{(k+1)} = \arg\max_{\mathbf{x}\in\mathbf{X}} \mathrm{EI}(\mathbf{x}) \tag{6}$$

Algorithm 1 describes the procedure of EGO. More details can be found in Refs. [22] and [29].

Algorithm 1 Efficient Global Optimization (EGO)

1 Generate initial samples $\mathbf{x}^s = [\mathbf{x}^{(1)}; \mathbf{x}^{(2)}; \cdots; \mathbf{x}^{(k)}]$

2 Compute $\mathbf{y}^s = [g(\mathbf{x}^{(1)}), g(\mathbf{x}^{(2)}), \cdots, g(\mathbf{x}^{(k)})]$; set $m = 1$

3 **While** $\{m = 1\}$ **or** $\{\max_{\mathbf{x}\in\mathbf{X}} \mathrm{EI}(\mathbf{x}) < \varepsilon_{EI}\}$ **do**

4 Construct a Kriging model $\hat{y} = \hat{g}(\mathbf{X})$ using $\{\mathbf{x}^s, \mathbf{y}^s\}$

5 Find $y^* = \max_{i=1,2,\cdots,k+m-1} \{g(\mathbf{x}^{(i)})\}$

6 Search for $\mathbf{x}^{(k+m)} = \arg\max_{\mathbf{x}\in\mathbf{X}} \mathrm{EI}(\mathbf{x})$, where $\mathrm{EI}(\mathbf{x})$ is computed by Eq. (4)

7 Scale $\max_{\mathbf{x}\in\mathbf{X}} \mathrm{EI}(\mathbf{x}) = \max_{\mathbf{x}\in\mathbf{X}} \mathrm{EI}(\mathbf{x}) / |\beta(1)|$, where $\beta(1)$ is the first element of the trend coefficients $\boldsymbol{\beta}$ given in Eq. (1)

8 Compute $g(\mathbf{x}^{(k+m)})$; update $\mathbf{y}^s = [\mathbf{y}^s, g(\mathbf{x}^{(k+m)})]$ and $\mathbf{x}^s = [\mathbf{x}^s; \mathbf{x}^{(k+m)}]$

9 $m = m + 1$

10 **End While**

In Step 3, ε_{EI} is the convergence criterion of EI. The maximum EI is scaled in Line 7 as suggested in [19].

2.2. Time-dependent reliability

For a general limit-state function $Y = g(\mathbf{X}, t)$, a failure occurs if

$$Y = g(\mathbf{X}, t) > e \tag{7}$$

in which e is the failure threshold.

For a time interval $[t_0, t_s]$, the time-dependent reliability is defined by [5]

$$R(t_0, t_s) = \Pr\{Y = g(\mathbf{X},\ t) < e, \forall t \in [t_0, t_s]\} \tag{8}$$

where $\Pr\{\cdot\}$ stands for a probability, and $\forall t \in [t_0, t_s]$ means all time instants on $[t_0, t_s]$.

The time-dependent probability of failure is defined

$$p_f(t_0, t_s) = \Pr\{Y = g(\mathbf{X},\ t) > e, \exists t \in [t_0, t_s]\} \tag{9}$$

where $\exists$ stands for "there exists".

$p_f(t_0, t_s)$ is a non-decreasing function of the length of $[t_0, t_s]$. The longer is the period of time, generally, the higher is $p_f(t_0, t_s)$.

2.3. Time-dependent reliability analysis with surrogate models

The failure event in Eq. (7) is equivalent to $Y_{\max} > e$, where $Y_{\max}$ is the global maximum response on $[t_0, t_s]$ and is given by

$$Y_{\max} = \underset{t \in [t_0, t_s]}{\arg\max}\{g(\mathbf{X},\ t)\} \tag{10}$$

Then $p_f(t_0, t_s)$ is rewritten as

$$p_f(t_0, t_s) = \Pr\{Y_{\max} > e\} \tag{11}$$

For many problems, $Y_{\max}$ is highly nonlinear with respect $\mathbf{X}$ and may follow a multimodal distribution. Using the current approximation reliability methods, such as the First and Second Order Reliability Methods (FORM and SORM), may result in large errors. Monte Carlo simulation becomes a choice if a surrogate model, $Y_{\max} = \hat{g}_{\max}(\mathbf{X})$, of $Y_{\max}$, can be built. As discussed previously, the direct EGO method, e.g., the approach in [20], builds $Y_{\max} = \hat{g}_{\max}(\mathbf{X})$ at two nested loops. The outer loop generates samples of $\mathbf{X}$.

At each sample of $\mathbf{X}$, the inner loop is executed to find the time $t_{\max}$ when the response is maximum. Samples of t are generated by EGO in the inner loop.

A more direct and general independent EGO procedure is summarized below.

- Outer loop: Sampling on $\mathbf{X}$ for building $Y_{\max} = \hat{g}_{\max}(\mathbf{X})$.
- Inner loop: EGO for $y_{\max} = \max\limits_{t\in[t_0, t_s]}\{g(\mathbf{x}, t)\}$ at $\mathbf{x}$, which a sample of $\mathbf{X}$.

The associated algorithm or Algorithm 2 is shown as follows.

Algorithm 2 Independent EGO method

1 Generate initial samples $\mathbf{x}^s = [\mathbf{x}^{(1)}; \mathbf{x}^{(2)}; \cdots; \mathbf{x}^{(k)}]$

2 Solve for $\mathbf{y}^s_{\max} = [g_{\max}(\mathbf{x}^{(1)}), g_{\max}(\mathbf{x}^{(2)}), \cdots, g_{\max}(\mathbf{x}^{(k)})]$, where

$g_{\max}(\mathbf{x}^{(i)}) = \max\limits_{t\in[t_0, t_s]}\{g(\mathbf{x}^{(i)}, t)\}$, using EGO; set $m = 1$

3 **While** $\{m = 1\}$ **or** $\{\max\limits_{\mathbf{x}\in\mathbf{X}} \mathrm{MSE}(\mathbf{x}) < \varepsilon_{MSE}\}$ **do**

4 Construct a Kriging model $Y_{\max} = \hat{g}_{\max}(\mathbf{X})$ using $\{\mathbf{x}^s, \mathbf{y}^s_{\max}\}$

5 Find $\mathbf{x}^{(k+m)} = \arg\max\limits_{\mathbf{x}\in\mathbf{X}}\{\mathrm{MSE}(\mathbf{x})\}$

6 Search for $g_{\max}(\mathbf{x}^{(k+m)}) = \max\limits_{t\in[t_0, t_s]}\{g(\mathbf{x}^{(k+m)}, t)\}$ using EGO

7 Update $\mathbf{x}^s = [\mathbf{x}^s; \mathbf{x}^{(k+m)}]$ and $\mathbf{y}^s_{\max} = [\mathbf{y}^s_{\max}, g_{\max}(\mathbf{x}^{(k+m)})]$

8 $m = m + 1$

9 **End While**

10 Reliability analysis using $Y_{\max} = \hat{g}_{\max}(\mathbf{X})$

In Step 3, ε_{MSE} is a small positive number used as the convergence criterion of MSE, where MSE stands for the mean square error.

The independent EGO method may not be efficient because of the following two reasons. First, the one-dimensional EGO with respect to *t* is performed repeatedly at each sample point of $\mathbf{X}$. As mentioned previously, $\mathbf{X}$ and t are treated independently at two separate levels, the interaction of $\mathbf{X}$ and t cannot be considered at either level. The efficiency will be low. Second, the surrogate model should have a very small *MSE* when

it is applied to the reliability analysis. If $Y_{\max}$ is highly nonlinear or its distribution is multimodal, constructing a surrogate model with a low *MSE* is computationally expensive.

3. Efficient Global Optimization Reliability Analysis (EGORA)

In this section, the EGORA method that overcomes the drawbacks of the independent EGO method is discussed. The new method builds a surrogate model $Y_{\max} = \hat{g}_{\max}(\mathbf{X})$ for the global extreme response through another surrogate model $Y = \hat{g}(\mathbf{X}, t)$ for the original limit-state function $Y = g(\mathbf{X}, t)$. The new method is still based on EGO and is much more efficient than the independent EGO method. It is therefore called the Efficient Global Optimization Reliability Analysis (EGORA) method. It is efficient because of the following reasons:

- With the use of the surrogate model $Y = \hat{g}(\mathbf{X}, t)$, the interaction effects of $\mathbf{X}$ and t can be effectively considered. This will reduce the numbers of samples of both $\mathbf{X}$ and t.
- EGORA employs the convergence criterion developed in [19] and can efficiently and accurately approximate the extreme responses at or near the limit state without using the *MSE*. High accuracy at or near the limit state also helps reduce the number of samples of $\mathbf{X}$.

3.1. Overview

Let the surrogate model of the extreme response be $Y_{\max} = \hat{g}_{\max}(\mathbf{X})$. As discussed in [19], the accuracy of reliability analysis is only affected by the accuracy of the surrogate model at the limit state or $Y_{\max} = g_{\max}(\mathbf{X}) = e$. For this reason, achieving high accuracy for $Y_{\max} = \hat{g}_{\max}(\mathbf{X})$ at or near the limit state is the focus. By doing so, the number of samples can be reduced. Since the limit-state $Y_{\max} = g_{\max}(\mathbf{X}) = e$ is of the greatest concern, the sample updating criterion needs to be modified. In this work, the

modified Expected Improvement (EI) in [19] is extended for time-independent problems into present time-dependent problems.

The overall procedure of EGORA is provided in Table 1, and the detailed algorithm will be discussed in Subsections 3.3 and 3.4 and will be summarized in Section. 4.

Table 1 Major Procedure of EGORA

Step 1: Initial sampling
1. Generate initial samples $\mathbf{x}^s$ and $\mathbf{t}^s$
Step 2: Build initial extreme response model (Algorithm 3)
2. Build time-dependent surrogate model $Y = \hat{g}(\mathbf{X}, t)$
3. Solve for the maximum responses $Y_{\max}$ at $\mathbf{x}^s$ based on $Y = \hat{g}(\mathbf{X}, t)$
4. Build initial extreme response model $Y_{\max} = \hat{g}_{\max}(\mathbf{X})$
Step 3: Update extreme response model (**Algorithm 4**)
5. Adding new samples of $\mathbf{X}$ though updating and using $Y = \hat{g}(\mathbf{X}, t)$
6. Obtain final model $Y_{\max} = \hat{g}_{\max}(\mathbf{X})$
Step 4: Reliability analysis
7. Monte Carlo simulation based on $Y_{\max} = \hat{g}_{\max}(\mathbf{X})$.

The major difference between the independent EGO method and EGORA is that $\mathbf{X}$ and t are sampled at two separate levels in the former method while $\mathbf{X}$ and t are sampled simultaneously in the latter method.

3.2. Initial sampling

The initial samples $\mathbf{x}^s$ are used to create an initial surrogate model for $Y_{\max}$. The commonly used sampling approaches include the Random Sampling (RS), Latin Hypercube Sampling (LHS), and Hammersley Sampling (HS) [30]. In this work, the HS method is used as it is better than LHS and RS in providing uniformity properties over multi-dimensional space [31].

Suppose that the dimension of $\mathbf{X}$ is *n* and that *k* initial samples are generated. The samples $\mathbf{x}^s$ are

$$\mathbf{x}^s = \left[\mathbf{x}^{(1)}; \mathbf{x}^{(2)}; \cdots; \mathbf{x}^{(k)}\right] = \begin{bmatrix} x_1^{(1)} & x_2^{(1)} & \cdots & x_n^{(1)} \\ x_1^{(2)} & x_2^{(2)} & \cdots & x_n^{(2)} \\ \vdots & \vdots & \ddots & \vdots \\ x_1^{(k)} & x_2^{(k)} & \cdots & x_n^{(k)} \end{bmatrix} \tag{12}$$

in which $\mathbf{x}^{(i)} = [x_1^{(i)}, x_2^{(i)}, \cdots, x_n^{(i)}]$ is the *i*-th sample point.

k initial samples of *t* are also generated along with those of $\mathbf{X}$. The combined initial samples are then given by

$$[\mathbf{x}^s, \mathbf{t}^s] = \begin{bmatrix} x_1^{(1)} & x_2^{(1)} & \cdots & x_n^{(1)}, & t^{(1)} \\ x_1^{(2)} & x_2^{(2)} & \cdots & x_n^{(2)}, & t^{(2)} \\ \vdots & \vdots & \ddots & \vdots & \\ x_1^{(k)} & x_2^{(k)} & \cdots & x_n^{(k)}, & t^{(k)} \end{bmatrix} \tag{13}$$

The limit-function is called to obtain responses at the above samples and build a mixed EGO model $Y = \hat{g}(\mathbf{X}, t)$ with respect to $\mathbf{X}$ and *t*. $Y = \hat{g}(\mathbf{X}, t)$ is called a mixed model because it is a function of $\mathbf{X}$ and *t*. Then, the extreme value responses $\mathbf{y}_{\max}^s$ at $\mathbf{x}^s$ are identified by the mixed EGO model that will be discussed in the following section.

3.3. Construct initial $Y_{\max} = \hat{g}_{\max}(\mathbf{X})$ with the mixed EGO model

This is Step 2 of EGORA in Table 1. With *t*, the EI in Eq. (4) is rewritten as

$$EI(\mathbf{x}^{(i)}, t) = (\mu(\mathbf{x}^{(i)}, t) - y_i^*)\Phi\left(\frac{\mu(\mathbf{x}^{(i)}, t) - y_i^*}{\sigma(\mathbf{x}^{(i)}, t)}\right) + \sigma(\mathbf{x}^{(i)}, t)\phi\left(\frac{\mu(\mathbf{x}^{(i)}, t) - y_i^*}{\sigma(\mathbf{x}^{(i)}, t)}\right) \tag{14}$$

where y_i^* is the current best solution (maximum response), and $\mu(\mathbf{x}^{(i)}, t)$ and $\sigma(\mathbf{x}^{(i)}, t)$ are the mean and standard deviation at $[\mathbf{x}^{(i)}, t]$.

The expressions of EI are the same for the independent EGO method and the mixed EGO model. The difference lies in the way of computing $\mu(\mathbf{x}^{(i)}, t)$ and $\sigma(\mathbf{x}^{(i)}, t)$. For the independent EGO method, $\mu(\mathbf{x}^{(i)}, t)$ and $\sigma(\mathbf{x}^{(i)}, t)$ are obtained from the one-dimensional Kriging model $Y = \hat{g}(t)$, which is constructed in the inner loop for *t* when $\mathbf{X}$

is fixed. For the mixed EGO model, they are computed from the Kriging model $Y = \hat{g}(\mathbf{X},\ t)$, which is constructed when $\mathbf{X}$ and t change simultaneously.

Once convergence is reached, the maximum responses with respect to $\mathbf{x}^s$ will be available. Then the initial model $Y_{\max} = \hat{g}_{\max}(\mathbf{X})$ can be built.

The algorithm (Algorithm 3) for the initial $Y_{\max} = \hat{g}_{\max}(\mathbf{X})$ is given as follows.

Algorithm 3 Mixed EGO model for initial $Y_{\max} = \hat{g}_{\max}(\mathbf{X})$

---

1 At initial samples points, compute $\mathbf{y}^s = [y^{(i)}]_{i=1,\ldots,k} = [g(\mathbf{x}^{(i)},\ t^{(i)})]_{i=1,\ldots,k}$

2 Set $\mathbf{x}_t^s = \mathbf{x}^s$, $m = 1$, and the initial current best solution vector $\mathbf{y}_{\max}^s = \mathbf{y}^s$

3 **While** $\{m = 1\}$ **or** $\{I_{\max} < \varepsilon_{EI}\}$ **do**

4 Construct Kriging model $Y = \hat{g}(\mathbf{X},\ t)$ using $\{[\mathbf{x}_t^s, \mathbf{t}^s], \mathbf{y}^s\}$

5 Find a point with maximum EI: $[\mathbf{x}^{(i_{\mathrm{EI}})}, t^{\mathrm{EI}}] = \underset{i=1,\,2,\cdots,\,k}{\arg\max}\{\max_{t\in[t_0,\,t_s]}\{\mathrm{EI}(\mathbf{x}^{(i)}, t)\}\}$,

where $i_{\mathrm{EI}} \in [1,\ldots,k]$ and $\mathrm{EI}(\mathbf{x}^{(i)}, t)$ is computed based on $Y = \hat{g}(\mathbf{X},\ t)$;

calculate $I_{\max} = \mathrm{EI}(\mathbf{x}^{(i_{\mathrm{EI}})}, t^{\mathrm{EI}}) / \left|\beta_{(\mathbf{x},\,t)}(1)\right|$.

6 Compute $y^{\mathrm{EI}} = g(\mathbf{x}^{(i_{\mathrm{EI}})}, t^{\mathrm{EI}})$

7 Update current best solution $y_{\max}^s(i_{\mathrm{EI}}) = \begin{cases} y^{\mathrm{EI}} & \text{if } y^{\mathrm{EI}} > y_{\max}^s(i_{\mathrm{EI}}) \\ y_{\max}^s(i_{\mathrm{EI}}) & \text{otherwise} \end{cases}$

8 Update data points $\mathbf{x}_t^s = [\mathbf{x}_t^s; \mathbf{x}^{(i_{\mathrm{EI}})}]$, $\mathbf{t}^s = [\mathbf{t}^s;\ t^{\mathrm{EI}}]$, and $\mathbf{y}^s = [\mathbf{y}^s, y^{\mathrm{EI}}]$

9 $m = m + 1$

10 **End While**

11 Record $\mathbf{y}_{\max}^s$, $[\mathbf{x}_t^s, \mathbf{t}^s]$, and $\mathbf{y}^s$

12 Construct $Y_{\max} = \hat{g}_{\max}(\mathbf{X})$ using $\{\mathbf{x}^s, \mathbf{y}_{\max}^s\}$

In Line 2, $\mathbf{x}^s$ contains initial samples used to construct $Y_{\max} = \hat{g}_{\max}(\mathbf{X})$, and $\mathbf{x}_t^s$ contains $\mathbf{x}^s$ and added samples of $\mathbf{X}$ for model $Y = \hat{g}(\mathbf{X},\ t)$. In Line 3, ε_{EI} is the

convergence criterion of maximum EI. In Line 5, $\mathrm{EI}(\mathbf{x}^{(i)}, t)$ is computed by plugging $y^s_{\max}(i)$, $\mu_Y(\mathbf{x}^{(i)}, t)$ and $\mu_Y(\mathbf{x}^{(i)}, t)$, which are obtained from $Y = \hat{g}(\mathbf{X}, t)$, into Eq. (14).

In the mixed EGO model, all the sampled data of both $\mathbf{X}$ and t are used to update the training points of t. But in the independent EGO model, only the sampled data of t are used to update training points of t. This is the reason why the mixed EGO model is more efficient.

From the outputs of the mixed EGO model, the extreme values $\mathbf{y}^s_{\max}$ are obtained corresponding to the samples $\mathbf{x}^{(i)}$, $i = 1, 2, \cdots, k$. In the following section, it discusses how to get a new training point $\mathbf{x}^{(k+1)}$ and the associated $g_{\max}(\mathbf{x}^{(k+1)})$.

3.4. Update $Y_{\max} = \hat{g}_{\max}(\mathbf{X})$

The initial model of the extreme response $Y_{\max} = \hat{g}_{\max}(\mathbf{X})$ obtained above may not be accurate. This work now discusses how to update the model. The criterion originally developed in [19] is adopted, where the expected improvement function (EIF) is modified to the expected feasibility function (EFF). The method is for only time-independent problems. It is now extended to time-dependent problems.

Other than the use of EFF, the other steps are the same as the EGO model. Specifically, an initial Kriging model is built first. Then a new training point is identified by maximizing the expected feasibility (EF). The advantage of using the EF is that it helps generate new training points near the limit state. Consequently, the surrogate model is accurate near the limit state; other regions away from the limit state are not concerned. This allows for an accurate surrogate model for reliability analysis with reduced samples.

As mentioned previously, the EF in [19] is for a time-independent problem, where the following probability needs to be approximated.

$$P = \Pr\{g(\mathbf{X}) > e\} \tag{15}$$

The surrogate model $\hat{\mathrm{g}}(\mathbf{X})$ for $g(\mathbf{X})$ is to be constructed. EF is defined by [19]

$$\begin{aligned}\mathrm{EF}(\mathbf{x}) = (\mu_g(\mathbf{x}) - e)\left[2\Phi\left(\frac{e-\mu_g(\mathbf{x})}{\sigma_g(\mathbf{x})}\right) - \Phi\left(\frac{e^- - \mu_g(\mathbf{x})}{\sigma_g(\mathbf{x})}\right) - \Phi\left(\frac{e^+ - \mu_g(\mathbf{x})}{\sigma_g(\mathbf{x})}\right)\right] \\ -\sigma_g(\mathbf{x})\left[2\phi\left(\frac{e-\mu_g(\mathbf{x})}{\sigma_g(\mathbf{x})}\right) - \phi\left(\frac{e^- - \mu_g(\mathbf{x})}{\sigma_g(\mathbf{x})}\right) - \phi\left(\frac{e^+ - \mu_g(\mathbf{x})}{\sigma_g(\mathbf{x})}\right)\right] \\ +\delta\left[\Phi\left(\frac{e^+ - \mu_g(\mathbf{x})}{\sigma_g(\mathbf{x})}\right) - \Phi\left(\frac{e^- - \mu_g(\mathbf{x})}{\sigma_g(\mathbf{x})}\right)\right]\end{aligned} \tag{16}$$

where $\mu_g(\mathbf{x})$ and $\sigma_g(\mathbf{x})$ are mean and standard deviation at point $\mathbf{x}$ obtained from the outputs of predictor $\hat{\mathrm{g}}(\mathbf{x})$, $e^- = e - \delta$, $e^+ = e + \delta$, and δ is a parameter which is proportional to $\sigma_g(\mathbf{x})$.

The new training point of $\mathbf{x}$ is then identified by maximizing EF. After the new training point is identified, a new surrogate model is constructed. Then, new training point is obtained based on EF again. The iteration continues until the convergence criterion is satisfied. More details are available in [19].

The same strategy can be used for present time-dependent problem for finding a training point. As discussed in Sec. 3.1, an initial Kriging model $Y_{\max} = \hat{g}_{\max}(\mathbf{X})$ is first constructed using $\{\mathbf{x}^s, \mathbf{y}^s_{\max}\}$. By using the EFF, a new training point of $\mathbf{x}$ is obtained as follows

$$\mathbf{x}^{(k+1)} = \arg\max_{\mathbf{x}\in\mathbf{X}}\{\mathrm{EF}(\mathbf{x})\} \tag{17}$$

where $\mathrm{EF}(\mathbf{x})$ is obtained by plugging $\mu_{y_{\max}}(\mathbf{x})$, $\sigma_{y_{\max}}(\mathbf{x})$, e, $e^- = -\delta$, and $e^+ = \delta$ into Eq. (16). $\mu_{y_{\max}}(\mathbf{x})$ and $\sigma_{y_{\max}}(\mathbf{x})$ are outputs of the predictor $\hat{g}_{\max}(\mathbf{X})$.

With the new training point $\mathbf{x}^{(k+1)}$, the associated extreme response $g_{\max}(\mathbf{x}^{(k+1)})$ is needed to update the surrogate model for $Y_{\max}$.

Obtaining $g_{\max}(\mathbf{x}^{(k+1)})$ is equivalent to solving the following one dimensional global optimization problem:

$$t^{(k+1)}_{\max} = \arg\max_{t\in[t_0, t_s]}\{y = g(\mathbf{x}^{(k+1)}, t)\} \tag{18}$$

To reduce the number of function calls, the mixed EGO model presented in the last subsection is still used, and the data set of $[\mathbf{x}_t^s, \mathbf{t}^s]$ and $\mathbf{y}^s$ obtained as discussed in Section 3.3 are used as well. Algorithm 4 presents the procedure for the sampling update on $\mathbf{x}^{(k+1)}$ and associated $g_{\max}(\mathbf{x}^{(k+1)})$.

Algorithm 4 Sampling update

Set p=1

While { $p=1$ **}** **or** { $\max_{\mathbf{x}\in\mathbf{X}} EF(\mathbf{x}) < \varepsilon_{EF}$ } **do**

  Construct a Kriging model of $Y_{\max} = \hat{g}_{\max}(\mathbf{X})$ using $\{\mathbf{x}^s, \mathbf{y}_{\max}^s\}$

  Find a point with maximum EF: $\mathbf{x}^{(k+p)} = \arg\max_{\mathbf{x}\in\mathbf{X}}\{\mathrm{EF}(\mathbf{x})\}$

  Generate a new random t_r that follows uniform distribution on $[t_0, t_s]$

  Compute $y^{\mathrm{EF}} = g(\mathbf{x}^{(k+p)}, t_r)$; Update $\mathbf{x}_t^s = [\mathbf{x}_t^s; \mathbf{x}^{(k+p)}]$ $\mathbf{t}^s = [\mathbf{t}^s;\ t_r]$ and $\mathbf{y}^s = [\mathbf{y}^s, y^{\mathrm{EF}}]$

  Set $y_{\max}^s(k+p) = y^{\mathrm{EF}}$ and $q=1$

  While { $q=1$ } or { $\max_{t\in[t_0,t_s]} \mathrm{EI}(\mathbf{x}^{(k+p)}, t) < \varepsilon_{EI}$ } **do**

    Construct an $n+1$ dimensional Kriging model $Y = \hat{g}(\mathbf{X},\ t)$ using $\{[\mathbf{x}_t^s, \mathbf{t}^s], \mathbf{y}^s\}$

    Find a point with maximum EI: $t^{\mathrm{EI}} = \max_{t\in[t_0,t_s]}\{\mathrm{EI}(\mathbf{x}^{(k+p)}, t)\}$, where $\mathrm{EI}(\mathbf{x}^{(k+p)}, t)$ is computed based on $Y = \hat{g}(\mathbf{X},\ t)$

    Scale $\mathrm{EI}(\mathbf{x}^{(k+p)}, t^{\mathrm{EI}}) = \mathrm{EI}(\mathbf{x}^{(k+p)}, t^{\mathrm{EI}}) / \left|\beta_{(\mathbf{x},\,t)}(1)\right|$, where $\beta_{(\mathbf{x},\,t)}(1)$ is the first element of the trend coefficients of $Y = \hat{g}(\mathbf{X},\ t)$ model

    Compute $y^{\mathrm{EI}} = g(\mathbf{x}^{(k+p)}, t^{\mathrm{EI}})$

    Update current best solution $y_{\max}^s(k+p) = \begin{cases} y^{\mathrm{EI}}, & \text{if } y^{\mathrm{EI}} > y_{\max}^s(k+p) \\ y_{\max}^s(k+p), & \text{otherwise} \end{cases}$

    Update data points $\mathbf{x}_t^s = [\mathbf{x}_t^s; \mathbf{x}^{(k+p)}]$, $\mathbf{t}^s = [\mathbf{t}^s;\ t^{\mathrm{EI}}]$, $\mathbf{y}^s = [\mathbf{y}^s, y^{\mathrm{EI}}]$

15: $q = q + 1$

16: **End While**

17: Record $\mathbf{y}^s_{\max}$, $\mathbf{x}^s = [\mathbf{x}^s; \mathbf{x}^{(k+p)}]$, $\mathbf{x}^s_t$, $\mathbf{t}^s$, and $\mathbf{y}^s$

18: $p = p + 1$

19: **End While**

In Line 10, $\mathrm{EI}(\mathbf{x}^{(k+p)}, t)$ is computed by plugging $y^s_{\max}(k+p)$, $\mu_Y(\mathbf{x}^{(k+p)}, t)$ and $\mu_Y(\mathbf{x}^{(k+p)}, t)$, which are obtained from $Y = \hat{g}(\mathbf{X}, t)$, into Eq. (14). When the convergence criterion is satisfied, the surrogate model $Y_{\max} = \hat{g}_{\max}(\mathbf{X})$ is obtained.

MCS is then used to calculate reliability. As $Y_{\max} = \hat{g}_{\max}(\mathbf{X})$ is accurate, so will be the reliability calculated by MCS with a sufficiently large sample. Note that MCS will not call the original limit-state state function any more.

All the algorithms for the new method are now available. Next everything is put together and give the complete algorithm.

4. Summary of EGORA

Combining Algorithms 3 and 4 yields the complete algorithm of EGORA, or Algorithm 5, given below.

Algorithm 5 Efficient Global Optimization Reliability Analysis (EGORA)

---

1) **Step 1: Initialization**

   a) Generate initial samples $\mathbf{x}^s = [\mathbf{x}^{(1)}; \mathbf{x}^{(2)}; \cdots; \mathbf{x}^{(k)}]$ and $\mathbf{t}^s = [t^{(1)}; t^{(2)}; \cdots; t^{(k)}]$ using the Harmmersley sampling method.

2) **Step 2: Build initial model** $Y_{\max} = \hat{g}_{\max}(\mathbf{X})$ **(Algorithm 3)**

   a) Compute $\mathbf{y}^s = [y^{(i)}]_{i=1,\cdots,k} = [g(\mathbf{x}^{(1)}, t^{(1)})]_{i=1,\cdots,k}$

   b) Set $\mathbf{x}^s_t = \mathbf{x}^s$, $m = 1$, and the initial current best solution vector $\mathbf{y}^s_{\max} = \mathbf{y}^s$

   c) **While** $\{ m = 1 \}$ **or** $\{ I_{\max} < \varepsilon_{EI} \}$ **do**

      i) Construct an $n+1$ dimensional Kriging model $Y = \hat{g}(\mathbf{X}, t)$

using $\{[\mathbf{x}_t^s, \mathbf{t}^s], \mathbf{y}^s\}$

ii) Find a point with maximum EI:

$[\mathbf{x}^{(i_{\text{EI}})}, t^{\text{EI}}] = \arg\max_{i=1,2,\cdots,k}\{\max_{t\in[t_0,t_s]}\{EI(\mathbf{x}^{(i)}, t)\}\}$, where $i_{\text{EI}} \in [1, \cdots, k]$;

calculate $I_{\max} = EI(\mathbf{x}^{(i_{\text{EI}})}, t^{\text{EI}}) / \left|\beta_{(\mathbf{x},\,t)}(1)\right|$.

iii) Compute $y^{\text{EI}} = g(\mathbf{x}^{(i_{\text{EI}})}, t^{\text{EI}})$

iv) Update current best solution $y_{\max}^s(i_{\text{EI}}) = \begin{cases} y^{\text{EI}}, & \text{if } y^{\text{EI}} > y_{\max}^s(i_{\text{EI}}) \\ y_{\max}^s(i_{\text{EI}}), & \text{otherwise} \end{cases}$

v) Update data points $\mathbf{x}_t^s = [\mathbf{x}_t^s; \mathbf{x}^{(i_{\max})}]$, $\mathbf{t}^s = [\mathbf{t}^s; t^{\text{EI}}]$, $\mathbf{y}^s = [\mathbf{y}^s, y^{\text{EI}}]$

vi) $m = m+1$

End While

d) Record $\mathbf{y}_{\max}^s$, $[\mathbf{x}_t^s, \mathbf{t}^s]$ and $\mathbf{y}^s$; Set $p = 1$.

3) **Step 3: Update $Y_{\max} = \hat{g}_{\max}(\mathbf{X})$ (Algorithm 4)**

While { $p = 1$ **} or {** $\max_{\mathbf{x}\in\mathbf{X}} EF(\mathbf{x}) < \varepsilon_{EF}$ **} do**

a) Construct a Kriging model $Y_{\max} = \hat{g}_{\max}(\mathbf{X})$ using $\{\mathbf{x}^s, \mathbf{y}_{\max}^s\}$

b) Find a point with maximum EF: $\mathbf{x}^{(k+p)} = \arg\max_{\mathbf{x}\in\mathbf{X}}\{\text{EF}(\mathbf{x})\}$

c) Generate a new random t_r that follows uniform distribution $[t_0, t_s]$

d) Compute $y^{\text{EF}} = g(\mathbf{x}^{(k+p)}, t_r)$ and update $\mathbf{x}_t^s = [\mathbf{x}_t^s; \mathbf{x}^{(k+p)}]$, $\mathbf{t}^s = [\mathbf{t}^s; t_r]$, and $\mathbf{y}^s = [\mathbf{y}^s, y^{\text{EF}}]$

e) Set $y_{\max}^s(k+p) = y^{\text{EF}}$ and $q = 1$

f) **While {** $q = 1$ **} or {** $\max_{t\in[t_0,t_s]} EI(\mathbf{x}^{(k+p)}, t) < \varepsilon_{EI}$ **} do**

i) Construct an $n+1$ dimensional Kriging model $Y = \hat{g}(\mathbf{X}, t)$ using $\{[\mathbf{x}_t^s, \mathbf{t}^s], \mathbf{y}^s\}$

ii) Find a point with maximum EI: $t^{\text{EI}} = \max_{t\in[t_0,t_s]}\{\text{EI}(\mathbf{x}^{(k+p)}, t)\}$, $\text{EI}(\mathbf{x}^{(k+p)}, t)$ is computed based on $Y = \hat{g}(\mathbf{X}, t)$

iii) Scale $\mathrm{EI}(\mathbf{x}^{(k+p)}, t^{\mathrm{EI}}) = \mathrm{EI}(\mathbf{x}^{(k+p)}, t^{\mathrm{EI}}) / \left|\beta_{(\mathbf{x},\,\mathrm{t})}(1)\right|$, where $\beta_{(\mathbf{x},\,\mathrm{t})}(1)$ is the first element of the trend coefficients of $Y = \hat{g}(\mathbf{X},\ t)$

iv) Compute $y^{\mathrm{EI}} = g(\mathbf{x}^{(k+p)}, t^{\mathrm{EI}})$

v) Update current best solution

$$y^{s}_{\max}(k+p) = \begin{cases} y^{\mathrm{EI}}, \text{ if } y^{\mathrm{EI}} > y^{s}_{\max}(k+p) \\ y^{s}_{\max}(k+p), \text{ otherwise} \end{cases}$$

vi) Update data points $\mathbf{x}^{s}_{t} = [\mathbf{x}^{s}_{t}; \mathbf{x}^{(k+p)}]$, $\mathbf{t}^{s} = [\mathbf{t}^{s}; t^{\mathrm{EI}}]$, $\mathbf{y}^{s} = [\mathbf{y}^{s}, y^{\mathrm{EI}}]$

vii) $q = q + 1$

End While

g) Record $\mathbf{y}^{s}_{\max}$, $\mathbf{x}^{s} = [\mathbf{x}^{s}; \mathbf{x}^{(k+p)}]$, $\mathbf{x}^{s}_{t}$, $\mathbf{t}^{s}$, and $\mathbf{y}^{s}$;

h) $p = p + 1$

End While

4) **Step 4: Reliability Analysis**

a) Reliability analysis using $Y_{\max} = \hat{g}_{\max}(\mathbf{X})$

---

5. Numerical examples

In this section, three numerical examples are employed to demonstrate the effectiveness of the proposed approach. Each of the examples is analyzed using the following four methods.

- The outcrossing rate method based on the Rice's formula and First Order Reliability Method (FORM) [14, 32].
- The independent EGO method.
- The proposed EGORA method.
- Direct MCS using the original limit-state function.

The reason other methods is used is to evaluate the accuracy and efficiency of EGORA.

5.1. A nonlinear mathematical model

A function of X and t is given in Eq. (19), where X is a random variable following a normal distribution $X \sim N(10, 0.5^2)$.

$$y(X, t) = \frac{1}{X^2 + 4} \sin(2.5\,\mathrm{X}) \cos(t + 0.4)^2 \tag{19}$$

The time-dependent probability of failure is given by

$$p_f(t_0, t_s) = \Pr\{y(X, \tau) > 0.014, \exists \tau \in [1, 2.5]\} \tag{20}$$

According to Eq. (8), $p_f(t_0, t_s)$ is equivalent to the following probability:

$$p_f(t_0, t_s) = \Pr\{Y_{\max} > 0.014\} \tag{21}$$

Before calculating reliability, the mixed EGO model (i.e. Algorithm 3) was at first evaluated because it is the core component of the proposed EGORA method. Different numbers of initial samples of $\mathbf{X}$ and t were generated. $\mathbf{y}^s_{\max}$ corresponding to $\mathbf{x}^s$ were then identified using the existing independent EGO method and the mixed EGO method, respectively. The convergence criterion of the two methods was $\varepsilon_{EI} = 10^{-5}$. The numbers of initial samples of $\mathbf{X}$ were set to 10, 15, 18, and 20. The numbers of function evaluations (NOF) required for identifying $\mathbf{y}^s_{\max}$ for different numbers of initial samples of $\mathbf{X}$ are given in Table 2. Fig. 1 shows the values of $Y_{\max}$ (i.e. $\mathbf{y}^s_{\max}$) obtained from the two methods, as well as the true $Y_{\max}$, for the case that the number of initial samples of $\mathbf{X}$ is ten.

Table 2 NOF required for different number of samples of $\mathbf{X}$

Number of samples of $\mathbf{X}$	NOF	
	Independent EGO	Mixed EGO
10	85	49
15	127	59
18	153	66
20	170	69

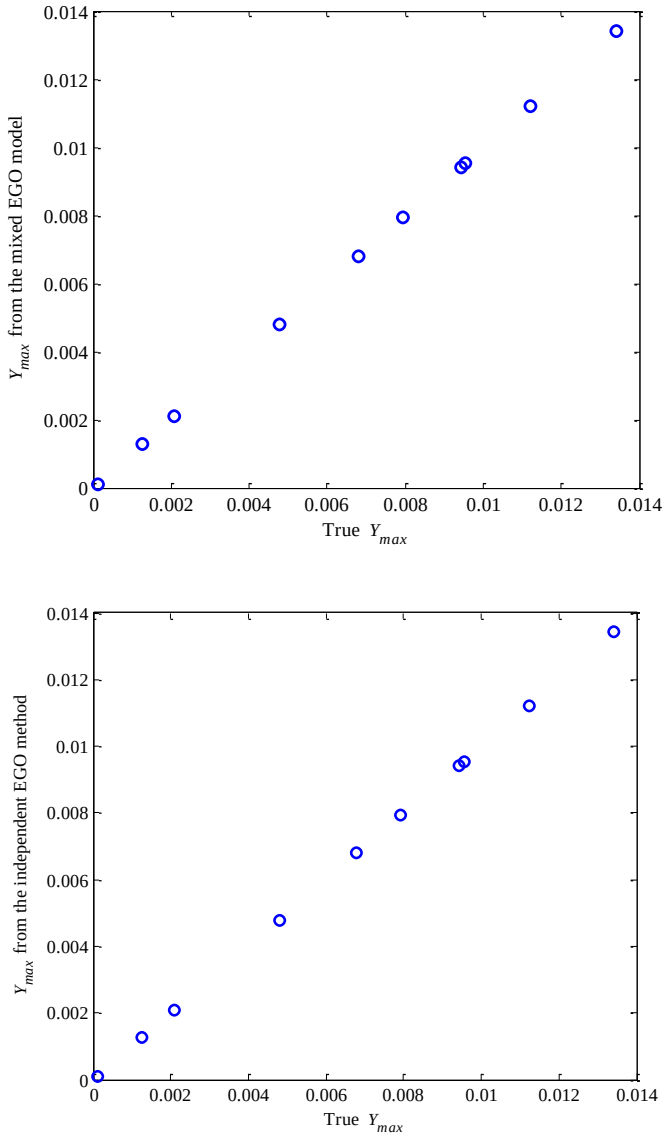

Fig. 1 $Y_{\max}$ obtained from different methods

The results show that both models could accurately extract the extreme responses. The number of function evaluations by the mixed EGO model, however, is less than that by the independent EGO method. This indicates that the mixed EGO model is more efficient. This becomes more apparent when the number of samples of **X** becomes larger.

EGORA was then performed. The number of initial samples of **X** was ten. Fig. 2 shows the constructed surrogate model from EGORA and the true function of the extreme response. The initial samples and the added new samples are also plotted in the figure. The total number of samples of **X** was 18.

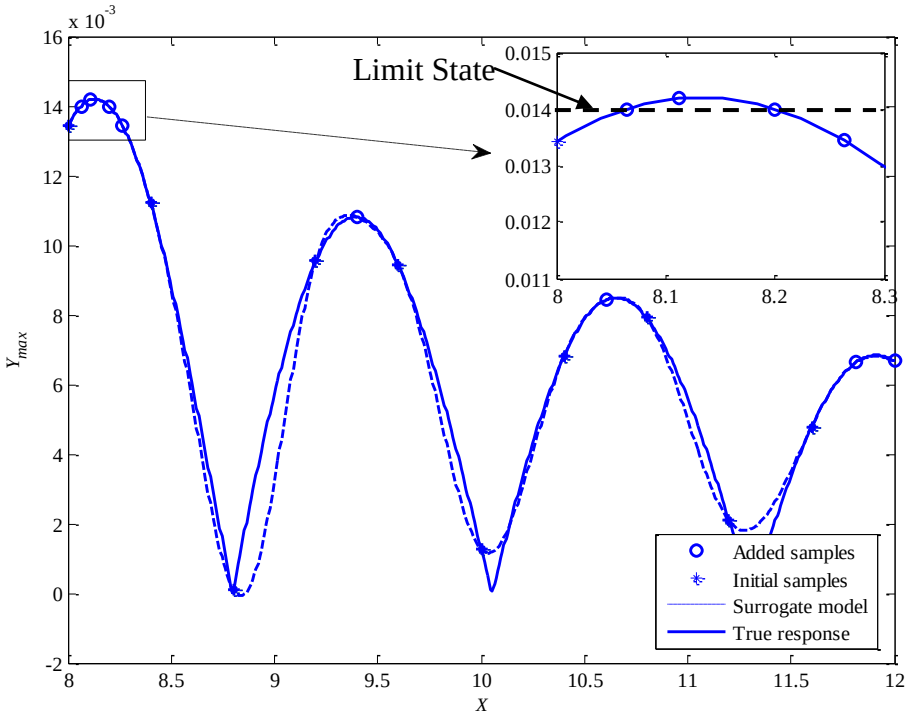

Fig. 2 Surrogate model from EGORA and the true extreme response

The figure shows that the proposed method adds more new samples near the limit state. As revealed in the enlarged section near the limit state in Fig. 2, the surrogate model and the true extreme response curve overlap and are not distinguishable. This makes the surrogate model highly accurate near the limit state and therefore ensures the high accuracy of the reliability analysis.

The surrogate model was also constructed using the independent EGO method. 25 samples of $\mathbf{X}$ were used and a maximum mean square error less than 10^{-5} was achieved. Fig. 3 gives the constructed surrogate model and the true extreme response function. Although the overall accuracy of the surrogate model is better than the one from EGORA, the former is less accurate than the latter near the limit state.

The two surrogate models from independent EGO and EGORA were then used to calculate the time-dependent probability of failure. The calculations were through Monte Carlo simulation (MCS) with sample size of 10^6. To evaluate the accuracy, MCS was also performed using the original limit-state function and used it as a benchmark for the accuracy comparison. The percentage of error is computed by

$$\varepsilon\% = \frac{\left| p_f^{MCS} - p_f \right|}{p_f^{MCS}} \times 100\% \tag{22}$$

where p_f^{MCS} is from MCS based on the original limit-state function, and p_f is from other methods.

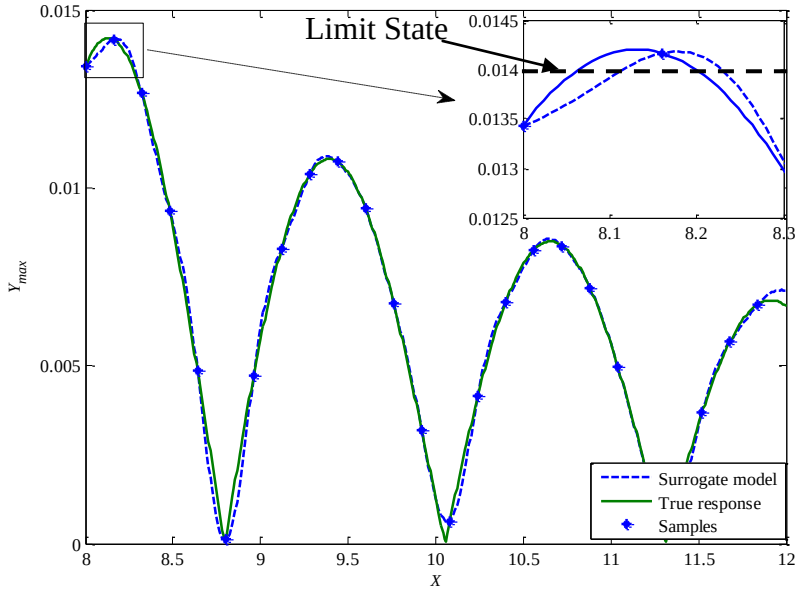

Fig. 3 Surrogate model from independent EGO and the true response

The Rice's formula with FORM was also employed for the accuracy comparison. The results are shown in Table 3.

The results show that the accuracy and efficiency of EGORA are much better than the outcrossing rate method (Rice's formula) and the independent EGO method.

Table 3 Results of example 1

Method	NOF	$p_f(t_0, t_s)$ $(\times 10^{-4})$	Error (%)
Rice	1017	0	100
Independent EGO	212	1.31	20.18
EGORA	69	1.09	0
MCS	5×10^8	1.09	N/A

5.2. A vibration problem

A vibration problem as shown in Fig. 4 was modified from Ref. [33] by treating the stiffness of spring k_2, damping coefficient c_2, and mass m_2 as deterministic parameters and the stiffness of spring k_1 and mass m_1 as random variables. The variables are given in Table 4.

Table 4 Variables and parameters of Example 2

Variable	Mean	Standard deviation	Distribution
k_1 (N/m)	3×10^6	2×10^4	Normal
m_1 (kg)	1.6×10^4	2×10^2	Normal
k_2 (N/m)	8.5×10^4	0	Deterministic
m_2 (kg)	480	0	Deterministic
c_2 (Ns/m)	300	0	Deterministic

The amplitude of the vibration of mass m_1 subjected to force $f_0\sin(\Omega t)$ is given by

$$q_{1\max} = f_0\left(\frac{c_2^2\Omega^2+(k_2-m_2\Omega^2)^2}{c_2^2\Omega^2(k_1-m_1\Omega^2-m_2\Omega^2)^2+(k_2m_2\Omega^2-(k_1-m_1\Omega^2)(k_2-m_2\Omega^2))^2}\right)^{1/2} \quad (23)$$

where Ω is the excitation frequency, which is considered as time, or $t=\Omega$.

Eq. (23) can be nondimensionalized using a 'static' deflection of the main system. The non-dimensional displacement of m_1 is given by [33]

$$Y = g(\mathbf{X},\Omega) = k_1\ K_1/\ K_2+K_3^2\ ^{1/2} \quad (24)$$

where $\mathbf{X}=[k_1, m_1]$, and K_i, $i=1,2,3$, are given by

$$K_1 = c_2^2\Omega^2+(k_2-m_2\Omega^2)^2 \quad (25)$$

$$K_2 = c_2^2\Omega^2(k_1-m_1\Omega^2-m_2\Omega^2)^2 \quad (26)$$

$$K_3 = k_2m_2\Omega^2-(k_1-m_1\Omega^2)(k_2-m_2\Omega^2) \quad (27)$$

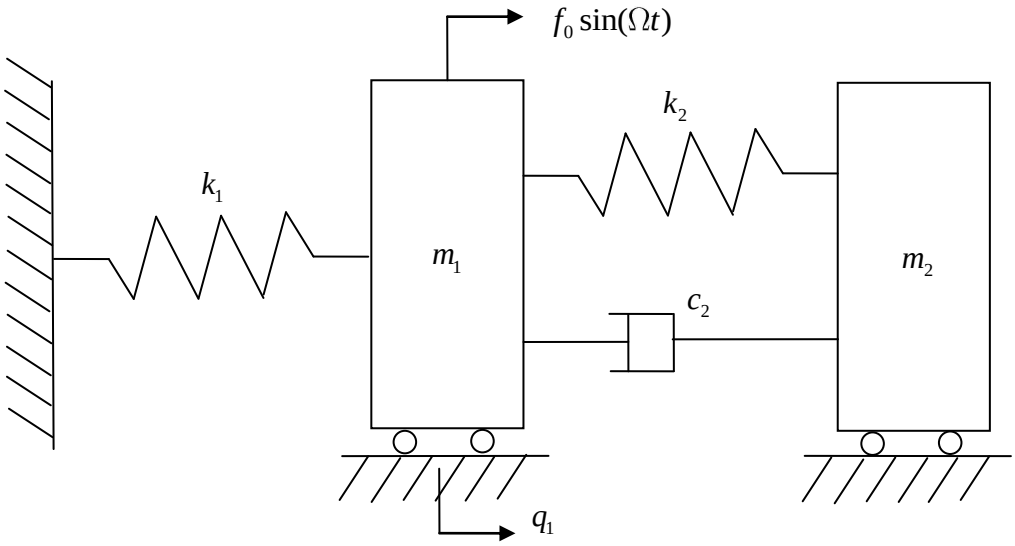

Fig. 4 A vibration problem

Y is considered over a wide excitation frequency band, $8 \le \Omega \le 28$ (rad/s). Since Ω is treated as t, the period of time is $[8, 28]$ rad/s. A failure is defined as the event when Y is larger than 31. The probability of failure on $[8, 28]$ rad/s is given by

$$p_f(8, 28) = \Pr\{g(\mathbf{X}, \Omega) > 31, \exists \Omega \in [8, 28]\} \tag{28}$$

Fig. 5 shows one response of Y at fixed values of k_1 and m_1. It is highly nonlinear.

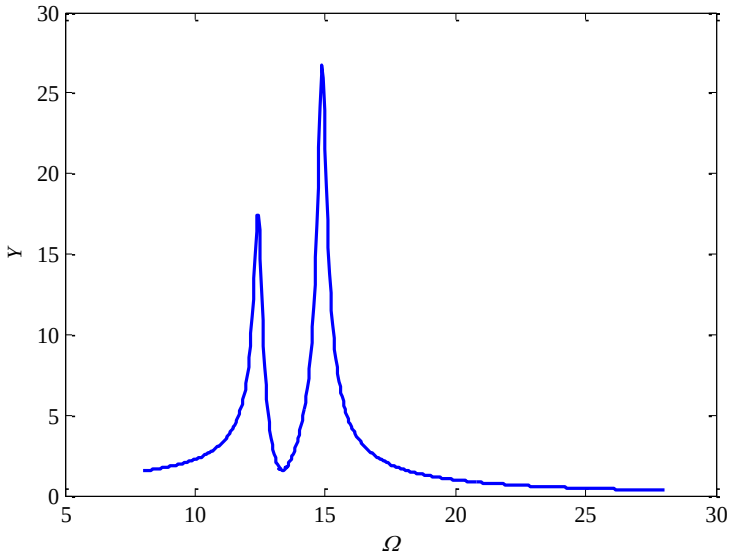

Fig. 5 One response Y at a given set of k_1 and m_1

The maximum response $Y_{\max}$ is even more highly nonlinear as shown by its contours in Fig. 6 and the 3-D plot in Fig. 7.

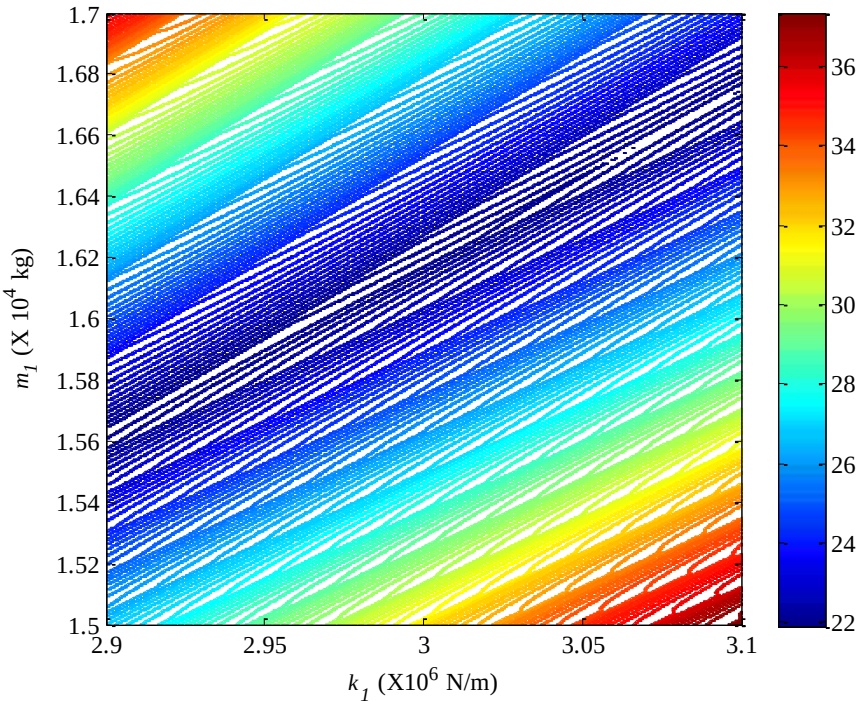

Fig. 6 Exact contours of extreme response $Y_{\max}$

EGORA was used to construct an accurate surrogate model of $Y_{\max}$ in spite the high nonlinearity. 30 initial samples were used, and additional samples were added afterwards. The total number of function calls was 704, and the convergence criterion was $\varepsilon_{EI} = 10^{-5}$ and $\varepsilon_{EF} = 10^{-2}$. The independent EGO method with 140 initial samples was also used, the number of function calls was 2663.

Figs. 8 and 9 show the samples, the contours of the extreme responses, and the limit state from independent EGO and EGORA, respectively. EGORA effectively generated more samples near the limit state as shown in Fig. 9. The independent EGO method produced more evenly distributed samples over the entire design region than the proposed method, but the samples far away from the limit state are not useful. Figs. 10 through 12 give the contours of the extremes responses in the entire design space and

near the two limit state boundaries. The figures indicate that EGORA is more accurate than the independent EGO method near the limit state.

The results of the reliability analysis are given in Table 5, which confirms that EGORA is more accurate than the independent EGO method and the upcrossing rate method.

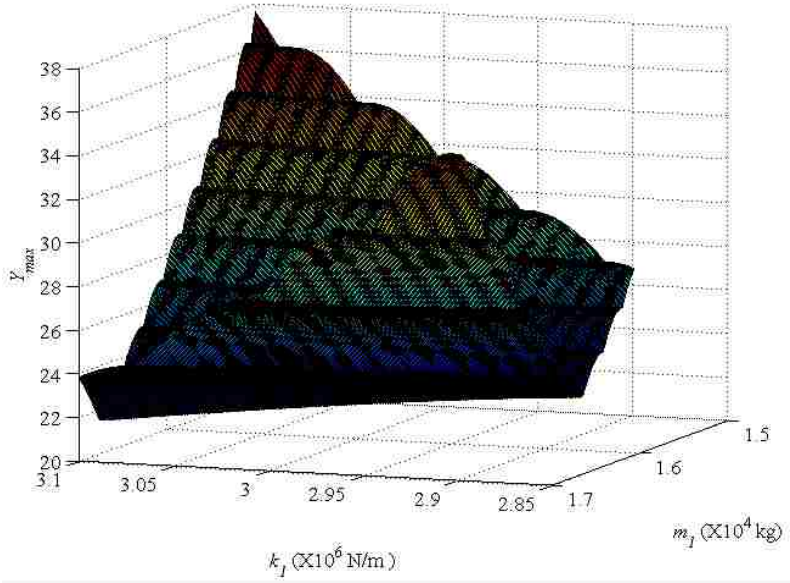

Fig. 7 Three dimensional plot of the extreme response $Y_{\max}$

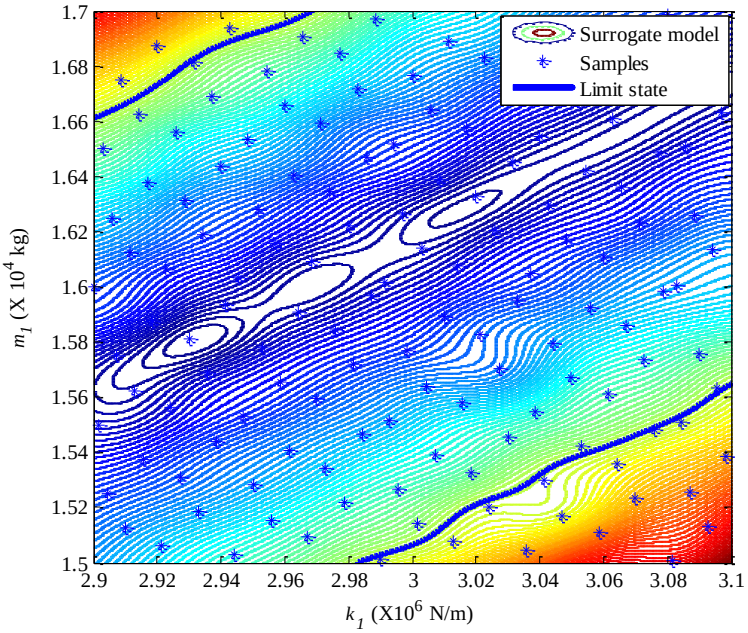

Fig. 8. Samples and contours of $Y_{\max}$ from the independent EGO

Similar to Example 1, the effectiveness of the mixed EGO method was studied by identifying extreme responses under different number of samples of $\mathbf{X}$. The numbers of function calls in Table 6 indicate that the mixed EGO is more efficient than the independent EGO method. The mixed EGO actually reduced more than half of the function evaluations required by the independent EGO method. The former method becomes much more efficient than the latter method when more samples of $\mathbf{X}$ are used.

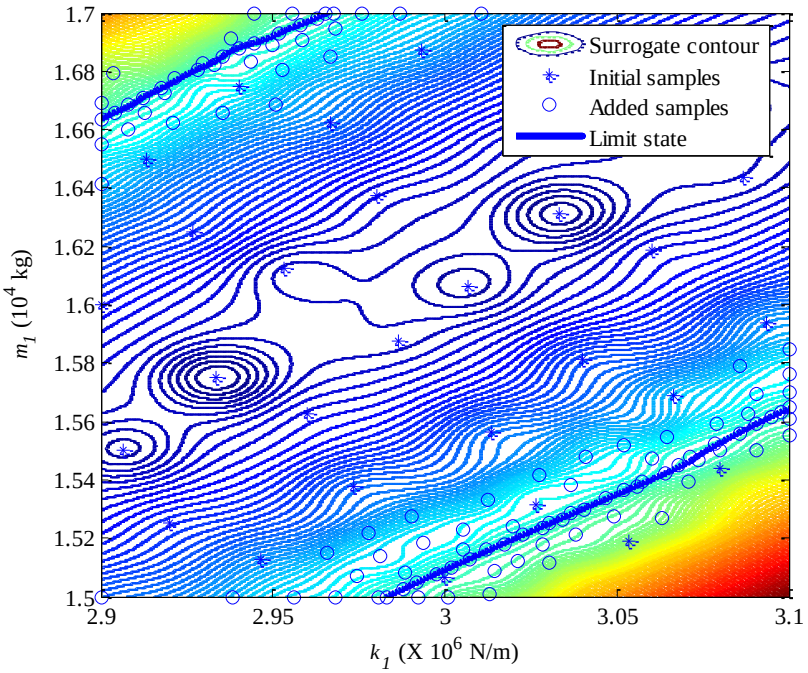

Fig. 9. Samples and contours of $Y_{\max}$ from EGORA

Table 5 Results of Example 2

Method	NOF	p_f $(\times 10^{-5})$	Error (%)
Rice	34235	0	100
Independent EGO	2663	3.9	20
EGORA	704	3.25	0
MCS	1×10^9	3.25	N/A

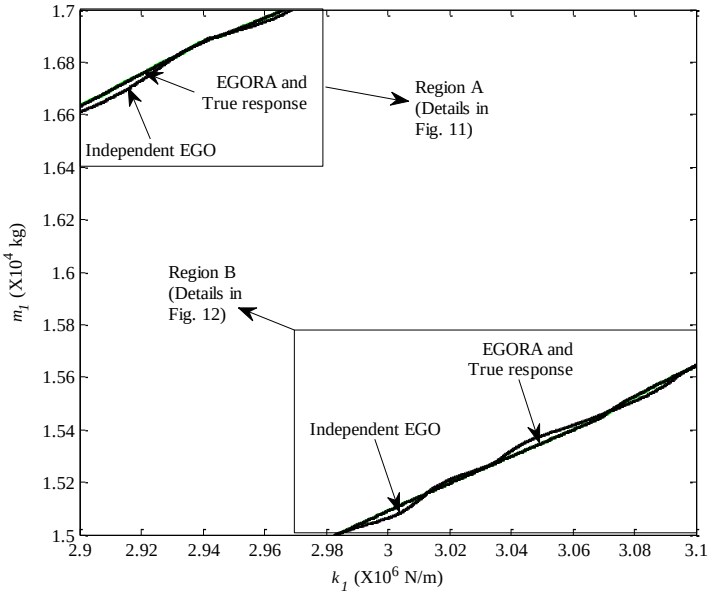

Fig. 10. Contours of extreme response from independent EGO and EGORA at limit state

5.3. A function generator mechanism

A function generator mechanism in Fig. 13 [32] is designed to realized a functional relationship between motion input and motion output. The limit-state function is given by

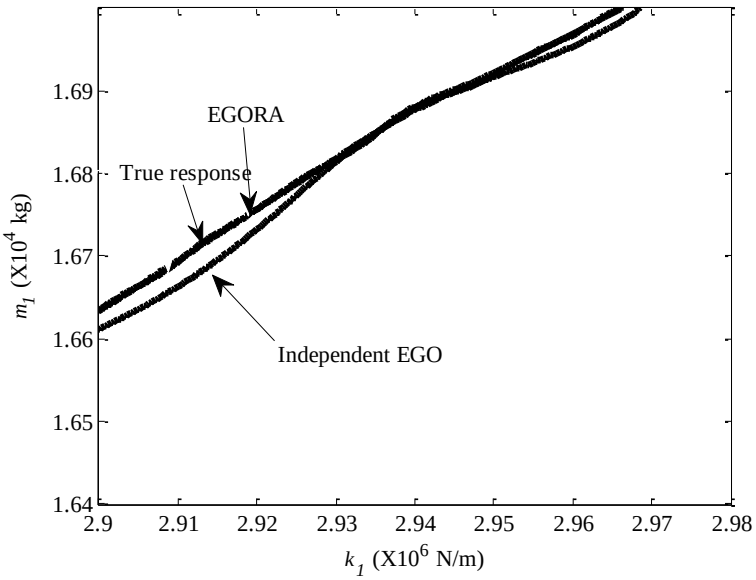

Fig. 11. Enlarged region A

$$\varepsilon(\mathbf{X}, t) = 2\arctan\left(\frac{-E \pm \sqrt{E^2 + D^2 - F^2}}{F - D}\right) - (60^o + 60^o \sin[0.75(t - 97^o)]) \quad (29)$$

where the $\mathbf{X} = [L_1, L_2, L_3, L_4]$, $D = 2L_4(L_1 - L_2\cos(t))$, $E = 2L_2L_4\sin(t)$, $F = L_1^2 + L_2^2 + L_4^2 - L_3^2 - 2L_1L_2\cos(t)$, and the time t represent the motion input, or the angle between links *AB* and *AD*.

The time-dependent probability of failure is computed by

$$p_f(t_0, t_s) = \Pr\{\varepsilon(\mathbf{X}, \tau) > 0.75, \exists\tau \in [97^\circ, 217^\circ]\} \quad (30)$$

The distributions of random variables are given in Table 7.

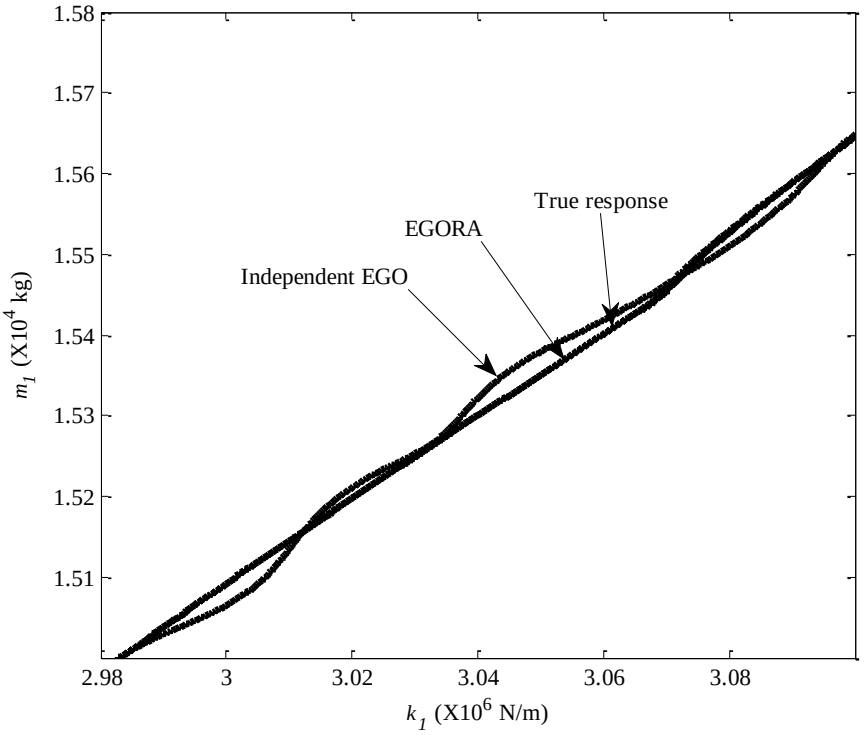

Fig. 12. Enlarged region B

The results from different methods are given in Table 8. 25 initial samples were taken for EGORA and the independent EGO method. As the nonlinearity of the extreme response is not high, both methods converged with the initial samples and produced identical solutions. The number of function evaluations indicates that EGORA is still

more efficient than the independent EGO method for the case where the nonlinearity of the extreme response is not high.

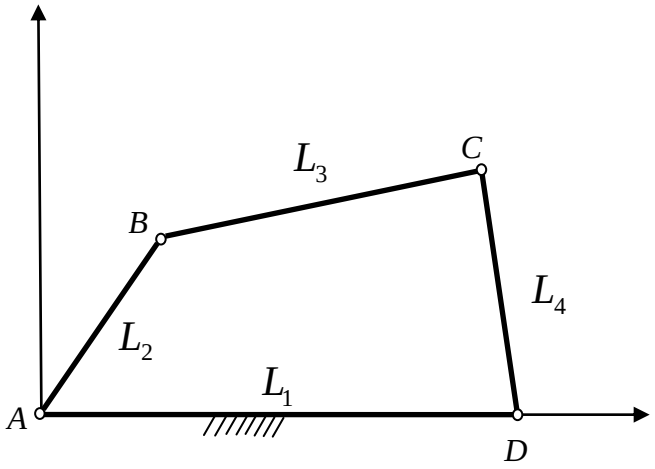

Fig. 13. A four-bar function generator mechanism

Table 6 Number of function evaluations required for different number of samples of **X**

Number of samples of **X**	NOF	
	Nested	Mixed EGO
30	579	156
80	1521	482
110	2142	513
140	2663	588

Table 7 Variables and parameters of Example 3

Variable	Mean	Standard deviation	Distribution
L_1 (mm)	100	0.05	Normal
L_2 (mm)	55.5	0.05	Normal
L_3 (mm)	144.1	0.05	Normal
L_4 (mm)	72.5	0.05	Normal

6. Conclusion

The distribution of the extreme value of a time-dependent limit-state function is required to evaluate the reliability defined within a period of time. The extreme value may be highly nonlinear with a multimodal distribution with respect to random input variables. For this reason, existing approximation methods, such as FORM, SORM, and the upcrossing method, may produce large errors. Using Monte Carlo simulation based on the surrogate model of the extreme response becomes more practical.

Table 8 Results of Example 3

Method	NOF	p_f $(\times 10^{-1})$	Error (%)
Rice	21677	1.986	10.86
Independent EGO	181	2.231	1.3
EGORA	123	2.231	1.3
MCS	5×10^8	2.228	N/A

This works develops a new reliability method that can efficiently and accurately construct surrogate models of extreme responses. The Efficient Global Optimization (EGO) is employed, and the sample points of both the input random variables and time are simultaneously generated. With this treatment, the new method is much more efficient than the existing method where the two sets of samples are generated independently in two nested loops. The surrogate model from the new method is accurate near or at the limit state, and its accuracy in other area is not important for the reliability assessment. This is another reason for the high efficiency. After the surrogate model is available, the reliability can then be easily estimated by Monte Carlo simulation, which will not call the original limit-state function any more.

The new method is based on the Kriging model, and during the sampling and model updating process, the Kriging model is called repeatedly with the cost of computational time. The cost, however, is minor or moderate compared to the time for calling a limit-state function whose evaluation may be computationally expensive. Besides, as a fundamental drawback of Kriging based approaches, high dimensionality

might be a problem. In future, how to overcome this drawback by employing other surrogate model methods will be investigated.

Acknowledgement

This material is based upon work supported by the National Science Foundation through grant CMMI 1234855. The support from the Intelligent Systems Center (ISC) at the Missouri University of Science and Technology is also acknowledged.

References

[1] Du, X., and Hu, Z., 2012, "First order reliability method with truncated random variables," Journal of Mechanical Design, Transactions of the ASME, 134(9).

[2] Zhang, J., and Du, X., 2010, "A second-order reliability method with first-order efficiency," Journal of Mechanical Design, Transactions of the ASME, 132(10).

[3] Li, J., Mourelatos, Z., and Singh, A., 2012, "Optimal Preventive Maintenance Schedule Based on Lifecycle Cost and Time-Dependent Reliability," SAE International Journal of Materials and Manufacturing, 5(1), pp. 87-95.

[4] Singh, A., Mourelatos, Z. P., and Li, J., 2010, "Design for lifecycle cost using time-dependent reliability," Journal of Mechanical Design, Transactions of the ASME, 132(9), pp. 0910081-09100811.

[5] Singh, A., Mourelatos, Z. P., and Nikolaidis, E., 2011, "An importance sampling approach for time-dependent reliability," Proceedings of the ASME Design Engineering Technical Conference, 2011, 5, pp. 1077-1088.

[6] Rice, S. O., 1945, "Mathematical analysis of random noise," Bell Syst.Tech. J.,, 24, pp. 146-156.

[7] Lindgren, G., 1984, "Extremal ranks and transformation of variables or extremes of functions of multivariate Gaussian processes," Stochastic Process and Their Applications, 17, pp. 285-312.

[8] Breitung, K., 1984, "Asymptotic crossing rates for stationary Gaussian vector processes," Tech. Report, 1, Dept. of Math, and Statistics, Univ. of Lund, Lund, Sweden.

[9] Breitung, K., 1988, "Asymptotic approximations for the outcrossing rates of stationary vector processes," Stochast Process Appl, , 13, pp. 195–207.

[10] Ditlevsen, O., 1983, "GAUSSIAN OUTCROSSINGS FROM SAFE CONVEX POLYHEDRONS," Journal of Engineering Mechanics, 109(1), pp. 127-148.

[11] Hagen, O., and Tvedt, L., 1991, "Vector process out-crossing as parallel system sensitivity measure," Journal of Engineering Mechanics, 117(10), pp. 2201-2220.

[12] Hagen, O., and Tvedt, L., 1992, "Parallel system approach for vector out-crossing," Journal of Offshore Mechanics and Arctic Engineering, 114(2), pp. 122-128.

[13] Andrieu-Renaud, C., Sudret, B., and Lemaire, M., 2004, "The PHI2 method: A way to compute time-variant reliability," Reliability Engineering and System Safety, 84(1), pp. 75-86.

[14] Hu, Z., and Du, X., 2012, "Reliability analysis for hydrokinetic turbine blades," Renewable Energy, 48, pp. 251-262.

[15] Vanmarcke, E. H., 1975, "On the distribution of the first-passage time for normal stationary random processes," Journal of Applied Mechanics, 42, pp. 215-220.

[16] Madsen, P. H., and Krenk, S., 1984, "Integral equation method for the first-passage problem in random vibration," Journal of Applied Mechanics, Transactions ASME, 51(3), pp. 674-679.

[17] Hu, Z., and Du, X., 2013, "Time-dependent reliability analysis with joint upcrossing rates," Structural and Multidisciplinary Optimization, pp. 1-15.

[18] Hu, Z., Li, H., Du, X., and Chandrashekhara, K., 2012, "Simulation-based time-dependent reliability analysis for composite hydrokinetic turbine blades," Structural and Multidisciplinary Optimization, pp. 1-17.

[19] Bichon, B. J., Eldred, M. S., Swiler, L. P., Mahadevan, S., and McFarland, J. M., "Multimodal reliability assessment for complex engineering applications using efficient global optimization," pp. 3029-3040.

[20] Wang, Z., and Wang, P., 2012, "A nested extreme response surface approach for time-dependent reliability-based design optimization," Journal of Mechanical Design, Transactions of the ASME, 134(12).

[21] Chen, J. B., and Li, J., 2007, "The extreme value distribution and dynamic reliability analysis of nonlinear structures with uncertain parameters," Structural Safety, 29(2), pp. 77-93.

[22] Jones, D. R., Schonlau, M., and Welch, W. J., 1998, "Efficient Global Optimization of Expensive Black-Box Functions," Journal of Global Optimization, 13(4), pp. 455-492.

[23] Hu, Z., and Du, X., 2013, "A sampling approach to extreme value distribution for time-dependent reliability analysis," Journal of Mechanical Design, Transactions of the ASME, 135(7).

[24] Hu, Z., and Du, X., 2013, "Lifetime cost optimization with time-dependent reliability," Engineering Optimization(ahead-of-print), pp. 1-22.

[25] Grogan, J. A., Leen, S. B., and McHugh, P. E., 2013, "Optimizing the design of a bioabsorbable metal stent using computer simulation methods," Biomaterials, 34(33), pp. 8049-8060.

[26] Lockwood, B., and Mavriplis, D., 2013, "Gradient-based methods for uncertainty quantification in hypersonic flows," Computers and Fluids, 85, pp. 27-38.

[27] Raghavan, B., and Breitkopf, P., 2013, "Asynchronous evolutionary shape optimization based on high-quality surrogates: Application to an air-conditioning duct," Engineering with Computers, 29(4), pp. 467-476.

[28] Steponaviče, I., Ruuska, S., and Miettinen, K., 2014, "A solution process for simulation-based multiobjective design optimization with an application in the paper industry," CAD Computer Aided Design, 47, pp. 45-58.

[29] Lophaven;, S. N., Nielsen;, H. B., and Søndergaard, J., 2002, "DACE-A MATLAB Kriging Toolbox," Technical University of Denmark.

[30] Chen, W., Tsui, K.-L., Allen, J. K., and Mistree, F., "Integration of the response surface methodology with the compromise decision support problem in developing a general robust design procedure," Proc. American Society of Mechanical Engineers, Design Engineering Division (Publication) DE 82 (1), pp. 485-492 pp. 485-492.

[31] Hosder, S., Walters, R. W., and Balch, M., "Efficient sampling for non-intrusive polynomial chaos applications with multiple uncertain input variables," pp. 2946-2961.

[32] Zhang, J., and Du, X., 2011, "Time-dependent reliability analysis for function generator mechanisms," Journal of Mechanical Design, Transactions of the ASME, 133(3).

[33] Zang, C., Friswell, M. I., and Mottershead, J. E., 2005, "A review of robust optimal design and its application in dynamics," Computers and Structures, 83(4-5), pp. 315-326.

PAPER
III. SIMULATION-BASED TIME-DEPENDENT RELIABILITY ANALYSIS FOR COMPOSITE HYDROKINETIC TURBINE BLADES

Zhen Hu, Haifeng Li, Xiaoping Du[2], K. Chandrashekhara
Department of Mechanical and Aerospace Engineering
Missouri University of Science and Technology

Abstract

The reliability of blades is vital to the system reliability of a hydrokinetic turbine. A time-dependent reliability analysis methodology is developed for river-based composite hydrokinetic turbine blades. Coupled with the blade element momentum theory, finite element analysis is used to establish the responses (limit-state functions) for the failure indicator of the Tsai-Hill failure criterion and blade deflections. The stochastic polynomial chaos expansion method is adopted to approximate the limit-state functions. The uncertainties considered include those in river flow velocity and composite material properties. The probabilities of failure for the two failure modes are calculated by means of time-dependent reliability analysis with joint upcrossing rates. A design example for the Missouri river is studied, and the probabilities of failure of the turbine blade over twelve months are studied.

1. Introduction

River-based hydrokinetic turbines extract kinetic energy from flowing water of a stream, river, or current [1, 2]. They have similar working principles as wind turbines. The main difference between hydrokinetic turbines and wind turbines is their working environment. The density of water, in which hydrokinetic turbines are put into operation, is about 800 times higher than that of air. Hydrokinetic turbines are advantageous over conventional hydro-power and wind power in the following aspects [3]: A hydrokinetic

[2] Corresponding author, 400 West 13th Street, Toomey Hall 290D, Rolla, MO 65401, U.S. A., Tel:1-573-341-7249, email: dux@mst.edu

turbine does not alter natural pathways of rivers; its energy extraction is much higher than the other renewable power technologies; it requires less civil engineering work and introduces less hazards to the environment; the application of hydrokinetic turbines is more flexible. Due to the significant advantages of hydrokinetic turbines, this technology has attracted increasing attention of researchers in recent years [4, 5].

As the most important part of the hydrokinetic turbine system, the turbine blade has a high requirement for its performance and strength [6]. Composite materials offer several advantages, such as high ratio of strength to weight, resistance to corrosion, excellent fatigue resistance, and design flexibility. These make composite materials an attractive choice for the construction of turbine blades. Besides, applications of composite materials in the marine and ocean engineering demonstrated that the load-induced deformations of composite elliptic hydrofoils can delay cavitation inception while maintaining the overall lift and drag [7].

Due to the complex manufacturing process, the material properties of composites tend to be more random than metallic materials [8]. For instance, the overall performance of composite turbine blades can be affected by fiber misalignments, voids, laminate properties, boundary conditions and so on [9-11]. There are also many uncertain factors existing in the working environment of turbines and composite structures. In recent years, efforts have been made to reduce the effects of uncertainties on the performance of composite structures and turbine blades. For example, Toft and Sørensen [12] established a probabilistic framework for design of wind turbine blades by adopting a reliability-based design approach. Val and Chernin [13] assessed the reliability of tidal turbine blades with respect to the failure in bending. Motley [14] presented a reliability-based global optimization technique for the design of a marine rotor made of advanced composite. Similarly, Young et al. [8] used a reliability-based design and optimization methodology for adaptive marine structures. They mitigated the influence of composite material uncertainty on the performance of self-adaptive marine rotors. Christopher and Masoud [15] applied the probabilistic design modeling and reliability-based design optimization methodology to the optimization of a composite submarine structure. More developments about the probabilistic design method in the design and optimization of composite structures can be found in [16].

The most commonly used methods for the probabilistic design of composite structures and turbine blades can be classified into two categories: reliability-based design optimization (RBDO) and the inverse reliability design (IRD). RBDO is a methodology that ensures the reliability is satisfied at a desired level by introducing the reliability constraints into the design optimization framework [17]. IRD identifies the design loading using the inverse reliability analysis method [18]. Even though the existing RBDO and IRD methods can be employed for the design of regular composite structures and wind turbine blades, it is hard to use them to guarantee the reliability of composite hydrokinetic blades over the service life. The reason is that most existing RBDO and IRD methods employed for the design of composite structures and turbine blades are based on time-invariant reliability analysis, while the uncertainties in hydrokinetic turbine blades always change with time. For instance, the river flow climate, which governs the loading of turbine blades, is a stochastic process with strong auto-correlations [19, 20]. This means that the monthly river flow velocity has much longer memory than the wind climate and that the reliability of hydrokinetic turbine blades is time dependent. The Monte Carlo simulation (MCS) can be used for time-dependent reliability analysis, but it is computationally expensive. Efficient time-dependent reliability analysis methods, therefore, need to be employed for the probabilistic design of composite hydrokinetic turbine blades.

In the past decades, many methods have been proposed for the time-dependent reliability analysis, such as the Gamma distribution method, Markov method [21], and the upcrossing rate method [22]. Amongst the above methods, the upcrossing rate method is the most widely used one [23, 24], which has been applied to the time-dependent reliability analysis for function generator mechanism [25], steel beam under stochastic loading [26], and hydrokinetic turbine blades [27]. As the method in [25-27] is based on the simple Poisson assumption, it cannot well take into account the correlation of river velocities at different time instants. A more accurate method called the first order reliability method with joint upcrossing rate (JUR/FORM) has been recently developed [28]. This method combines the joint upcrossing rates (JUR) with First Order Reliability Method (FORM). It is suitable for the time-dependent reliability analysis of composite hydrokinetic turbine blades in this work.

The objective of this work is to develop a reliability analysis model for composite hydrokinetic turbine blades by quantifying the effects of uncertainties in river flow velocity and composite material properties on the performance of hydrokinetic turbine blades over the design life. It is an improved work of the reliability analysis method of hydrokinetic turbine blades presented in [27]. The finite element method (FEM) is employed to analyze the performances of the hydrokinetic turbine blade. The JUR/FORM reliability analysis method is adopted for reliability analysis. A three-blade horizontal-axis hydrokinetic turbine system developed for the Missouri river is studied. The probabilities of failure of turbine blades according to the Tsai-Hill failure criterion and excessive deflections are analyzed.

The remainder of the paper is organized as follows: In Section 2, the state of the art of the time-dependent reliability analysis methods is provided. Following that, in Section 3, uncertainties that affect the performance of composite hydrokinetic turbine blades are analyzed and the potential failure modes of turbine blades are studied. In Section 4, the way of modeling the loading of turbine blades and the methods employed to establish the limit-state functions are discussed. A design example is given in Section 5 and conclusions are made in Section 6.

2. The State of the Art of Time-Dependent Reliability Analysis Methods

Reliability analysis problems can be divided into the following two categories:

- Time-invariant reliability problems with random variables
- Time-dependent reliability problems with stochastic processes

In the past decades, many methods have been developed for time-invariant reliability problems. These methods include FORM, Second Order Reliability Analysis Method (SORM), and Importance Sampling Method (ISM).

For the time-dependent reliability analysis problems, such as the reliability analysis of composite hydrokinetic turbine blades under stochastic river flow loading, are much more complicated. To show the complexities, in the following subsections, this work first discusses the differences between the two reliability problems and then reviews several methodologies for time-dependent reliability analysis.

2.1. Time-dependent reliability and time-invariant reliability

Time-invariant reliability does not change over time while the time-dependent reliability does. Let a general limit-state function be

$$G = g(\mathbf{X}, \mathbf{Y}(t), t) \tag{1}$$

in which $\mathbf{X} = [X_1, X_2, \cdots, X_n]$ is a vector of random variables, and $\mathbf{Y}(t) = [Y_1(t), Y_2(t), \cdots Y_m(t)]$ is a vector of stochastic processes.

(a) Time-dependent reliability

For the general limit-state function in Eq. (1), the response variable G is a random variable at any instant of time. Let the threshold of a failure be e. If a failure occurs when $G = g(\mathbf{X}, \mathbf{Y}(t), t) > e$, the time-dependent probability of failure over a time interval $[t_0, t_s]$ is given by

$$P_f(t_0, t_s) = \Pr\left\{g(\mathbf{X}, \mathbf{Y}(t)) > e, \exists\, t \in [t_0, t_s]\right\} \tag{2}$$

where $\Pr\{\cdot\}$ stands for the probability.

The corresponding time-dependent reliability is given by

$$R(t_0, t_s) = \Pr\left\{g(\mathbf{X}, \mathbf{Y}(t)) < e, \forall\, t \in [t_0, t_s]\right\} \tag{3}$$

The time-dependent reliability tells us the likelihood that no failure will occur over a time period.

(b) Time-invariant reliability

At a specified time instant t_i, the reliability is given by

$$R(t_i) = \Pr\left\{g(\mathbf{X}, \mathbf{Y}(t_i)) < e\right\} \tag{4}$$

This reliability is called instantaneous reliability or time-invariant reliability. It is the probability that the response variable is not greater than the threshold at t_i, thereby not in the failure region, regardless whether a failure has occurred or not prior to t_i. It is meaningful for only time-invariant limit-state functions $g(\mathbf{X})$, which does not depend on time, resulting a constant reliability. For a time-dependent problem over $[t_0, t_s]$, the instantaneous reliability is only used for the initial reliability at $t = t_0$.

The methods for the time-invariant reliability, however, may not be directly used to calculate the time-dependent reliability. The major reason is that the time-dependent reliability is defined over a time period, which consists of infinite numbers of time instants where the response variables are dependent.

2.2. Methodologies for time-dependent reliability analysis

2.2.1. MCS for time-dependent reliability analysis

The implementation of MCS for time-dependent reliability analysis is quite different from that for time-invariant one. The differences lie on the ways of counting failure events and generating random samples.

If stochastic processes are involved, trajectories (sample traces) of the processes need to be generated first. Since a trajectory is a continuous function of time, many discretization points (time instants) need to be used to accurately represent the function. At each of the time instants, a stochastic process is a random variable and the random variables at all the time instants are usually dependent. As a result, the random samples are stored in a two-dimensional array – one is indexed by time instants, and the other is indexed by random trajectories. For a time-invariant problem, the samples are represented by just a one-dimensional array because no time is involved. The size of the samples of a time-dependent problem is therefore much higher than that of a time-invariant one.

After the samples are generated, a limit-state function will be evaluated at all the sample points. Compared to a time-invariant problem, the number of function calls for a time-dependent problem will be much higher because of the above reason. By comparing the value of a limit-state function against the failure threshold, if a failure occurs will be known. If the limit-state function value is greater than the threshold at any discretized time instant, the event is considered as a failure. The details of MCS for time-dependent reliability analysis are provided in Appendix A.

Due to its high computational cost, MCS is not practically used for time-dependent reliability analysis, but may be used as a benchmark for the accuracy assessment for other reliability analysis methods.

2.2.2. Poisson assumption based upcrossing rate method

Given its high efficiency, the Poisson assumption based upcrossing rate method has been widely used [25-27]. With this method, the time-dependent probability of failure over time interval $[t_0, t_s]$ is computed by

$$p_f(t_0, t_s) = 1 - [1 - p_f(t_0)] \exp\left\{-\int_{t_0}^{t_s} v^+(t)dt\right\} \tag{5}$$

in which $v^+(t)$ is the upcrossing rate at time *t*, and $p_f(t_0)$ stands for the instantaneous probability of failure at the initial time.

It is difficult to obtain the upcrossing rate $v^+(t)$. One effective way is using FORM. FORM transforms random variables $\{\mathbf{X}, \mathbf{Y}(t)\}$ into the standard normal variables $\mathbf{U}(t) = [\mathbf{U}_\mathbf{X}, \mathbf{U}_\mathbf{Y}(t)]$. Then the limit state function becomes $G = g(\mathbf{U}(t), t)$ [25]. After the linearization of the limit-state function at the Most Probable Point (MPP) $\mathbf{u}^*(t)$, the upcrossing rate $v^+(t)$ is computed using the Rice's formula [29, 30] as follows:

$$v^+(t) = \omega(t)\phi\big(\beta(t)\big)\{\phi(\dot{\beta}(t)/\omega(t)) - [\dot{\beta}(t)/\omega(t)]\Phi(-\dot{\beta}(t)/\omega(t))\} \tag{6}$$

where $\phi(\cdot)$ and $\Phi(\cdot)$ represent the probability density function (PDF) and cumulative distribution function (CDF) of a standard normal random variable, respectively,
and

$$\beta(t) = \left\|\mathbf{u}^*(t)\right\| \tag{7}$$

in which $\|\cdot\|$ stands for the magnitude of a vector.

$\omega(t)$ is given by

$$\omega^2(t) = \dot{\boldsymbol{\alpha}}(t)\dot{\boldsymbol{\alpha}}^T(t) + \boldsymbol{\alpha}(t)\ddot{\mathbf{C}}_{12}(t, t)\boldsymbol{\alpha}^T(t) \tag{8}$$

where

$$\boldsymbol{\alpha}(t) = \nabla\mathbf{g}(\mathbf{u}^*(t), t) / \left\|\nabla\mathbf{g}(\mathbf{u}^*(t), t)\right\| \tag{9}$$

and

$$\ddot{\mathbf{C}}_{12}(t_1,t_2)=\ddot{\mathbf{C}}_{21}(t_1,t_2)=\begin{bmatrix}\mathbf{0} & \mathbf{0} & \cdots & \mathbf{0}\\ \mathbf{0} & \partial^2\rho^{Y_1}(t,t)/\partial t_1\partial t_2 & \cdots & 0\\ \vdots & \vdots & \ddots & \vdots\\ \mathbf{0} & 0 & \cdots & \partial^2\rho^{Y_m}(t,t)/\partial t_1\partial t_2\end{bmatrix}_{(n+m)\times(n+m)} \tag{10}$$

in which $\rho^{Y_i}(t,t)$ is the autocorrelation coefficient function of stochastic process Y_i.

$\dot{\boldsymbol{\alpha}}(t)$ and $\dot{\beta}(t)$ are the derivatives of $\boldsymbol{\alpha}(t)$ and $\beta(t)$, respectively.

Even if the Poisson assumption based upcrossing rate method has been widely used, large errors have been reported for this method by Madsen etc. [31-34]. One of the main error sources is the Poisson assumption, which assumes that the events that the response upcrosses the failure threshold are completely independent from each other. This assumption does not hold for many cases because there are always some correlations between the failure events and failures may occur in clusters. To overcome this drawback, Madsen [31] proposed a method to consider the correlation between two time instants of a Gaussian process. His method focuses on only Gaussian processes. Vanmarcke [32] has made some empirical modifications to the Poisson assumption based method. His modifications, however, are limited to stationary Gaussion process. Most recently, Singh [34] has established a "composite" limit-state function method, which can accurately estimate the time-dependent reliability problems with limit-state functions in a form of $G=g(\mathbf{X},t)$, where there are no input stochastic processes. The JUR/FORM [28] method has recently been developed by extending Madsen's method [31] for more general problems with both random variables and non-stationary stochastic processes. The main idea of the JUR/FORM is then reviewed.

2.2.3. JUR/FORM

JUR/FORM aims to release the Poisson assumption by considering the correlations between the limit-state function at two time instants. It can be applied to general problems with both random variables and stochastic processes. Since it is based on FORM, it is much more efficient than MCS while the accuracy is higher than the traditional upcrossing method. With this method, the time-dependent probability of failure $p_f(t_0,t_s)$ is computed by

$$p_f(t_0,t_s)=\Pr\{g(\mathbf{X},\mathbf{Y}(t_0),t_0)>e\}+\Pr\{g(\mathbf{X},\mathbf{Y}(t_0),t_0)<e\}\int_{t_0}^{t_s} f_{T_1}(t)\,dt \quad (11)$$

where $f_{T_1}(t)$ is the PDF of the first-time to failure. $\Pr\{g(\mathbf{X},\mathbf{Y}(t_0),t_0)>e\}$ is the probability of failure at the initial time, and $\Pr\{g(\mathbf{X},\mathbf{Y}(t_0),t_0)<e\}\int_{t_0}^{t_s} f_{T_1}(t)\,dt$ is the probability of failure over $[t_0,t_s]$ given that no failure occurs at the initial time.

$f_{T_1}(t)$ can be obtained by solving the following integral equation [31]:

$$v^+(t)=f_{T_1}(t)+\int_{t_0}^{t} v^{++}(t,\tau)\,f_{T_1}(\tau)/v^+(\tau)d\tau \quad (12)$$

in which $v^+(\tau)$ is given in Eq. (6), and $v^{++}(t,\tau)$ stands for the joint probability that there are upcrossings at both *t* and τ. The equations for $v^{++}(t,\tau)$ are given in Appendix B.

Given its advantages, JUR/FORM is used for the reliability analysis of the composite hydrokinetic turbine blades. MCS is also used to verify the accuracy of JUR/FORM.

Fig. 1 shows the three steps of JUR/FORM [28]. In the first step, the time-interval is divided into discretized time instants. FORM is then used to search for MPPs at every time instant and calculate $\boldsymbol{\alpha}(t_i),\boldsymbol{\beta}(t_i),\dot{\boldsymbol{\alpha}}(t_i),\dot{\boldsymbol{\beta}}(t_i)$ and $\mathbf{C}(t_i,t_j)$. The PDF $f_{T_1}(t)$ can then be obtained using Eqs. (6) and (12), and the formulas in Appendix B. Finally, the time-dependent probability of failure is calculated by Eq. (11).

In the following section, this work discusses how to apply the time-dependent reliability analysis method to evaluate the reliability of composite hydrokinetic turbine blades over the design life.

3. Uncertainty and Failure Modes Analysis for Composite Hydrokinetic Turbine Blades

3.1. Uncertainty analysis

3.1.1. River flow velocity

Due to the natural variability, the river flow velocity is the major uncertainty inherent in the working environment of hydrokinetic turbine blades. It is directly related to the safety of the turbine blade. Analyzing the uncertainty of the river flow velocity is

critical to the reliability analysis of hydrokinetic turbine blades. The river flow velocity, however, is difficult to be modeled exactly since it varies both in space and time. To present the variation of river flow velocity over space and time, many historical river flow velocity data at different locations of the river cross section are needed. This kind of data is not available at most of the time. In order to overcome this limitation, Hu and Du [27] proposed to present the river flow velocity in the form of river discharge, of which the data have been recorded for many rivers.

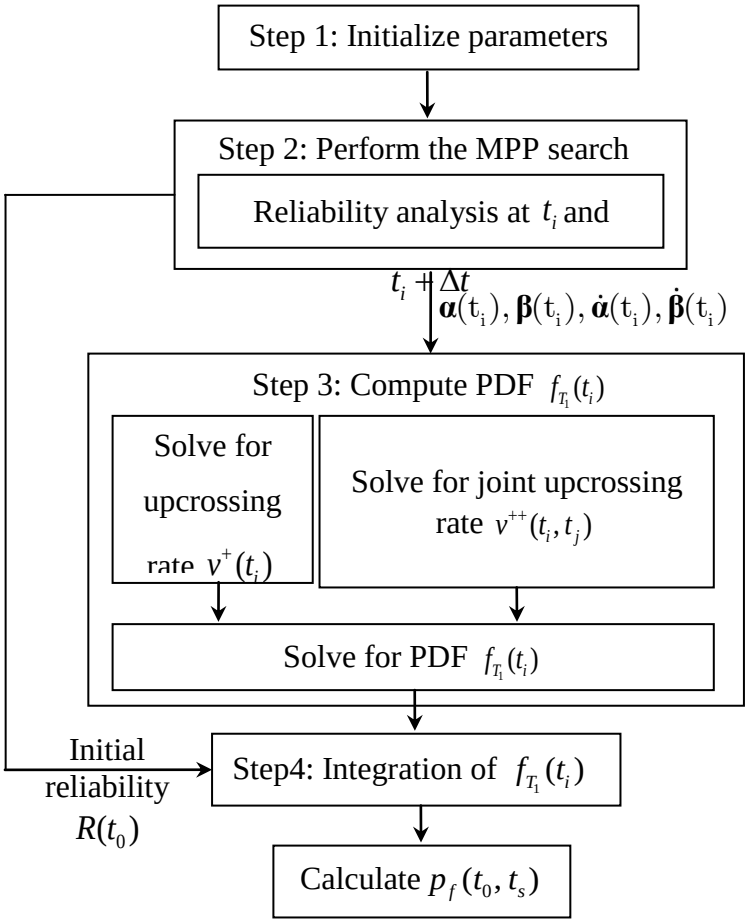

Fig. 1. Numerical procedure of JUR/FORM

With the river discharge and the assumption that the shape of a river bed is a rectangle, the cross section average river flow velocity is calculated by the Manning-Strickler formula as follows [35-37]:

$$v(t) = n_r^{-1} Q(t)^{2/3} S^{1/2} \tag{13}$$

in which $v(t)$ is the river water flow velocity (m/s), n_r is the river bed roughness, S is the river slope (m/m), and $Q(t)$ is given by [27, 37]

$$Q(t) = \frac{0.946 d_m^{0.898}}{0.698 d_m^{0.341} + 2.71 d_m^{0.557}} \tag{14}$$

where d_m is the monthly discharge of the river $(\mathrm{m}^3/\mathrm{s})$.

The distribution of d_m is lognormal [38, 39], and its CDF is given by

$$F_{D_m}(d_m) = \Phi\left(\frac{\ln(d_m) - \mu_{D_m}(t)}{\sigma_{D_m}(t)}\right) \tag{15}$$

in which $\mu_{D_m}(t)$ and $\sigma_{D_m}(t)$ are the mean and standard deviation of $\ln(d_m)$, respectively. These two parameters are time-dependent because the river discharge varies seasonally.

The autocorrelation coefficient of the normalized and standardized monthly river discharge is approximated by [20, 40]

$$\rho_{D_m}(t_1, t_2) = \exp\left(-\left(\frac{t_2 - t_1}{\zeta}\right)^2\right) \tag{16}$$

where ζ is the correlation length. Therefore, after normalization and standardization, the monthly river discharge can be presented by its underlying Gaussian process with autocorrelation coefficient function given in Eq. (16).

3.1.2. Uncertainties in composite materials

The hydrokinetic turbine blade is made of fiberglass/epoxy laminates with $[0/90/0/90/0]_s$ symmetric configurations. Due to the natural variability in laminate properties, fiber misalignment, and the fabrication process of composite materials, uncertainties exist in the stiffness of composite materials. Herein, four variables are represented by probability distributions. These random variables are E_{11} and E_{22} (E_{33}) (elastic modulus along direction 1, 2 and 3), G_{12} (G_{13}), and G_{23} (shear modulus). All the random variables are normally distributed. As suggested in [8], a 2% coefficient of variation was assigned to the material parameters of the composite material as shown in Table 1. The coefficient of variation is the ratio of the standard deviation to the mean of a random variable.

Table 1. Distributions of random variables of the composite material

Variable	Value		Distribution type
	Mean	Coefficient of variation	
Young's modulus	E_{11}=45.6 GPa	0.02	Gaussian
	E_{22}=E_{33}=16.2 GPa	0.02	Gaussian
Shear Modulus	G_{12}= G_{13}=5.83 GPa	0.02	Gaussian
	G_{23}=5.786 GPa	0.02	Gaussian

After identifying the uncertainties in the composite hydrokinetic turbine blade, the potential failure modes that may occur during the operation of turbine blades are identified.

3.2. Failure modes of composite hydrokinetic turbine blades

The failure modes of wind turbine blades have been reported in literature. They can be used as a reference for analyzing hydrokinetic turbine blades because both wind and hydrokinetic turbine blades share similar working principles. For wind turbine blades, the commonly studied failure modes include failures due to fatigue [41, 42], extreme stresses [43, 44], excessive deflections [45], corrosion [46, 47], and so on. Based on the studied failure modes, in this work, the failure modes with respect to the Tsai-Hill failure criterion and excessive deflection are the main focuses. The major reason of doing this is that the extreme stress and deflection can be obtained from static analysis and that the two failure modes can be analyzed using the same kind of reliability analysis method.

The fatigue of turbine blades is also critical to the reliability of a turbine system. The fatigue reliability analysis requires a stress cycle distribution of blades obtained from a large number of simulations or experiments. It also needs stochastic S-N curve to account for uncertainties in material fatigue tests. It is a much more challenging task and will be one of the future works.

3.2.1. The Tsai-Hill failure criterion for composite turbine blades

For plane stresses, the failure indicator of the Tsai-Hill criterion is

$$f_{ind} = \frac{\sigma_1^2}{s_L^2} - \frac{\sigma_1\sigma_2}{s_L^2} + \frac{\sigma_2^2}{s_T^2} + \frac{\tau_{12}^2}{s_{LT}^2} \tag{17}$$

where σ_1, σ_2 and τ_{12} are local stresses in a lamina with reference to the material axes. s_L, s_T and s_{LT} are the failure strengthes in the principal material directions. s_L stands for the longitudinal strength in fiber direction (direction 1), s_T denotes transverse strength in matrix direction (direction 2), and s_{LT} indicates the in-plane shear strength (in plane 1-2).

If $\sigma_1 > 0$, use longitudinal tensile strength for s_L; if $\sigma_2 > 0$, use transverse tensile strength for s_T; otherwise, use the compressive strength for s_L and s_T. To determine whether the composite blade laminate will fail due to applied loading, the method first calculates stresses across the different plies, followed by applying the Tsai-Hill interactive failure criterion based on these stress levels. The composite blade laminate is considered to fail when a first ply fails. This point of failure is the first ply failure (FPF) [48, 49], beyond which the laminate may still carry the load. For a safe design, the composite laminates should not experience stress high enough to cause FPF. Fig. 2 shows a failure evaluation of hydrokinetic turbine blade using the Tsai-Hill criterion in ABAQUS.

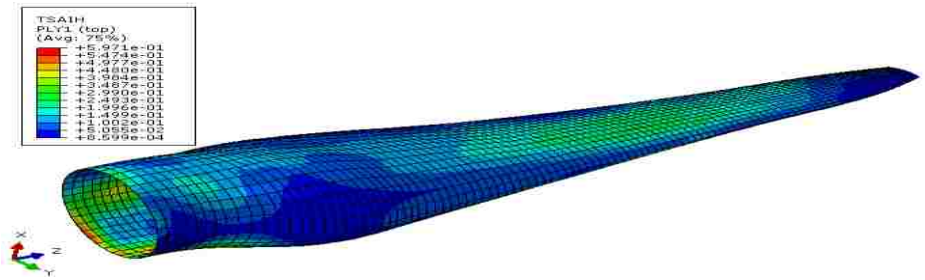

Fig. 2. Blade failure evaluation under hydrokinetic loadings (based on the Tsai-Hill criterion)

The limit-state function with respect to the Tsai-Hill failure criterion is defined by

$$g_1\left(\mathbf{X}_b, \mathbf{Y}_b(t), t\right) = f_{ind}\left(\mathbf{X}_b, \mathbf{Y}_b(t), t\right) - f_{allow} \quad t \in [t_0, t_s] \tag{18}$$

where $f_{ind}\left(\mathbf{X}_b, \mathbf{Y}_b(t), t\right)$ is the failure indicator of the composite blade based on the Tsai-Hill criterion, f_{allow} is the allowable value, $\mathbf{X}_b = [E_{11}, E_{22}, G_{12}, G_{23}]$ is the vector of

random variables, and $\mathbf{Y}_b(t)=[v(t)]$ is the vector of stochastic process. When $g\left(\mathbf{X}_b, \mathbf{Y}_b(t), t\right)>0$, a failure occurs based on the Tsai-Hill criterion.

3.2.2. Excessive deflection of turbine blades

Fig. 3 shows the deflection of the hydrokinetic turbine blade due to the river flow loading. The deflection of the blade is inevitable during the operation. It is correlated with various turbine performances, such as the power production, cavitation characteristics, possible failure modes of composite materials, and so on [7, 8]. It is one of the critical parameters that need to be investigated during the turbine blade design phase.

Since the river climate varies over time, it results in the variation of the tip deflection of the turbine blade during operation. The actual deflection of the turbine blade should not exceed the allowable one. The following limit-state function is then defined:

$$g_2\left(\mathbf{X}_b, \mathbf{Y}_b(t), t\right)=\varepsilon_{actual}(\mathbf{X}_b, \mathbf{Y}_b(t), t)-\varepsilon_{allow},\ t\in[t_0, t_s] \tag{19}$$

where $\varepsilon_{actual}(\mathbf{X}_b, \mathbf{Y}_b(t), t)$ and ε_{allow} are the actual and allowable deflections of the turbine blade at time t, respectively.

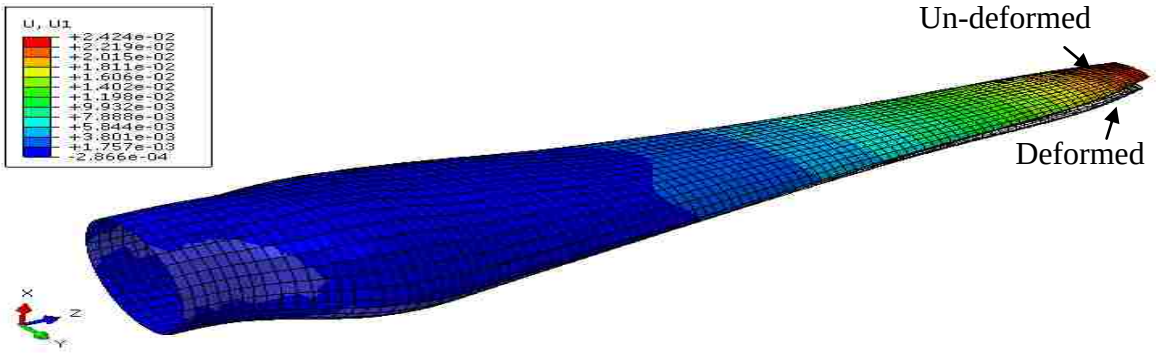

Fig. 3. Deformed and un-deformed geometry of the hydrokinetic turbine blade

Based on the failure modes and limit-state functions defined, the reliability analysis of the composite turbine blade is then discussed.

4. Simulation-Based Time-Dependent Reliability Analysis for Composite Hydrokinetic Turbine Blades

To perform the time-dependent reliability analysis for the composite hydrokinetic turbine blades, two more challenges need to be addressed. The first one is how to analyze the performance responses of turbine blades under the stochastic river flow loading. The other one is how to build the limit-state functions in terms of the blade response for reliability analyses. In this paper, the BEM-FEM coupled method was used to compute the responses of composite turbine blades. By applying the simulation results from BEM-FEM, surrogate models were built for the responses through the stochastic polynomial chaos expansion (SPCE) method. Finally, the time-dependent reliability analyses are performed on these surrogate models.

4.1. Construction of surrogate models

4.1.1. BEM-FEM coupled method

The blade element momentum theory (BEM), proposed by Glauert in 1935, has been widely used to calculate the load of turbine blades. It is applicable to estimate the steady loads, the thrust and power for different settings of speed, rotational speed and pitch angle of turbines [50]. Since it is based on the momentum theory and the local events taking place at the blade elements, it may not be as accurate as that from the 3-dimentional computational fluid dynamics (CFD) simulations. However, the BEM calculation is much faster than the CFD simulation. Given its high efficiency and many corrections to the original model, BEM provides engineers with an effective way of approximating the aerodynamic/hydrodynamic loadings on turbine blades.

In the present work, BEM is employed to compute the loadings on the composite hydrokinetic turbine blades in reliability analysis. The load produced by BEM serves as the input of FEM, which generates the stress distribution of the turbine blade. This procedure is referred as the BEM-FEM coupled method.

Fig. 4 shows the flowchart of the BEM-FEM coupled method. For BEM, it assumes that there is no-radial-dependency among blade elements. However, the Prandtil's tip loss, Glauert correction, and hub loss are incorporated into the model to ensure reliable results. The hydrodynamic loadings obtained from BEM codes have been validated with Blade Tidal, which is a design tool for tidal current turbines [51].

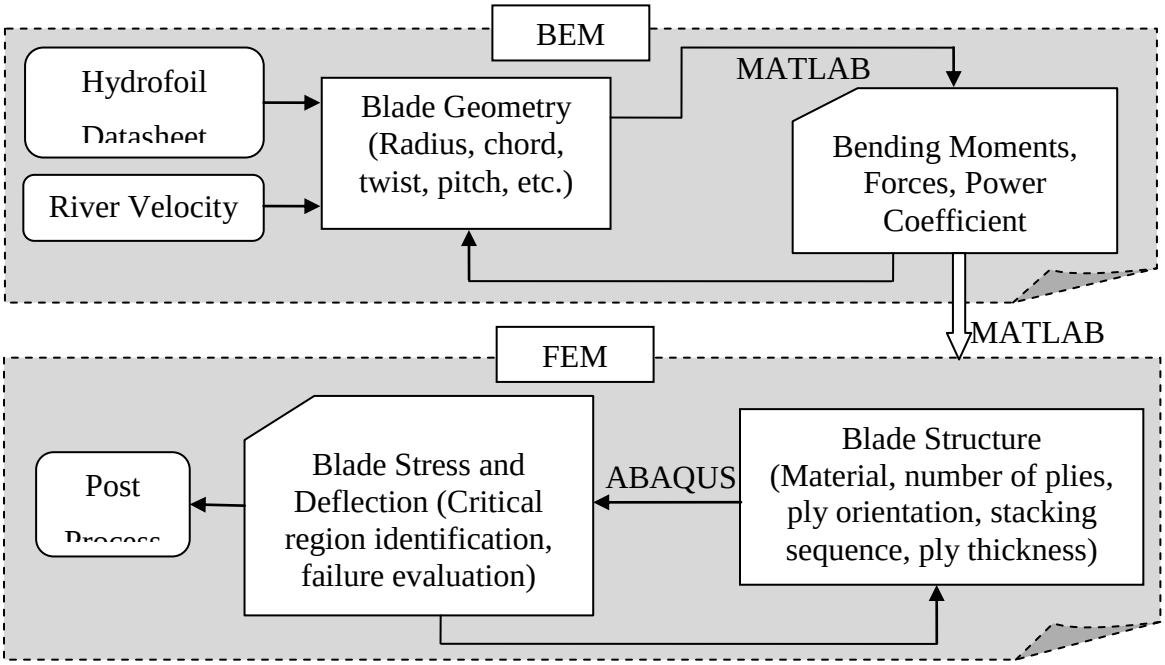

Fig. 4. Flowchart of the BEM-FEM

Fig. 5 presents the finite element mesh of the blade, which is divided into eight stations, and each station is applied with concentrated hydrodynamic forces on the blade surface using multipoint constraints (MPC) technique.

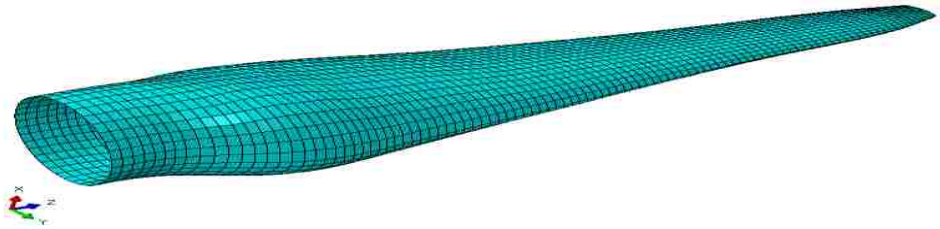

Fig. 5. Finite element mesh of the blade

If BEM-FEM is directly employed for the time-dependent reliability analysis, the efficiency will be very low, as the number of FEM runs is much higher than that of the time-invariant reliability analysis. Since the time-dependent reliability analysis will be later integrated into an optimization framework, the direct use of BEM-FEM may not be affordable in terms of computational efforts. Therefore, surrogate models are constructed

based on limited and selected BEM-FEM analyses. In the next section, a method will be introduced to construct the surrogate models based on the FEM simulations.

4.1.2. SPCE method

Since the uncertainties are all modeled by random variables, the SPCE method is used to get the surrogate models for the two limit-state functions. As an efficient tool for multi-disciplinary design optimization (MDO) in various engineering applications, SPCE has drawn much attention in the past decades. With SPCE, the chaos expansion for a response Z is given by [52, 53]

$$Z = \sum_{i=0}^{P} \chi_i \Gamma_i(\boldsymbol{\xi}) \tag{20}$$

where χ_i are deterministic coefficients, $\Gamma_i(\boldsymbol{\xi})$ are the i-th order random basis functions, $\boldsymbol{\xi} = [\xi_1, \xi_2, \cdots \xi_n]$ is a vector of independent standard random variables, and P is the number of terms. The total number of terms for a complete polynomial chaos expansion of order p and n random variables is given by

$$1 + P = \frac{(n+p)!}{n!\,p!} \tag{21}$$

The use of independent standard random variables in Eq. (20) is critical because it allows decoupling of the multidimensional integrals in a mixed basis expansion [54]. $\Gamma_i(\boldsymbol{\xi})$ are multivariable polynomials, which involve products of one-dimensional polynomials. For the expansion of a response with different kinds of random variables, mixed bases will be used. There are different kinds of basis functions for different uncertainty distributions [52]. For a normal (Gaussian) uncertain variable, the ideal basis function is the Hermit polynomial. For a uniform or exponential distribution, the ideal basis function is Legendre or Laguerre polynomial.

In this work, the point collocation method is applied to get the deterministic coefficients χ_i in Eq. (20). For the point collocation method, sampling of input random variables is the key to ensure the efficiency and accuracy of the approximation. The most commonly used sampling methods include the Random Sampling (RS), Latin Hypercube Sampling (LHS), and Hammersley Sampling (HS) [55]. HS is used to generate samples

for input random variables because it is capable of providing better uniformity properties over multi-dimensional space than LHS and RS.

For the time-dependent reliability analysis of composite hydrokinetic turbine blades, the uncertainties in the material are modeled as Gaussian random variables, which can be expanded using the Hermit polynomial basis. The flow velocity is a stochastic process that varies randomly over time. As a result, at different time instants, the velocity distributions will be different. There is no single distribution that can be used for the expansion. Therefore, the flow velocity is treated as a variable with unknown distribution and then it is treated with a uniform distribution bounded by the cut-out and cut-in velocity as shown in Fig. 6. This treatment is similar to expand a general variable. As shown in the example in this paper, this treatment works well for the reliability analysis of turbine blades. For stochastic polynomial chaos expansion, the Hermit polynomials are therefore used for E_{11}, E_{22} (E_{33}), G_{12} (G_{13}), and G_{23}; and Legendre polynomials for the river velocity. For multivariate basis functions, the mixed bases are used for expansion.

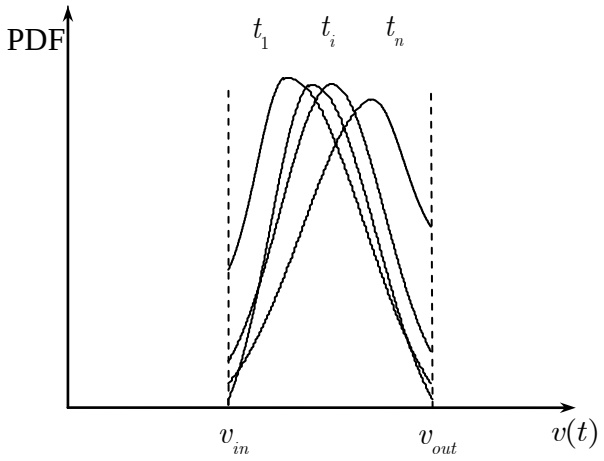

Fig. 6. Distribution of river flow velocity

With the expansion order of two, the polynomial chaos expansion model for the studied problem in this work is given by

$$Z^s = \sum_{k=0}^{20} \chi_i^s \Gamma_i(\boldsymbol{\xi}) = \chi_0^s + \sum_{i=1}^{4} \chi_i^s H_1(\xi_i) + \chi_5^s L_1(\xi_5(t)) + \sum_{i=1}^{4} \chi_{5+i}^s H_1(\xi_i) L_1(\xi_5(t)) + \sum_{i=1}^{3} \sum_{j=i+1}^{4} \chi_{(i,j)}^s H_1(\xi_i) H_1(\xi_j) + \sum_{i=1}^{4} \chi_{15+i}^s H_2(\xi_i) + \chi_{20}^s L_2(\xi_5(t)) \tag{22}$$

$$\xi_j = \frac{x_j - \mu_{X_j}}{\sigma_{X_j}},\ j = 1, \cdots, 4 \tag{23}$$

and

$$\xi_5(t) = \frac{2v(t) - v_L - v_U}{v_U - v_L} \tag{24}$$

in which

— $\xi_j,\ j = 1, \cdots, 4$, are the standard normal random variables corresponding to material strengths

— $\xi_5(t)$ is a normalized uniform random variable bounded in [-1, 1], which is associated with the stochastic process of river velocity $v(t)$ at time t

— $\mathbf{x} = [x_1, x_2, x_3, x_4]$ is a vector of specific values for random variables $[E_{11}, E_{22}, G_{12}, G_{23}]$

— μ_{X_j} and σ_{X_j} are the mean and standard deviation of random variable X_j, respectively

— v_L is the lower bound of tip river velocity expansion interval

— v_U is the upper bound of river velocity expansion interval

— $H_i(\cdot),\ i = 1, 2$, is the i^{th} order Hermit polynomial basis

— $L_i(\cdot),\ i = 1, 2$, is the i^{th} order Legendre polynomial basis

— $Z^s,\ s = 1, 2$, represents the limit-state functions, s=1 for limit-state function 1 in Eq. (18), and s=2 for limit-state function 2 in Eq. (19)

— $\chi_i^s,\ s = 1, 2$ and $i = 0, 1, 2, \cdots, 20$, stand for the deterministic coefficients of the surrogate models. s=1 for surrogate model associated with limit-state function 1 and s=2 for surrogate model associated with limit-state function 2

Assume that N_p simulations are performed for the turbine blades at the sample points generated from HS, the deterministic coefficients χ_i^s, $s=1,2$ and $i=0,1,2,\cdots,20$, are then solved by the point collocation method as follows:

$$\begin{pmatrix} \Gamma_0(\xi^1) & \Gamma_1(\xi^1) & \cdots & \Gamma_{20}(\xi^1) \\ \Gamma_0(\xi^2) & \Gamma_1(\xi^2) & \cdots & \Gamma_{20}(\xi^2) \\ \vdots & \vdots & \cdots & \vdots \\ \Gamma_0(\xi^{N_p}) & \Gamma_1(\xi^{N_p}) & \cdots & \Gamma_{20}(\xi^{N_p}) \end{pmatrix} \begin{pmatrix} \chi_0^s \\ \chi_1^s \\ \vdots \\ \chi_{20}^s \end{pmatrix} = \begin{pmatrix} Z^s(\xi^1) \\ Z^s(\xi^2) \\ \vdots \\ Z^s(\xi^{N_p}) \end{pmatrix} \tag{25}$$

where $\xi^i = [\xi_1^i, \xi_2^i, \xi_3^i, \xi_4^i, \xi_5^i(t)], i=1,\cdots,N_p$ is the i^{th} group of sample points generated from HS, and $Z^s(\xi^i)$ is the blade response of Z^s with the i^{th} group of sample points obtained from the simulation.

4.2. Reliability analysis of composite hydrokinetic turbine blades

It assumes that the seasonal effects of river flow velocity repeat in the same time periods of any year. This assumption is reasonable given the fact that the Earth circulates around the Sun annually with the same seasonal effects. Based on this assumption, the probability of failures during *T*-years operation can be calculated by

$$p_f^i(T) = 1-[1-p_f^i(Y_e)]^T \tag{26}$$

where $p_f^i(T)$ is the probability of failure during *T* years; $p_f^i(Y_e)$ is the annual probability of failure. *i* stands for the two failure modes as follows:

- $i=1$ for the failure with respect to the Tsai-Hill failure criterion
- $i=2$ for the failure of excessive deflection

In Eq. (26) the annual probability of failure $p_f^i(Y_e)$ is defined over a time interval $[0,t]$, where *t* is equal to one year. The anuual probability of failure $p_f^i(Y_e)$ can be solved by applying JUR/FORM given in Section 2 and using the surrogate models in Section 4.1.

4.3. Numerical procedure

In this section, the numerical implementation of the reliability analysis method discussed above is summarized. Fig. 7 depicts the procedure of the implementation.

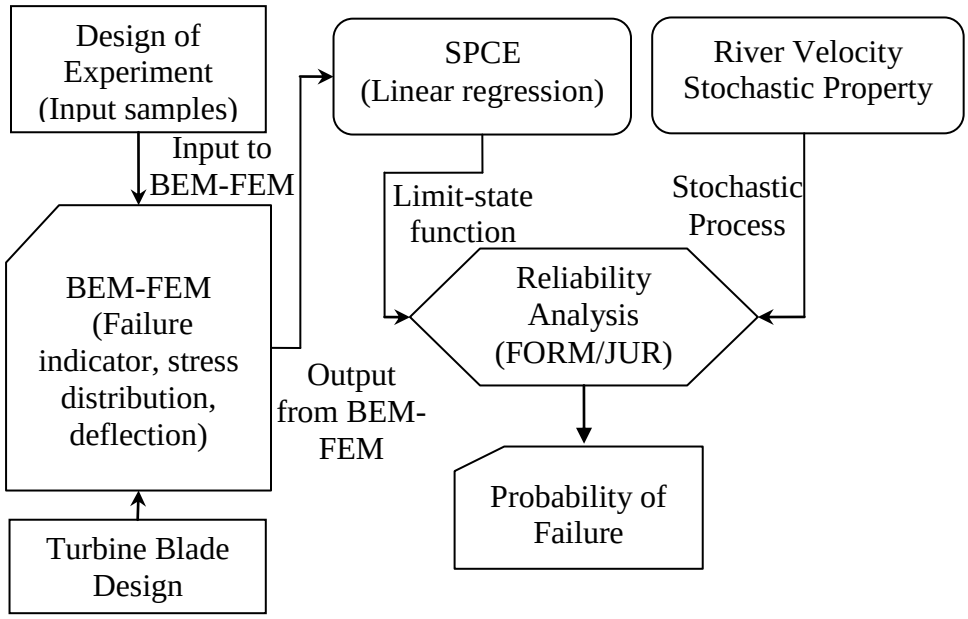

Fig. 7. Flowchart of simulation-based time-dependent reliability analysis

- Step 1: Sample generation: generate the samples of random variables using the Hammersley Sampling method based on their distribution.
- Step 2: BEM-FEM coupled analysis: with the input samples from step 1, analyze the failure indicator with respect to the Tsai-Hill failure criterion and deflection of the hydrokinetic turbine blade using BEM-FEM.
- Step 3: Design of experiments: construct surrogate models using the outputs from simulations and approximate the responses with the stochastic polynomial chaos expansion method.
- Step 4: Reliability analysis: Perform time-dependent reliability analysis by applying the JUR/FORM method.

5. Case study

A one-meter long composite hydrokinetic turbine blade with varying chord lengths, cross sections and an eight-degree twist angle was studied. This blade is for a hydrokinetic turbine system that is intended to put into operation in the Missouri River. During the design process, the reliability of the hydrokinetic turbine over a 20-year design period was evaluated.

5.1. Data

5.1.1. River discharge of the Missouri River

Based on the historical river discharge data of Missouri river from 1897 to 1988 at Hermann station, the mean and standard deviation of the monthly river discharge were fitted as functions of *t* as follows [27]

$$\mu_{D_m}(t) = a_0^{mean} + \sum_{i=1}^{5}[a_i^{mean}\cos(i\omega_{mean}t) + b_i^{mean}\sin(i\omega_{mean}t)] \tag{27}$$

$$\sigma_{D_m}(t) = a_0^{std} + \sum_{j=1}^{5}[a_j^{std}\cos(j\omega_{std}t) + b_j^{std}\sin(j\omega_{std}t)] \tag{28}$$

where

$$\begin{aligned} &a_0^{mean} = 2335,\ a_1^{mean} = -1076,\ a_2^{mean} = 241.3,\ a_3^{mean} = 61.69,\\ &a_4^{mean} = -30.92,\ a_5^{mean} = 32.38,\ b_1^{mean} = 57.49,\ b_2^{mean} = -174.9,\\ &b_3^{mean} = -296.2,\ b_4^{mean} = 213.6,\ b_5^{mean} = -133.6,\ \omega_{mean} = 0.5583 \end{aligned} \tag{29}$$

$$\begin{aligned} &a_0^{std} = 1280,\ a_1^{std} = -497.2,\ a_2^{std} = 145.8,\ a_3^{std} = 225.4,\\ &a_4^{std} = -203.1,\ a_5^{std} = 99.47, b_1^{std} = -82.58,\ b_2^{std} = -19.06,\\ &b_3^{std} = -178.7,\ b_4^{std} = 36.15,\ b_5^{std} = -52.47,\ \omega_{std} = 0.5887 \end{aligned} \tag{30}$$

The auto-correlation coefficient function of the normalized and standardized monthly discharge was assumed to be

$$\rho_{D_m}(t_1, t_2) = \exp\{-[20(t_2 - t_1)/3]^2\} \tag{31}$$

5.1.2. Deterministic parameters for time-dependent reliability analysis

Table 2 presents the deterministic parameters for the reliability analysis, which include the limit states and time step size.

Table 2. Deterministic parameters used for reliability analysis

Parameter	f_{allow}	ε_{allow}	Δt
Value	1	3.5×10^{-2} (m)	5×10^{-3} (month)

5.2. Sampling of random variables

According to the distributions of random variables and their bases for expansion, samples were generated. Since there are five variables to be expanded using the SPCE method and the expansion order is two, the minimal number of samplings required is 21 according to Eq. (21). To achieve a good accuracy of approximation, more samples (32 samples) were generated. The samples are depicted in Fig. 8.

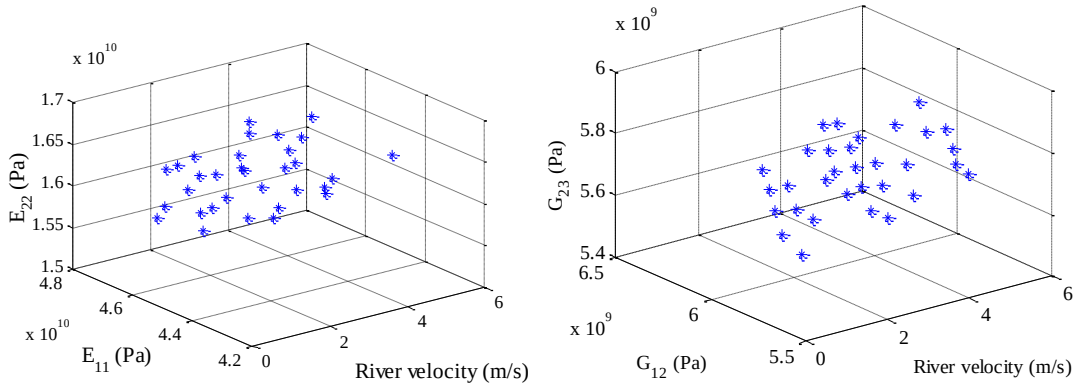

Fig. 8. Samples of random variables

5.3. Responses from FEM simulation

BEM-FEM coupled simulations were performed at the sample points generated in Section 5.2. Based on the simulation results, surrogate models were constructed. Fig. 9

presents the failure indicators of the Tsai-Hill failure criterion from simulations versus the predicted ones from the surrogate model. Fig. 10 shows the deflections obtained from simulations versus the predicted ones from the surrogate model.

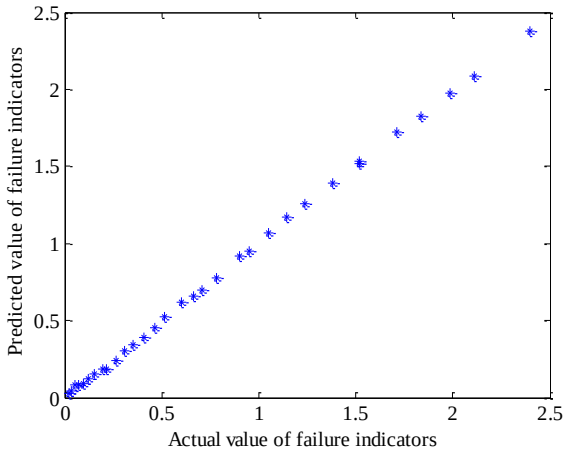

Fig. 9. Values of failure indicators from simulation and predicted values

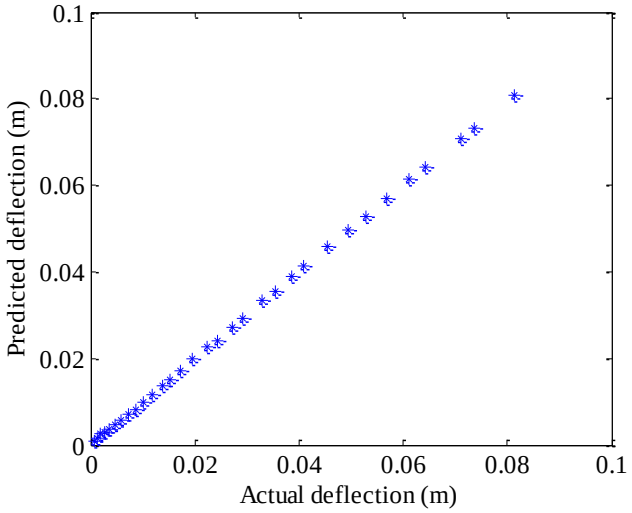

Fig. 10. Deflections from simulation versus predicted deflections

The figures indicate that the SPCE method well approximates the responses because the two curves are almost linear. Thus the approximated models could be confidently used for assessing the reliability of the turbine blade. Figs. 11 and 12 illustrate the response of failure indicator of the Tsai-Hill failure criterion and that of the deflection versus the river velocity and composite material property, respectively.

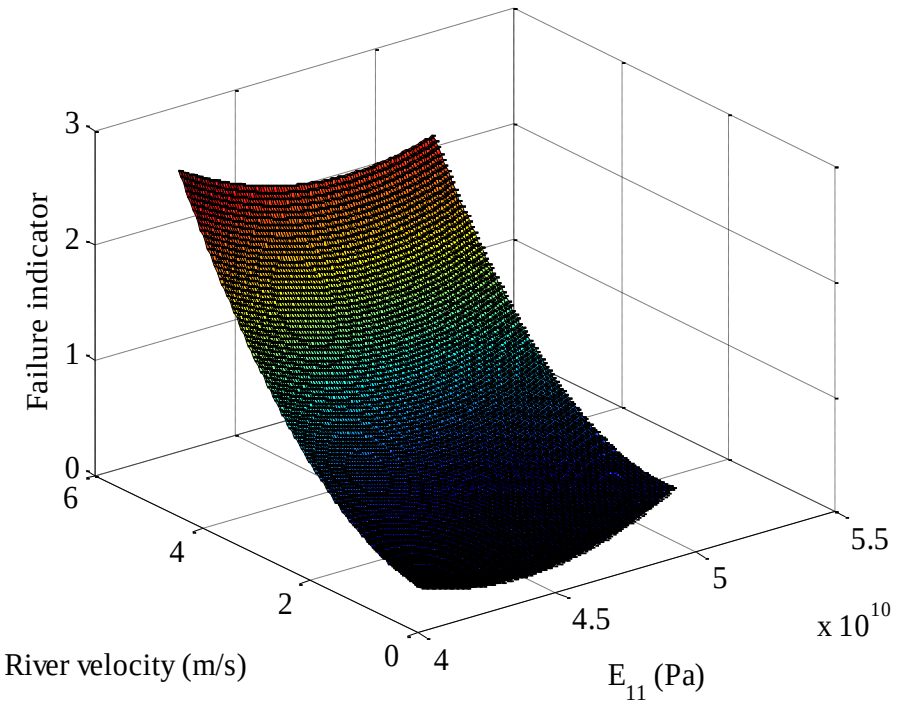

Fig.11. Failure indicator for Tsai-Hill failure criterion

5.4. Reliability analysis and results

The probability of failure of the hydrokinetic turbine blade over a one-year time period $[t_0, t_s] = [0, 1]$ yr was calculated. The probability of failure over the life time $[t_0, t_s] = [0, 20]$ yr was then computed using Eq. (26).

5.4.1. Time-dependent probabilities of failure

Figs. 13 and 14 give the time-dependent probabilities of failure of composite hydrokinetic turbine blades over a one-year time period with respect to the failure modes of the Tsai-Hill failure criterion and excessive deflection, respectively. To verify the accuracy of the reliability analysis, MCS with a sample size of 2×10^6 was also performed.

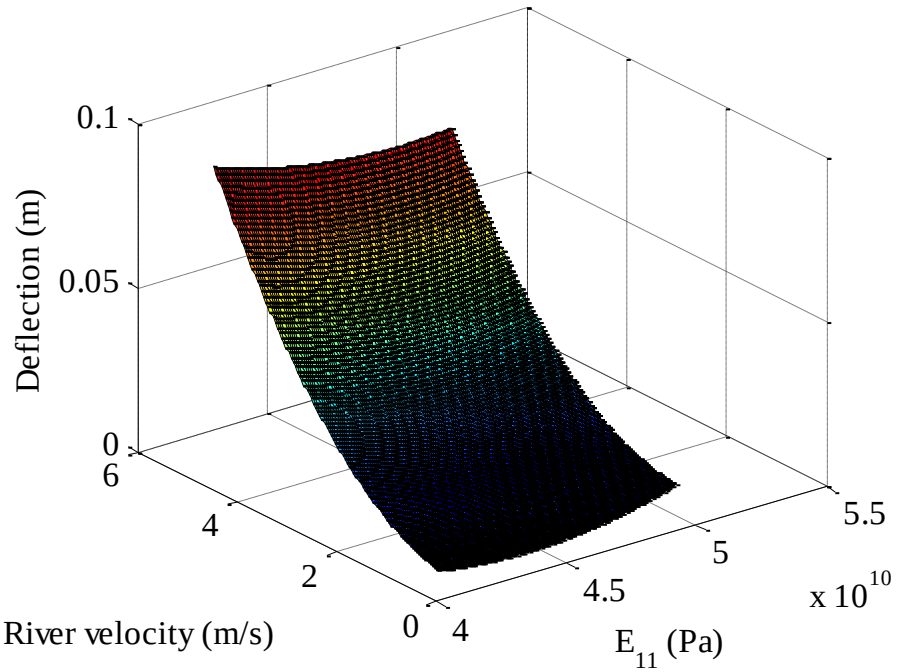

Fig.12. Deflection of turbine blades

The results indicate that the accuracy of the reliability analysis from JUR/FORM is good. The probability of failure for the Tsai-Hill failure criterion is 5.6312×10^{-4} over a one-year period. The probability of failure due to excessive deflection is 11.0843×10^{-4} over a one-year time period. The failure mode of the Tsai-Hill failure criterion is less likely to happen than that of excessive deflection for this design. The probabilities of failure for the Tsai-Hill failure criterion and excessive deflection over a 20-year life period are 1.12×10^{-2} and 2.19×10^{-2}, respectively.

Tables 3 and 4 present the actual computational costs and numbers of function calls required by JUR/FORM and MCS for the two failure modes, respectively. The analyses were run on a Dell personal computer with Intel (R) Core (TM) i5-2400 CPU and 8GB system memory. The results indicate that JUR/FORM is much more efficient than MCS. This means that the computational effort will decrease significantly when JUR/FORM is employed to substitute MCS for the time-dependent reliability analysis. This is especially beneficial when the time-dependent reliability analysis is embedded in

the hydrokinetic turbine blade optimization framework where the reliability analysis is called repeatedly.

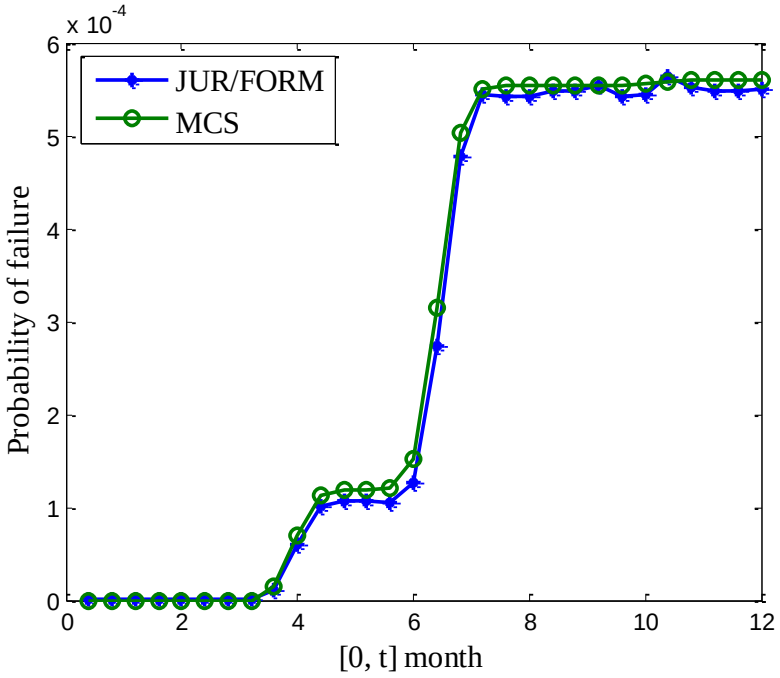

Fig. 13 Time-dependent probabilities of failure with respect to Tsai-Hill failure criterion

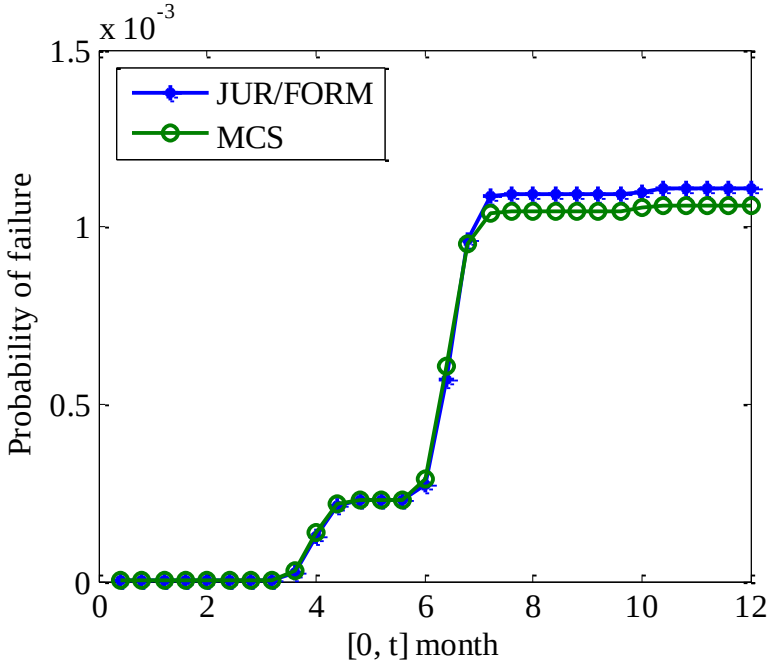

Fig. 14 Time-dependent probabilities of failure with respect to excessive deflection

Table 3 Number of function calls and actual computational cost for Tsai-Hill failure criterion

$[t_0, t_s]$ months	JUR/FORM		MCS	
	Time (s)	Function Calls	Time (s)	Function Calls
[0, 4]	27.83	11403	1.47×10^3	2×10^8
[0, 6]	30.55	11167	2.03×10^3	3×10^8
[0, 8]	30.20	11427	3.26×10^3	4×10^8
[0, 10]	26.45	11870	4.91×10^3	5×10^8
[0, 12]	28.69	11821	6.89×10^3	6×10^8

Table 4 Number of function calls and actual computational cost for excessive deflection

$[t_0, t_s]$ months	JUR/FORM		MCS	
	Time (s)	Function Calls	Time (s)	Function Calls
[0, 4]	23.97	9449	1.28×10^3	2×10^8
[0, 6]	23.64	9692	2.86×10^3	3×10^8
[0, 8]	25.95	9625	3.87×10^3	4×10^8
[0, 10]	23.04	9933	5.67×10^3	5×10^8
[0, 12]	23.72	9827	7.78×10^3	6×10^8

5.4.2. Sensitivity analysis of random variables

Sensitivity factors [56] are used to quantify the importance of random variables to the probability of failure. Given the transformed limit-state function $\mathbf{g}(\mathbf{U}(t),t)$ and MPP $\mathbf{U}^*(t)$, the sensitivity factor of random variable $U_i(t)$ at time instant t is given by [56]

$$s_i(t) = -U_i^*(t) / [\sum_{j=1}^{n+m} (U_j^*(t))^2]^{0.5} \tag{32}$$

Based on this, the sensitivities factors of random variables were obtained at every time instant.

Figs. 15 and 16 show sensitivity factors of the five random variables for the Tsai-Hill failure criterion and excessive deflection, respectively.

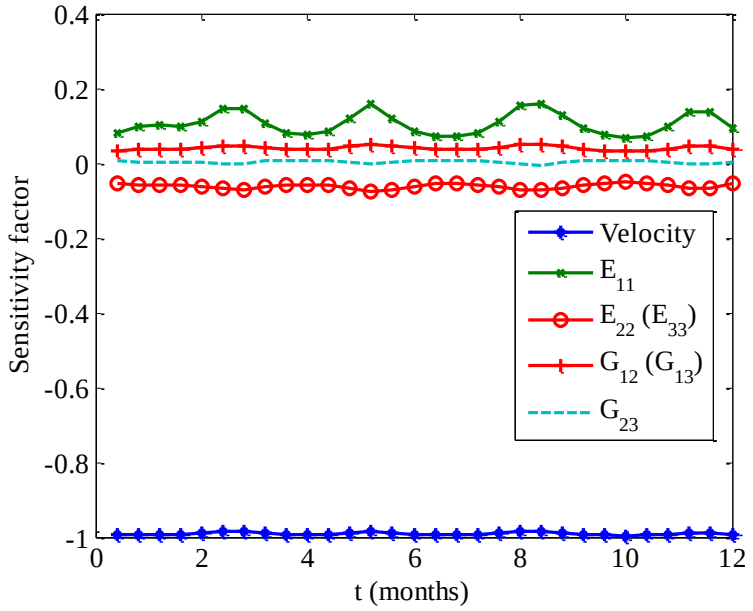

Fig. 15. Sensitivity factors for the Tsai-Hill failure criterion

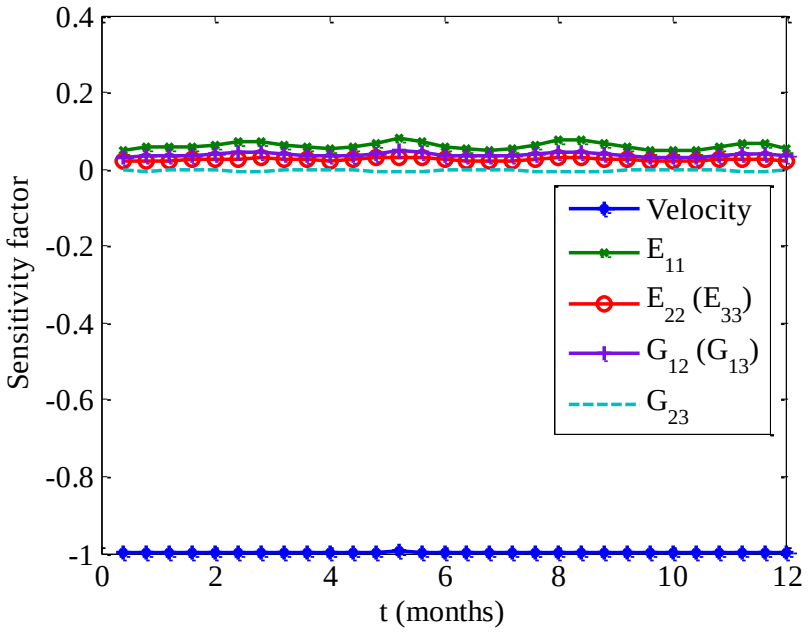

Fig. 16. Sensitivity factors for the excessive deflection failure

With the results of sensitivity analyses in Figs. 15 and 16, the major findings are summarized as follows:

- The river velocity makes the highest contributions to the probability of failure, while the uncertainties in material properties make smaller contributions.
- The river velocity always makes negative contribution to the reliability of composite turbine blades. This means that an increase in velocity will result in a decrease in reliability.
- With respect to the failure mode of excessive deflection, elastic modulus along direction 1 (i.e. E_{11}), irrespective of river velocity, makes the highest positive contributions to the reliability of composite hydrokinetic turbine blades. It is followed by the shear modulus G_{12} (G_{13}).
- For the failure mode of the Tsai-Hill failure criterion, E_{22} turns out to make negative contributions to the reliability of turbine blades while the sensitivity with respect to E_{11} is positive and the largest.
- The shear modulus G_{23} always makes negligible contributions to both of the failure modes.

6. Conclusions

Using an appropriate reliability analysis method is critical for the probabilistic design of composite hydrokinetic turbine blades. In this work, a simulation based time-dependent reliability model was developed for composite hydrokinetic turbine blades. The BEM-FEM coupled method was used to get the responses of failure indicator of the Tsai-Hill failure criterion and deflections of turbine blades. The SPCE method was adopted to establish the limit-state functions, and JUR/FORM was employed to perform time-dependent reliability analysis. By incorporating these analysis methods, the influence of uncertainties in river flow velocity and composite material properties on the performance of turbine blades was evaluated.

The results illustrated that the composite hydrokinetic turbine blade has larger probability of failure for the excessive deflection than that due to the Tsai-Hill failure criterion. The former, therefore, needs to be paid more attention during the design phase.

Sensitivity analysis of random variables showed that the river flow velocity makes the highest contribution to the probability of failure of the composite hydrokinetic

turbine blade for both failure modes. The sensitivity analysis of the composite material parameters showed that E_{11} always makes a positive contribution and is the most important composite material parameter for the reliability of turbine blades. Therefore, this parameter should be focused on during the design stage. The shear modulus G_{23} makes negligible contributions to the two failure modes. E_{22} makes a positive contribution to the reliability of turbine blades against excessive deflection while this contribution turns to be negative for the reliability against the failure mode of Tsai-Hill failure criterion. This demonstrated that the material parameters of the composite material make different contributions to the reliability of turbine blades.

The future work includes coupling the CFD simulation with FEM to improve accuracy and applying the developed method to the reliability-based design optimization (RBDO) of composite hydrokinetic turbine blades. Fatigue reliability analysis will also be the future work.

Appendix A: MCS for time-dependent reliability analysis

The MCS for time-dependent reliability analysis involves both a stochastic process (river flow discharge) and random variables. To generate samples for the stochastic process, the time interval $[t_0, t_s]$ is discretized into *N* points. Then the samples of the normalized and standardized river flow discharge process $\mathbf{D_m}$ is generated by

$$\mathbf{D_m} = \boldsymbol{\mu}_{D_m} + \mathbf{M}\boldsymbol{\varsigma} \tag{33}$$

where $\boldsymbol{\varsigma} = (\varsigma_1, \varsigma_2, \cdots, \varsigma_N)^T$ is the vector of *N* independent standard normal random variables; $\boldsymbol{\mu}_{D_m} = (\mu_{D_m}(t_1), \mu_{D_m}(t_2), \cdots, \mu_{D_m}(t_N))^T$ is the vector of mean values of $\mathbf{D_m} = (D_m(t_1), D_m(t_2), \cdots, D_m(t_N))^T$; and $\mathbf{M}$ is a lower triangular matrix obtained from the covariance matrix of $\mathbf{D_m}$.

Let the covariance matrix of $\mathbf{D_m}$ at the *N* points be $\mathbf{C}_{N\times N}$, it gives

$$\mathbf{C}_{N\times N}=\begin{pmatrix} \rho_{D_m}(t_1,t_1) & \rho_{D_m}(t_1,t_2) & \cdots & \rho_{D_m}(t_1,t_N) \\ \rho_{D_m}(t_2,t_1) & \rho_{D_m}(t_2,t_2) & \cdots & \rho_{D_m}(t_2,t_N) \\ \vdots & \vdots & \ddots & \vdots \\ \rho_{D_m}(t_N,t_1) & \rho_{D_m}(t_N,t_2) & \cdots & \rho_{D_m}(t_N,t_N) \end{pmatrix}_{N\times N} \tag{34}$$

Then $\mathbf{M}$ can be obtained by

$$\mathbf{C}_{N\times N}=\mathbf{PDP}^{-1}=\mathbf{MM}^{T} \tag{35}$$

in which $\mathbf{D}$ is a diagonal eigenvalue matrix of the covariance matrix $\mathbf{C}_{N\times N}$, and $\mathbf{P}$ is the $N\times N$ square matrix whose *i*-th column is the *i*-th eigenvector of $\mathbf{C}_{N\times N}$.

After samples of the stochastic process of river flow discharge are generated, they are plugged into the limit-state functions, and then the samples (trajectories) of the limit-state functions are obtained. A trajectory is traced from the initial time to the end of the time period. Once the trajectory upcrosses the limit state, then a failure occurs; and the remaining curve will not be checked anymore. The process is illustrated in Fig. 17.

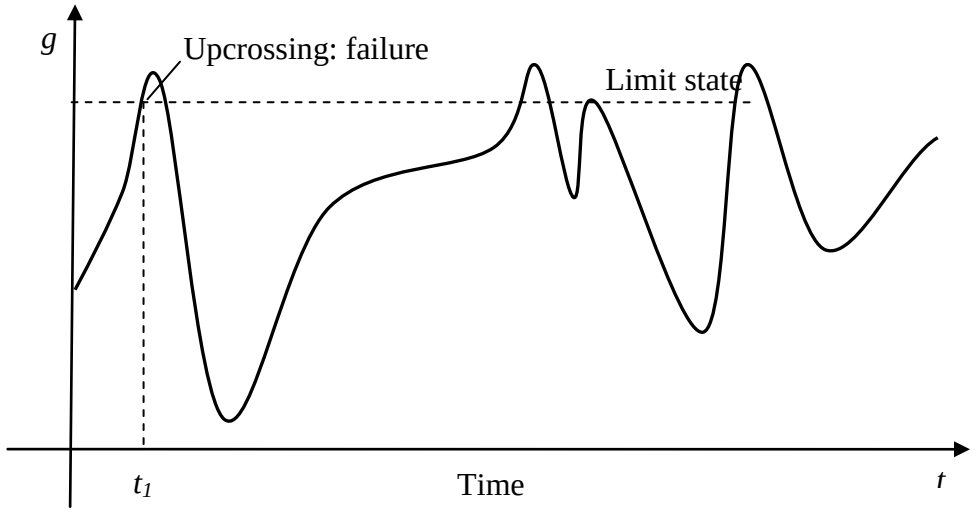

Fig. 17. A trajectory of a limit-state function

Appendix B: Computation of $v^{++}(t_1,t_2)$

Madsen has derived the expression for $v^{++}(t_1,t_2)$ as follows [31]

$$
\begin{aligned}
\nu^{++}(t_1,t_2) &= \lambda_1\lambda_2 f_{\mathbf{W}}(\boldsymbol{\beta})\Psi\left((\dot{\beta}_1-\mu_1)/\lambda_1\right)\Psi\left((\dot{\beta}_2-\mu_2)/\lambda_2\right) \\
&+\lambda_1\lambda_2 f_{\mathbf{W}}(\boldsymbol{\beta})\kappa\Phi\left((\mu_1-\dot{\beta}_1)/\lambda_1\right)\Phi\left((\mu_2-\dot{\beta}_2)/\lambda_2\right) \\
&+\lambda_1^2\lambda_2^2 f_{\mathbf{W}}(\boldsymbol{\beta})\int_0^{\kappa}(\kappa-K)\, f_{\dot{\mathbf{W}}|\mathbf{W}}\left(\dot{\boldsymbol{\beta}}\,|\,\boldsymbol{\beta};K\right)dK
\end{aligned} \tag{36}
$$

in which

$$
f_{\mathbf{W}}(\boldsymbol{\beta}) = \{\exp[(\beta_1^2 - 2\rho\beta_1\beta_2 + \beta_2^2)/(2-2\rho^2)]\}/(2\pi\sqrt{1-\rho^2}) \tag{37}
$$

$\boldsymbol{\beta} = [\beta_1, \beta_2]$ represents the time-invariant reliability index at time t_1 and t_2. μ_1 and μ_2, and λ_1 and λ_2, κ are the mean values, standard deviations, and correlation coefficient of $\dot{L}(t_1)\big|\boldsymbol{\beta}$ and $\dot{L}(t_2)\big|\boldsymbol{\beta}$, respectively. They are calculated by the following equations [28]:

$$
\mu = \begin{bmatrix}\mu_1\\ \mu_2\end{bmatrix} = \mathbf{c}_{\dot{\mathbf{L}}\mathbf{L}}\mathbf{c}_{\mathbf{L}\mathbf{L}}^{-1}\boldsymbol{\beta} = \begin{bmatrix}(\beta_2-\rho\beta_1)\rho_1\\ (\beta_1-\rho\beta_2)\rho_2\end{bmatrix}/(1-\rho^2) \tag{38}
$$

$$
\sum = \mathbf{c}_{\dot{\mathbf{L}}|\mathbf{L}} = \mathbf{c}_{\dot{\mathbf{L}}\dot{\mathbf{L}}} - \mathbf{c}_{\dot{\mathbf{L}}\mathbf{L}}\mathbf{c}_{\mathbf{L}\mathbf{L}}^{-1}\mathbf{c}_{\mathbf{L}\dot{\mathbf{L}}} = \begin{bmatrix}\lambda_1^2 & \kappa\lambda_1\lambda_2\\ \kappa\lambda_1\lambda_2 & \lambda_2^2\end{bmatrix} \tag{39}
$$

where

$$
\begin{bmatrix}\mathbf{c}_{\dot{\mathbf{L}}\dot{\mathbf{L}}} & \mathbf{c}_{\dot{\mathbf{L}}\mathbf{L}}\\ \mathbf{c}_{\mathbf{L}\dot{\mathbf{L}}} & \mathbf{c}_{\mathbf{L}\mathbf{L}}\end{bmatrix} = \begin{bmatrix}\omega^2(t_1) & \rho_{12} & 0 & \rho_1\\ \rho_{21} & \omega^2(t_2) & \rho_2 & 0\\ 0 & \rho_2 & 1 & \rho\\ \rho_1 & 0 & \rho & 1\end{bmatrix} \tag{40}
$$

$$
\rho_1 = \dot{\boldsymbol{\alpha}}(t_1)\mathbf{C}(t_1,t_2)\boldsymbol{\alpha}^T(t_2) + \boldsymbol{\alpha}(t_1)\dot{\mathbf{C}}_1(t_1,t_2)\boldsymbol{\alpha}^T(t_2) \tag{41}
$$

$$
\rho_2 = \boldsymbol{\alpha}(t_1)\mathbf{C}(t_1,t_2)\dot{\boldsymbol{\alpha}}^T(t_2) + \boldsymbol{\alpha}(t_1)\dot{\mathbf{C}}_2(t_1,t_2)\boldsymbol{\alpha}^T(t_2) \tag{42}
$$

$$
\begin{aligned}
\rho_{12} &= \dot{\boldsymbol{\alpha}}(t_1)\dot{\mathbf{C}}_2(t_1,t_2)\boldsymbol{\alpha}^T(t_2) + \dot{\boldsymbol{\alpha}}(t_1)\mathbf{C}(t_1,t_2)\dot{\boldsymbol{\alpha}}^T(t_2) \\
&+\boldsymbol{\alpha}(t_1)\ddot{\mathbf{C}}_{12}(t_1,t_2)\boldsymbol{\alpha}^T(t_2) + \boldsymbol{\alpha}(t_1)\dot{\mathbf{C}}_1(t_1,t_2)\dot{\boldsymbol{\alpha}}^T(t_2)
\end{aligned} \tag{43}
$$

$$
\begin{aligned}
\rho_{21} &= \dot{\boldsymbol{\alpha}}(t_1)\mathbf{C}(t_1,t_2)\dot{\boldsymbol{\alpha}}^T(t_2) + \boldsymbol{\alpha}(t_1)\dot{\mathbf{C}}_1(t_1,t_2)\dot{\boldsymbol{\alpha}}^T(t_2) \\
&+\boldsymbol{\alpha}(t_1)\ddot{\mathbf{C}}_{21}(t_1,t_2)\boldsymbol{\alpha}^T(t_2) + \dot{\boldsymbol{\alpha}}(t_1)\dot{\mathbf{C}}_2(t_1,t_2)\boldsymbol{\alpha}^T(t_2)
\end{aligned} \tag{44}
$$

$$\mathbf{C}(t_1,t_2)=\begin{bmatrix}\mathbf{1} & \mathbf{0} & \cdots & \mathbf{0}\\ \mathbf{0} & \rho^{Y_1}(t_1,t_2) & \cdots & 0\\ \vdots & \vdots & \ddots & \vdots\\ \mathbf{0} & 0 & \cdots & \rho^{Y_m}(t_1,t_2)\end{bmatrix}_{(n+m)\times(n+m)} \tag{45}$$

and

$$\dot{\mathbf{C}}_j(t_1,t_2)=\partial\mathbf{C}(t_1,t_2)/\partial t_j=\begin{bmatrix}\mathbf{0} & \mathbf{0} & \cdots & \mathbf{0}\\ \mathbf{0} & \dfrac{\partial\rho^{Y_1}(t_1,t_2)}{\partial t_j} & \cdots & 0\\ \vdots & \vdots & \ddots & \vdots\\ \mathbf{0} & 0 & \cdots & \dfrac{\partial\rho^{Y_m}(t_1,t_2)}{\partial t_j}\end{bmatrix}_{(n+m)\times(n+m)},\ j=1,2 \tag{46}$$

Acknowledgements

The authors gratefully acknowledge the support from the Office of Naval Research through contract ONR N000141010923 (Program Manager - Dr. Michele Anderson) and the Intelligent Systems Center at the Missouri University of Science and Technology.

Reference

[1] D.A. Brooks, The hydrokinetic power resource in a tidal estuary: The Kennebec River of the central Maine coast, Renewable Energy, 36 (2011) 1492-1501.

[2] M.S. Guney, Evaluation and measures to increase performance coefficient of hydrokinetic turbines, Renewable and Sustainable Energy Reviews, 15 (2011) 3669-3675.

[3] L.I. Lago, F.L. Ponta, L. Chen, Advances and trends in hydrokinetic turbine systems, Energy for Sustainable Development, 14 (2010) 287-296.

[4] V.J. Ginter, J.K. Pieper, Robust gain scheduled control of a hydrokinetic turbine, IEEE Transactions on Control Systems Technology, 19 (2011) 805-817.

[5] R. Hantoro, I.K.A.P. Utama, Erwandi, A. Sulisetyono, An experimental investigation of passive variable-pitch vertical-axis ocean current turbine, ITB Journal of Engineering Science, 43 B (2011) 27-40.

[6] T.Y. Kam, H.M. Su, B.W. Wang, Development of glass-fabric composite wind turbine blade, Advanced Materials Research, (2011), pp. 2482-2485.

[7] M.R. Motley, Y.L. Young, Performance-based design and analysis of flexible composite propulsors, Journal of Fluids and Structures, 27 (2011) 1310-1325.

[8] Y.L. Young, J.W. Baker, M.R. Motley, Reliability-based design and optimization of adaptive marine structures, Composite Structures, 92 (2010) 244-253.

[9] B. Kriegesmann, R. Rolfes, C. Hühne, A. Kling, Fast probabilistic design procedure for axially compressed composite cylinders, Composite Structures, 93 (2011) 3140-3149.

[10] M.R. Motley, Y.L. Young, Influence of uncertainties on the response and reliability of self-adaptive composite rotors, Composite Structures, 94 (2011) 114-120.

[11] R.J. Pimenta, S.M.C. Diniz, G. Queiroz, R.H. Fakury, A. Galvão, F.C. Rodrigues, Reliability-based design recommendations for composite corrugated-web beams, Probabilistic Engineering Mechanics, 28 (2012) 185-193.

[12] H.S. Toft, J.D. Sørensen, Reliability-based design of wind turbine blades, Structural Safety, 33 (2011) 333-342.

[13] D.V. Val, L. Chernin, Reliability of tidal stream turbine blades, in: 11th International Conference on Applications of Statistics and Probability in Civil Engineering, ICASP, Zurich, 2011, pp. 1817-1822.

[14] M.R. Motley, Y.L. Young, Reliability-based global design of self-adaptive marine rotors, in: ASME 2010 3rd Joint US-European Fluids Engineering Summer Meeting, FEDSM 2010, Montreal, QC, 2010, pp. 1113-1122.

[15] C.D. Eamon, M. Rais-Rohani, Integrated reliability and sizing optimization of a large composite structure, Marine Structures, 22 (2009) 315-334.

[16] M. Chiachio, J. Chiachio, G. Rus, Reliability in composites - A selective review and survey of current development, Composites Part B: Engineering, 43 (2012) 902-913.

[17] X. Du, A. Sudjianto, Reliability-based design with the mixture of random and interval variables, Journal of Mechanical Design, Transactions of the ASME, 127 (2005), pp. 1068-1076.

[18] X. Du, A. Sudjianto, W. Chen, An integrated framework for optimization under uncertainty using inverse reliability strategy, Journal of Mechanical Design, Transactions of the ASME, 126 (2004) 562-570.

[19] M. Muste, K. Yu, T. Pratt, D. Abraham, Practical aspects of ADCP data use for quantification of mean river flow characteristics; Part II: Fixed-vessel measurements, Flow Measurement and Instrumentation, 15 (2004) 17-28.

[20] M.Y. Otache, M. Bakir, Z. Li, Analysis of stochastic characteristics of the Benue River flow process, Chinese Journal of Oceanology and Limnology, 26 (2008) 142-151.

[21] J.N. Yang, M. Shinozuka, On the first excursion probability in stationary narrow-band random vibration, Journal of Applied Mechanics, Transactions ASME, 38 Ser E (1971) 1017-1022.

[22] B. Sudret, Analytical derivation of the outcrossing rate in time-variant reliability problems, Structure and Infrastructure Engineering, 4 (2008) 353-362.

[23] F.M.H. Schall G, Rackwitz R., The ergodicity assumption for sea states in the reliability estimation of offshore structures. , Journal of Offshore Mechanics and Arctic Engineering, 113 (1991) 241–246.

[24] S. Engelund, R. Rackwitz, C. Lange, Approximations of first-passage times for differentiable processes based on higher-order threshold crossings, Probabilistic Engineering Mechanics, 10 (1995) 53-60.

[25] J. Zhang, X. Du, Time-dependent reliability analysis for function generator mechanisms, Journal of Mechanical Design, Transactions of the ASME, 133 (2011).

[26] C. Andrieu-Renaud, B. Sudret, M. Lemaire, The PHI2 method: A way to compute time-variant reliability, Reliability Engineering and System Safety, 84 (2004) 75-86.

[27] Z. Hu, X. Du, Reliability analysis for hydrokinetic turbine blades, Renewable Energy, 48 (2012) 251-262.

[28] Z. Hu, X. Du, Time-Dependent Reliability Analysis with Joint Upcrossing Rates, Submitted to Structural and Multidisciplinary Optimization, (2011).

[29] S.O. Rice, Mathematical Analysis of Random Noise, Bell System Technical Journal, 23 (1944) 282–332.

[30] S.O. Rice, Mathematical analysis of random noise, Bell Syst.Tech. J., 24 (1945) 146-156.

[31] P.H. Madsen, and Krenk, S.,, An integral equation method for the first passage problem in random vibration, Journal of Applied Mechanics 51 (1984) 674-679.

[32] E.H. Vanmarcke, On the distribution of the first-passage time for normal stationary random processes, Journal of Applied Mechanics, Transactions ASME, 42 Ser E (1975) 215-220.

[33] A. Preumont, On the peak factor of stationary Gaussian processes, Journal of Sound and Vibration, 100 (1985) 15-34.

[34] A. Singh, Z. Mourelatos, J. Li, Design for lifecycle cost using time-dependent reliability, Journal of Mechanical Design, Transactions of the ASME, 132 (2010) 091008.

[35] V.K. Arora, G.J. Boer, A variable velocity flow routing algorithm for GCMs, Journal of Geophysical Research D: Atmospheres, 104 (1999) 30965-30979.

[36] K. Schulze, M. Hunger, P. Döll, Simulating river flow velocity on global scale, Advances in Geosciences, 5 (2005) 133-136.

[37] P.M. Allen, J.G. Arnold, B.W. Byars, Downstream channel geometry for use in planning-level models, Water Resources Bulletin, 30 (1994) 663-671.

[38] J.J. Beersma, T.A. Buishand, Joint probability of precipitation and discharge deficits in the Netherlands, Water Resources Research, 40 (2004) 1-11.

[39] H.T. Mitosek, On stochastic properties of daily river flow processes, Journal of Hydrology, 228 (2000) 188-205.

[40] P.H.A.J.M. W. Wang, Van Gelder and J.K. Vrijling, Long-memory in streamflow processes of the yellow river, IWA International Conference on Water Economics, Statistics, and Finance Rethymno, Greece, July 8-10, (2005) 481-490.

[41] K.O. Ronold, C.J. Christensen, Optimization of a design code for wind-turbine rotor blades in fatigue, Engineering Structures, 23 (2001) 993-1004.

[42] D. Veldkamp, A probabilistic evaluation of wind turbine fatigue design rules, Wind Energy, 11 (2008) 655-672.

[43] K.O. Ronold, G.C. Larsen, Reliability-based design of wind-turbine rotor blades against failure in ultimate loading, Engineering Structures, 22 (2000) 565-574.

[44] K. Saranyasoontorn, L. Manuel, Design loads for wind turbines using the environmental contour method, Journal of Solar Energy Engineering, Transactions of the ASME, 128 (2006) 554-561.

[45] M. Grujicic, G. Arakere, B. Pandurangan, V. Sellappan, A. Vallejo, M. Ozen, Multidisciplinary design optimization for glass-fiber epoxy-matrix composite 5 MW horizontal-axis wind-turbine blades, Journal of Materials Engineering and Performance, 19 (2010) 1116-1127.

[46] C.K. Lee, Corrosion and wear-corrosion resistance properties of electroless Ni-P coatings on GFRP composite in wind turbine blades, Surface and Coatings Technology, 202 (2008) 4868-4874.

[47] K. Mühlberg, Corrosion protection of offshore wind turbines - A challenge for the steel builder and paint applicator, Journal of Protective Coatings and Linings, 27 (2010) 20-32.

[48] A.L. Araújo, C.M. Mota Soares, C.A. Mota Soares, J. Herskovits, Optimal design and parameter estimation of frequency dependent viscoelastic laminated sandwich composite plates, Composite Structures, 92 (2010) 2321-2327.

[49] Y.X. Zhang, C.H. Yang, Recent developments in finite element analysis for laminated composite plates, Composite Structures, 88 (2009) 147-157.

[50] O.L.H. Martin, Aerodynamics of wind turbines, Second edition, Earthscan, Sterling, VA., 2008.

[51] Blade Tidal, Demonstration version, GL Garrad Hassan, www.gl-garradhassan.com.

[52] M.S. Eldred, J. Burkardt, Comparison of non-intrusive polynomial chaos and stochastic collocation methods for uncertainty quantification, in: 47th AIAA Aerospace Sciences Meeting including the New Horizons Forum and Aerospace Exposition , art. no. 2009-0976 2009.

[53] B. Sudret, Global sensitivity analysis using polynomial chaos expansions, Reliability Engineering and System Safety, 93 (2008) 964-979.

[54] M.S. Eldred, Recent advances in non-intrusive polynomial chaos and stochastic collocation methods for uncertainty analysis and design, in: 50th AIAA/ASME/ASCE/AHS/ASC Structures, Structural Dynamics and Materials Conference , art. no. 2009-2274 2009.

[55] W. Chen, K.-L. Tsui, J.K. Allen, F. Mistree, Integration of the response surface methodology with the compromise decision support problem in developing a general robust design procedure, in: American Society of Mechanical Engineers, Design Engineering Division (Publication) DE 82 (1), pp. 485-492 1995.

[56] S.K. Choi, R.V. Grandhi, R.A. Canfield, Reliability-based structural design, Springer, 2007.

PAPER
IV. A RANDOM FIELD APPROACH TO RELIABILITY ANALYSIS WITH RANDOM AND INTERVAL VARIABLES

Zhen Hu and Xiaoping Du[3]

Abstract

Reliability analysis with random and interval variables predicts the lower and upper bounds of reliability. The analysis is computationally intensive because the global extreme values of a limit-state function with respect to interval variables must be obtained during the reliability analysis. In this work a random field approach is proposed to reduce the computational cost. This work consists of two major developments. The first development is the treatment of a response variable as a random field, which is spatially correlated at different locations of interval variables. Equivalent reliability bounds are defined from a random field perspective. The definitions can avoid the direct use of the extreme values of the response. The second development is the employment of the First Oder Reliability Method (FORM) to show the feasibility of the random field modeling. This development results in a new random field method based on FORM. The new method converts a general response variable into a Gaussian field at its limit state and then builds surrogate models for the auto-correlation function and reliability index function with respect to interval variables. Then Monte Carlo simulation is employed to estimate the reliability bounds without calling the original limit-state function. Three examples demonstrated the effectiveness of the proposed method.

1. Introduction

The major task of reliability analysis is to predict reliability in a design stage. Because of this advantage, reliability analysis has been used in many applications, such

[3]400 West 13th Street, Toomey Hall 290D,Rolla, MO 65401, U.S.A., Tel: 1-573-341-7249, e-mail: dux@mst.edu

as those of automobile vehicles [1], wind/hydrokinetic turbines [2], and airplanes [3]. The reliability analysis requires knowing a limit-state function, which specifies the functional relationship between input variables and output variables (responses), and the joint probability distribution of the input variables.

In many applications, the data of some input variables are too limited to fit probability distributions. For this situation, the fuzzy set [4], evidence theory [5], and intervals [6, 7] are employed to model the uncertainty in these input variables. Interval variables are used for the highest degree of uncertainty – only the lower and upper bounds of an input variable are available. For instance, the contact resistance in the vehicle crash [8] and the parameters of a new design [9] are examples of interval variables. As a result, the input variables of a limit-state function may contain both random and interval variables, and the reliability is therefore also bounded within its minimum and maximum values.

Many methods are available for the reliability analysis with the mixture of random and interval variables. For example, Jiang *et al.* [10] developed a reliability analysis method based on a hybrid uncertain model. In their model, parameters such as mean and standard deviation of some random variables are described as interval variables. Adduri and Penmetsa [11] investigated the method of approximating the bounds of structural system reliability in the presence of interval variables. Luo *et al.* [12, 13] developed an iterative procedure to obtain the worst-case point of interval variables and the Most Probable Point (MPP) using a probability and convex set model. Penmetsa and Grandhi [14] used function approximation methods to improve the efficiency of reliability analysis with random and interval variables. By combining simulation process with interval analysis, Zhang *et al.* [15] proposed an interval Monte Carlo method to estimate the interval probability of failure. In order to perform reliability-based design optimization for problems with interval variables, Du et al. developed a sequential single loop (SSL) procedure [16, 17]. To improve the stability of SSL, Jiang *et al* designed a new algorithm [9].

Although many reliability methods are available for interval variables as reviewed above, there are still some challenges that need to be resolved. First, the reliability analysis requires global extreme values of a response with respect to interval variables.

As a result, the reliability analysis usually involves two loops. In the inner loop, global optimization is used to find the extreme values of the response with respect to interval variables while the outer loop is responsible for reliability analysis with respect to random variables. Even though single loop procedures have been proposed [9, 16, 17], efficient global optimization is still indispensable. Second, the extreme values of the response may be highly nonlinear with respect to interval variables and may have multiple MPPs. This may lead to large errors if the First Order and Second Order Reliability Methods (FORM and SORM) are used based on the extreme values of the response. Third, most of current methods only focus on the worst case reliability, or the lower bound of the reliability. To understand the uncertainty in the reliability, the upper bound of reliability is also needed.

The objective of this work is to deal with above challenges by developing a new random filed approach for reliability analysis with both random and interval variables. The contributions and significance of the new method are as follows: (1) This work develops a new way to model the reliability with random and interval variables. A response variable is viewed as a random field that is spatially correlated at different locations of interval variables. This allows for using random field methodologies to calculate the lower and upper bounds of reliability. (2) A new FORM-based random field approach is developed for the reliability analysis with random and interval variables. The method transforms the general random filed of the response into a Gaussian field, which is then expanded as a function of a number of Gaussian variables. This avoids the use of global optimization and makes it possible to use Monte Carlo simulation to obtain both the maximum and minimum values of the reliability simultaneously. (3) An efficient algorithm of the Kriging model method is developed to build the mean and autocorrelation functions of the transformed Gaussian field. This makes it accurate and efficient to fully define the transformed Gaussian field.

The remainder of this paper is organized as follows. Sec. 2 reviews the methods of reliability analysis with both random and interval variables. Sec. 3 discusses the idea of reliability analysis with a random field approach, followed by the numerical implementation in Sec. 4. Three examples are presented Sec. 5. Conclusions and future work are given in Sec. 6.

2. Review of Reliability Analysis with Random and Interval Variables

A response variable G may be a function of random variables $\mathbf{X}=[X_i]_{i=1,n}$ and interval variables $\mathbf{Y}=[Y_j]_{j=1,m}$. If only $\mathbf{Y}$ exists, the response is given by

$$G = g(\mathbf{Y}) \tag{1}$$

where $\mathbf{Y} \in [\underline{\mathbf{Y}}, \overline{\mathbf{Y}}]$; $\underline{\mathbf{Y}}=[\underline{Y}_j]_{j=1,m}$ and $\overline{\mathbf{Y}}=[\overline{Y}_j]_{j=1,m}$ are the lower and upper bounds, respectively.

G is also an interval, whose lower and upper bounds are defined by

$$\underline{G} = \min_{\mathbf{Y}\in[\underline{\mathbf{Y}}, \overline{\mathbf{Y}}]} \{g(\mathbf{Y})\} \tag{2}$$

and

$$\overline{G} = \max_{\mathbf{Y}\in[\underline{\mathbf{Y}}, \overline{\mathbf{Y}}]} \{g(\mathbf{Y})\} \tag{3}$$

respectively. Fig. 1 shows an interval response for a two-dimensional case.

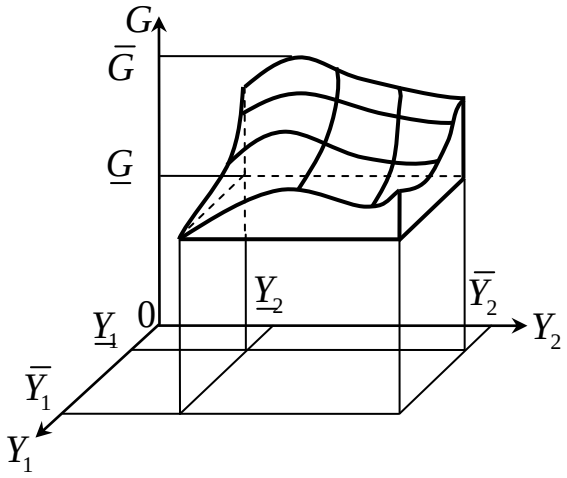

Fig. 1. Limit-state function with interval variables

If both $\mathbf{X}$ and $\mathbf{Y}$ exist, the response is given by

$$G = g(\mathbf{X}, \mathbf{Y}) \tag{4}$$

The extreme responses $\overline{G}$ and $\underline{G}$ are now random variables. If a failure occurs when $G < e$, where e is a limit state, the probability of failure is defined by

$$p_f(\mathbf{Y}) = \Pr\{g(\mathbf{X}, \mathbf{Y}) < e\} \tag{5}$$

Since p_f depends on $\mathbf{Y}$, p_f is bounded between its lower and upper bounds given below.

$$\underline{p}_f = \Pr\{\overline{G} < e\} = \Pr\{\max_{\mathbf{Y}\in[\underline{\mathbf{Y}}, \overline{\mathbf{Y}}]} \{g(\mathbf{X}, \mathbf{Y})\} < e\} \tag{6}$$

and

$$\overline{p}_f = \Pr\{\underline{G} < e\} = \Pr\{\min_{\mathbf{Y}\in[\underline{\mathbf{Y}}, \overline{\mathbf{Y}}]} \{g(\mathbf{X}, \mathbf{Y})\} < e\} \tag{7}$$

As obtaining the extreme responses $\overline{G}$ and $\underline{G}$ requires the global optimization on $[\underline{\mathbf{Y}}, \overline{\mathbf{Y}}]$, calculating $\underline{p}_f$ and $\overline{p}_f$ is extremely costly in computation. Next two common types of reliability analysis methods for problems with both random and interval variables are briefly reviewed.

The first type includes methodologies that combine reliability analysis (RA), such as FORM, and interval analysis (IA). If FORM is used for RA, $\mathbf{X}$ is transformed into standard normal variables $\mathbf{U}$ [18], and the transformation is denoted by $\mathbf{X} = T[\mathbf{U}]$. Then the reliability indexes ($\overline{\beta}$ and $\underline{\beta}$) are searched for by

$$\begin{cases} \overline{\beta} = \min_{\mathbf{U}} \sqrt{\mathbf{U}\mathbf{U}^T} \\ \text{s. t. } \max_{\mathbf{Y}} \{g(T[\mathbf{U}], \mathbf{Y})\} = e \end{cases} \tag{8}$$

and

$$\begin{cases} \underline{\beta} = \min_{\mathbf{U}} \sqrt{\mathbf{U}\mathbf{U}^T} \\ \text{s. t. } \min_{\mathbf{Y}} \{g(T[\mathbf{U}], \mathbf{Y})\} = e \end{cases} \tag{9}$$

Then the probabilities of failure are given by

$$\underline{p}_f = \Phi(-\overline{\beta}) \tag{10}$$

and

$$\overline{p}_f = \Phi(-\underline{\beta}) \tag{11}$$

The optimal point from Eq. (8) or (9) is called a MPP, denoted by $\overline{\mathbf{u}}^*$ for Eq. (8) and $\underline{\mathbf{u}}^*$ for Eq. (9).

Evaluating the equality constraint functions in Eqs. (8) and (9) requires global optimization on $\mathbf{Y} \in [\underline{\mathbf{Y}}, \overline{\mathbf{Y}}]$, and the entire analysis needs a double-loop optimization process, thereby computationally expensive. The following are some examples of the first type methodologies. An iterative procedure [12] using a probability and convex mixed model was reported in [13]. By applying the performance measure approach, the method transforms the nested double-loop optimization problem into an approximate single-loop minimization problem. Similarly, a SSL method, as mentioned in the introduction section, decouples the double loop procedure into a sequential single loop [16, 17].

After the SSL method, Jiang *et al.*[9] proposed an equivalent model method to improve the robustness of the single loop algorithm. The method demonstrates that solving Eq. (9) is equivalent to solving a general MPP problem after treating the interval variables as uniformly distributed random variables [9]. The method is efficient compared with other single loop methods, but similar to other methods that uses FORM, its accuracy may not be good. When G is highly nonlinear with respect to $\mathbf{Y}$, the linearization of the limit-state function at the MPP with respect to $\mathbf{Y}$ will result in large errors. The above methods also need to be performed twice to obtain the lower and upper bounds of p_f, thereby increasing the computational cost.

The second type of methodologies uses design of experiments. A surrogate model of $G = g(\mathbf{X}, \mathbf{Y})$ is built first, and then the extreme probabilities of failure are estimated by MCS. In this group of methods, interval variables are usually treated as variables following uniform distributions. For instance, Zhuang and Pan approximate limit-state functions with interval variables using the Kriging method [19]. Li *et al.* [20] also use the Kriging method to build a surrogate model for a bi-level limit-state function with only random variables. The function is constructed by applying the probability theory at the random variable level and non-probabilistic reliability method at the interval variable level. Yoo and Lee [21] perform the sensitivity analysis with respect to interval variables, and surrogate models are employed to approximate the reliability. Zhang and Hosder [22] expand the random and interval variables using the stochastic expansion methods.

Although all the aforementioned methods can deal with both random and interval variables, their accuracy and efficiency may still need to be improved. From a different perspective, this work views limit-state functions with interval variables as general

random fields, and this leads to a new modeling and analysis method that can potentially improve the efficiency and accuracy of reliability analysis.

3. Reliability Modeling from a Random Field Perspective

This work now shows that the reliability analysis problem can be approached from a random field perspective. The advantages of doing so are discussed as well. A random filed is essentially a spatial-variant random variable [23]. In other words, its distribution changes at different locations, and the random variable at one location is usually dependent on that at another location. Random fields have been used to describe spatially varying and dependent quantities, such as mechanical properties of materials, including Young's modulus, Poisson's ratio, and yield stress [24], as well as temperature, deformation, and surface forces.

For example, the thickness, D, of a metal sheet shown in Fig. 2, is a random field. At a specific location (y_1, y_2), D is a random variable with a specific distribution. The distribution of D is different at another location (y_1', y_2'), and $D(y_1, y_2)$ is dependent on $D(y_1', y_2')$. In this case, the spatial variables are Y_1 - and Y_2 -coordinates.

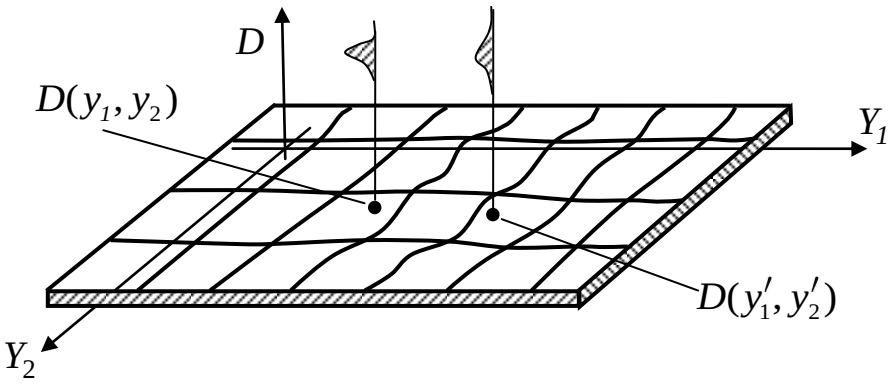

Fig. 2. Random field thickness of a metal sheet

The response $G = g(\mathbf{X}, \mathbf{Y})$ is considered as a random field. The reasons are below.

- G is a random variable. If $\mathbf{Y}$ is fixed at $\mathbf{y}$, $G = g(\mathbf{X}, \mathbf{y})$ is random, and its distribution is determined by $g(\cdot)$ and the joint probability density function (PDF) of $\mathbf{X}$.
- The distribution of G changes with respect to $\mathbf{Y}$. The distribution at $\mathbf{y}$ may be different from that at $\mathbf{y}'$ because $G = g(\mathbf{X}, \mathbf{y})$ may be different from $G' = g(\mathbf{X}, \mathbf{y}')$ as shown in the metal sheet example in Fig. 2 and another two-dimensional example in Fig. 3.
- $G = g(\mathbf{X}, \mathbf{y})$ and $G' = g(\mathbf{X}, \mathbf{y}')$ may be dependent because they share common random variables $\mathbf{X}$.
- For any given $\mathbf{X} = \mathbf{x}$, $G = g(\mathbf{x}, \mathbf{Y})$ is a realization of the field;

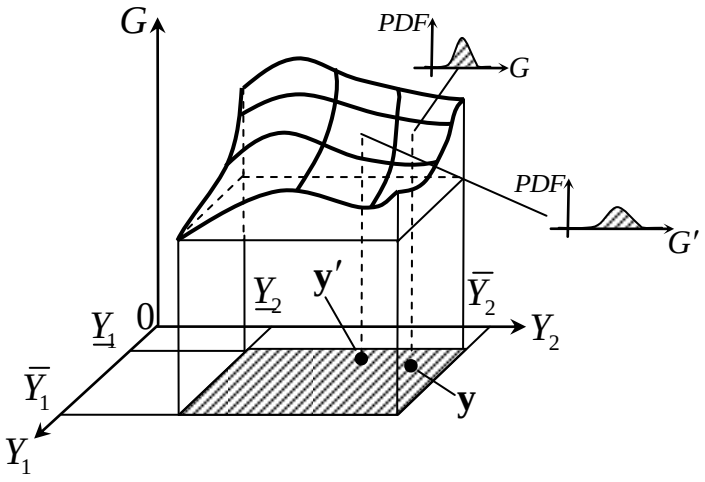

Fig. 3. Responses with both random and interval variables

For the above reasons, G is indeed a random field whose spatial variables are intervals $\mathbf{Y}$. G is actually a general non-stationary random field since its distributions are not constant (varying with respect to $\mathbf{Y}$) and the dimensions of the spatial variable $\mathbf{Y}$ is m, maybe greater than two or three.

The random field perspective allows us to use random field methodologies to calculate the probability of failure. To do so, the bounds of the probability of failure are redefined as follows.

$$\underline{p}_f = \Pr\{G = g(\mathbf{X}, \mathbf{y}) < e, \forall\, \mathbf{y} \in [\underline{\mathbf{Y}}, \overline{\mathbf{Y}}]\} \tag{12}$$

where $\forall$ stands for "for all". The minimum probability of failure is the probability that all the interval bounds are completely in the failure region.

$$\overline{p}_f = \Pr\{G = g(\mathbf{X}, \mathbf{y}) < e, \exists\, \mathbf{y} \in [\underline{\mathbf{Y}}, \overline{\mathbf{Y}}]\} \tag{13}$$

where $\exists$ stands for "there exists at least one". The maximum probability is the probability that the interval bounds intersect with in the failure region.

Let us examine why the new definitions are equivalent to the original definitions given in Eqs. (6) and (7). Recall that the original maximum probability of failure $\overline{p}_f$ is defined as $\overline{p}_f = \Pr\{\underline{G} = \min_{\mathbf{Y} \in [\underline{\mathbf{Y}}, \overline{\mathbf{Y}}]} \{g(\mathbf{X}, \mathbf{Y})\} < e\}$ in Eq. (7). The definition is equivalent to the definition given in Eq. (13). The reason is that the two events $A = \underline{G} < e$ in Eq. (7) and $B = G = g(\mathbf{X}, \mathbf{y}) < e, \exists\, \mathbf{y} \in [\underline{\mathbf{Y}}, \overline{\mathbf{Y}}]$ in Eq. (13) are equivalent. For event *B*, at least at one point of $\mathbf{Y}$, $G < e$. There are two cases.

Case 1: There is only one point $\mathbf{y}'$ where $G < e$, and event *B* becomes $B = g(\mathbf{X}, \mathbf{y}') < e$. This mean that at other points on $[\underline{\mathbf{Y}}, \overline{\mathbf{Y}}]$, except at $\mathbf{y}'$, $G \geq e$. Then $\mathbf{y}'$ is the point where G is minimum, or $\underline{G} = g(\mathbf{X}, \mathbf{y}')$. Thus event *A* becomes $A = \underline{G} = g(\mathbf{X}, \mathbf{y}') < e$. Event *A* is therefore equivalent to event *B*.

Case 2: There are multiple points $[\mathbf{y}'_i]_{i=1,h}$ where $G < e$. Event *B* is then an intersection expressed by $B = \bigcap_{i=1}^{h} g(\mathbf{X}, \mathbf{y}'_i) < e$. At all the other points on $[\underline{\mathbf{Y}}, \overline{\mathbf{Y}}]$, $G \geq e$. Let $\mathbf{y}'' \in [\mathbf{y}'_i]_{i=1,h}$ be the point where G is minimum, or $\underline{G} = g(\mathbf{X}, \mathbf{y}'')$. Event *B* can be rewritten as $B = \min_{\mathbf{y}'_i} g(\mathbf{X}, \mathbf{y}'_i) < e \;=\; \underline{G} = g(\mathbf{X}, \mathbf{y}'') < e$, which is equivalent to event A.

Similarly, the original minimum probability of failure $\underline{p}_f$, defined as $\underline{p}_f = \Pr\{\overline{G} = \max_{\mathbf{Y} \in [\underline{\mathbf{Y}}, \overline{\mathbf{Y}}]} \{g(\mathbf{X}, \mathbf{Y})\} < e\}$ in Eq. (6), is equivalent to the definition given in Eq. (12) because event $C = \overline{G} < e$ in Eq. (6) is equivalent to event $D = g(\mathbf{X}, \mathbf{y}) < e, \forall\, \mathbf{y} \in [\underline{\mathbf{Y}}, \overline{\mathbf{Y}}]$ in Eq. (12). The equivalency holds because

$g(\mathbf{X}, \mathbf{y}) \le \bar{G}$ for all $\mathbf{y} \in [\underline{\mathbf{Y}}, \bar{\mathbf{Y}}]$, and thus $C = \bar{G} < e = g(\mathbf{X}, \mathbf{y}) \le \bar{G} < e, \forall\, \mathbf{y} \in [\underline{\mathbf{Y}}, \bar{\mathbf{Y}}] = D$.

The advantages of the new definitions are multifold. First, it avoids the direct use of the global responses with respect to interval variables. The elimination of global optimization can improve the computational efficiency significantly for responses that are highly nonlinear with respect to interval variables. Second, defining the probability of failure with a random field approach enables us to use existing random field methodologies to estimate the bounds of the probability of failure differently, potentially more accurately and efficiently than the traditional methods. Third, as discussed in the next section, the definitions also make it easy to integrate the traditional reliability methods and a random field approach to solve the problems with both random and interval variables.

As the second task of this work, the feasibility of the proposed random approach is demonstrated by developing a new numerical procedure that employs FORM and a random field expansion method. The details are given in the next section.

4. First Order Reliability Method Using Random Field Approach

As indicated in Eqs. (12) and (13), the lower and upper bounds of p_f can be calculated by considering G as a random field. Directly using random field G, however, is difficult because it is in general a non-Gaussian and non-stationary random field and no analytical solutions exist. One possible way is using the direct MCS, but it will be computationally expensive.

In this work, FORM is used to transform G into a Gaussian random field $\tilde{G}$. A similar strategy has been applied to the time-dependent reliability analysis involving stochastic processes [25]. Herein, the strategy is extended to the problem with interval variables. Based on the probability equivalency between G and $\tilde{G}$, samples are generated on $\tilde{G}$ by discretizing $\tilde{G}$. With the samples, the probability of failure is then estimated. In the following subsections, the discretization methods of a Gaussian field are introduced first and then the details of the implementation procedure are discussed.

4.1. Discretization methods of a Gaussian random field

The discretization of a Gaussian field has been extensively studied. There are three groups of discretization methods, including the point discretization method, the average discretization method, and the series expansion method [24]. The review of the discretization methods is available in [26]. Herein, the expansion optimal linear estimation method (EOLE) [26] that used in this work is briefly reviewed. Let $\tilde{G}$ be a Gaussian field with mean $\mu(\mathbf{y})$, standard deviation $\sigma(\mathbf{y})$, and autocorrelation function $\rho(\mathbf{y}, \mathbf{y}')$. After discretizing $[\underline{\mathbf{Y}}, \overline{\mathbf{Y}}]$ into p points $\mathbf{y}_i$, $i = 1, 2, \cdots, p$, EOLE expands $\tilde{G}$ as follows:

$$\tilde{G} \approx \mu(\mathbf{y}) + \sigma(\mathbf{y}) \sum_{i=1}^{r} \frac{\xi_i}{\sqrt{\eta_i}} \boldsymbol{\varphi}_i^T \boldsymbol{\rho}_G(\mathbf{y}), \quad \forall \mathbf{y} \in [\underline{\mathbf{Y}}, \overline{\mathbf{Y}}] \tag{14}$$

where η_i and $\boldsymbol{\varphi}_i^T$ are the eigenvalues and eigenvectors of the correlation matrix $\boldsymbol{\rho}$ with element $\rho_{ij} = \rho(\mathbf{y}_i, \mathbf{y}_j)$, $i, j = 1, 2, \cdots, p$, $\boldsymbol{\rho}_G(\mathbf{y}) = [\rho(\mathbf{y}, \mathbf{y}_1), \rho(\mathbf{y}, \mathbf{y}_2), \cdots, \rho(\mathbf{y}, \mathbf{y}_p)]^T$, and $r \le p$ is the number of terms of expansion. Note that the eigenvalues η_i are sorted in decreasing order.

As discussed above, a Gaussian field can be completely characterized and discretized once its mean value function $\mu(\mathbf{y})$, standard deviation function $\sigma(\mathbf{y})$, and autocorrelation function $\rho(\mathbf{y}, \mathbf{y}')$ are known. Next it discusses how to obtain $\tilde{G}$ and its mean, standard deviation, and autocorrelation functions.

4.2. Construction of an equivalent Gaussian field $\tilde{G}$

To use EOLE in Eq. (14), t the general random field G needs to be transformed into an equivalent Gaussian field $\tilde{G}$. This work does so by using FORM.

4.2.1. Transformation by FORM

FORM has been widely used in reliability analysis with only random variables [27-29]. It can also be used for problems with both random and interval variables. It requires searching for the MPP. For a given $\mathbf{y} \in [\underline{\mathbf{Y}}, \overline{\mathbf{Y}}]$, the MPP of $g(\mathbf{X}, \mathbf{y})$ is obtained by

$$\begin{cases} \min\limits_{\mathbf{u}} \sqrt{\mathbf{U}\mathbf{U}^T} \\ \text{s. t. } G = g(T(\mathbf{U}), \mathbf{y}) \le e \end{cases} \tag{15}$$

where $T(\mathbf{U})$ is an operator that transforms standard normal variables $\mathbf{U}$ to $\mathbf{X}$ [18].

After the MPP search, $g(T(\mathbf{U}), \mathbf{y})$ is linearized at the MPP point $\mathbf{u}^*(\mathbf{y})$ using Taylor's series expansion as follows:

$$g(T(\mathbf{U}), \mathbf{y}) \approx \hat{g}(\mathbf{U}, \mathbf{y}) = g(\mathbf{u}^*(\mathbf{y}), \mathbf{y}) + \nabla g(\mathbf{u}^*(\mathbf{y}), \mathbf{y})(\mathbf{U} - \mathbf{u}^*(\mathbf{y}))^T \tag{16}$$

where

$$\nabla g(\mathbf{u}^*(\mathbf{y}), \mathbf{y}) = \left(\left.\frac{\partial g(\mathbf{U}, \mathbf{y})}{\partial U_1}\right|_{\mathbf{u}^*(\mathbf{y})}, \left.\frac{\partial g(\mathbf{U}, \mathbf{y})}{\partial U_2}\right|_{\mathbf{u}^*(\mathbf{y})}, \cdots, \left.\frac{\partial g(\mathbf{U}, \mathbf{y})}{\partial U_n}\right|_{\mathbf{u}^*(\mathbf{y})} \right) \tag{17}$$

The accuracy loss of the Taylor expansion is minimal at the MPP, where $g(\mathbf{u}^*(\mathbf{y}), \mathbf{y}) = e$, for $\mathbf{y} \in [\underline{\mathbf{Y}}, \overline{\mathbf{Y}}]$. It gives

$$\Pr\{G = g(\mathbf{X}, \mathbf{y}) < e\} \approx \Pr\{\nabla g(\mathbf{u}^*(\mathbf{y}), \mathbf{y})(\mathbf{U} - \mathbf{u}^*(\mathbf{y}))^T < 0\} \tag{18}$$

Eq. (18) is rewritten as

$$\Pr\{G = g(\mathbf{X}, \mathbf{y}) < e\} \approx \Pr\{\frac{\nabla g(\mathbf{u}^*(\mathbf{y}), \mathbf{y})}{\left\|\nabla g(\mathbf{u}^*(\mathbf{y}), \mathbf{y})\right\|} \mathbf{U}^T < \frac{\nabla g(\mathbf{u}^*(\mathbf{y}), \mathbf{y})}{\left\|\nabla g(\mathbf{u}^*(\mathbf{y}), \mathbf{y})\right\|} \mathbf{u}^*(\mathbf{y})^T\} \tag{19}$$

At the MPP point, it also has $\dfrac{\nabla g(\mathbf{u}^*(\mathbf{y}), \mathbf{y})}{\left\|\nabla g(\mathbf{u}^*(\mathbf{y}), \mathbf{y})\right\|} = -\dfrac{\mathbf{u}^*(\mathbf{y})}{\left\|\mathbf{u}^*(\mathbf{y})\right\|}$; Eq. (19) then becomes

$$\Pr\{G = g(\mathbf{X}, \mathbf{y}) < e\} \approx \Pr\{-\frac{\mathbf{u}^*(\mathbf{y})}{\left\|\mathbf{u}^*(\mathbf{y})\right\|} \mathbf{U}^T < -\frac{\mathbf{u}^*(\mathbf{y})}{\left\|\mathbf{u}^*(\mathbf{y})\right\|} \mathbf{u}^*(\mathbf{y})^T\} \tag{20}$$

Define $\boldsymbol{\alpha}(\mathbf{y}) = -\dfrac{\mathbf{u}^*(\mathbf{y})}{\left\|\mathbf{u}^*(\mathbf{y})\right\|}$ and $\beta(\mathbf{y}) = \left\|\mathbf{u}^*(\mathbf{y})\right\|$, it gives

$$\Pr\{G = g(\mathbf{X}, \mathbf{y}) < e\} \approx \Pr\{\boldsymbol{\alpha}(\mathbf{y})\mathbf{U}^T < -\beta(\mathbf{y})\} \tag{21}$$

Thus the probability if failure is

$$\Pr\{G = g(T(\mathbf{U}), \mathbf{y}) \le e\} \approx \Pr\{\tilde{G} = \tilde{g}(\mathbf{U}, \mathbf{y}) = \boldsymbol{\alpha}(\mathbf{y})\mathbf{U}^T + \beta(\mathbf{y}) < 0\} \tag{22}$$

The mean and standard deviation functions of $\tilde{G}$ are then given by

$$\mu_{\tilde{G}}(\mathbf{y}) = E\{\boldsymbol{\alpha}(\mathbf{y})\mathbf{U}^T\} + \beta(\mathbf{y}) = \beta(\mathbf{y}) \tag{23}$$

$$\sigma_{\tilde{G}}(\mathbf{y}) = \|\boldsymbol{\alpha}(\mathbf{y})\| = 1 \tag{24}$$

where $E\{\cdot\}$ stands for expectation.

Eqs. (23) and (24) indicate that for any $\mathbf{y} \in [\underline{\mathbf{Y}}, \bar{\mathbf{Y}}]$, the equivalent response $\tilde{G}$ is a Gaussian random variable with mean $\mu_{\tilde{G}}(\mathbf{y}) = \beta(\mathbf{y})$ and standard deviation $\sigma_{\tilde{G}}(\mathbf{y}) = 1$.

4.2.2. Properties of $\tilde{G}$

If the MPP search is performed at two points, $\mathbf{y}, \mathbf{y}' \in [\underline{\mathbf{Y}}, \bar{\mathbf{Y}}]$, it has

$$\Pr\{G = g(T(\mathbf{U}), \mathbf{y}) \le e\} \approx \Pr\{\tilde{G}(\mathbf{y}) = \boldsymbol{\alpha}(\mathbf{y})\mathbf{U}^T + \beta(\mathbf{y}) < 0\} \tag{25}$$

$$\Pr\{G = g(T(\mathbf{U}), \mathbf{y}) \le e\} \approx \Pr\{\tilde{G}(\mathbf{y}') = \boldsymbol{\alpha}(\mathbf{y}')\mathbf{U}^T + \beta(\mathbf{y}') < 0\} \tag{26}$$

Since $\tilde{G}(\mathbf{y})$ and $\tilde{G}(\mathbf{y}')$ share common random variables $\mathbf{U}$, they are generally correlated. The correlation coefficient between $\tilde{G}(\mathbf{y})$ and $\tilde{G}(\mathbf{y}')$ is given by

$$\rho(\mathbf{y}, \mathbf{y}') = \frac{E\{\tilde{G}(\mathbf{y})\tilde{G}(\mathbf{y}')\} - E\{\tilde{G}(\mathbf{y})\}E\{\tilde{G}(\mathbf{y}')\}}{\sigma_{\tilde{G}(\mathbf{y})}\sigma_{\tilde{G}(\mathbf{y}')}} \tag{27}$$

The above expression can be simplified as

$$\rho(\mathbf{y}, \mathbf{y}') = \boldsymbol{\alpha}(\mathbf{y})\boldsymbol{\alpha}(\mathbf{y}')^T, \ \mathbf{y}, \mathbf{y}' \in [\underline{\mathbf{Y}}, \bar{\mathbf{Y}}] \tag{28}$$

From the above discussions, it is known that $\tilde{G}$ has he following properties:

- $\tilde{G}$ is a Gaussian random variable for any given $\mathbf{y} \in [\underline{\mathbf{Y}}, \bar{\mathbf{Y}}]$.
- The distribution of $\tilde{G}$ changes with respect to $\mathbf{y}$ as its mean $\mu_{\tilde{G}}(\mathbf{y}) = \beta(\mathbf{y})$ is a function of $\mathbf{y}$.
- For any two points $\mathbf{y}, \mathbf{y}' \in [\underline{\mathbf{Y}}, \bar{\mathbf{Y}}]$, $\tilde{G}(\mathbf{y})$ and $\tilde{G}(\mathbf{y}')$ are in general correlated with correlation coefficient given in Eq. (28).

The properties of $\tilde{G}$ show that $\tilde{G}$ is indeed a Gaussian field with mean $\mu_{\tilde{G}}(\mathbf{y}) = \beta(\mathbf{y})$, standard deviation $\sigma_{\tilde{G}}(\mathbf{y}) = 1$, and autocorrelation function $\rho(\mathbf{y}, \mathbf{y}')$. By performing FORM at every point $\mathbf{y} \in [\underline{\mathbf{Y}}, \bar{\mathbf{Y}}]$, the random field G can be mapped to an equivalent Gaussian field $\tilde{G}$.

Based on the equivalency given in Eq. (22), the minimum and maximum probabilities of failure are then computed with $\tilde{G}$ as follows:

$$\begin{aligned} \underline{p}_f &= \Pr\{G = g(\mathbf{X}, \mathbf{y}) < e, \forall\, \mathbf{y} \in [\underline{\mathbf{Y}}, \overline{\mathbf{Y}}]\} \\ &\approx \Pr\{\tilde{G} = \tilde{g}(\mathbf{U}, \mathbf{y}) < 0, \forall\, \mathbf{y} \in [\underline{\mathbf{Y}}, \overline{\mathbf{Y}}]\} \end{aligned} \tag{29}$$

$$\begin{aligned} \overline{p}_f &= \Pr\{G = g(\mathbf{X}, \mathbf{y}) < e, \exists\, \mathbf{y} \in [\underline{\mathbf{Y}}, \overline{\mathbf{Y}}]\} \\ &\approx \Pr\{\tilde{G} = \tilde{g}(\mathbf{U}, \mathbf{y}) < 0, \exists\, \mathbf{y} \in [\underline{\mathbf{Y}}, \overline{\mathbf{Y}}]\} \end{aligned} \tag{30}$$

The task now is to obtain $\mu_{\tilde{G}}(\mathbf{y})$ (or $\beta(\mathbf{y})$) and $\rho(\mathbf{y}, \mathbf{y}')$ as a function of $\mathbf{y}$ because they fully define $\tilde{G}$. One possible way to determine $\mu_{\tilde{G}}(\mathbf{y})$ and $\rho(\mathbf{y}, \mathbf{y}')$ is to perform the MPP search at a number of points of interval variables that are uniformly distributed on $[\underline{\mathbf{Y}}, \overline{\mathbf{Y}}]$. This approach, however, is not efficient. In this work, the Kriging method is used to create models for $\beta(\mathbf{y})$ and $\rho(\mathbf{y}, \mathbf{y}')$. This approach is much more efficient as discussed next.

4.2.3. Surrogate models of $\beta(\mathbf{y})$ and $\rho(\mathbf{y}, \mathbf{y}')$

As discussed previously, if the MPP search is performed at $\mathbf{y}$, $\beta(\mathbf{y})$ is obtained. If the MPP search is also performed at $\mathbf{y}'$, $\rho(\mathbf{y}, \mathbf{y}')$ is obtained. In this work, the Kriging model method [30] is used, which determines the locations of $\mathbf{y}$ and $\mathbf{y}'$ iteratively without using uniformly distributed points of $\mathbf{y}$ and $\mathbf{y}'$. This way the number of MPP searches can be reduced.

The output of a Kriging model is assumed to be a stochastic process [30-33]. The Kriging model of a function $f(\mathbf{y})$ is given by

$$\hat{f}(\mathbf{y}) = \boldsymbol{\upsilon}^T \mathbf{h}(\mathbf{y}) + \varepsilon(\mathbf{y}) \tag{31}$$

where $\boldsymbol{\upsilon} = [\upsilon_1, \upsilon_2, \cdots, \upsilon_p]^T$ is a vector of unknown coefficients, $\mathbf{h}(\mathbf{y}) = [h_1(\mathbf{y}), h_2(\mathbf{y}), \cdots, h_p(\mathbf{y})]^T$ is a vector of regression functions, $\boldsymbol{\upsilon}^T \mathbf{h}(\mathbf{y})$ is the polynomial parts and the trend of prediction, and $\varepsilon(\mathbf{y})$ is a Gaussian process with zero mean and covariance $Cov[\varepsilon(\mathbf{y}_i), \varepsilon(\mathbf{y}_j)]$. Reviews of the Kriging model are available in [34, 35], and a Kriging toolbox DACE is also available [36]. Herein the application of the Kriging model for $\beta(\mathbf{y})$ and $\rho(\mathbf{y}, \mathbf{y}')$ is the focus.

Even if $\beta(\mathbf{y})$ and $\rho(\mathbf{y}, \mathbf{y}')$ are two different functions, they share common input variables on $[\underline{\mathbf{Y}}, \overline{\mathbf{Y}}]$. The result of the MPP search for $\beta(\mathbf{y})$ can also be used for $\rho(\mathbf{y}, \mathbf{y}')$. Surrogate models for $\beta(\mathbf{y})$ and $\rho(\mathbf{y}, \mathbf{y}')$ are therefore constructed simultaneously. In addition, Eq. (28) gives $\rho(\mathbf{y}, \mathbf{y}') = 1$ for any $\mathbf{y} = \mathbf{y}'$. Taking advantage of these features of $\beta(\mathbf{y})$ and $\rho(\mathbf{y}, \mathbf{y}')$, an efficient algorithm can be designed to create the surrogate models. Fig. 4 shows such a procedure. The detailed steps are explained below.

Step 1 through Step 3: Create initial Kriging models

Step 1: Generate evenly distributed initial samples $\mathbf{y}^s = [\mathbf{y}_i^s]_{i=1,k}$ on $[\underline{\mathbf{Y}}, \overline{\mathbf{Y}}]$.

Step 2: Obtain initial samples of $\boldsymbol{\beta}$ and $\boldsymbol{\rho}$ for surrogate models

(1) Perform MPP searches at $\mathbf{y}_i^s$, $i = 1, k$, using Eq. (15); obtain $\boldsymbol{\alpha}(\mathbf{y}_i^s)$ and $\beta(\mathbf{y}_i^s)$.

(2) Obtain $\boldsymbol{\beta} = [\beta_i]_{i=1,k}$, $\mathbf{yy}^s = [\mathbf{y}_i^s, \mathbf{y}_j^s]_{i,j=1,k}$, and $\boldsymbol{\rho} = [\rho(\mathbf{y}_i^s, \mathbf{y}_j^s)]_{i,j=1,k}$ using Eq. (28).

Step 3: Construct the initial Kriging models of $\beta(\mathbf{y})$ and $\rho(\mathbf{y}, \mathbf{y}')$ using $\{\mathbf{y}^s, \boldsymbol{\beta}\}$ and $\{\mathbf{yy}^s, \boldsymbol{\rho}\}$, respectively.

Step 4 through Step 8: Update models and create final models

Step 4: Identify the maximum mean square error and the associated new sample point

(1) Find the maximum mean square errors of $\beta(\mathbf{y})$ and $\rho(\mathbf{y}, \mathbf{y}')$ using $[\mathbf{y}^\beta, \varepsilon_\beta^{\max}] = \arg\max_{\mathbf{y} \in [\mathbf{Y}^L, \mathbf{Y}^U]} \mathrm{MSE}_\beta(\mathbf{y})$ and $[(\mathbf{y}_1^\rho, \mathbf{y}_2^\rho), \varepsilon_\rho^{\max}] = \arg\max_{\mathbf{y}_1, \mathbf{y}_2 \in [\mathbf{Y}^L, \mathbf{Y}^U]} \mathrm{MSE}_\rho(\mathbf{y}_1, \mathbf{y}_2)$, respectively.

$\mathrm{MSE}_\beta(\mathbf{y})$ and $\mathrm{MSE}_\rho(\mathbf{y}_1, \mathbf{y}_2)$ are obtained from the outputs of Kriging model directly [36].

(2) If $\varepsilon_\rho^{\max} > \varepsilon_\beta^{\max}$, let $\varepsilon^{\max} = \varepsilon_\rho^{\max}$, $\mathbf{y}^{\text{new}} = [\mathbf{y}_1^\rho, \mathbf{y}_2^\rho]$; otherwise, let $\varepsilon^{\max} = \varepsilon_\beta^{\max}$, $\mathbf{y}^{\text{new}} = \mathbf{y}^\beta$.

Step 5: Check convergence: If $\varepsilon^{\max} > \varepsilon_{MSE}$, go to next step; otherwise, obtain surrogate models of $\beta(\mathbf{y})$ and $\rho(\mathbf{y}, \mathbf{y}')$.

Step 6: Perform MPP searches at $\mathbf{y}^{\text{new}}$, and obtain $\boldsymbol{\alpha}(\mathbf{y}^{\text{new}})$ and $\beta(\mathbf{y}^{\text{new}})$

Step 7: Update $\mathbf{y}^s$, $\boldsymbol{\beta}$, $\mathbf{yy}^s$, and $\boldsymbol{\rho}$: $\mathbf{y}^s = [\mathbf{y}^s, \mathbf{y}^{\text{new}}]$, $\boldsymbol{\beta} = [\boldsymbol{\beta}, \beta(\mathbf{y}^{\text{new}})]$, $\mathbf{yy}^s = [\mathbf{y}_i^s, \mathbf{y}_j^s]_{i,\, j=1,\, h}$, and $\boldsymbol{\rho} = [\rho(\mathbf{y}_i^s, \mathbf{y}_j^s)]_{i,\, j=1,\, h}$, where h is the number of samples of $\mathbf{y}^s$.

Step 8: Construct new Kriging models $\beta(\mathbf{y})$ and $\rho(\mathbf{y}, \mathbf{y}')$ using $\{\mathbf{y}^s, \boldsymbol{\beta}\}$ and $\{\mathbf{yy}^s, \boldsymbol{\rho}\}$, and then go to Step 4.

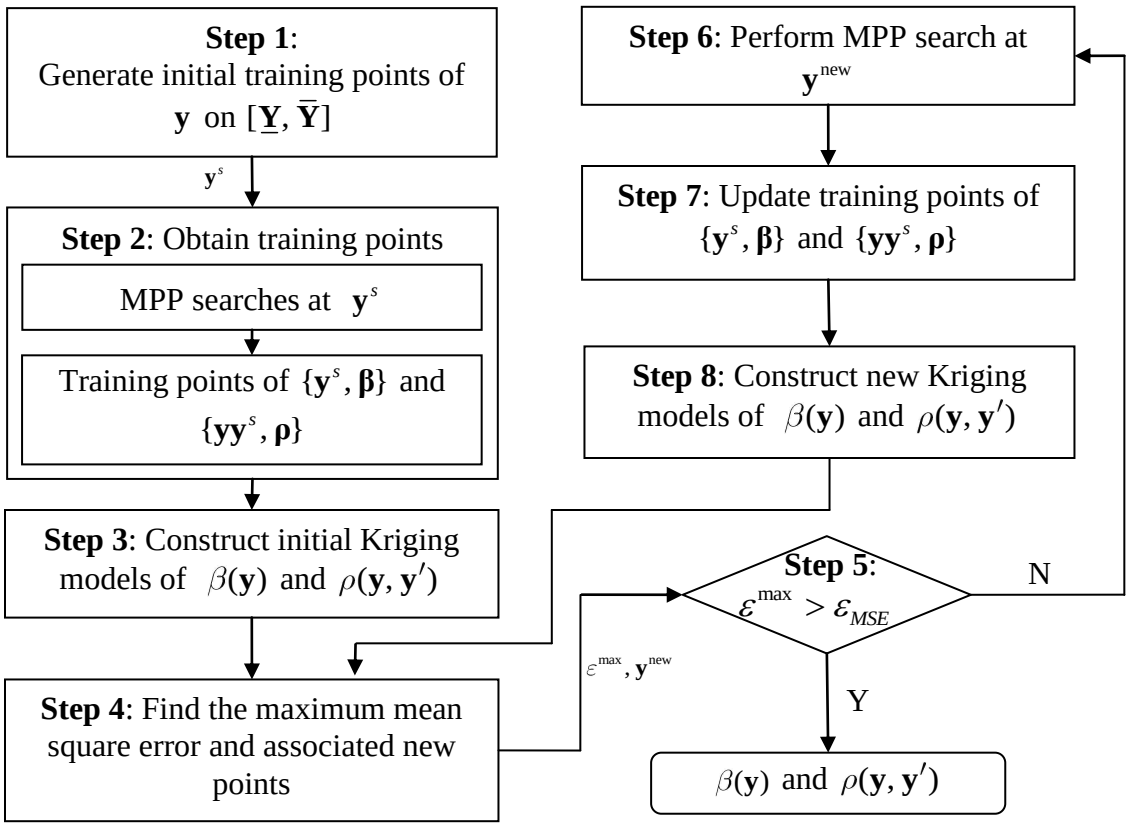

Fig. 4. Flowchart of constructing surrogate models of $\beta(\mathbf{y})$ and $\rho(\mathbf{y}, \mathbf{y}')$

In Step 1, many sampling generation methods can be used, such as the Random sampling method (RS) [37], the Latin hypercube sampling (LHS) method [38], and the Hammersley sampling method (HS) [39]. In this work, the HS method is used as it is

capable of generating more evenly distributed samples than other methods. In Step 2, MPP searches are performed at a number of $\mathbf{y}$. To reduce the number of function calls, a good starting point should be carefully selected for the MPP search. The MPP that has been already obtained is picked as the starting point. The MPP of the sample point, which is the closest to the current sample point $\mathbf{y}_i^s$, is selected as the starting point of $\mathbf{y}_i^s$. In Step 4, the maximum mean square errors are used as the stopping criteria. Since they are calculated by the Kriging models, there is no need to call the limit-state function in this step. Any optimization methods can be used to determine the maximum mean square errors, for example, the DIRECT algorithm [40].

The numerical procedure shows that MPP searches are performed in Steps 2 and 6.

4.3. Discretization *of* $\tilde{G}$

Once the surrogate models of $\beta(\mathbf{y})$ and $\rho(\mathbf{y}, \mathbf{y}')$ are obtained, the equivalent Gaussian field $\tilde{G}$ is fully defined. The original limit-state function is no longer needed for the reliability analysis. $\tilde{G}$ is usually a non-stationary Gaussian field, and there is no analytical solution available to find whether there exists an instant of $\mathbf{y}$ on $[\underline{\mathbf{Y}}, \overline{\mathbf{Y}}]$ when a failure occurs. For this reason, $\tilde{G}$ needs to be approximated or discretized with respect to $\mathbf{Y}$ so that the instants of $\mathbf{Y}$, where failure occurs, can be captured. As discussed in Sec. 4.1, there are many discretization methods available. Here, the EOLE [41] method is used.

s points for the interval variables are first generated on $[\underline{\mathbf{Y}}, \overline{\mathbf{Y}}]$ using the HS sampling method. Let the s points be $\mathbf{y}_i$, $i = 1, s$, using the Kriging model of $\rho(\mathbf{y}, \mathbf{y}')$, the correlation matrix of these points is obtained as follows:

$$\boldsymbol{\Sigma} = \begin{pmatrix} \rho(\mathbf{y}_1, \mathbf{y}_1) & \rho(\mathbf{y}_1, \mathbf{y}_2) & \cdots & \rho(\mathbf{y}_1, \mathbf{y}_s) \\ \rho(\mathbf{y}_2, \mathbf{y}_1) & \rho(\mathbf{y}_2, \mathbf{y}_2) & \cdots & \rho(\mathbf{y}_2, \mathbf{y}_s) \\ \vdots & \vdots & \ddots & \vdots \\ \rho(\mathbf{y}_s, \mathbf{y}_1) & \rho(\mathbf{y}_s, \mathbf{y}_2) & \cdots & \rho(\mathbf{y}_s, \mathbf{y}_s) \end{pmatrix}_{s \times s} \tag{32}$$

where $\rho\left(\mathbf{y}_i, \mathbf{y}_j\right)$, $i, j = 1, s$, are correlation coefficients of $\tilde{G}(\mathbf{y}_i)$ and $\tilde{G}(\mathbf{y}_j)$, which are obtained by plugging $\mathbf{y}_i$ and $\mathbf{y}_j$ into surrogate model $\rho(\mathbf{y}, \mathbf{y}')$.

Based on the correlation matrix and Eq. (14), $\tilde{G}$ is then discretized as

$$\tilde{G} \approx \beta(\mathbf{y}) + \sum_{i=1}^{s} \frac{Z_i}{\sqrt{\eta_i}} \boldsymbol{\varphi}_i^T \boldsymbol{\rho}_{\tilde{G}}(\mathbf{y}), \qquad \forall \mathbf{y} \in [\underline{\mathbf{Y}}, \bar{\mathbf{Y}}] \tag{33}$$

where Z_i, $i = 1, s$, are independent standard normal variables, η_i and $\boldsymbol{\varphi}_i$ are eigenvalues and eigenvectors of correlation matrix $\boldsymbol{\Sigma}$, and $\boldsymbol{\rho}_{\tilde{G}}(\mathbf{y}) = [\rho(\mathbf{y}, \mathbf{y}_1), \rho(\mathbf{y}, \mathbf{y}_2), \cdots, \rho(\mathbf{y}, \mathbf{y}_s)]^T$.

Upon the discretization of $\tilde{G}$, MCS can be performed by plugging random samples of Z_i, $i = 1, s$, and samples of $\mathbf{Y}$ into Eq. (33). Suppose n_{MCS} samples are generated for each random variable Z_i and n_y samples are generated for $\mathbf{Y}$ on $[\underline{\mathbf{Y}}, \bar{\mathbf{Y}}]$ using the HS method, the following sampling matrix of $\tilde{G}$ is then obtained.

$$\tilde{\mathbf{G}} = \begin{pmatrix} \tilde{G}\left(\mathbf{y}_1, 1\right) & \tilde{G}\left(\mathbf{y}_2, 1\right) & \cdots & \tilde{G}\left(\mathbf{y}_{n_Y}, 1\right) \\ \tilde{G}\left(\mathbf{y}_1, 2\right) & \tilde{G}\left(\mathbf{y}_2, 2\right) & \cdots & \tilde{G}\left(\mathbf{y}_{n_Y}, 2\right) \\ \vdots & \vdots & \ddots & \vdots \\ \tilde{G}\left(\mathbf{y}_1, n_{MCS}\right) & \tilde{G}\left(\mathbf{y}_2, n_{MCS}\right) & \cdots & \tilde{G}\left(\mathbf{y}_{n_Y}, n_{MCS}\right) \end{pmatrix}_{n_{MCS} \times n_Y} \tag{34}$$

4.4. Reliability analysis

To approximate the lower and upper bounds of the probability of failure, the following indicator function is first defined:

$$F(i, j) = \begin{cases} 1, \text{ if } \tilde{G}(\mathbf{y}_j, i) < 0, & i = 1, \ n_{MCS}; \ j = 1, n_Y; \\ 0, \text{ otherwise} \end{cases} \tag{35}$$

According to Eqs. (29) and (30), $\underline{p}_f$ and $\bar{p}_f$ are then estimated by

$$\underline{p}_f \approx \frac{1}{n_{MCS}} \sum_{i=1}^{n_{MCS}} F^L(i) \tag{36}$$

$$\bar{p}_f \approx \frac{1}{n_{MCS}} \sum_{i=1}^{n_{MCS}} F^U(i) \tag{37}$$

where

$$F^L(i) = \begin{cases} 1, \text{ if } \sum_{j=1}^{n_Y} F(i,\ j) = n_Y \\ 0, \text{ otherwise} \end{cases} \tag{38}$$

$$F^U(i) = \begin{cases} 1, \text{ if } \sum_{j=1}^{n_Y} F(i,\ j) > 0 \\ 0, \text{ otherwise} \end{cases} \tag{39}$$

As indicated above, with the new approach, $\underline{p}_f$ and $\overline{p}_f$ can be estimated simultaneously, and no global optimization with respect to interval variables is required.

5. Examples

In this section, three examples are used to demonstrate the accuracy and efficiency of the proposed method. Each example is solved using the following four methods:

- The proposed random field approach, denoted by *Random Field*.
- The direct Kriging model method, denoted by *Direct Kriging*, which constructs a surrogate model of the response with respect to both random and interval variables and then uses Monte Carlo simulation (MCS) to calculate the extreme probabilities of failure.
- The equivalent model method proposed by Jiang et al. [9], denoted by *Equivalent MPP*.
- The direct Monte Carlo simulation (MCS).

The solution from MCS with a sufficiently large sample size is used as a benchmark for the accuracy comparison, and the efficiency is measured by the number of function calls for the response variable.

5.1. A mathematical example

The model is given in Eq. (40) with four random variables and one interval variable defined in Table 1. The response function is nonlinear with respect to the interval variable.

$$g(\mathbf{X}, \mathbf{Y}) = -10.5 + 2.1X_1^2 X_2 \sin^2(Y_1 + 0.3) - 2X_3(Y_1 + 0.3) + (X_1 + X_4)(Y_1 - 0.7)^2 \quad (40)$$

The limit state is $e = -10$, and thus the probability of failure is given by

$$p_f = \Pr\{g(\mathbf{X}, \mathbf{Y}) < -10\} \quad (41)$$

where $\mathbf{X} = [X_i]_{i=1,4}$.

In the table, for a random variable, parameters 1 and 2 are the mean and stadard deviation, repectively. For an interval varaible, the two parameters are the lower and upper bounds, respectively.

Building the surrogate models for $\beta(\mathbf{y})$ and $\rho(\mathbf{y}, \mathbf{y}')$ is critical for the proposed random field approach, and the results of the two models are now shown in Figs. 5 and 6. The initial training points and added training points of $\mathbf{Y}$ are also plotted in the figures. The convergence criterion of the two surrogate models is $\varepsilon_{MSE} = 1 \times 10^{-4}$. 13 training points, in total, were used, and thus the MPP search was performed 13 times. The results show that both $\beta(\mathbf{y})$ and $\rho(\mathbf{y}, \mathbf{y}')$ are nonlinear with respect to the interval variable.

Table 1 Variables and parameters of Example 1

Variable	Parameter 1	Parameter 2	Distribution
X_1	2	0.2	Normal
X_2	3	0.3	Normal
X_3	3.5	0.35	Normal
X_4	2	0.4	Normal
Y_1	0	1.5	Interval

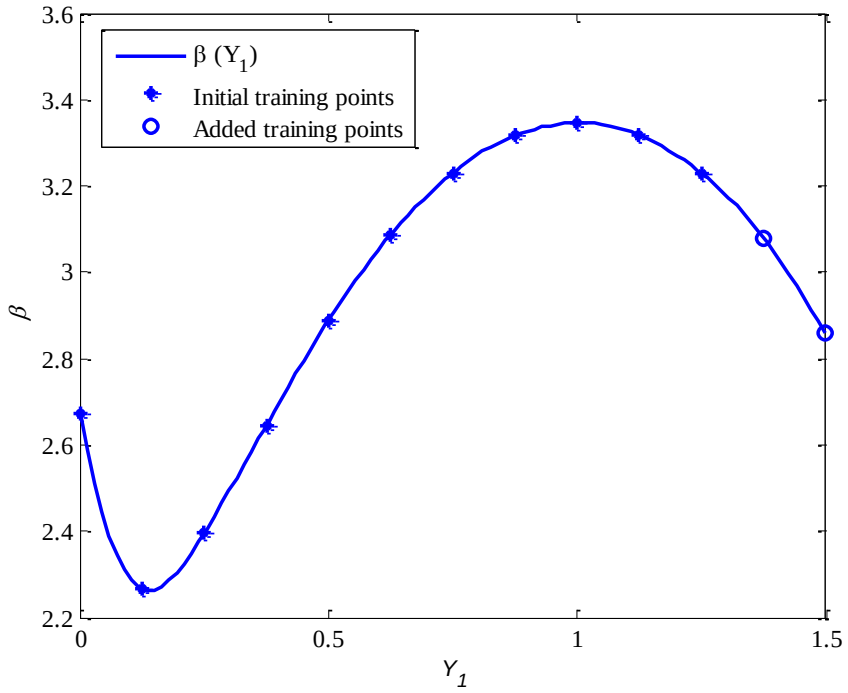

Fig. 5 Surrogate model of $\beta(\mathbf{y})$

Recall that the probability of failure p_f can be evaluated with the equivalent Gaussian random field $\tilde{G}$ through Eqs. (29) and (30). With $\beta(\mathbf{y})$ and $\rho(\mathbf{y}, \mathbf{y}')$ available, $\tilde{G}$ is fully defined. Then $\tilde{G}$ could be expanded, followed by MCS. The final results are given in Table 2, where NOF is the number of function calls. The random field approach called the function 335 times.

For a fair comparison, 500 training points were used for the direct Kiging method to generate a direct Kiging model for the response with respect to $\mathbf{X}$ and Y. The number of the training points was much higher than that of the random field approach. The range of a random variable X was set to $[\mu_{\mathbf{X}} - 5\sigma_{\mathbf{X}}, \mu_{\mathbf{X}} + 5\sigma_{\mathbf{X}}]$, and the training points were generated by the Hammersley sampling (HS) method. The equivalent MPP method and MCS were also executed.

All the results are given in Table 2. $\underline{\varepsilon}$ and $\overline{\varepsilon}$ are the percentage errors of the lower and upper probabilities of failure with respect to MCS solutions, respectively. The results show that the proposed random field approach is more efficient and accurate than the direct Kriging method. Note that the equivalent MPP method used the fewest number

of function calls, but this does not mean it is more efficient than the random field approach because it calculated only the upper probability of failure, and its accuracy is much worse. If they had been used to calculate lower and upper probabilities of failure, the number of functions would have doubled and would be therefore be higher than that of the random field approach.

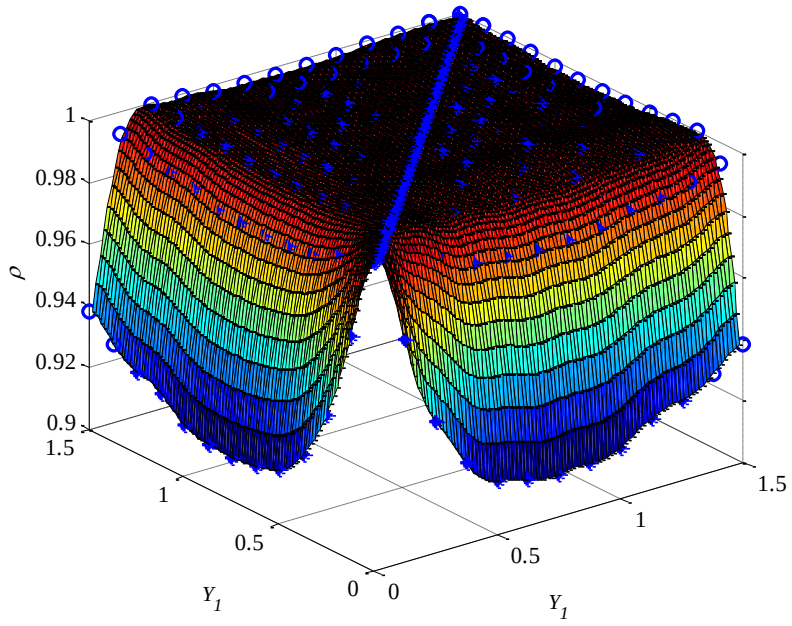

Fig. 6 Surrogate model of $\rho(\mathbf{y}, \mathbf{y}')$

Table 2 Results of Example 1

Method	$[\underline{p}_f, \overline{p}_f]$	$[\underline{\varepsilon}, \overline{\varepsilon}]$ (%)	NOF
Random field	$[4.21\times10^{-4}, 1.25\times10^{-2}]$	[0.94, 2.8]	335
Direct Kriging	$[3.50\times10^{-4}, 1.08\times10^{-2}]$	[17.65, 16.18]	500
Equivalent MPP	[N/A, 1.0×10^{-2}]	[N/A, 22.48]	242
MCS	$[4.25\times10^{-4}, 1.29\times10^{-2}]$	N/A	4×10^{8}

5.2. A cantilever tube

The cantilever tube example shown in Fig. 7 is modified from [16]. The component is subjected to three forces F_1, F_2, and P; and torque T. A failure occurs when the maximum von Moses stress $\sigma_{\max}$ is larger than the yield strength S_y. The limit-state function is given by

$$G = g(\mathbf{X}, \mathbf{Y}) = S_y - \sigma_{\max} \tag{42}$$

where $\mathbf{X} = [S_y, t, d, F_1, F_2, P, T]$, $\mathbf{Y} = [\theta_1, \theta_2]$, and $\sigma_{\max}$ is given by

$$\sigma_{\max} = \sqrt{\sigma_x^2 + 3\tau_{zx}^2} \tag{43}$$

in which

$$\sigma_x = \frac{P}{A} + \frac{M}{I} \tag{44}$$

$$\tau_{xz} = \frac{[2T + F_1 d \sin(\theta_1) - F_2 d \sin(\theta_2)]d}{8I} \tag{45}$$

$$I = \frac{\pi}{64}[d^4 - (d - 2t)^4] \tag{46}$$

$$A = \frac{\pi}{4}[d^2 - (d - 2t)^2] \tag{47}$$

and

$$M = F_1 L_1 \cos(\theta_1) - F_2 L_2 \cos(\theta_2) \tag{48}$$

where $L_1 = 120$ mm and $L_2 = 60$ mm.

All the input variables are given in Table 3. Parameters 1 and 2 have the same meanings as those in Example 1. The probability of failure is defined by $p_f = \Pr\{G = g(\mathbf{X}, \mathbf{Y}) < 0\}$, and the limit state is $e = 0$. This problem involves seven independent random variables and two interval variables.

Fig. 8 shows the maximum von Moses stress with respect to interval variables θ_1 and θ_2 while all the random variables are fixed at their mean values. The surface is quite

nonlinear. Given that the maximum von Moses stress is part of the response, the response is therefore also highly nonlinear with respect to the interval variables.

The results of all the methods are provided in Table 4. For the direct Kriging model method, 400 training points were used, which are more than the training points used by the random field approach.

Table 3 Variables of Example 2

Variable	Parameter 1	Parameter 2	Distribution
t (mm)	6	0.2	Normal
d (mm)	43	0.2	Normal
F_1 (N)	1000	50	Normal
F_2 (N)	1700	80	Normal
P (N)	1000	50	Normal
T (Nm)	350	20	Normal
S_y (MPa)	360	0	Normal
θ_1 (^{o})	-5	10	Interval
θ_2 (^{o})	-10	6	Interval

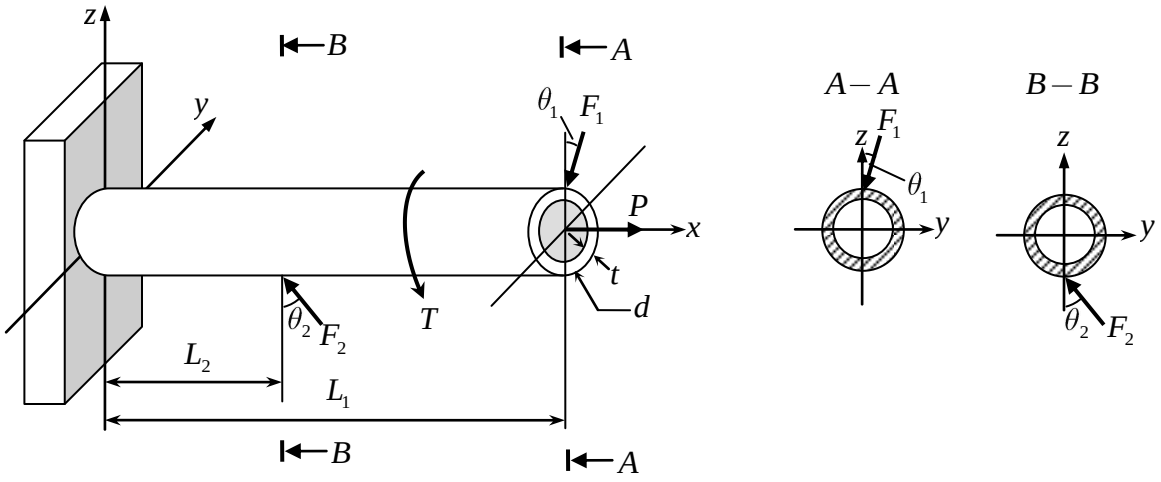

Fig. 7 A cantilever tube

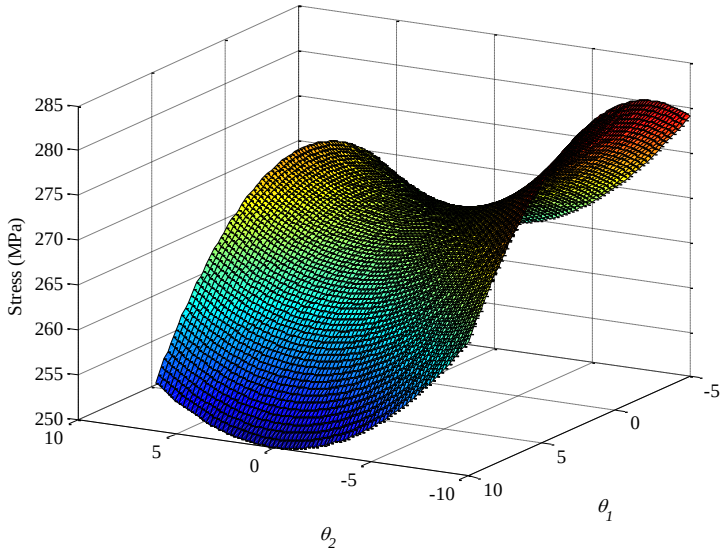

Fig. 8 Maximum von Moses stress of the tube for a given θ_1 and θ_2

Table 4 Results of Example 2

Method	$[\underline{p}_f, \overline{p}_f]$	$[\underline{\varepsilon}, \overline{\varepsilon}]$ (%)	NOF
Random field	$[2.07\times10^{-4}, 9.86\times10^{-4}]$	[1.90, 1.89]	371
Direct Kriging	$[1.2\times10^{-4}, 7.10\times10^{-3}]$	[43.13, 576.19]	400
Equivalent MPP	[N/A, 5.64×10^{-4}]	[N/A, 43.62]	257
MCS	$[2.11\times10^{-4}, 1.0\times10^{-3}]$	N/A	3×10^{9}

The results also show the high accuracy and efficiency of the random field method.

5.3. A ten-bar aluminum truss

This example is modified from Refs. [9, 13, 42]. As shown in Fig. 9, a ten-bar aluminum truss is subject to forces F_1, F_2, and F_3. The vertical displacement of joint 2 is of interest. Its allowable value is $d_{\max} = 0.046$ m. The Young's modulus of the material is $E = 68.948$ GPa. The lengths of the horizontal and vertical bars are all $L = 9.144$ m.

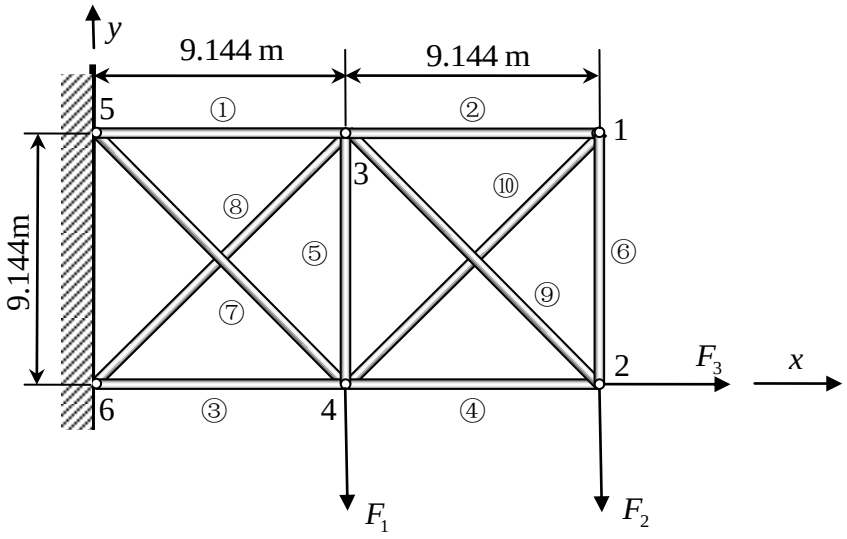

Fig. 9 A ten-bar aluminum truss

The probability of failure is given by

$$p_f = \Pr\{G = g(\mathbf{X}, \mathbf{Y}) = d_{\max} - d < 0\} \tag{49}$$

in which d is computed by [42]

$$d = \left(\sum_{i=1}^{6} \frac{N_i^0 N_i}{A_i} + \sqrt{2} \sum_{i=7}^{10} \frac{N_i^0 N_i}{A_i} \right) \frac{L}{E} \tag{50}$$

where

$$\begin{cases} N_1 = F_2 - \dfrac{\sqrt{2}}{2} N_8,\ N_2 = -\dfrac{\sqrt{2}}{2} N_{10} \\ N_3 = -F_1 - 2F_2 + F_3 - \dfrac{\sqrt{2}}{2} N_8 \\ N_4 = -F_2 + F_3 - \dfrac{\sqrt{2}}{2} N_{10} \\ N_5 = -F_2 - \dfrac{\sqrt{2}}{2} N_8 - \dfrac{\sqrt{2}}{2} N_{10},\ N_6 = -\dfrac{\sqrt{2}}{2} N_{10} \\ N_7 = \sqrt{2}(F_1 + F_2) + N_8,\ N_8 = \dfrac{a_{22} b_1 - a_{12} b_2}{a_{11} a_{22} - a_{12} a_{21}} \\ N_9 = \sqrt{2} F_2 + N_{10},\ N_{10} = \dfrac{a_{11} b_2 - a_{21} b_1}{a_{11} a_{22} - a_{12} a_{21}} \end{cases} \tag{51}$$

$$\begin{cases} a_{11} = \left(\dfrac{1}{A_1} + \dfrac{1}{A_3} + \dfrac{1}{A_5} + \dfrac{2\sqrt{2}}{A_7} + \dfrac{2\sqrt{2}}{A_8} \right) \dfrac{L}{2E} \\ a_{12} = a_{21} = \dfrac{L}{2A_5 E} \\ a_{22} = \left(\dfrac{1}{A_2} + \dfrac{1}{A_4} + \dfrac{1}{A_6} + \dfrac{2\sqrt{2}}{A_9} + \dfrac{2\sqrt{2}}{A_{10}} \right) \dfrac{L}{2E} \\ b_1 = \left(\dfrac{F_2}{A_1} - \dfrac{F_1 + 2F_2 - F_3}{A_3} - \dfrac{F_2}{A_5} - \dfrac{2\sqrt{2}(F_1 + F_2)}{A_7} \right) \dfrac{\sqrt{2}L}{2E} \\ b_2 = \left(\dfrac{\sqrt{2}(F_3 - F_2)}{A_4} - \dfrac{\sqrt{2}F_2}{A_5} - \dfrac{4F_2}{A_9} \right) \dfrac{L}{2E} \end{cases} \tag{52}$$

and N_i^0, $i = 1, 2, \cdots, 10$ are obtained by plugging $F_1 = F_3 = 0$ and $F_2 = 1$ into Eqs. (51) and (52).

There are 10 independent random variables and 3 interval variables as shown in Table 5. The results are provided in Table 6. For the direct Kriging model method, the HS method was used to generate 1000 training points, which were more than the training points used by the random field approach. This example again shows the high accuracy and efficiency of the random field approach.

6. Conclusions

Interval variables are usually used to model uncertain with limited information. As a result, the probability of failure is also an interval variable. Most of reliability analysis methods for both random and interval variables rely on the global extreme values of a response with respect to interval variables. When the response is a nonlinear function of interval variables, the accuracy and efficiency of reliability analysis are not good. This work shows that the response is a random filed with respect to interval variables. From this perspective, the reliability or probability of failure can be redefined using a random field approach. The new definition allows for a new reliability analysis method that maps the random field response into a Gaussian field through the First Order Reliability Method (FORM). The Kriging model method is employed to determine the mean and autocorrelation functions of the Gaussian field, which is then expanded with a

number of Gaussian variables. Then the bounds of the probability of failure are estimated by Monte Carlo simulation.

The proposed method avoids global optimization with respect to interval variables and therefore avoids performing FORM on the extreme values of the response. In addition, the proposed method obtains the lower and upper bounds of the probability of failure simultaneously. As the three examples demonstrate, the proposed method is accurate and efficient.

Table 5 Variables of Example 3

Variable	Parameter 1	Parameter 2	Distribution
A_1 (mm^2)	4000	50	Normal
A_2 (mm^2)	4000	50	Normal
A_3 (mm^2)	4000	50	Normal
A_4 (mm^2)	4000	80	Normal
A_5 (mm^2)	4000	80	Normal
A_6 (mm^2)	4000	80	Normal
A_7 (mm^2)	4000	100	Lognormal
A_8 (mm^2)	4000	100	Lognormal
A_9 (mm^2)	4000	100	Lognormal
A_{10} (mm^2)	4000	100	Lognormal
F_1 (N)	442800	446800	Interval
F_2 (N)	442800	446800	Interval
F_3 (N)	1709200	1849200	Interval

It is critical to construct the models of the mean and autocorrelation functions of the Gaussian field. The Kriging method is used in this work for this task. Other surrogate model methods can also be employed. When the dimension of interval variables is high, the proposed method may not perform well because the Kriging method may not be efficient for large scale problems. Large number of interval variables, however, should be

avoided because this situation will lead to too conservative reliability analysis results. More information should be collected to reduce the number of interval variables. The future work in this area is the sensitivity analysis that identifies the most important interval variables, for which more information needs to be collected.

Table 6 Results of Example 3

Method	$[\underline{p}_f, \overline{p}_f]$	$[\underline{\varepsilon}, \overline{\varepsilon}]$ (%)	NOF
Random field	$[0, 4.153\times10^{-3}]$	$[0, 1.49]$	401
Direct Kriging	$[0, 3.88\times10^{-3}]$	$[0, 5.18]$	1000
Equivalent MPP	$[\text{N/A}, 4.82\times10^{-2}]$	$[\text{N/A}, 1077.91]$	605
MCS	$[0, 4.092\times10^{-3}]$	N/A	3×10^{9}

Although the FORM-based random field approach does not approximate the limit-state function with respect to interval variables, it linearizes the limit-state function with respect to the transformed random variables. Even though the accuracy of FORM is acceptable for many engineering problems, its error will be large if the limit-state function is highly nonlinear with respect to the transformed random variables. The future work is to use more accurate reliability method, such the Second Order Reliability (SORM) method, to replace FORM.

Acknowledgment

This material is based upon work supported by the National Science Foundation through grant CMMI 1234855. The support from the Intelligent Systems Center (ISC) at the Missouri University of Science and Technology is also acknowledged.

Reference

[1] Du, X., Sudjianto, A., and Huang, B., 2005, "Reliability-based design with the mixture of random and interval variables," Journal of Mechanical Design, Transactions of the ASME, 127(6), pp. 1068-1076.

[2] Hu, Z., and Du, X., 2012, "Reliability analysis for hydrokinetic turbine blades," Renewable Energy, 48, pp. 251-262.

[3] Qiu, Z., and Wang, J., 2010, "The interval estimation of reliability for probabilistic and non-probabilistic hybrid structural system," Engineering Failure Analysis, 17(5), pp. 1142-1154.

[4] Du, L., Youn, B. D., Gorsich, D., and Choi, K., 2006, "Possibility-based design optimization method for design problems with both statistical and fuzzy input data," Journal of Mechanical Design, 128(4), pp. 928-935.

[5] Mourelatos, Z. P., and Zhou, J., 2006, "A design optimization method using evidence theory," Journal of Mechanical Design, 128(4), pp. 901-908.

[6] Zaman, K., Rangavajhala, S., McDonald, M. P., and Mahadevan, S., 2011, "A probabilistic approach for representation of interval uncertainty," Reliability Engineering & System Safety, 96(1), pp. 117-130.

[7] Xiao, N.-C., Huang, H.-Z., Wang, Z., Pang, Y., and He, L., 2011, "Reliability sensitivity analysis for structural systems in interval probability form," Structural and Multidisciplinary Optimization, 44(5), pp. 691-705.

[8] Bayarri, M. J., Berger, J. O., Paulo, R., Sacks, J., Cafeo, J. A., Cavendish, J., Lin, C.-H., and Tu, J., 2007, "A framework for validation of computer models," Technometrics, 49(2).

[9] Jiang, C., Lu, G., Han, X., and Liu, L., 2012, "A new reliability analysis method for uncertain structures with random and interval variables," International Journal of Mechanics and Materials in Design, 8(2), pp. 169-182.

[10] Jiang, C., Han, X., Li, W., Liu, J., and Zhang, Z., 2012, "A hybrid reliability approach based on probability and interval for uncertain structures," Journal of Mechanical Design, 134(3), p. 031001.

[11] Adduri, P. R., and Penmetsa, R. C., 2007, "Bounds on structural system reliability in the presence of interval variables," Computers & structures, 85(5), pp. 320-329.

[12] Luo, Y., Kang, Z., and Li, A., 2009, "Structural reliability assessment based on probability and convex set mixed model," Computers & Structures, 87(21), pp. 1408-1415.

[13] Kang, Z., and Luo, Y., 2010, "Reliability-based structural optimization with probability and convex set hybrid models," Structural and Multidisciplinary Optimization, 42(1), pp. 89-102.

[14] Penmetsa, R. C., and Grandhi, R. V., 2002, "Efficient estimation of structural reliability for problems with uncertain intervals," Computers & structures, 80(12), pp. 1103-1112.

[15] Zhang, H., Mullen, R. L., and Muhanna, R. L., 2010, "Interval Monte Carlo methods for structural reliability," Structural Safety, 32(3), pp. 183-190.

[16] Du, X., Sudjianto, A., and Huang, B., 2005, "Reliability-based design with the mixture of random and interval variables," Journal of mechanical design, 127(6), pp. 1068-1076.

[17] Guo, J., and Du, X., 2010, "Reliability analysis for multidisciplinary systems with random and interval variables," AIAA journal, 48(1), pp. 82-91.

[18] Choi, S.-K., Grandhi, R. V., and Canfield, R. A., 2007, Reliability-based structural design, Springer.

[19] Zhuang, X., and Pan, R., "Epistemic uncertainty in reliability-based design optimization," Proc. Reliability and Maintainability Symposium (RAMS), 2012 Proceedings-Annual, IEEE, pp. 1-6.

[20] Li, G., Lu, Z., Lu, Z., and Xu, J., 2014, "Regional sensitivity analysis of aleatory and epistemic uncertainties on failure probability," Mechanical Systems and Signal Processing, 46(2), pp. 209-226.

[21] Yoo, D., and Lee, I., 2013, "Sampling-based approach for design optimization in the presence of interval variables," Structural and Multidisciplinary Optimization, pp. 1-14.

[22] Zhang, Y., and Hosder, S., 2013, "Robust Design Optimization Under Mixed Uncertainties With Stochastic Expansions," Journal of Mechanical Design, 135(8), p. 081005.

[23] Adler, R. J., and Taylor, J. E., 2009, Random fields and geometry, Springer.

[24] Sudret, B., and Der Kiureghian, A., 2000, Stochastic finite element methods and reliability: a state-of-the-art report, Department of Civil and Environmental Engineering, University of California.

[25] Hu, Z., Du, X.,, 2014, "First Order Reliability Method for Time-Variant Problems Using Series Expansions," Structural and Multidisciplinary Optimization, Under Review.

[26] Li, C.-C., and Der Kiureghian, A., 1993, "Optimal discretization of random fields," Journal of Engineering Mechanics, 119(6), pp. 1136-1154.

[27] Du, X., and Hu, Z., 2012, "First order reliability method with truncated random variables," Journal of Mechanical Design, 134(9), p. 091005.

[28] Der Kiureghian, A., and Dakessian, T., 1998, "Multiple design points in first and second-order reliability," Structural Safety, 20(1), pp. 37-49.

[29] Der Kiureghian, A., Zhang, Y., and Li, C.-C., 1994, "Inverse reliability problem," Journal of Engineering Mechanics, 120(5), pp. 1154-1159.

[30] Kbiob, D., 1951, "A statistical approach to some basic mine valuation problems on the Witwatersrand," Jnl. C'hem. Met. and Min. Soc. S. Afr.

[31] Kaymaz, I., 2005, "Application of kriging method to structural reliability problems," Structural Safety, 27(2), pp. 133-151.

[32] Xiong, Y., Chen, W., Apley, D., and Ding, X., 2007, "A non- stationary covariance- based Kriging method for metamodelling in engineering design," International Journal for Numerical Methods in Engineering, 71(6), pp. 733-756.

[33] Kleijnen, J. P., 2009, "Kriging metamodeling in simulation: A review," European Journal of Operational Research, 192(3), pp. 707-716.

[34] Echard, B., Gayton, N., and Lemaire, M., 2011, "AK-MCS: an active learning reliability method combining Kriging and Monte Carlo simulation," Structural Safety, 33(2), pp. 145-154.

[35] Bichon, B. J., Eldred, M. S., Swiler, L. P., Mahadevan, S., and McFarland, J. M., 2008, "Efficient global reliability analysis for nonlinear implicit performance functions," AIAA journal, 46(10), pp. 2459-2468.

[36] Lophaven, S. N., Nielsen, H. B., and Søndergaard, J., 2002, "DACE-A Matlab Kriging toolbox, version 2.0."

[37] Vitter, J. S., 1985, "Random sampling with a reservoir," ACM Transactions on Mathematical Software (TOMS), 11(1), pp. 37-57.

[38] Helton, J. C., and Davis, F. J., 2003, "Latin hypercube sampling and the propagation of uncertainty in analyses of complex systems," Reliability Engineering & System Safety, 81(1), pp. 23-69.

[39] Hammersley, J. M., 1960, "Monte Carlo methods for solving multivariable problems," Annals of the New York Academy of Sciences, 86(3), pp. 844-874.

[40] Björkman, M., and Holmström, K., 1999, "Global optimization using DIRECT algorithm in matlab."

[41] Sudret, B., and Der Kiureghian, A., 2002, "Comparison of finite element reliability methods," Probabilistic Engineering Mechanics, 17(4), pp. 337-348.

[42] Au, F., Cheng, Y., Tham, L., and Zeng, G., 2003, "Robust design of structures using convex models," Computers & structures, 81(28), pp. 2611-2619.

PAPER
V. RELIABILITY-BASED DESIGN OPTIMIZATION WITH STATIONARY STOCHASTIC PROCESSES

Zhen Hu and Xiaoping Du[4]

Department of Mechanical and Aerospace Engineering

Missouri University of Science and Technology

Abstract

Form time-dependent engineering problems, time-dependent reliability-based design ensures reliability requirements are met for a given period of time, but it is challenging to maintain high efficiency and accuracy. This work develops an accurate and efficient reliability-based design methodology for problems whose responses are nonlinear functions of both stationary stochastic processes and random variables. The high efficiency is achieved by performing deterministic design optimization and time-dependent reliability analysis with sequential single loops where optimization and reliability analysis are completely decoupled. The time-dependent reliability analysis method employed in this work also helps reduce the computational cost. Its accuracy is ensured by using the Orthogonal Series Expansion (OSE) method. Two numerical examples demonstrated that the proposed method is able to design the product to specific reliabilities with less than 10% error.

1. Introduction

Stochastic processes, such as time-variant random excitations and loadings, are commonly encountered in aerospace applications. For problems with input stochastic processes, the responses are also stochastic processes. To quantify the effects of time-dependent uncertainties in the input stochastic processes, time-dependent reliability

[4]400 West 13th Street, Toomey Hall 290D,Rolla, MO 65401, U.S.A., Tel: 1-573-341-7249, e-mail: dux@mst.edu

methods should be employed [1-3] because they can provide the probability that a system or component still works properly after it has been put into operation for a period of time $[0,t]$.

Let $\mathbf{X} = [X_1, X_2, \cdots, X_n]$ be a vector of random variables and $\mathbf{Y}(t) = [Y_1(t), Y_2(t), \cdots, Y_m(t)]$ be a vector of stochastic processes, the time-dependent reliability $R(t)$ over $[0,t]$ is defined by

$$R(t) = \Pr\{G(\tau) = g(\mathbf{X}, \mathbf{Y}(\tau)) < 0, \forall \tau \in [0,t]\} \tag{1}$$

where $g(\mathbf{X}, \mathbf{Y}(\tau))$ is the limit-state function, $G(\tau)$ is the response variable, $\forall \tau \in [0,t]$ stands for all time instants over $[0,t]$, and $g(\mathbf{X}, \mathbf{Y}(\tau)) < 0$ indicates a working state.

The time-dependent probability of failure is

$$p_f(t) = 1 - R(t) \tag{2}$$

It can also be computed by

$$p_f(t) = \Pr\{g(\mathbf{X}, \mathbf{Y}(\tau)) > 0, \exists \tau \in [0,t]\} \tag{3}$$

The probability of failure indicates that if there exists one time instant τ in $[0,t]$, such that $g(\mathbf{X}, \mathbf{Y}(\tau)) > 0$, a failure occurs. It is therefore also called the probability of the first-passage failure.

For special problems with only random variables $\mathbf{X}$, the reliability becomes time independent or constant. Many reliability-based design optimization (RBDO) methods are for only time-independent reliability problems [4-7]. A typical time-independent RBDO model is given by

$$\begin{cases} \min\limits_{(\mathbf{d}, \boldsymbol{\mu}_\mathbf{X})} f(\mathbf{d}) \\ \text{s.t.} \\ \Pr\{g_{Pi}(\mathbf{d}, \mathbf{X}) > 0\} \le [p_{fi}], \ i = 1, 2, \cdots, n_p \\ g_{Dj}(\mathbf{d}) \le 0, \ \ j = 1, 2, \cdots, n_d \end{cases} \tag{4}$$

In the above model, $f(\mathbf{d})$ is the objective function, and $\mathbf{d}$ is a vector of deterministic design variables. $\mathbf{X} = [\mathbf{X}_R, \mathbf{X}_P]$ is a vector of random variables with $\mathbf{X}_R$ being random design variables and $\mathbf{X}_P$ being random parameters. The difference

between $\mathbf{X}_R$ and $\mathbf{X}_P$ is that the distribution parameters of the former are controllable while those of the latter are uncontrollable. The mean values of $\mathbf{X}_R$, $\boldsymbol{\mu}_{\mathbf{X}}$, are also usually treated as design variables. $g_P(\cdot)$ is a constraint function for which reliability is concerned, and $[p_f]$ is the permitted probability of failure. $g_{Dj}(\cdot)$ is a constraint function, for which no reliability is required.

Solving the above RBDO model is time consuming because the reliability analysis for $\Pr\{g_{Pi}(\mathbf{d}, \mathbf{X}) > 0\}$ is embedded within the optimization. Many methods have been proposed for improving computational efficiency. The commonly used methods is the sequential single-loop methods, including the efficient reliability and sensitivity analysis method [8, 9] and the Sequential Optimization and Reliability Analysis (SORA) method [10]. The methods decouple the RBDO process into a deterministic optimization process and reliability analysis process. The decoupling enables a RBDO problem to be solved in a sequential single-loop process with a reduced computational cost. Other progresses have also been made based on SORA [11-16].

When time-dependent uncertainties are involved [3], the RBDO model for a period of time $[0, t]$ becomes

$$\begin{cases} \min\limits_{(\mathbf{d},\, \boldsymbol{\mu}_{\mathbf{X}})} f(\mathbf{d}) \\ \text{s.t.} \\ \Pr\{g_{Pi}(\mathbf{d}, \mathbf{X}, \mathbf{Y}(\tau)) > 0, \exists \tau \in [0, t]\} \le [p_{fi}], i = 1, 2, \cdots, n_p \\ g_{Dj}(\mathbf{d}) \le 0, \quad j = 1, 2, \cdots, n_d \end{cases} \tag{5}$$

The time-dependent reliability constraint $\Pr\{g_P(\mathbf{d}, \mathbf{X}, \mathbf{Y}(\tau)) > 0, \exists \tau \in [0, t]\} \le [p_f(t)]$ is included in the above model.

Solving time-dependent RBDO problems are much more difficult than solving time-independent RBDO problems. There are two primary reasons. The first reason is that many time-dependent reliability analysis methods are not accurate. Developing accurate and efficient time-dependent reliability analysis methods is still a research issue [17-21]. Even if many methodologies have been developed in recent years, they are limited either by their assumptions or by their application scopes [1-3, 22-25]. A brief review about time-dependent reliability analysis methods is available in [26].

The second reason is that solving time-dependent RBDO is much more time consuming than solving time-independent RBDO. The higher computational cost is due to the higher computational demand by the time-dependent reliability analysis [1-3].

Methodologies for time-dependent RBDO have been proposed and used in many applications. For instance, Kuschel and Rackwitz [27] developed a structure design optimization model by using the outcrossing rate method for time-dependent reliability analysis. Mourelatos et al. [1] introduced the time-dependent reliability analysis into the lifecycle cost optimization. Based on a nonlinear interior point algorithm and a line search strategy, Jensen et al. [28] carried out RBDO for structural systems under stochastic excitations. Wang and Wang [3] proposed a sequential design optimization method based on a nested extreme response method. A RBDO model was also developed in [29] for the degradation of reliability over time.

The accuracy and efficiency of above time-dependent RBDO methodologies can be further improved. For example, most of the current methods imbed the reliability constraints in the optimization framework [1, 27-29], and this may increase the number of function evaluations significantly. SORA is a feasible way to improve the efficiency by decoupling the reliability analysis model from the optimization framework [3]. The direct application of SORA to problems with stochastic processes, however, may not be accurate. In this work, a new time-dependent SORA method is developed to accurately and efficiently solve time-dependent RBDO problems.

The main contributions of this work include the following: (1) the extension of SORA so that stationary stochastic processes can also be accommodated in RBDO, (2) a concept of the equivalent Most Probable Point (MPP), which allows for decoupling deterministic optimization and time-dependent reliability analysis, (3) an efficient approach to the equivalent MPP search, and (4) a new efficient time-dependent reliability analysis approach. The developed method is applicable to the general time-dependent RBDO problems with nonlinear response functions in the time-dependent reliability constraint functions.

The paper is organized as follows: The original SORA is reviewed in Section 2, and the new time-dependent SORA is discussed in Section 3, followed by the detailed

numerical procedure in Section 4. Two numerical examples are given in Section 5, and conclusions are made in Section 6.

2. Review of SORA

The original Sequential Optimization and Reliability Analysis (SORA) method is for the time-independent RBDO defined in Eq. (4) [10]. It is based on the First Order Reliability Method (FORM), which approximates a limit-state function in the space of standard normal random variables.

SORA performs RBDO with sequential cycles of deterministic optimization and reliability analysis. After an optimal design point is found in the deterministic optimization loop, at this point FORM is employed in the reliability analysis loop. The output of the reliability analysis is then used to reformulate the deterministic optimization model for the next cycle so that the reliability will be improved. The process continues cycle by cycle till convergence as shown in Fig. 1.

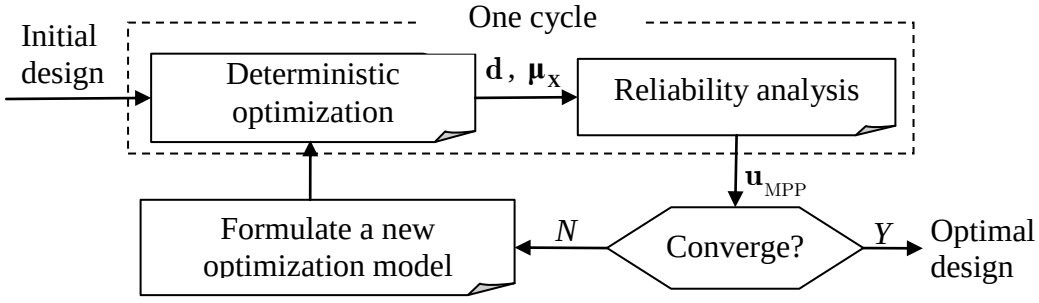

Fig. 1 Flowchart of SORA

The deterministic optimization in the *k*-th cycle is formulated as

$$\begin{cases} \min\limits_{[\mathbf{d},\boldsymbol{\mu}_\mathbf{X}]} f(\mathbf{d}) \\ \text{s.t.} \\ g_{Pi}(\mathbf{d},\, T[\mathbf{u}_{\text{MPP}}^{(k-1)}]) < 0,\, i = 1, 2, \cdots, n_p \\ g_{Dj}(\mathbf{d}) \le 0,\, j = 1, 2, \cdots, n_d \end{cases} \tag{6}$$

where $\mathbf{u}_{\mathrm{MPP},\,i}^{(k-1)}$ is the Most Probable Point (MPP) in the standard normal variable space for the *i*-th probabilistic constraint from the reliability analysis in the (*k*-1)-th cycle. $T[\cdot]$ is the transformation operator given by $\mathbf{x} = T[\mathbf{u}]$ [30]. The result of the optimization is the optimal point $[\mathbf{d}^{(k)}, \boldsymbol{\mu}_{\mathbf{X}}^{(k)}]$.

Then reliability analysis or the inverse MPP search is perform at $[\mathbf{d}^{(k)}, \boldsymbol{\mu}_{\mathbf{X}}^{(k)}]$ for each of the probabilistic constraint functions The MPP $\mathbf{u}_{\mathrm{MPP},\,i}^{(k-1)}$ the solution to the following MPP search model:

$$\begin{cases} \max\limits_{\mathbf{u}_{\mathbf{X},i}} \; g_{Pi}(\mathbf{d}^{(k)},\, T(\mathbf{u}_{\mathbf{X},i})) \\ \text{s.t.} \\ \left\| \mathbf{u}_{\mathbf{X},i} \right\| = \beta_i \end{cases} \tag{7}$$

in which $\|\cdot\|$ stands for the determinant of a vector, and β is called a reliability index and is given by

$$\beta_i = -\Phi^{-1}([p_{fi}]) \tag{8}$$

in which $\Phi^{-1}(\cdot)$ is the inverse cumulative density function (CDF) of a standard normal variable. The approximation of the probability of failure is by means of a standard normal distribution as indicated in Eq. (8). The obtained CDF of the limit-state function this way, however, is not necessarily normally distributed.

The MPP $\mathbf{u}_{\mathrm{MPP},\,i}^{(k-1)}$ corresponds directly to the permitted probability of failure $[p_{fi}]$ as shown in Eq. (8). If the constraint function at $\mathbf{u}_{\mathrm{MPP},\,i}^{(k-1)}$ is less than 0, p_{fi} will be less than $[p_{fi}]$. Therefore, $g_{Pi}(\mathbf{d},\, T[\mathbf{u}_{\mathrm{MPP}}^{(k-1)}]) < 0$ in the deterministic optimization leads to the satisfaction of reliability.

After the *k*-th cycle, if no convergence is reached, the (*k*+1)-th cycle is performed.

SORA has been proofed efficient for time-independent RBDO [14-16]. It might also be efficient for time-dependent RBDO. However, there is no direct correspondence of the MPP to the permitted time-dependent probability of failure. Major modifications of

SORA are needed for time-dependent RBDO. In this work, modifying SORA for time-dependent RBDO problems involving only stationary stochastic processes and random variables is the focus.

3. Time-Dependent SORA (t-SORA)

In this section, the main idea of SORA for time-dependent RBDO is first introduced. The new method is called the time-dependent SORA (t-SORA). Details of t-SORA are then discussed.

3.1. Overview of t-SORA

In this work, limit-state function $g_P(\mathbf{X}, \mathbf{Y}(\tau))$ where the components of $\mathbf{Y}(\tau)$ are independent stationary stochastic processes, whose distributions do not change with time, are of interest. $\mathbf{Y}(\tau)$ may or may not include Gaussian stochastic processes. Since the distributions of $\mathbf{Y}(\tau)$ at all the instants of time over $[0,t]$ are the same, the MPP of $g_P(\mathbf{X}, \mathbf{Y}(\tau))$ is also identical at all the instants of time over $[0,t]$.

Fig. 2 shows the flowchart of t-SORA. As the new method inherits from the original SORA, the steps are very similar to those in Fig. 1. The entire optimization is still performed cycle by cycle till convergence. Each cycle consists of decoupled deterministic optimization and time-dependent reliability analysis. However, the major difference or challenge is that the MPP corresponding to the permitted probability of failure $[p_f]$ cannot be directly used in the deterministic optimization. Its direct use cannot ensure that the reliability requirement be met. The reason is explained as follows.

With the involvement of $\mathbf{Y}(\tau)$, the random variables at τ become $\mathbf{Z} = [\mathbf{X}, \mathbf{Y}(\tau)]$. If the inverse MPP search is performed as in the original SORA, the MPP $\mathbf{u_Z}$ can be obtained from

$$\begin{cases} \max\limits_{\mathbf{u_Z}} \; g_P(\mathbf{d}, T(\mathbf{u_Z})) \\ \text{s.t.} \\ \left\| \mathbf{u_Z} \right\| = -\Phi^{-1}([p_{fi}]) \end{cases} \tag{9}$$

Then at the MPP $\mathbf{u_Z}$,

$$\Pr\{g_P(\mathbf{d}, \mathbf{X}, \mathbf{Y}(\tau)) > g_P(\mathbf{d}, T(\mathbf{u_Z}))\} = [p_{f_i}] \tag{10}$$

However, the probability $\Pr\{g(\mathbf{X}, \mathbf{Y}(\tau)) > g_P(\mathbf{d}, T(\mathbf{u_Z})), \exists\tau \in [0,t]\}$ over $[0,t]$ is always greater than or equal to the instantaneous probability $\Pr\{g_P(\mathbf{d}, \mathbf{X}, \mathbf{Y}(\tau)) > g_P(\mathbf{d}, T(\mathbf{u_Z}))\}$ [1, 2, 31], and therefore

$$\Pr\{g(\mathbf{X}, \mathbf{Y}(\tau)) > g_P(\mathbf{d}, T(\mathbf{u_Z})), \exists\tau \in [0,t]\} \geq [p_{f_i}] \tag{11}$$

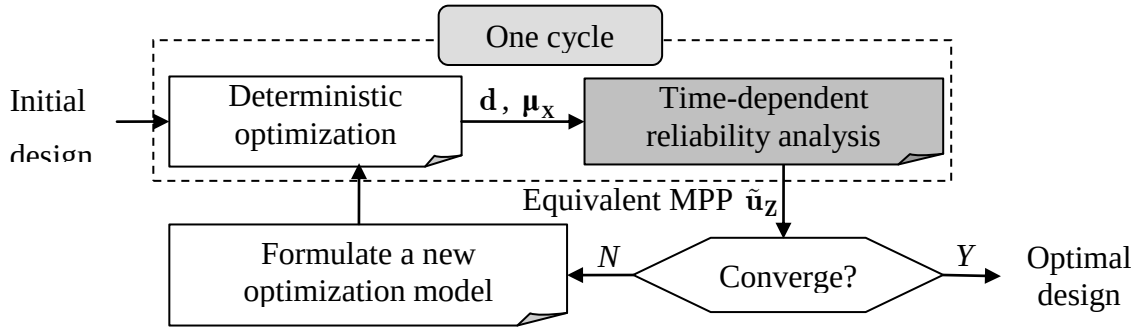

Fig. 2 Flowchart of t-SORA

As a result, the constraint $g_P(\mathbf{d}, T(\mathbf{u_Z})) \leq 0$ in the deterministic optimization can only satisfy $\Pr\{g_P(\mathbf{d}, \mathbf{X}, \mathbf{Y}(\tau)) > 0\} \leq [p_{f_i}]$ at τ, and it may not satisfy the time-dependent reliability requirement $\Pr\{g(\mathbf{X}, \mathbf{Y}(\tau)) > 0, \exists\tau \in [0,t]\} \leq [p_{f_i}]$.

To address the above challenge, a concept of equivalent MPP is proposed and denote it by $\tilde{\mathbf{u}}_\mathbf{Z}$. It is the MPP at which the limit-state function satisfies

$$\Pr\{g(\mathbf{X}, \mathbf{Y}(\tau)) > g_P(\mathbf{d}, T(\tilde{\mathbf{u}}_\mathbf{Z})), \exists\tau \in [0,t]\} = [p_{f_i}] \tag{12}$$

$\tilde{\mathbf{u}}_\mathbf{Z}$ can be obtained by adding the above condition to the inverse MPP search model. The new model is given by

$$\begin{cases} \max\limits_{[\mathbf{u_Z},\beta]} g_P(T(\mathbf{u_Z})) \\ \text{s.t.} \\ \left\|\mathbf{u_Z}\right\| = \beta \\ \Pr\{g(\mathbf{X}, \mathbf{Y}(\tau)) > g_P(T(\tilde{\mathbf{u}}_\mathbf{Z})), \exists\tau \in [0,t]\} = [p_{f_i}] \end{cases} \tag{13}$$

The reliability index β is also treated as a design variable in the MPP search since it cannot be predetermined.

Then the task of time-dependent reliability analysis is to search for the equivalent MPPs based on Eq. (13) for all the reliability constraint functions. Solving for the MPP using Eq. (13), however, is too computationally expensive. The details of developing an efficient algorithm for Eq. (13) will be presented in Section 3.3.

Now that the equivalent MPP $\tilde{\mathbf{u}}_{\mathbf{Z}}$ is directly associated with $[p_f]$. Its use in the deterministic optimization can therefore guarantee the satisfaction of the reliability requirement. The deterministic optimization model with the equivalent MPPs will be given in the next section.

3.2. Deterministic optimization

With the equivalent MPP, for the *k*-th cycle, the deterministic design optimization is formulated as

$$\begin{cases} \min\limits_{(\mathbf{d},\, \boldsymbol{\mu}_{\mathbf{X}})} \; f(\mathbf{d}) \\ \text{s.t.} \\ g_{Pi}(\mathbf{d},\, T(\tilde{\mathbf{u}}_{\mathbf{Z},i}^{(k-1)}) \le 0,\; i = 1, 2, \cdots, n_p \\ g_{Dj}(\mathbf{d}) \le 0, \quad j = 1, 2, \cdots, n_d \end{cases} \tag{14}$$

in which $\tilde{\mathbf{u}}_{\mathbf{Z},i}^{(k-1)}$ is the equivalent MPP for the *i*-th reliability constraint. How to obtain $\tilde{\mathbf{u}}_{\mathbf{Z},i}^{(k-1)}$ will be discussed in Section 3.3. The optimization model is similar to the optimization model in the original SORA. The only difference is that the MPPs are replaced by the equivalent MPPs. As discussed above, the use of the equivalent MPPs in constraints $g_{Pi}(\mathbf{d},\, T(\tilde{\mathbf{u}}_{\mathbf{Z},i}^{(k-1)}) \le 0,\; i = 1, 2, \cdots, n_p$, will satisfy the time-dependent reliability requirements.

3.3. Time-dependent reliability analysis

The purpose of the time-dependent reliability analysis is to identify the equivalent MPPs. For a general limit-state function $g_P(\mathbf{X},\, \mathbf{Y}(\tau)) = g_P(\mathbf{Z})$, where $\mathbf{Z} = [\mathbf{X}, \mathbf{Y}(\tau)]$, the task is to search for the equivalent MPP $\tilde{\mathbf{u}}_{\mathbf{Z}}$ given the design variables $[\mathbf{d}, \boldsymbol{\mu}_{\mathbf{X}}]$. As

indicated in the new inverse MPP search model in Eq. (13), there are two research issues. The first is how to calculate the time-dependent probability $\Pr\{g(\mathbf{X}, \mathbf{Y}(\tau)) > g_P(\mathbf{d}, T(\mathbf{u_Z})), \exists\tau \in [0,t]\}$, and the second is how to solve Eq. (13) efficiently.

3.3.1. Calculation of $\Pr\{g(\mathbf{X}, \mathbf{Y}(\tau)) > g_P(\mathbf{d}, T(\mathbf{u_Z})), \exists\tau \in [0,t]\}$

The task is to calculate the time-dependent probability $\Pr\{g(\mathbf{X}, \mathbf{Y}(\tau)) > c, \exists\tau \in [0,t]\}$, where $c = g_P(\mathbf{d}, T(\tilde{\mathbf{u}}_\mathbf{Z}))$ on the condition that c is known. It is nothing but the time-dependent analysis with the limit state c.

Time-dependent reliability analysis methods have been extensively studied [1-3, 32-39]. Amongst them, the most commonly used one is the upcrossing rate method that integrates the Rice's formula [36, 37] and FORM. An upcrossing is defined as the event that the limit-state function upcrosses the failure threshold from the safe region to the failure region. The method assumes that upcrossings are independent. The time-dependent probability of failure can then be approximated easily. Even though the Rice's formula is based on Gaussian processes, its integration with FORM and the upcrossing rate method makes it applicable to general problems with non-Gaussian stochastic process responses.

The upcrossing rate method is accurate when the probability of failure is low, but inaccurate when the probability of failure is high. Many improvements have been made for the Rice's formula, such as considering the correlation between upcrossing events [40], making empirical corrections to the formula of upcrossing rate [41], employing the important sampling method [1, 2], and constructing surrogate models for the extreme response [3]. Since the Rice's formula based upcrossing rate method is widely used and is also compared with the new method, its brief review is given in Appendix A.

In this work, a first order sampling method is used, which approximates the limit-state function at the MPP and then use an efficient sampling approach based on the Orthogonal Series Expansion (OSE) method to estimate the probability of failure. A brief review about the OSE method is given in Appendix B.

3.3.2. MPP search

It is computationally costly to directly search for the equivalent MPP using Eq. (13) because it involves the probability calculation for $\Pr\{g(\mathbf{X}, \mathbf{Y}(\tau)) > g_P(\mathbf{d}, T(\mathbf{u_Z})), \exists\tau \in [0,t]\}$, and the probability calculation itself is also a reliability analysis. The other disadvantage is that the existing efficient MPP search algorithms cannot be used because of the constraint $\Pr\{g(\mathbf{X}, \mathbf{Y}(\tau)) > g_P(\mathbf{d}, T(\mathbf{u_Z})), \exists\tau \in [0,t]\} = [p_f]$ in the MPP search model. The MPP search then becomes a double-loop procedure. To ease the computational intensity, using the same strategy as SORA, the MPP search is performed with a sequential procedure. The idea is to separate the MPP search from the probability calculation. Both of them are described below.

The analysis that is performed first is the inverse MPP search without the probability calculation. It is conditional on a known reliability index β. The inverse MPP search is given by

$$\begin{cases} \max\limits_{\mathbf{u_Z}} g_P(T(\mathbf{u_Z})) \\ \text{s.t.} \\ \left\|\mathbf{u_Z}\right\| = \beta \end{cases} \tag{15}$$

It is the regular MPP search, and any existing MPP search algorithms can be used. The solution is the MPP $\mathbf{u_Z}$ given β .

Then the next analysis is performed to update the reliability index β on the condition that $\mathbf{u_Z}$ is known. The task is to find a new reliability index so that the time-dependent probability of failure is equal to its permitted value, or $\Pr\{g(\mathbf{X}, \mathbf{Y}(\tau)) > g_P(\mathbf{d}, T(\mathbf{u_Z})), \exists\tau \in [0,t]\} = [p_f]$. How to update β will be discussed in Sec. 3.3.3. The result of the MPP search is the equivalent MPP $\tilde{\mathbf{u}}_\mathbf{Z}$. Then the convergence is checked. If convergence is not reached, the process repeats. The procedure of time-dependent reliability analysis is illustrated in Fig. 3.

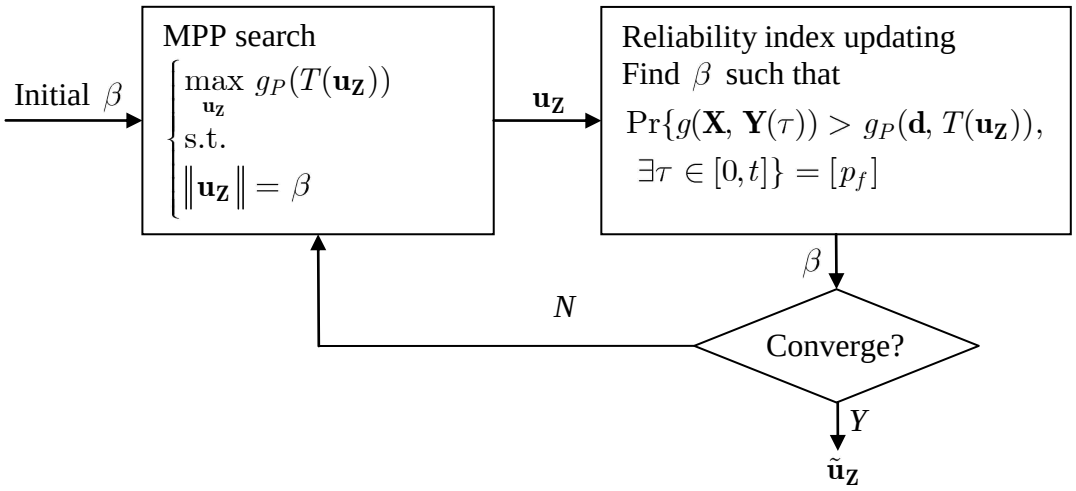

Fig. 3 Time-dependent MPP search

3.3.3. Reliability index updating

This section now discusses how to obtain the reliability index so that $p_f(t) = \Pr\{g_P(T(\mathbf{U_Z})) > 0, \exists \tau \in [0,t]\} = [p_f]$. Since FORM is used, the limit-state function $g_P(T(\mathbf{U_Z}))$ is approximated at $\mathbf{u_Z}$ for updating β. As shown in Appendix A, after approximation, the time-dependent probability is

$$p_f(t) = \Pr\{g_P(T(\mathbf{U_Z})) > 0 \; \exists \tau \in [0,t]\} \approx \Pr\{L(\tau) = \boldsymbol{\alpha}\mathbf{U}_\mathbf{Z}^T > \|\mathbf{u_Z}\|, \exists \tau \in [0,t]\} \quad (16)$$

where $L(\tau) = \boldsymbol{\alpha}\mathbf{U}_\mathbf{Z}^T$ is a linear combination of $\mathbf{U_Z}$, and $\boldsymbol{\alpha}$ is a constant vector evaluated at $\mathbf{u_Z}$ and is given in Eq. (A4). If $p_f(t) > [\mathrm{p}_f]$, a new reliability index β is obtained so that $p_f(t) = [p_f]$.

Note that original limit-state function $G(\tau) = g_P(T(\mathbf{U_Z}))$ in general is a non-Gaussian process, after the approximation, its new version $L(\tau) = \boldsymbol{\alpha}\mathbf{U}_\mathbf{Z}^T$ becomes a stationary and standard Gaussian process. Given a different limit state, $G(\tau) = g_P(T(\mathbf{U_Z}))$ will be approximated by another Gaussian process $L(\tau) = \boldsymbol{\alpha}\mathbf{U}_\mathbf{Z}^T$ with a difference vector $\boldsymbol{\alpha}$. With the different coefficients $\boldsymbol{\alpha}$, the approximated limit-state function this way will not be in general a Gaussian process.

Let the global maximum of $L(\tau)$ over $[0,t]$ be W; namely

$$W = \max_{\tau}\{L(\tau), \tau \in [0, t]\} \tag{17}$$

$p_f(t)$ can then be calculated by

$$p_f(t) = \Pr\{W > \left\|\mathbf{u_Z}\right\|\} \tag{18}$$

If $p_f(t) > [\mathrm{p}_f]$, the old reliability index $\left\|\mathbf{u_Z}\right\|$ should be reduced and an updated reliability index β is obtained such that

$$\Pr\{L(\tau) > \beta, \exists\tau \in [0,t]\} = [\mathrm{p}_f] \tag{19}$$

or

$$\Pr\{\mathrm{W} > \beta\} = [p_f] \tag{20}$$

It is obvious that $\beta < \left\|\mathbf{u_Z}\right\|$.

The problem now becomes to find the percentile value of W given a probability level $[p_f]$. It is a difficult task because there may not be a close-form solution to the distribution of the extreme value W. Wang [3] proposed a kriging model method to approximate the extreme value distribution, but the method is limited to limit-state functions in the form of $g(\mathbf{X}, t)$ without any input stochastic processes. Herein a sampling method is used.

Recall that $L(\tau) = \boldsymbol{\alpha}\mathbf{U}_\mathbf{Z}^T$ is a stationary Gaussian process with known coefficients $\boldsymbol{\alpha}$. Simulations can then be used to obtain its sample trajectories, and for each trajectory, the maximum value can be found. Then the samples of W will be available for the estimation of the CDF of W. The CDF will then produce β as indicated in Eq. (20). The samples can be efficiently generated using the Orthogonal Series Expansion (OSE) [42], which is given in Appendix B.

Once the samples of W are available, the percentile value of W in Eq. (20) is approximated. Since $[p_f]$ is small, β is in the far right tail of the distribution of W. To obtain an accurate result, the saddlepoint approximation (SPA) method [43] is used. The details are provided in Appendix C. Since the sampling approach is based on $L(\tau) = \boldsymbol{\alpha}\mathbf{U}_\mathbf{Z}^T$, the original limit-state function $g_P(\cdot)$ will not be called.

3.3.4. Numerical procedure of the time-dependent reliability analysis

The strategy of the time-dependent reliability analysis and its procedure are now summarized. As discussed above, the analysis is an iterative process. For a general limit-state function $g_P(\mathbf{X}, \mathbf{Y}(\tau)) = g_P(\mathbf{Z})$, when it is approximated at an MPP, a number of iterations are needed to solve the following model:

$$\begin{cases} \max\limits_{[\mathbf{u_Z},\beta]} g_P(T(\mathbf{u_Z})) \\ \text{s.t.} \\ \left\|\mathbf{u_Z}\right\| = \beta \\ \Pr\{\mathrm{W} > \beta\} = [p_f] \end{cases} \tag{21}$$

It is derived from the original model in Eq. (13) when FORM is employed. The model is solved with the procedure shown in Fig. 3 where the MPP search and reliability index updating are performed separately and sequentially. The main steps are as follows:

Step 1: Initialization: set the initial reliability index β. The following initial value is recommended:

$$\beta = -1.2\Phi^{-1}([p_f]) \tag{22}$$

Step 2: MPP search: Search for the MPP using Eq. (15). The results are the MPP $\mathbf{u_Z}$ and vector $\boldsymbol{\alpha}$ (given in Eq. (A4)).

Step 3: Update the reliability index: (1) Construct $L(\tau)$ by $L(\tau) = \boldsymbol{\alpha}\mathbf{U}_\mathbf{Z}^T$. (2) Use the OSE method to generate samples for $L(\tau)$ over $[0, t]$. (3) Obtain the samples of the extreme value of W. (4) Use SPA to compute the reliability index β.

Step 4: Check convergence: If the difference between the current β value and previous β is larger than a predefined tolerance, repeat Steps 2 through 4; otherwise, set the equivalent MPP $\tilde{\mathbf{u}}_\mathbf{Z} = \mathbf{u_Z}$ and stop. The convergence tolerance can be set as 0.01 or 0.001 or other small numbers.

A more detailed flowchart is given in Fig. 4. The above procedure is for a general limit-state function. It should be executed for all the limit-state functions in the overall RBDO model.

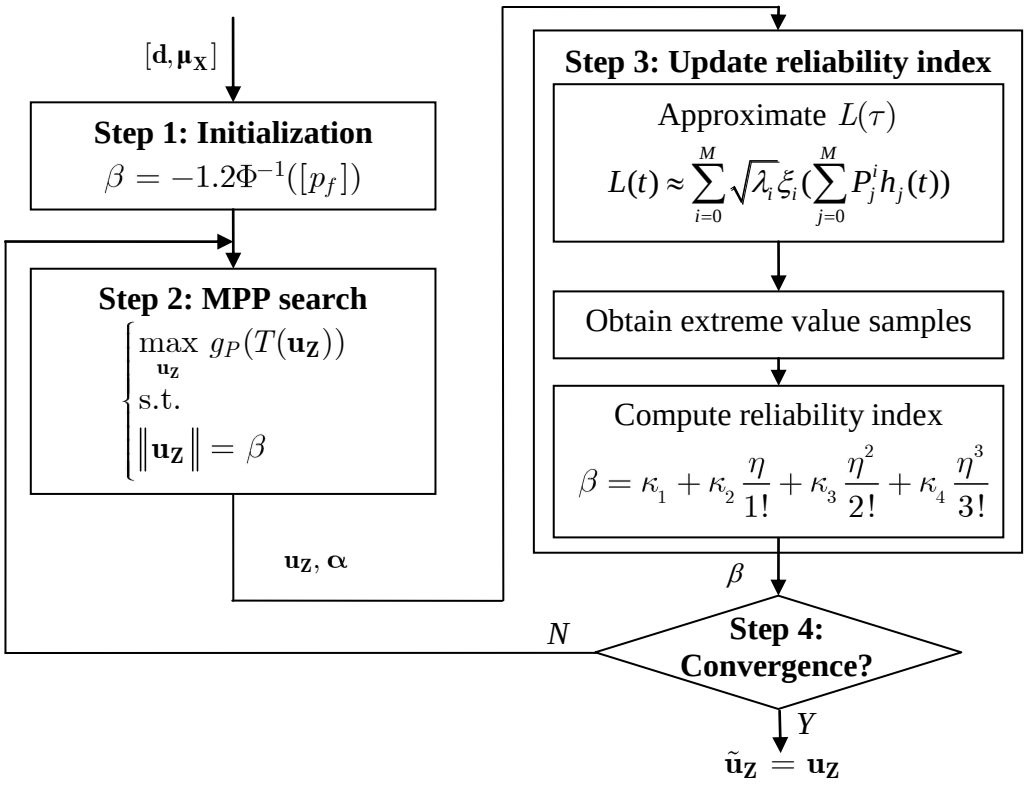

Fig. 4 Detailed flowchart for time-dependent reliability analysis

4. Summary of Numerical Procedure

The procedure of the entire RBDO is now summarized and is shown in Fig. 5.

Step 1: Initialize parameters. (1) Define the initial design variables. (2) Set the cycle counter $k = 1$.

Step 2: Perform deterministic optimization. If $k = 1$, solve deterministic optimization at mean values of random variables and main functions of stochastic processes. If $k > 1$, formulate the deterministic optimization model using the equivalent MPPs $\tilde{\mathbf{u}}_{\mathbf{Z},i}^{(k-1)}$, where $i = 1, 2, \ldots, n_p$, obtained from the $(k-1)$-th cycle; then solve the optimization model given in Eq. (14). The optimal solution is $[\mathbf{d}^{(k)}, \boldsymbol{\mu}_X^{(k)}]$.

Step 3: Perform time-dependent reliability analysis at $[\mathbf{d}^{(k)}, \boldsymbol{\mu}_X^{(k)}]$ following the procedure in Fig. 4. The solution is the equivalent MPPs $\tilde{\mathbf{u}}_{\mathbf{Z},i}^{(k)}$, where $i = 1, 2, \ldots, n_p$.

Step 4: Check convergence. If the limit-state functions satisfy

$$g_{P_i}(\mathbf{d}^{(k)}, T(\tilde{\mathbf{u}}_{\mathbf{Z},i}^{(k)})) \leq \varepsilon \tag{23}$$

where ε is a small positive number, then the optimal solution is found and stop. Otherwise, update the cycle counter by $k = k + 1$, and repeat Steps 2 through 4.

Similar to the original SORA, the efficiency of t-SORA is high because it can converge within a few cycles, and the typical number of cycles is between three and five. In addition to the decoupling between optimization and reliability analysis, the proposed approach to the equivalent MPP search converges quickly, and this also makes t-SORA fast.

5. Numerical Example

Two examples are presented. In example one, there are one stochastic process and two time-dependent reliability constraints. In example two, there are two stochastic processes and one time-dependent reliability constraint.

5.1. A two-bar frame under stochastic force

A two-bar frame is subjected to a stochastic force $F(t)$ as shown in Fig. 6. The distances O_1O_3 and O_1O_2 are random parameters and are denoted by l_1 and l_2, respectively. Failures occur when the maximum stresses of the two bars are larger than their material yield strengths S_1 and S_2. The diameters D_1 and D_2 of the two bars are random design variables.

The limit-state functions are given by

$$g_1(\mathbf{d}, \mathbf{X}, \mathbf{Y}(\tau)) = \frac{4F(\tau)\sqrt{l_1^2 + l_2^2}}{l_2 \pi D_1^2 S_1} - 1 \tag{24}$$

$$g_2(\mathbf{d}, \mathbf{X}, \mathbf{Y}(\tau)) = \frac{4F(\tau)l_1}{l_2 \pi D_2^2 S_2} - 1 \tag{25}$$

where $\mathbf{X} = [\mathbf{X}_R, \mathbf{X}_P]$, $\mathbf{X}_R = [D_1, D_2]$, $\mathbf{X}_P = [l_1, l_2, S_1, S_2]$, $\mathbf{d} = [\mu_{D_1}, \mu_{D_2}]$, and $\mathbf{Y}(t) = [F(t)]$.

The information known is given in Table 1, where STD and GP stand for a standard deviation and a Gaussian process, respectively.

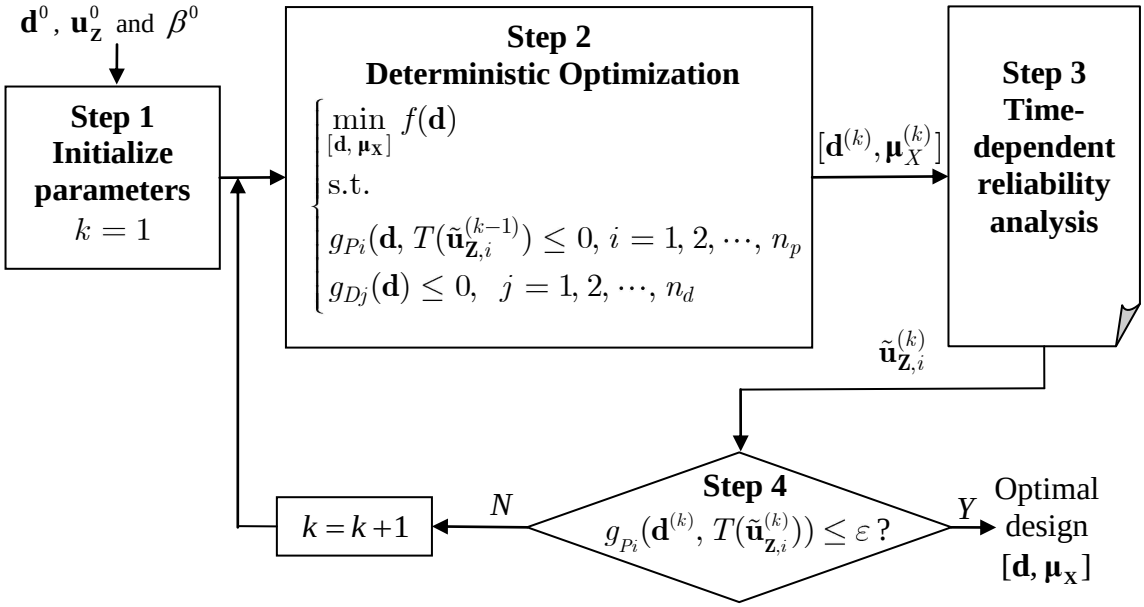

Fig. 5 Numerical procedure of t-SORA

Table 1. Random variables and stochastic process

Variable	Mean	STD	Distribution	Autocorrelation
D_1	μ_{D_1}	1×10^{-3} m	Normal	N/A
D_2	μ_{D_2}	1×10^{-3} m	Normal	N/A
S_1	1.7×10^{8} Pa	1.7×10^{7} Pa	Lognormal	N/A
S_2	1.7×10^{8} Pa	1.7×10^{7} Pa	Lognormal	N/A
l_1	0.4m	1×10^{-3} m	Normal	N/A
l_2	0.3m	1×10^{-3} m	Normal	N/A
$F(t)$	2.2×10^{6} N	2×10^{5} N	GP	Eq. (26)

The auto-correlation coefficient functions of $F(\tau)$ is

$$\rho^F(\tau_1, \tau_2) = \exp\left\{-\left[\frac{(\tau_2 - \tau_1)}{\zeta}\right]^2\right\} \tag{26}$$

in which $\zeta = 0.1$ year is the correlation length.

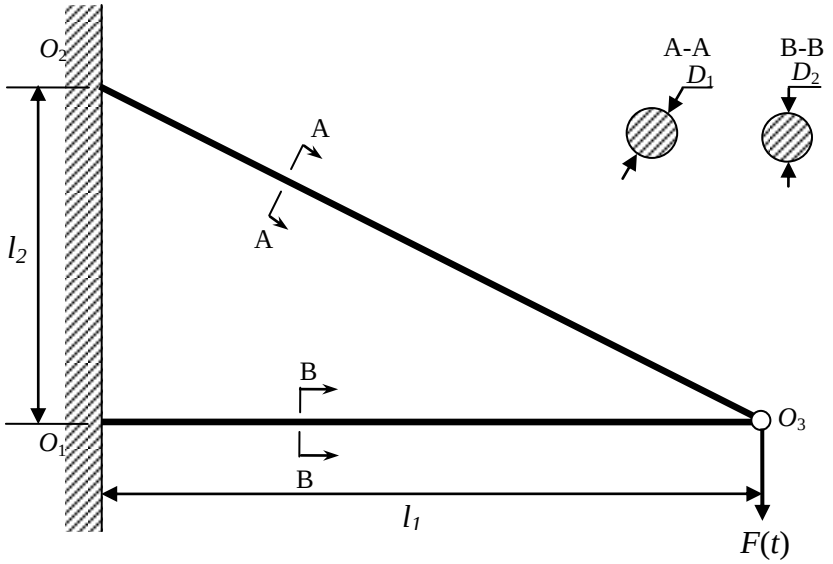

Fig. 6 A two-bar frame under stochastic force

The objective is to minimize the weight of the two bars, and the RBDO model for a service period of $[0,10]$ years is formulated as

$$\begin{cases} \min\limits_{(\mathbf{d},\,\boldsymbol{\mu}_\mathbf{X})} f(\mathbf{d}) = \dfrac{\pi\mu_{l_1}\mu_{D_1}^2}{4} + \dfrac{\pi\sqrt{\mu_{l_1}^2 + \mu_{l_2}^2}\,\mu_{D_2}^2}{4} \\ \text{s.t.} \\ \Pr\{g_i(\mathbf{d}, \mathbf{X}, \mathbf{Y}(\tau)) > 0, \exists\tau \in [0, t]\} \le [p_{fi}],\ i = 1, 2 \\ 0.07\ \text{m} \le \mu_{D_1} \le 0.25\ \text{m} \\ 0.07\ \text{m} \le \mu_{D_2} \le 0.25\ \text{m} \end{cases} \tag{27}$$

where $[p_{f1}] = 0.01$, $[p_{f2}] = 0.001$, and $t = 10$ years.

To evaluate the accuracy and efficiency of t-SORA, three methods were used to solve the problem with the same starting point. The three methods are the t-SORA with the Orthogonal Series Expansion (OSE) method presented in Appendix B, the double-loop method using the same time-dependent reliability analysis method as t-SORA, and

the double-loop method with the Rice's formula for time-dependent reliability analysis presented in Appendix A. Next the latter two methods were called the Double (OSE) and Double (Rice).

The parameters of OSE used by t-SORA and Double (OSE) are given below.

- The number of time instants dividing: $[0, t]$, $Q = 500$
- The number of samples generated at each time instant: $N = 10^6$
- The number of terms used in the OSE model: $M = 200$

Table 2 shows the convergence history of t-SORA. The optimal solution was obtained within three cycles. After the first cycle, the two limit-state functions were much larger than zero, and this is the indication that the reliability requirements were not met. After the third cycle, the two limit-state functions were close to zero. Then the time-dependent probabilities of failure were almost at their target values.

Table 2 Convergence history of t-SORA

k	f (m^3)	(μ_{D_1}, μ_{D_2}) (m)	β_1	β_2	$g_{P1}(\mathbf{d}, T(\tilde{\mathbf{u}}_{\mathbf{Z},1}))$	$g_{P2}(\mathbf{d}, T(\tilde{\mathbf{u}}_{\mathbf{Z},2}))$
1	0.0173	(0.0831, 0.0743)	3.5662	4.2095	0.6049	0.7541
2	0.0290	(0.1051, 0.0981)	3.5715	4.2111	9.44×10^{-4}	9.24×10^{-4}
3	0.0290	(0.1051, 0.0982)	3.5721	4.2138	2.50×10^{-4}	4.88×10^{-4}

Table 3 shows the final results from the three methods. The number of function calls (NOFC) is used to measure the efficiency. t-SORA and Double (OSE) produced almost identical results. t-SORA is much more efficient than the Double (OSE) and Double (Rice) methods. The fourth and fifth columns of Table 3 present the probabilities of failure after the optimization. Since t-SORA does not compute the probabilities of failure directly, their values are not available. The probabilities of failure of the Double (OSE) and Double (Rice) methods are computed by the OSE-based sampling method (Appendix B) and Rice's formula (Appendix A), respectively. The results show that the reliability constraints were satisfied by the three optimization methods.

Table 3 Optimal results

Method	f (m^3)	(μ_{D_1}, μ_{D_2})(m)	$p_{f1}(t)$	$p_{f2}(t)$	NOFC
t-SORA	0.0290	(0.1051, 0.0982)	N/A	N/A	715
Double (OSE)	0.0290	(0.1051, 0.0982)	0.0099	0.0010	18840
Double (Rice)	0.0297	(0.1066, 0.0990)	0.0100	0.0010	11050

To verify the accuracy, Monte Carlo Simulation was also performed at the optimal design points in Table 3 from the three methods. In MCS, the time interval $[0, t]$ was discretized into 200 time instants, and 10^6 samples were generated at each time instants. Table 4 gives the percentage errors, and Table 5 gives the 95% confidence intervals of the MCS solutions.

The percentage error is computed by

$$\varepsilon = \frac{\left| p_f(t) - p_f^{\mathrm{MCS}}(t) \right|}{p_f^{\mathrm{MCS}}(t)} \times 100\% \tag{28}$$

For t-SORA and Double (OSE), $p_f(t)$ is calculated by the OSE-based sampling method, and for Double (Rice), it is calculated by the method based on Rice's method. $p_f^{\mathrm{MCS}}(t)$ is the probability of failure obtained from MCS.

Table 4 Accuracy comparison

	$p_{f1}(t)$	$p_{f1}^{\mathrm{MCS}}(t)$	Error (%)	$p_{f2}(t)$	$p_{f2}^{\mathrm{MCS}}(t)$	Error (%)
t-SORA	0.01	0.0094	5.3	0.001	9.4×10^{-4}	6.38
Double (OSE)	0.01	0.0094	5.3	0.001	9.4×10^{-4}	6.38
Double (Rice)	0.01	0.0046	117.39	0.001	5.4×10^{-4}	85.19

The results indicate that the accuracy of t-SORA is good. It is more accurate than the Double (RICE) method. For the t-SORA and Double (OSE) methods, at the optimal design points, the actual time-dependent probabilities of failure are very close to the permitted ones. The probabilities of failure from the Double (Rice) method are much lower than the permitted ones. The reason is that the Rice's formula overestimates the

probability of failure [3], which resulted in an over-design for this problem because the cross-sectional area is larger than those of the other two methods as indicated in Table 3.

Table 5 95% confidence intervals of MCS solutions

	t-SORA	Double (OSE)	Double (Rice)
p_{f1}^{MCS}	[0.0092, 0.0096]	[0.0092, 0.0096]	[0.0044, 0.0047]
p_{f2}^{MCS}	[8.77, 9.97] $\times 10^{-4}$	[8.77, 9.97] $\times 10^{-4}$	[4.96, 5.88]$\times 10^{-4}$

5.2. A simply supported beam under stochastic loadings

A simply supported beam shown in Fig. 7 is subjected to two stochastic loadings, which are the stochastic force $F(t)$, and the uniformly distributed loading $q(t)$. The cross section of the beam is rectangular. The height a and width b are random design variables. A failure of the beam occurs when the stress exceeds the ultimate strength of the material S. The weight of the beam is expected to be minimized under the constraint that the time-dependent probability of failure of the beam over 30 years is less than 0.05.

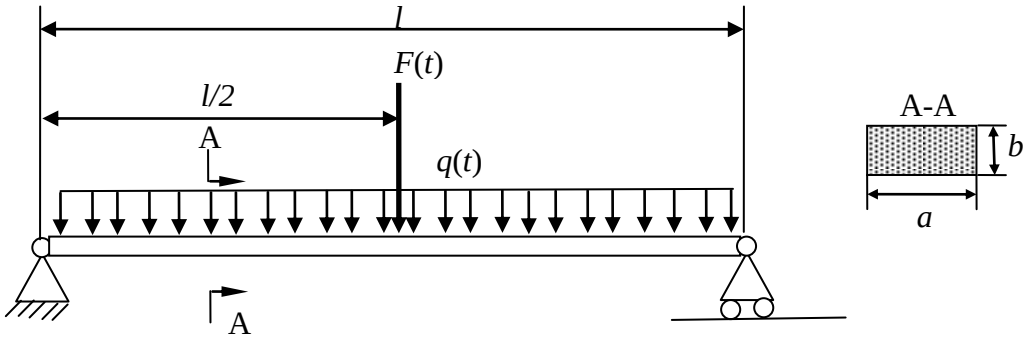

Fig. 7 A beam under stochastic loadings

The limit-state function of the beam is given by

$$g(\mathbf{d},\mathbf{X},\mathbf{Y}(\tau)) = \left(\frac{F(\tau)l}{4} + \frac{q(\tau)l^2}{8} + \frac{\rho_{st}abl^2}{8}\right)\frac{4}{ab^2S} - 1 \tag{29}$$

where $\mathbf{X} = [\mathbf{X}_R, \mathbf{X}_P]$, $\mathbf{X}_R = [a, b]$, $\mathbf{X}_P = [S]$, $\mathbf{d} = [\mu_a, \mu_b]$, and $\mathbf{Y}(\tau) = [F(\tau), q(\tau)]$, S is the ultimate strength, ρ_{st} is the density, and l is the length of the beam.

Table 6 gives the random variables, parameters, and stochastic processes.

The auto-correlation coefficient functions of $F(\tau)$ and $q(\tau)$ are

$$\rho_F(\tau_1, \tau_2) = \exp\left\{-\left(\frac{\tau_2 - \tau_1}{\zeta}\right)^2\right\} \tag{30}$$

and

$$\rho_q(\tau_1, \tau_2) = \cos(\pi(\tau_2 - \tau_1)) \tag{31}$$

respectively, where $\zeta = 0.8$ year is the correlation length of $F(\tau)$.

Table 6 Variables, parameters, and stochastic processes

Variable	Mean	STD	Distribution	Autocorrelation
a	μ_a	5×10^{-3} m	Lognormal	N/A
b	μ_b	5×10^{-3} m	Lognormal	N/A
S	2.4×10^{8} Pa	2.4×10^{7} Pa	Lognormal	N/A
$F(\tau)$	6000 N	600 N	GP	Eq. (30)
$q(\tau)$	900 N/m	90 N/m	GP	Eq. (31)
l	15 m	N/A	Deterministic	N/A
ρ_{st}	78.5 kN/m^3	N/A	Deterministic	N/A

The RBDO model is given by

$$\begin{cases} \min\limits_{[\mathbf{d},\, \boldsymbol{\mu}_\mathbf{X}]} f(\mathbf{d}) = \mu_a \mu_b \\ \text{s.t.} \\ \Pr\{g(\mathbf{d}, \mathbf{X}, \mathbf{Y}(\tau)) > 0, \exists \tau \in [0, t]\} \le [p_f] \\ \mu_b \le 4\mu_a \\ 0.04\text{ m} \le \mu_a \le 0.15\text{ m} \\ 0.15\text{ m} \le \mu_b \le 0.25\text{ m} \end{cases} \tag{32}$$

where $[p_f] = 0.05$ and $t = 30$ years.

The RBDO model was solved by the t-SORA, Double (OSE), and Double (Rice) methods with the same initial design point. Table 7 gives the convergence history of t-SORA. The results show that t-SORA converged with three cycles.

Table 7 Convergence history of t-SORA

k	f (m^2)	(μ_a, μ_b) (m)	β	$g(\mathbf{d}, T(\tilde{\mathbf{u}}_{\mathbf{Z},1}))$
1	0.0065	(0.0403, 0.1613)	2.2726	0.4384
2	0.0085	(0.0460, 0.1840)	2.2887	0.0036
3	0.0085	(0.0461, 0.1842)	2.2887	1.29×10^{-5}

Table 8 presents the final results from the three methods. The results show that t-SORA is much more efficient than the other two methods.

Table 8 Optimal results

Method	f (m^2)	(μ_a, μ_b) (m)	$p_f(t)$	NOFC
t-SORA	0.0085	(0.0461, 0.1842)	N/A	156
Double (OSE)	0.0085	(0.0463, 0.1836)	0.0500	7756
Double (Rice)	0.0092	(0.0478, 0.1914)	0.0500	1612

Table 9 gives the probabilities of failure from MCS at the optimal design points from the three aforementioned methods. Table 10 presents the 95% confidence intervals of the MCS solutions. The time interval [0, 30] year was divided into 600 time instants, and 10^6 samples were generated at each time instant for MCS.

The t-SORA and Double (OSE) methods are more accurate than the Rice's formula, which overestimated the probability of failure. The optimal design obtained from the Double (Rice) method is therefore conservative.

6. Conclusion

In this work, the time-dependent Sequential Optimization and Reliability Analysis (t-SORA) method is developed for problems with both random variables and stochastic processes. To address the limitation that there is no direct connection between time-dependent reliability and the Most Probable Point (MPP), t-SORA uses the equivalent MPP, which directly corresponds to the required time-dependent reliability. This ensures that the overall optimization be solved sequentially in cycles of deterministic optimization and reliability analysis. The results show that t-SORA can effectively solve design optimization with time-dependent reliability constraints.

Table 9 Accuracy comparison

	$p_f(t)$	$p_f^{\mathrm{MCS}}(t)$	Error (%)
t-SORA	0.05	0.0522	4.2
Double (OSE)	0.05	0.0522	4.2
Double (Rice)	0.05	0.0093	440.96

Table 10 95% confidence intervals of MCS solutions

	t-SORA	Double (OSE)	Double (Rice)
$p_f^{\mathrm{MCS}}(t)$	[0.0517 0.0526]	[0.0518 0.0527]	[0.0091 0.0094]

The proposed method is based on the First Order Reliability Method (FORM). Its accuracy is then affected by the linearization made by FORM [30, 44]. However, the proposed method may not be limited to FORM. If the limit-state function in the transformed normal variable space is highly nonlinear, more accurate reliability analysis methods, such as the Second Order Reliability Method (SORM), can also be used.

t-SORA is for problems with only stationary stochastic processes. When the stochastic processes are non-stationary, the method may be extended. Future work can be conducted with the following two tasks. The first task is to extend t-SORA to problems with non-stationary stochastic processes. This task is much more challenging because the

MPPs will change over time, and it will be more difficult to obtain the equivalent MPPs. The second task is to extend t-SORA to problems where time-dependent system reliability is concerned.

Acknowledgement

This material is based upon the work supported by the National Science Foundation through grant CMMI 1234855 and the Intelligent Systems Center at the Missouri University of Science and Technology.

Appendix A. Reliability analysis with the Rice's formula and FORM

For a limit-state function $g_P(\mathbf{d}, \mathbf{X}, \mathbf{Y}(t)) = g_P(\mathbf{d}, \mathbf{Z}(t))$, where $\mathbf{Z}(t) = [\mathbf{X}, \mathbf{Y}(t)]$, its Most Probable Point (MPP) is obtained from

$$\begin{cases} \min \left\| \mathbf{U}_{\mathbf{Z}} \right\| \\ \text{s.t.} \\ g_P(T[\mathbf{U}_{\mathbf{Z}}(t)]) > 0 \end{cases} \tag{A1}$$

where $\mathbf{U}_{\mathbf{Z}}(t) = [\mathbf{U}_X, \mathbf{U}_Y(t)]$ is the vector of standard normal variables associated with $\mathbf{X}$ and $\mathbf{Y}(t)$.

After the MPP $\mathbf{u}(t) = [\mathbf{u}_{\mathbf{X}}, \mathbf{u}_Y(t)]$ is found, the limit-state function $g_P(\mathbf{d}, \mathbf{X}, \mathbf{Y}(t)) = g_P(\mathbf{d}, \mathbf{Z}(t))$ is linearized at the MPP, the time-dependent probability of failure given in Eq. (5) is then approximated by [20, 32]:

$$p_f(t) = \Pr\{g_P(\mathbf{d}, \mathbf{X}, \mathbf{Y}(\tau)) > 0, \exists \tau \in [0, t]\} \approx \Pr\{L(\tau) = \boldsymbol{\alpha}\mathbf{U}_{\mathbf{Z}}^T(\tau) > \beta(\tau), \exists \tau \in [0, t]\} \tag{A2}$$

in which β and $\boldsymbol{\alpha}$ are given by [22, 24]

$$\beta(\tau) = \left\| \mathbf{u}(\tau) \right\| \tag{A3}$$

$$\boldsymbol{\alpha} = \frac{\mathbf{u}(\tau)}{\beta} \tag{A4}$$

The Rice's formula gives the upcrossing rate by [36, 37]

$$v^{+}(t) = \omega(t)\phi(\beta(t))\Psi\left(\frac{\dot{\beta}(t)}{\omega(t)}\right) \tag{A5}$$

where $\phi(\cdot)$ is the probability density function (PDF) of a standard normal variable, and

$$\dot{\beta}(t) = \frac{\partial \beta(t)}{\partial t} \tag{A6}$$

$$\Psi(x) = \phi(x) - x\Phi(-x) \tag{A7}$$

and

$$\omega^2(t) = \dot{\boldsymbol{\alpha}}\dot{\boldsymbol{\alpha}}^T + \boldsymbol{\alpha}\ddot{\mathbf{C}}_{12}(t,t)\boldsymbol{\alpha}^T \tag{A8}$$

in which

$$\dot{\boldsymbol{\alpha}} = \frac{\partial \boldsymbol{\alpha}(t)}{\partial t} \tag{A9}$$

and

$$\ddot{\mathbf{C}}_{12}(t_1,t_2)\Big|_{t_1=t_2=t} = \begin{bmatrix} \mathbf{0} & 0 & 0 & \cdots & 0 \\ 0 & \dfrac{\partial^2 \rho_1(t_1,t_2)}{\partial t_1 \partial t_2} & 0 & \cdots & 0 \\ 0 & 0 & \ddots & \vdots & 0 \\ \vdots & \vdots & \vdots & \ddots & \vdots \\ 0 & 0 & 0 & \cdots & \dfrac{\partial^2 \rho_m(t_1,t_2)}{\partial t_1 \partial t_2} \end{bmatrix}\Bigg|_{t_1=t_2=t} \tag{A10}$$

in which $\rho_l(t_1,t_2)$, $l = 1, 2, \cdots m$, are the coefficients of the autocorrelation of stochastic process $U_{Y_l}(t)$, and m is the number of stochastic processes. Since the stochastic processes $\mathbf{Y}(t)$ are assumed to be stationary, $\dot{\boldsymbol{\alpha}} = 0$, and $\dot{\beta} = 0$.

p_f is computed by [32]

$$p_f(\mathrm{t}) = 1 - R(0)\exp\ \left(-\int_0^t v^{+}(\tau)d\tau\right) \tag{A11}$$

where $R(0)$ is the time instantaneous reliability at the initial time instant and is computed by

$$R(0) = \Phi(\beta) \tag{A12}$$

Appendix B. Orthogonal Series Expansion (OSE)

As shown in Eq. (A2), the time-dependent probability of failure $p_f(t)$ is approximated by $\begin{aligned} p_f(t) &= \Pr\{G(\tau) = g_P(\mathbf{d}, \mathbf{X}, \mathbf{Y}(\tau)) > 0, \exists\tau \in [0, t]\} \\ &\approx \Pr\{L(\tau) = \boldsymbol{\alpha}\mathbf{U}_{\mathbf{Z}}^T(\tau) > \beta, \exists\tau \in [0,t]\} \end{aligned}$, where $G(\tau)$ is a non-Gaussian stochastic process and $L(\tau)$ is a standard Gaussian stochastic process. If the maximum value of $L(\tau)$ over $[0,t]$, W, is available, according to Eq. (18), $p_f(t) = \Pr\{W > \beta\}$. The distribution of W can be obtained from the samples of $L(\tau)$, and the samples may be generated from the OSE method.

OSE approximates $L(\tau)$ as follows [42]:

$$L(\tau) \approx \sum_{i=0}^{M} \sqrt{\lambda_i}\xi_i\left(\sum_{j=0}^{M} P_j^i h_j(\tau)\right) \tag{B1}$$

in which λ_i is the *i*-th eigenvalue of covariance matrix $\boldsymbol{\Sigma}$, P_j^i is the projection of the *i*-th eigenvector of covariance matrix $\boldsymbol{\Sigma}$ on the *j*-th Legendre polynomial, and $h_j(t)$ is the *j*-th Legendre polynomial, ξ_i, where $i = 1, 2, \cdots, M$, are *M* independent standard normal variables, and $\boldsymbol{\Sigma}$ is a matrix with element Σ_{ij} given by [42, 45]

$$\Sigma_{ij} = \int_0^t \int_0^t \rho_{t_1 t_2} h_i(t_1) h_j(t_2) dt_1 dt_2 \tag{B2}$$

where

$$\rho_{\tau_1\tau_2} = \boldsymbol{\alpha}\mathbf{C}(\tau_1, \tau_2)\boldsymbol{\alpha}^T \tag{B3}$$

and $\mathbf{C}(\tau_1, \tau_2)$ is a diagonal matrix with the diagonal element being the covariance of $\mathbf{U}_{\mathbf{Z}}(\tau_1)$ and $\mathbf{U}_{\mathbf{Z}}^T(\tau_2)$.

Once the approximated response $L(\tau)$ is available, N samples can be generated at Q discretizing instants over $[0,t]$ [45]. The samples are given in matrix $\tilde{L}_{N\times Q}$ as below.

$$\tilde{L}_{N\times Q}=\begin{pmatrix} l(t_1,1) & l(t_2,1) & \cdots & l(t_Q,1) \\ l(t_1,2) & l(t_2,2) & \cdots & l(t_Q,2) \\ \vdots & \vdots & \ddots & \vdots \\ l(t_1,N) & l(t_2,N) & \cdots & l(t_Q,N) \end{pmatrix}_{N\times Q} \tag{B4}$$

N samples of the extreme value W can then available through the following equations:

$$w_j=\max\{l(t_1,j),l(t_2,j),\cdots,l(t_Q,j)\},\ \text{where } j=1,2,\cdots,N \tag{B5}$$

Appendix C. Saddlepoint Approximation (SPA)

At first, the cumulants of W are computed from the samples and are computed by [46]

$$\begin{cases} \kappa_1=\dfrac{m_1}{N} \\ \kappa_2=\dfrac{Nm_2-m_1^2}{N(N-1)} \\ \kappa_3=\dfrac{2m_1^3-3nm_1m_2+N^2m_3}{N(N-1)(N-2)} \\ \kappa_4=\dfrac{-6m_1^4+12nm_1^2m_2-3N(N-1)m_2^2}{N(N-1)(N-2)(N-3)} \\ +\dfrac{-4N(N+1)m_1m_3+N^2(N+1)m_4}{N(N-1)(N-2)(N-3)} \end{cases} \tag{C1}$$

where κ_i is the *i*-th cumulant of W, m_s ($s=1,2,3,4$) are the sums of the *s-th* power of the samples W and are given by

$$m_s=\sum_{i=1}^{N}w_i^s \tag{C2}$$

in which w_i is the *i*-th sample of W given in Eq. (B5).

In this work, the first four moments are used because numerical examples show the good accuracy. Higher order may also be used.

Once κ_j, $j=1,2,3,4$, are available, the reliability index β is updated by

$$\beta = \kappa_1 + \kappa_2 \frac{\eta}{1!} + \kappa_3 \frac{\eta^2}{2!} + \kappa_4 \frac{\eta^3}{3!} \tag{C3}$$

where η is the saddlepoint, which satisfies the following equations:

$$1 - [p_f] = \Phi(z) + \phi(z)\left(\frac{1}{z} - \frac{1}{v}\right) \tag{C4}$$

$$z = \text{sign}(\eta)\ \ 2\left[\eta K_L^{'}(\eta) - K_L(\eta)\right]^{1/2} \tag{C5}$$

$$v = \eta\left[K_L^{''}(\eta)\right]^{1/2} \tag{C6}$$

$$K_L(\eta) = \sum_{i=1}^{4} \kappa_i \frac{\eta^i}{i!} \tag{C7}$$

and

$$K_L^{''}(\eta) = \kappa_2 + \sum_{j=3}^{4} \kappa_j \frac{\eta^{j-2}}{(j-2)!} \tag{C8}$$

where $\text{sign}(\eta)$= +1, −1, or 0, depending on whether η is positive, negative, or zero.

Reference

[1] Li, J., Mourelatos, Z., and Singh, A., 2012, "Optimal Preventive Maintenance Schedule Based on Lifecycle Cost and Time-Dependent Reliability," SAE International Journal of Materials and Manufacturing, 5(1), pp. 87-95.

[2] Singh, A., Mourelatos, Z. P., and Li, J., 2010, "Design for lifecycle cost using time-dependent reliability," Journal of Mechanical Design, Transactions of the ASME, 132(9), pp. 0910081-09100811.

[3] Wang, Z., and Wang, P., 2012, "A nested extreme response surface approach for time-dependent reliability-based design optimization," Journal of Mechanical Design, Transactions of the ASME, 134(12).

[4] Kurtz, N., and Song, J., 2013, "Cross-entropy-based adaptive importance sampling using Gaussian mixture," Structural Safety, 42, pp. 35-44.

[5] Li, Y., Jiang, P., Gao, L., and Shao, X., 2013, "Sequential optimisation and reliability assessment for multidisciplinary design optimisation under hybrid uncertainty of randomness and fuzziness," Journal of Engineering Design, 24(5), pp. 363-382.

[6] Srivastava, R., and Deb, K., 2013, "An evolutionary based Bayesian design optimization approach under incomplete information," Engineering Optimization, 45(2), pp. 141-165.

[7] Yu, H., Gillot, F., and Ichchou, M., 2013, "Reliability based robust design optimization for tuned mass damper in passive vibration control of deterministic/uncertain structures," Journal of Sound and Vibration, 332(9), pp. 2222-2238.

[8] Wu, Y. T., 1994, "Computational methods for efficient structural reliability and reliability sensitivity analysis," AIAA Journal, 32(8), pp. 1717-1723.

[9] Wu, Y. T., and Wang, W., "New method for efficient reliability-based design optimization," pp. 274-277.

[10] Du, X., and Chen, W., 2004, "Sequential optimization and reliability assessment method for efficient probabilistic design," Journal of Mechanical Design, Transactions of the ASME, 126(2), pp. 225-233.

[11] Du, X., Guo, J., and Beeram, H., 2008, "Sequential optimization and reliability assessment for multidisciplinary systems design," Structural and Multidisciplinary Optimization, 35(2), pp. 117-130.

[12] Tang, Y., Chen, J., and Wei, J., 2012, "A sequential algorithm for reliability-based robust design optimization under epistemic uncertainty," Journal of Mechanical Design, Transactions of the ASME, 134(1).

[13] Du, X., 2008, "Saddlepoint approximation for sequential optimization and reliability analysis," Journal of Mechanical Design, Transactions of the ASME, 130(1).

[14] Cho, T. M., and Lee, B. C., 2010, "Reliability-based design optimization using convex approximations and sequential optimization and reliability assessment method," Journal of Mechanical Science and Technology, 24(1), pp. 279-283.

[15] Rouhi, M., and Rais-Rohani, M., 2013, "Modeling and probabilistic design optimization of a nanofiber-enhanced composite cylinder for buckling," Composite Structures, 95, pp. 346-353.

[16] Spence, S. M. J., and Gioffrè, M., 2012, "Large scale reliability-based design optimization of wind excited tall buildings," Probabilistic Engineering Mechanics, 28, pp. 206-215.

[17] Breitung, K., 1984, "Asymptotic crossing rates for stationary Gaussian vector processes," Tech. Report, 1, Dept. of Math, and Statistics, Univ. of Lund, Lund, Sweden.

[18] Breitung, K., 1988, "Asymptotic approximations for the outcrossing rates of stationary vector processes," Stochast Process Appl, , 13, pp. 195–207.

[19] Ditlevsen, O., 1983, "GAUSSIAN OUTCROSSINGS FROM SAFE CONVEX POLYHEDRONS," Journal of Engineering Mechanics, 109(1), pp. 127-148.

[20] Hagen, O., and Tvedt, L., 1991, "Vector process out-crossing as parallel system sensitivity measure," Journal of Engineering Mechanics, 117(10), pp. 2201-2220.

[21] Hagen, O., and Tvedt, L., 1992, "Parallel system approach for vector out-crossing," Journal of Offshore Mechanics and Arctic Engineering, 114(2), pp. 122-128.

[22] Andrieu-Renaud, C., Sudret, B., and Lemaire, M., 2004, "The PHI2 method: A way to compute time-variant reliability," Reliability Engineering and System Safety, 84(1), pp. 75-86.

[23] Zhang, J., and Du, X., 2011, "Time-dependent reliability analysis for function generator mechanisms," Journal of Mechanical Design, Transactions of the ASME, 133(3).

[24] Yang, J. N., and Shinozuka, M., 1971, "On the first excursion probability in stationary narrow- band random vibration," Journal of Applied Mechanics, Transactions ASME, 38 Ser E(4), pp. 1017-1022.

[25] Chen, J. B., and Li, J., 2007, "The extreme value distribution and dynamic reliability analysis of nonlinear structures with uncertain parameters," Structural Safety, 29(2), pp. 77-93.

[26] Hu, Z., Li, H., Du, X., and Chandrashekhara, K., 2012, "Simulation-based time-dependent reliability analysis for composite hydrokinetic turbine blades," Structural and Multidisciplinary Optimization, 47(5), pp. 765-781.

[27] Kuschel, N., and Rackwitz, R., 2000, "Optimal design under time-variant reliability constraints," Structural Safety, 22(2), pp. 113-127.

[28] Jensen, H. A., Kusanovic, D. S., Valdebenito, M. A., and Schuëller, G. I., 2011, "Reliability-based design optimization of uncertain stochastic systems: Gradient-based scheme," Journal of Engineering Mechanics, 138(1), pp. 60-70.

[29] Rathod, V., Yadav, O. P., Rathore, A., and Jain, R., 2012, "Reliability-based design optimization considering probabilistic degradation behavior," Quality and Reliability Engineering International, 28(8), pp. 911-923.

[30] Choi, S. K., Grandhi, R. V., and Canfield, R. A., 2007, Reliability-based structural design, Springer.

[31] Singh, A., and Mourelatos, Z. P., 2010, "On the time-dependent reliability of non-monotonic, non-repairable systems," SAE International Journal of Materials and Manufacturing, 3(1), pp. 425-444.

[32] Hu, Z., and Du, X., 2012, "Reliability analysis for hydrokinetic turbine blades," Renewable Energy, 48, pp. 251-262.

[33] Li, J., and Mourelatos, Z. P., 2009, "Time-dependent reliability estimation for dynamic problems using a niching genetic algorithm," Journal of Mechanical Design, Transactions of the ASME, 131(7), pp. 0710091-07100913.

[34] Singh, A., Mourelatos, Z., and Nikolaidis, E., 2011, "Time-Dependent Reliability of Random Dynamic Systems Using Time-Series Modeling and Importance Sampling," SAE International Journal of Materials and Manufacturing, 4(1), pp. 929-946.

[35] Singh, A., and Mourelatos, Z. P., 2010, "Time-dependent reliability estimation for dynamic systems using a random process approach," SAE International Journal of Materials and Manufacturing, 3(1), pp. 339-355.

[36] Rice, S. O., 1944, "Mathematical Analysis of Random Noise," Bell System Technical Journal, , 23, pp. 282–332.

[37] Rice, S. O., 1945, "Mathematical analysis of random noise," Bell Syst.Tech. J.,, 24, pp. 146-156.

[38] Wang, Z., and Wang, P., "Reliability-based product design with time-dependent performance deterioration," Proc. 2012 IEEE International Conference on Prognostics and Health Management: Enhancing Safety, Efficiency, Availability, and Effectiveness of Systems Through PHM Technology and Application, PHM 2012;Denver, CO;18 June 2012through21 June 2012;Code93398.

[39] Singh, A., Mourelatos, Z. P., and Nikolaidis, E., "An importance sampling approach for time-dependent reliability," Proc. Proceedings of the ASME Design Engineering Technical Conference,Washington, DC, pp:1077-1088, I. C. 2011, ed.

[40] Madsen, P. H., and Krenk, S., 1984, "Integral equation method for the first-passage problem in random vibration," Journal of Applied Mechanics, Transactions ASME, 51(3), pp. 674-679.

[41] Vanmarcke, E. H., 1975, "On the distribution of the first-passage time for normal stationary random processes," Journal of Applied Mechanics, 42, pp. 215-220.

[42] Zhang, J., and Ellingwood, B., 1994, "Orthogonal series expansions of random fields in reliability analysis," Journal of Engineering Mechanics, 120(12), pp. 2660-2677.

[43] HU, Z., and Du, X., 2013, "A Sampling Approach to Extreme Values of Stochastic Processes for Reliability Analysis," ASME Journal of Mechanical Design, In press.

[44] Adhikari, S., 2005, "Asymptotic distribution method for structural reliability analysis In high dimensions," Proceedings of the Royal Society A: Mathematical, Physical and Engineering Sciences, 461(2062), pp. 3141-3158.

[45] Hu, Z., Du, X.,, 2013, "First Order Simulation for Time Dependent Reliability," Submitted.

[46] Fisher, R. A., 1928, "Moments and Product Moments of Sampling Distribution," Proceeding of London Mathematical Society, 30(2), pp. 199-238.

SECTION
2. CONCLUSION

Time-dependent uncertainties such as stochastic loadings and time-dependent performances are very common in practical engineering applications. The uncertainties in the design environment result in biases of actual designs from the nominal design. To quantify the effect of time-dependent uncertainties on the system performance, time-dependent reliability analysis method needs to be employed. Time-dependent reliability provides the probability that a system can operate without failure over a certain lifetime cycle. It is directly related to the product lifecycle cost and maintenance activities. Accurate and efficient time-dependent reliability analysis methods are required to design high reliability into the product. It is essential to the design optimization of a product with the optimal lifecycle cost and guaranteed reliability targets.

Based on the independent assumption of upcrossing events, reliability analysis methods have been proposed for the time-dependent problems in the past decades. The independent assumption, however, does not hold when the failure threshold is low or the correlation of response at time instants is strong. In this dissertation, a joint-upcrossing rate method was presented to release the independent assumption. Expressions for the joint-upcrossing rate were derived. Numerical algorithm was developed to estimate the first-passage rate. The join-upcrossing rate method is applicable to general problems with non-stationary stochastic processes, non-Gaussian random variables, and time. In addition to the join-upcrossing rate method, an efficient global optimization reliability analysis method was proposed for problems with only random variables and time. The surrogate model of extreme value response was constructed based on the extreme values identified from a newly developed mixed efficient global optimization method. The developed reliability analysis methodologies were evaluated through classical engineering design problems as well as a composite hydrokinetic turbine blade. The results of engineering application examples demonstrated that the proposed methods can approximate the time-dependent reliability efficiently and accurately. Since there is a similarity between the time-dependent reliability problem and the reliability analysis with mixture of random and interval variables, the series expansion method was successfully

extended to problems with both random and interval variables. In order to design the time-dependent reliability into product, a time-dependent sequential optimization and reliability analysis (t-SORA) method was developed for problems subjected to stationary stochastic loadings. Numerical examples demonstrated that the new method can efficiently and accurately perform design optimization with time-dependent reliability constraints.

Four kinds of time-dependent reliability analysis method were developed by employing the joint-upcrossing rate, surrogate model method, series expansion method, and sampling approach. One optimization approach was developed for special problems under stationary stochastic loadings. More generalized time-dependent reliability-based design optimization methods for problems with non-stationary stochastic loadings and random variables will be one of the future works. As most of current time-dependent reliability analysis methods were developed based on the First-Order Reliability Method (FORM), the accuracy of reliability analysis methods is affected by the drawbacks of FORM. Improving the accuracy of time-dependent reliability analysis methods by overcoming the drawbacks of FORM is also one of the future works.

BIBLIOGRAPHY

[1] Y. W. Liu, and F. Moses, “A sequential response surface method and its application in the reliability analysis of aircraft structural systems”, Structural Safety, 16(1), 39-46, 1994.

[2] B. D. Youn, K.K. Choi, R.J. Yang, and L. Gu. "Reliability-based design optimization for crashworthiness of vehicle side impact", Structural and Multidisciplinary Optimization 26.3-4: 272-283, 2004.

[3] P. J. Tavner, J. Xiang, and F. Spinato. "Reliability analysis for wind turbines.", Wind Energy 10, no. 1: 1-18, 2007.

[4] X.P. Du, and W. Chen, "Sequential optimization and reliability assessment method for efficient probabilistic design." Journal of Mechanical Design 126.2: 225-233, 2004.

[5] B.D. Youn, K. K. Choi, and H.P. Young, "Hybrid analysis method for reliability-based design optimization.”, Journal of Mechanical Design 125.2: 221-232, 2003.

[6] X. Du, and Z. Hu. "First Order Reliability Method With Truncated Random Variables.", Journal of Mechanical Design 134.9: 091005, 2012.

[7] Z. P. Mourelatos, and J. Zhou. "Reliability estimation and design with insufficient data based on possibility theory.", AIAA journal 43.8: 1696-1705, 2005.

[8] J.F. Zhang, and X. Du. "Time-dependent reliability analysis for function generator mechanisms." Journal of Mechanical Design 133.3: 031005, 2011.

[9] J. Li, and Z. P. Mourelatos., "Time-dependent reliability estimation for dynamic problems using a niching genetic algorithm.", Journal of Mechanical Design 131.7: 071009, 2009.

[10] A. Singh, Z. P. Mourelatos, and J. Li. "Design for lifecycle cost using time-dependent reliability." Journal of Mechanical Design, 132.9: 091008, 2010.

[11] Z. Hu, and X. Du. "Lifetime cost optimization with time-dependent reliability." Engineering Optimization, ahead-of-print: 1-22, 2013.

[12] J. M. Noortwijk, J. A. Weide, M. J. Kallen, and M. D. Pandey, “Gamma processes and peaks-over-threshold distributions for time-dependent reliability.”, Reliability Engineering & System Safety, 92(12), 1651-1658, 2007.

[13] A. Singh, and Z. P. Mourelatos., “Time-dependent reliability estimation for dynamic systems using a random process approach.”, No. 2010-01-0644. SAE Technical Paper, 2010.

[14] A. Singh, Z. P. Mourelatos, and E. Nikolaidis, “Time-dependent reliability of random dynamic systems using time-series modeling and importance sampling.”, No. 2011-01-0728. SAE Technical Paper, 2011.

[15] Z. Hu, and X. Du., "Time-dependent reliability analysis with joint upcrossing rates.", Structural and Multidisciplinary Optimization, 48.5: 893-907, 2013.

[16] Z. Hu, and X. Du., “Efficient Global Optimization Reliability analysis for time-dependent limit-state functions,” The ASME 2014 International Design Engineering Technical Conferences (IDETC) and Computers and Information in Engineering Conference (CIE), August 17-20, 2014 in Buffalo, NY.

[17] Z. Hu, and X. Du., " First Order Reliability Method for Time-Dependent Problems using Series Expansions", Structural and Multidisciplinary Optimization, in press.

[18] Z. Hu, and X. Du., "A Sampling Approach to Extreme Value Distribution for Time-Dependent Reliability Analysis.", Journal of Mechanical Design 135.7: 071003, 2013.

[19] Z. Hu, and X. Du, “A Design Oriented Reliability Analysis Methodology for Fatigue Life of Structures under Stochastic Loadings,” The ASME 2013 International Design Engineering Technical Conferences (IDETC) and Computers and Information in Engineering Conference (CIE), August 4-7, 2013 in Portland, OR.

[20] Z. Hu, X. Du, D. Conrad, R. Twohy, and M. Walmsley, “A Fatigue Reliability Analysis Method for Structures with known loading trend”, Structural and Multidisciplinary Optimization, in press, DOI 10.1007/s00158-013-1044-0, 2014.

VITA

Zhen Hu was born on December 16, 1986 in Xinyang, Henan, China. He received his Bachelor of Science degree in Mechanical Engineering in June 2008 from Central South University, Changsha, China. In March 2011, he received his Master of Science degree in Mechatronics engineering from Huazhong University of Science and Technology, Wuhan, China. In August 2014, he received his Doctor of Philosophy in Mechanical Engineering from Missouri University of Science and Technology, Rolla, Missouri, USA. His research interests include probabilistic engineering design, reliability-based design optimization, robust design, renewable energy, decision making under uncertainty, and fatigue reliability analysis. He won the first place award for the paper entitled "Reliability Analysis for Hydrokinetic Turbine Blades under Random River Velocity Field" at the 7th Intelligent System Center (ISC) Graduate Research Symposium on April 24, 2013 at Missouri University of Science and Technology. His paper entitled "Time-Dependent Reliability Analysis by A Sampling Approach to Extreme Values of Stochastic Processes" was nominated for the "Best Paper Award", sponsored by Ford Motor Company at the 38th Design Automation Conference of the ASME International Design Engineering Technical Conferences, 2012, Chicago, USA. During his Ph.D. study, he authored and co-authored 12 journal papers and 7 conference papers.